

2012

## LOCALIZATION AND FUNCTIONAL CHARACTERIZATION OF OATP4C1 TRANSPORTER IN *IN VITRO* CELL SYSTEMS AND HUMAN/RAT TISSUES

Kuei-Ling Kuo

University of Kentucky, kkuo2@uky.edu

[Right click to open a feedback form in a new tab to let us know how this document benefits you.](#)

### Recommended Citation

Kuo, Kuei-Ling, "LOCALIZATION AND FUNCTIONAL CHARACTERIZATION OF OATP4C1 TRANSPORTER IN *IN VITRO* CELL SYSTEMS AND HUMAN/RAT TISSUES" (2012). *Theses and Dissertations--Pharmacy*. 9. [https://uknowledge.uky.edu/pharmacy\\_etds/9](https://uknowledge.uky.edu/pharmacy_etds/9)

This Doctoral Dissertation is brought to you for free and open access by the College of Pharmacy at UKnowledge. It has been accepted for inclusion in Theses and Dissertations--Pharmacy by an authorized administrator of UKnowledge. For more information, please contact [UKnowledge@lsv.uky.edu](mailto:UKnowledge@lsv.uky.edu).

## **STUDENT AGREEMENT:**

I represent that my thesis or dissertation and abstract are my original work. Proper attribution has been given to all outside sources. I understand that I am solely responsible for obtaining any needed copyright permissions. I have obtained and attached hereto needed written permission statements(s) from the owner(s) of each third-party copyrighted matter to be included in my work, allowing electronic distribution (if such use is not permitted by the fair use doctrine).

I hereby grant to The University of Kentucky and its agents the non-exclusive license to archive and make accessible my work in whole or in part in all forms of media, now or hereafter known. I agree that the document mentioned above may be made available immediately for worldwide access unless a preapproved embargo applies.

I retain all other ownership rights to the copyright of my work. I also retain the right to use in future works (such as articles or books) all or part of my work. I understand that I am free to register the copyright to my work.

## **REVIEW, APPROVAL AND ACCEPTANCE**

The document mentioned above has been reviewed and accepted by the student's advisor, on behalf of the advisory committee, and by the Director of Graduate Studies (DGS), on behalf of the program; we verify that this is the final, approved version of the student's dissertation including all changes required by the advisory committee. The undersigned agree to abide by the statements above.

Kuei-Ling Kuo, Student

Dr. Markos Leggas, Major Professor

Dr. Jim Pauly, Director of Graduate Studies

ABSTRACT OF DISSERTATION

Kuei-Ling Kuo

The Graduate School

University of Kentucky

2012

LOCALIZATION AND FUNCTIONAL CHARACTERIZATION OF OATP4C1  
TRANSPORTER IN *IN VITRO* CELL SYSTEMS AND HUMAN/RAT TISSUES

---

ABSTRACT OF DISSERTATION

---

A dissertation submitted in partial fulfillment of the  
requirements for the degree of Doctor of Philosophy in the  
College of Pharmacy at the University of Kentucky

By

Kuei-Ling Kuo

Lexington, Kentucky

Co-Directors: Dr. Markos Leggas, Assistant Professor of Pharmaceutical Sciences  
and Dr. Patrick J. McNamara, Professor of Pharmaceutical Sciences

Lexington, Kentucky

2012

Copyright © Kuei-Ling Kuo 2012



## ABSTRACT OF DISSERTATION

### LOCALIZATION AND FUNCTIONAL CHARACTERIZATION OF OATP4C1 TRANSPORTER IN *IN VITRO* CELL SYSTEMS AND HUMAN/RAT TISSUES

The organic anion transporting polypeptide 4c1 (Oatp4c1) was previously identified as a novel uptake transporter predominantly expressed at the basolateral membrane in the rat kidney proximal tubules. Its functional role was suggested to be a vectorial transport partner of an apically-expressed efflux transporter for the efficient translocation of physiological substrates into urine, some of which were suggested to be uremic toxins. *In vitro* studies in polarized cell lines showed that upon transfection rat Oatp4c1 localizes at the apical membrane. The objectives of this project were to further validate the subcellular localization of Oatp4c1/OATP4C1 in rat and human tissues as well as their localization and function in polarized cells.

Using several complementary biochemical, molecular and proteomic methods as well as antibodies amenable to immunohistochemistry, immunofluorescence, and immunoblotting, we investigated the expression pattern of Oatp4c1 in epithelial cell lines and in the rat kidney and mammary gland (MG). Collectively, these data demonstrated that rat Oatp4c1 localized at the apical cell surface of polarized epithelium and primarily in the proximal straight tubules, the S3 segment of proximal tubule, in the juxtamedullary cortex.

Drug uptake studies in Oatp4c1-expressing cells demonstrated that Oatp4c1-mediated estrone-3-sulfate (E3S) uptake was ATP-independent and pH-dependent. The increased E3S transport activity at acidic extracellular pH was ascribed to the increased maximum transport rate ( $V_{\max}$ ). In addition, E3S transport inhibition by various substrates suggests that Oatp4c1 possesses multiple substrate binding sites.

The apical localization of Oatp4c1 in the rat kidney and MG is a novel finding and implies that this transporter protein plays a role in the reabsorption, not vectorial secretion, of its substrates. In addition, the upregulation of Oatp4c1 expression during lactation indicates that it is involved in reuptake of xenobiotic from the milk, resulting in their reduced exposure to the suckling infants, or that it functions as a scavenger system. Further, studies to identify physiological substrates are needed to better understand the significance of Oatp4c1 function in renal and mammary epithelium.

KEYWORDS: Oatp4c1, polarity, renal transporter, tubular reabsorption, estrone-3-sulfate

Kuei-Ling Kuo  
\_\_\_\_\_  
Student's Signature

6/25/12  
\_\_\_\_\_  
Date

LOCALIZATION AND FUNCTIONAL CHARACTERIZATION OF OATP4C1  
TRANSPORTER IN AN *IN VITRO* CELL SYSTEM AND HUMAN/RAT TISSUES

By  
Kuei-Ling Kuo

---

Markos Leggas  
Co-Director of Dissertation

---

Patrick J McNamara  
Co-Director of Dissertation

---

Jim Pauly  
Director of Graduate Studies

---

6/25/12  
Date

## RULES FOR THE USE OF DISSERTATIONS

Unpublished dissertations submitted for the Doctor's degree and deposited in the University of Kentucky Library are as a rule open for inspection, but are to be used only with due regard to the rights of the authors.

Bibliographical references may be noted, but quotations or summaries of parts may be published only with the permission of the author, and with the usual scholarly acknowledgments.

Extensive copying or publication of the dissertation in whole or in part also requires the consent of the Dean of the Graduate School of the University of Kentucky.

A library that borrows this dissertation for use by its patrons is expected to secure the signature of each user.

Name

Date[illegible]

DISSERTATION

Kuei-Ling Kuo

The Graduate School

University of Kentucky

2012

LOCALIZATION AND FUNCTIONAL CHARACTERIZATION OF OATP4C1  
TRANSPORTER IN *IN VITRO* CELL SYSTEMS AND HUMAN/RAT TISSUES

---

DISSERTATION

---

A dissertation submitted in partial fulfillment of the  
requirements for the degree of Doctor of Philosophy in the  
College of Pharmacy at the University of Kentucky

By

Kuei-Ling Kuo

Lexington, Kentucky

Co-Directors: Dr. Markos Leggas, Assistant Professor of Pharmaceutical Sciences  
and Dr. Patrick J. McNamara, Professor of Pharmaceutical Sciences

Lexington, Kentucky

2012

Copyright © Kuei-Ling Kuo 2012

## ACKNOWLEDGEMENTS

I would like to first thank my parents and sister, Chin-An Kuo, Yingyue Wang and Kuan-Ling Kuo, for their continuous love and support.

I deeply thank my mentor Dr. Markos Leggas for all of his guidance, advice and support in these years. I will always be grateful for his patience and trust, and giving me the opportunity to develop as a scientist. I also thank my co-advisor Dr. Patrick McNamara for his helpful comments and suggestions. I also acknowledge the contributions of my committee members Drs. Mary Vore, Gregory Graf, Peter Wedlund, and that of my outside examiner, Dr. Rina Plattner. I would like to give my sincerest gratitude to Dr. Mamta Goswami who selflessly instructs me in most of the techniques used in my graduate studies. I would also like to thank the current and former Leggas Lab members, Eleftheria Tsakalozou, Tamer Ahmed, Dr. Jamie Horn, Dr. Eyob Adane, Marta Milewska, Yali Liang, Dr. Zhiwei Liu, Dr. Dominique Talbert, for technical assistance and friendships. I also thank Dr. Philip Empey from Dr. McNamara's lab for initiating this project and his comments and discussions. I also value the technical assistance of Dr. Lipeng Wang from Dr. McNamara's lab, and Dr. Jingjing Liu and Dr. Kai Su from Dr. Graf's lab.

I appreciate the assistance of Dr. Haining Zhu with proteomic analysis, Cynthia Long with histology, Dr. Jennifer Strange and Dr. Greg Bauman with FACS. I would also like to thank Catina Rossell in the College of Pharmacy for all her help. Finally, I would like to thank all my friends to be with me and endure ups and downs of graduate studies.

## TABLE OF CONTENTS

ACKNOWLEDGEMENTS .....	iii
TABLE OF CONTENTS .....	iv
LIST OF TABLES .....	viii
LIST OF FIGURES.....	ix
Chapter 1 : BACKGROUND.....	1
A . Drug transporters in lactating mammary epithelium.....	1
1. ATP-binding cassette (ABC) transporter superfamily .....	2
2. Solute carrier (SLC) superfamily .....	5
B . Renal physiology.....	8
C . Drug transporters in the kidney.....	11
1. ABC transporters .....	12
2. SLC transporters.....	15
D . OATP4C1 (Human: OATP4C1; rodent: Oatp4c1) .....	19
E . Summary.....	21
Chapter 2 : PLAN OF WORK.....	24
Hypothesis 1.....	24
Specific Aim 1a .....	24
Specific Aim 1b .....	24
Specific Aim 1c .....	24
Hypothesis 2.....	25
Specific Aim 2a .....	25
Specific Aim 2b .....	25
Hypothesis 3.....	25
Specific Aim 3a .....	25
Specific Aim 3b .....	26
Hypothesis 4.....	26
Specific Aim 4a .....	26
Specific Aim 4b .....	26
Specific Aim 4c .....	26
Specific Aim 4d .....	27
Chapter 3 : MATERIALS AND METHODS .....	28
A . Materials .....	28
B . Creation and validation of a rat Oatp4c1-expressing cell line .....	30
1. Development of rat Oatp4c1 antibody .....	30
2. Construction of plasmid vector.....	31
3. Cell culture and transfection .....	33
4. Single clone selection by fluorescence-activated cell sorting (FACS) with transiently expressed C-terminal-tagged green fluorescent protein (GFP).....	34



5. Single clone selection by immunofluorescence labeling and FACS .....	35
6. Single clone selection by serial dilution .....	35
7. Regulation of Oatp4c1 expression by sodium butyrate, blasticidin, simvastatin, glycerol, and MG132 .....	37
8. Western blot.....	37
9. Immunohistochemistry .....	38
10. Immunofluorescence microscopy.....	39
11. Surface protein biotinylation assay .....	40
C . Determination of Oatp4c1 expression and subcellular localization in rat tissues .....	41
1. Quantitative real time polymerase chain reaction (qRT-PCR) .....	41
2. Western blot.....	43
3. Immunohistochemistry .....	44
4. BBM (brush-border membrane) and BLM (basolateral membrane) isolation .....	44
5. Protein trypsin digestion and LC-MS/MS analysis .....	46
D . Functional characterization of Oatp4c1 in MDCKII-Oatp4c1 cells .....	47
1. [ <sup>3</sup> H]-E3S uptake and inhibition studies .....	47
2. [ <sup>3</sup> H]-MTX uptake and inhibition studies .....	49
E . Creation and validation of human OATP4C1-expressing cell lines.....	49
1. MDCKII cells .....	49
2. <i>Spodoptera frugiperda</i> (Sf9) insect cells .....	52
F . Validation of OATP4C1 expression in human kidney and cancer cells.....	56
1. Immunohistochemical analysis in human kidney sections .....	56
2. qRT-PCR analysis for <i>SLCO4C1</i> expression in cancer cells.....	56
3. OATP4C1/ <i>SLCO4C1</i> expression in lung tumor and adjacent normal lung tissue sections.....	58
Chapter 4 : RESULTS .....	60
A . Creation and validation of a rat Oatp4c1-expressing cell line .....	60
1. Specific Aim 1a: To develop and validate rat Oatp4c1 antibodies amenable for immunoblotting, immunohistochemistry and immunofluorescence. ....	60
2. Specific Aim 1b: To create and validate a stably transfected rat Oatp4c1-expressing cell line with appropriate characteristics for uptake studies.....	60
B . Determination of Oatp4c1 expression and subcellular localization in rat tissues .....	78
1. Specific Aim 1c: To determine the expression and subcellular localization of Oatp4c1 in the rat tissues (liver, kidney, lactating and non-lactating mammary gland). ....	78
2. Specific Aim 2a: To verify the apical localization of Oatp4c1 in the rat kidney cortex by proteomic analysis in the isolated brush-border membrane (BBM) and basolateral membrane (BLM). ....	87
3. Specific Aim 2b: To determine the precise expression pattern of Oatp4c1 at the organ and nephron level.....	90

C . Functional characterization of Oatp4c1 in MDCKII-Oatp4c1 cells .....	95
1. Specific Aim 3a: To investigate Oatp4c1 transport characteristics and driving force. ....	95
2. Specific Aim 3b: To identify potential Oatp4c1 substrates.....	105
D . Creation and validation of human OATP4C1-expressing cell lines .....	110
1. Specific Aim 4a: To develop and validate human OATP4C1 antibodies amenable for immunoblotting, immunohistochemistry and immunofluorescence. ....	110
2. Specific Aim 4b: To create and validate human OATP4C1-expressing cells with appropriate characteristics for functional studies.....	110
E . Validation of OATP4C1 expression in human kidney and cancer cells .....	127
1. Specific Aim 4c: To determine the expression and subcellular localization of OATP4C1 in the human kidney.....	127
2. Specific Aim 4d: To determine the expression of OATP4C1 in cancer cells. ....	129
Chapter 5 : Discussion .....	134
A . Creation and validation of a rat Oatp4c1-expressing cell line .....	134
B . Determination of Oatp4c1 expression and subcellular localization in rat tissues .....	140
C . Functional characterization of Oatp4c1 in MDCKII-Oatp4c1 cells .....	144
D . Creation and validation of human OATP4C1-expressing cell lines .....	149
E . Validation of OATP4C1 expression in human kidney and cancer cells .....	152
Chapter 6 : conclusions.....	155
appendices.....	159
Appendix 1: Lists of abbreviations.....	159
Appendix 2: Identification of Abcg2 as a potential transporter of uremic toxins .....	162
Introduction.....	162
Methods.....	162
Results and Discussion .....	163
Appendix 3: Creation and validation of human ABCG2-expressing Sf9 cells.....	168
Introduction.....	168
Methods.....	168
Results and Discussion .....	170
Appendix 4: Development of a mathematical model to simulate the transport of common substrate of apical uptake and apical efflux transporters across the renal proximal tubular cells .....	175
Introduction.....	175
Methods.....	175
Results and Discussion .....	178
References .....	184

VITA .....	204
------------	-----

## LIST OF TABLES

Table 1-1: Milk to plasma AUC ratios for certain drugs in wild-type and Abcg2 knockout (Abcg2 <sup>-/-</sup> ) mice. ....	5
Table 3-1: Slco4c1 and 18s rRNA primers information. ....	43
Table 3-2: SLCO4C1 and 18s rRNA primers information. ....	57
Table 3-3: TaqMan <sup>®</sup> Gene Expression Assay for SLCO4C1 and 18s rRNA.....	59
Table 4-1: Akaike Information Criterion (AIC) of model selection for transport kinetic parameter estimation of Oatp4c1-mediated E3S transport at pH 4.5, 5.5 and 7.4. ....	100
Table 4-2: Transport kinetic parameters of Oatp4c1-mediated E3S transport at pH 4.5, 5.5 and 7.4 (mean $\pm$ S.E.). ....	101
Table 4-3: Transport kinetic parameters of OATP4C1-mediated [ <sup>3</sup> H]-ouabain transport at pH 7.4 (mean $\pm$ S.E.). ....	117
Table 4-4: Transport kinetic parameters of OATP4C1-mediated [ <sup>3</sup> H]-ouabain transport in Sf9-OATP4C1 membrane vesicles at pH 7.4 (mean $\pm$ S.E.)......	123

## LIST OF FIGURES

Figure 1-1: Cross-sectional view of the kidney (34). .....	10
Figure 1-2: ABC and SLC transporters in proximal tubular cells (adapted from literature (37-39)). .....	12
Figure 3-1: Rat Oatp4c1 antibody antigen peptide sequence and location.....	31
Figure 3-2: pcDNA6.2/GFP-DEST/ Slco4c1 plasmid construct.....	33
Figure 3-3: Plate setup for serial dilution.....	36
Figure 3-4: pcDNA6.2/EmGFP-Bsd/V5-DEST/SLCO4C1 plasmid construct.....	51
Figure 3-5: Human OATP4C1 antibody antigen peptide sequence and location.....	52
Figure 3-6: pDEST8/SLCO4C1 plasmid construct. ....	53
Figure 4-1: Validation of Slco4c1 plasmid constructs.....	62
Figure 4-2: Validation of Oatp4c1 expression and subcellular localization in MDCKII-Oatp4c1 cells.....	63
Figure 4-3: Confocal microscopy of Oatp4c1 expression and subcellular localization in LLC-PK1-Oatp4c1 cells. ....	65
Figure 4-4: Immunofluorescence staining for Oatp4c1 expression in MDCKII-Oatp4c1 pooled cells and c94.....	68
Figure 4-5: Effect of 24 hr sodium butyrate (NaB) treatment on Oatp4c1 expression and subcellular localization in MDCKII-Oatp4c1 pooled cells.....	69
Figure 4-6: Effect of increasing blasticidin (Bsd) concentration for two passages on Oatp4c1 expression in MDCKII-Oatp4c1 pooled cells. ....	71
Figure 4-7: Effect of 24 hr simvastatin (Sim) treatment on Oatp4c1 expression in MDCKII-Oatp4c1 pooled cells.....	72
Figure 4-8: Effect of 48 hr glycerol treatment on Oatp4c1 expression in MDCKII-Oatp4c1 pooled cells.....	74
Figure 4-9: Effect of MG132 treatment on Oatp4c1 expression in MDCKII-Oatp4c1 pooled cells.....	75
Figure 4-10: Effect of sodium butyrate (NaB, 5 mM) and blasticidin (Bsd, 30 µg/ml) on Oatp4c1 expression in MDCKII-Oatp4c1 pooled cells and c94. ....	77

Figure 4-11: Immunofluorescence staining for Oatp4c1 expression in MDCKII-Oatp4c1 pooled cells and sodium butyrate (NaB) treated c94.....	77
Figure 4-12: Oatp4c1 expression in female adult rat liver, kidney, lactating and non-lactating MG.....	80
Figure 4-13: Ontogeny of Oatp4c1 in rat kidney. ....	81
Figure 4-14: Ontogeny of Oatp4c1 in rat liver. ....	82
Figure 4-15: Oatp4c1 localization in rat liver, kidney and lactating MG. ....	84
Figure 4-16: Verification of apical Oatp4c1 localization in rat renal tubules by four different antibodies.....	85
Figure 4-17: Double immunofluorescence staining for Oatp4c1 (green) and E-cadherin (red) in rat kidney. ....	86
Figure 4-18: A. Double immunofluorescence staining for Oatp4c1 (green) and Abcg2 (A, red) or E-cadherin (B, red) in rat lactating MG. ....	86
Figure 4-19: Expression of Oatp4c1 in isolated kidney brush border membrane (BBM) and basolateral membrane (BLM) fractions.....	89
Figure 4-20: Oatp4c1 location in rat kidney. ....	91
Figure 4-21: Double immunofluorescence staining for Oatp4c1 (red) and the proximal tubule marker AQP1 (A, green) or the distal tubule marker calbindin-D <sub>28K</sub> (B, green).....	92
Figure 4-22 (part 1 of 2): Oatp4c1 colocalization with major efflux transporters in the kidney cortex. ....	93
Figure 4-23: Inhibition of Oatp4c1-mediated 0.5 $\mu$ M [ <sup>3</sup> H]-E3S uptake by 100 $\mu$ M E3S at 1 min at pH 5.5 and pH 7.4. ....	96
Figure 4-24: Time-dependent Oatp4c1-mediated [ <sup>3</sup> H]-E3S (0.5 $\mu$ M) transport in MDCKII-Oatp4c1 c94 cells at pH 4.5, pH 5.5 and pH 7.4. ....	97
Figure 4-25: Concentration-dependent Oatp4c1-mediated [ <sup>3</sup> H]-E3S transport in MDCKII-Oatp4c1 c94 cells at pH 4.5, pH 5.5 and pH 7.4. ....	100
Figure 4-26: The effect of pH on uptake transport clearance.....	102
Figure 4-27: The relationship between proton concentration and E3S uptake. ....	102
Figure 4-28: Effect of ATP depletion on [ <sup>3</sup> H]-E3S uptake (0.5 $\mu$ M) via Oatp4c1.....	104
Figure 4-29: Effect of putative substrates on [ <sup>3</sup> H]-E3S uptake at pH 5.5 and 7.4. ....	106

Figure 4-30: Time-dependent Oatp4c1-mediated [ <sup>3</sup> H]-MTX (1 μM) transport in MDCKII-Oatp4c1 c94 cells at pH 5.5 and pH 7.4.....	108
Figure 4-31: Effect of putative substrates on [ <sup>3</sup> H]-MTX uptake at pH 5.5 and 7.4. ....	109
Figure 4-32: Validation of SLCO4C1 plasmid constructs.....	112
Figure 4-33: Validation of OATP4C1 expression and subcellular localization in MDCKII-OATP4C1 cells.....	114
Figure 4-34: Concentration-dependent OATP4C1-mediated [ <sup>3</sup> H]-ouabain transport in MDCKII-OATP4C1 cells at pH 7.4. ....	117
Figure 4-35: Concentration-dependent OATP4C1-mediated [ <sup>3</sup> H]-E3S transport in MDCKII-OATP4C1 cells at pH 7.4. ....	118
Figure 4-36: Validation of pDEST8-SLCO4C1 plasmid construct.....	120
Figure 4-37: Validation of OATP4C1 expression in Sf9-OATP4C1 membrane vesicles. ....	120
Figure 4-38: Time-dependent OATP4C1-mediated [ <sup>3</sup> H]-ouabain (0.5 μM) transport in Sf9-OATP4C1 membrane vesicles at pH 7.4.....	122
Figure 4-39: Concentration-dependent OATP4C1-mediated [ <sup>3</sup> H]-ouabain transport in Sf9-OATP4C1 membrane vesicles at pH 7.4.....	122
Figure 4-40: Time-dependent and concentration-dependent OATP4C1-mediated [ <sup>3</sup> H]-E3S transport in Sf9-OATP4C1 membrane vesicles at pH 7.4.....	125
Figure 4-41: Effect of pH on OATP4C1-mediated [ <sup>3</sup> H]-E3S transport in Sf9-OATP4C1 membrane vesicles.....	126
Figure 4-42: Immunohistochemical analysis for OATP4C1 subcellular localization in human kidney sections.....	128
Figure 4-43: Relative <i>SLCO4C1</i> expression in cancer cells calculated with the $2^{-\Delta\Delta Ct}$ method.....	131
Figure 4-44: Relative <i>SLCO4C1</i> expression in lung tumor and adjacent normal lung tissue of 9 patients calculated with the $2^{-\Delta\Delta Ct}$ method.....	132
Figure 4-45: OATP4C1 expression in the lung tumor and adjacent normal lung tissue of 4 patients.....	133

## **CHAPTER 1 : BACKGROUND**

### **A. Drug transporters in lactating mammary epithelium**

Breast milk offers the most complete nutrition for infant growth and development, and breastfeeding is widely advocated because of numerous benefits for infants and mothers. For infants, breastfeeding enhances cognitive development and immune system function, thus decreasing the risk of contracting infectious diseases. For mothers, breastfeeding promotes postpartum recovery, and decreases the risk of osteoporosis and incidences of both breast cancer and ovarian cancer (1, 2). However, maternal medications may pose exposure risks to nursing infants. The limited information regarding drug transfer into the milk makes patients and physicians hesitate when deciding between maternal therapeutic benefit and infant drug exposure risk. A better understanding of the mechanism of drug transfer into the milk will facilitate these therapeutic decisions regarding drug use during lactation.

The mammary gland is the organ that produces milk. It is comprised of epithelium and stroma (mammary fat pad), which is connective tissue. The epithelium consists of ducts and milk production unit, alveoli. Mammary epithelial cells are luminal secretory cells, which undergo extensive proliferation and differentiation during pregnancy and lactation to produce breast milk and secrete it into a central lumen, which opens to the body surface through the nipple. The luminal secretory cells form the barrier between the breast milk and the maternal circulation with an apical surface facing the lumen (milk) and a basolateral surface facing the blood. They are surrounded by basal myoepithelial cells, which are contractile following oxytocin stimuli, and subsequently eject the milk (3, 4).

During lactation, the mammary gland is responsible for delivering essential nutrients, as well as xenobiotics, to suckling infants via breast milk. Many substances



enter into breast milk by passive diffusion, and their exposure risks can therefore be predicted using mathematical models incorporating drug protein binding, ionization, and fat partitioning (5, 6). Nevertheless, some water soluble substances need transporters to efficiently cross the lactating mammary epithelial cells (LMEC). Several adenosine triphosphate (ATP)-binding cassette (ABC) transporters and solute carrier (SLC) have been reported to be expressed on the mammary epithelium. However, to date, only ABCG2 has been demonstrated to be important for drug transfer into the milk.

#### 1. ATP-binding cassette (ABC) transporter superfamily

The ABC transporter superfamily consists of 7 subfamilies categorized A - G, based on membrane topology and sequence homology. ABC transporters consist of a pair of cytoplasmic ATP-binding domains, also known as nucleotide binding domains (NBD), and two sets of transmembrane domains (TMD). The NBD contain three conserved sequences: Walker A and B motifs and a signature C motif. Walker A and B motifs can be found in all ATP-binding proteins, but the C motif is specific to ABC transporters. ABC transporters are organized as either full transporters containing two NBD and TMD or half transporters containing one of each domain. Half transporters assemble as either a homodimer or a heterodimer to be functional. ABC transporters are called primary active efflux transporters because they utilize energy derived from ATP hydrolysis to unidirectionally efflux a wide range of molecules against their concentration gradient (7).

Several ABC transporters have been identified in mammary gland. The prototypical ABC transporter is ABCB1, which is also known as multidrug resistance protein 1 (MDR1) or P-glycoprotein (P-gp). P-gp is a full length transporter with 12 TMD with cytoplasmic N- and C- terminals. P-gp was identified in human mammary gland by immunohistochemistry (8, 9), and mRNA and protein expression appears to be down-regulated during lactation in humans and mice (10, 11).

The ABCC family encodes multidrug resistance-associated proteins (MRPs). Larger MRPs (1, 2, 3, 6 and 7) contain 17 TMD with extracellular N-terminal and intracellular C-terminal. Smaller MRPs (4 and 5) consist of 12 TMD with intracellular N- and C-terminals (12). ABCC1, ABCC2, and ABCC5 mRNA were detected in both LMEC isolated from human breast milk and non-lactating mammary epithelial cells (MEC) isolated from reduction mammoplasty specimens, while ABCC3 and ABCC4 were not detected in either tissues. ABCC1 expression is lower in LMEC relative to MEC at mRNA and protein levels in humans and mice, respectively (10, 11). During lactation, mRNA expression of ABCC2 is not changed, whereas ABCC5 is increased 1.7-fold in LMEC as compared to MEC (11).

ABCG2 (Human: ABCG2; rodent: Abcg2), also known as breast cancer resistance protein (BCRP), is a half-transporter containing only 6 TMD, and forms a homodimer to acquire transport activity. ABCG2/Abcg2 localizes at the apical membrane in mouse, rat, cow, and human lactating mammary tissues. Its expression increases during mammary gland development and achieves highest levels during lactation (10, 13). Several studies using the Abcg2 knockout mouse model have demonstrated that Abcg2 plays an important role in xenobiotics as

well as riboflavin (vitamin B<sub>2</sub>) transfer into the milk (Table 1-1) (14-17). It is interesting to note that milk secretion of riboflavin in Abcg2 knockout mice is reduced 60-fold compared to wild-type mice. This suggests that Abcg2 is involved in nutrient transfer from mother to suckling infant via breast milk (14). In addition, drugs such as nitrofurantoin, cimetidine, acyclovir, and ciprofloxacin, for which milk to plasma ratio cannot be explained by passive diffusion, are shown to be ABCG2/Abcg2 substrates (16-19). This suggests that ABCG2/Abcg2 may be a major factor in facilitating drug transfer into the milk.

**Table 1-1: Milk to plasma AUC ratios for certain drugs in wild-type and Abcg2 knockout (Abcg2<sup>-/-</sup>) mice.**

	Wild-type	Abcg2 <sup>-/-</sup>	Ratio	Reference
Riboflavin	25.0	0.37	67.6	(14)
Nitrofurantoin	45.7	0.6	76.2	(15)
PhIP	12.8	0.5	28.1	(16)
Topotecan	6.7	0.7	10.1	
Cimetidine	13.7	2.3	6.0	
Aflatoxin B1	0.7	0.2	3.8	
IQ	0.9	0.3	3.4	
Acyclovir	1.3	0.4	3.3	
Trp-P-1	1.1	0.4	2.6	
Ciprofloxacin	4.44	2.19	2	(17)

## 2. Solute carrier (SLC) superfamily

The SLC family consists of 52 subfamilies, with over 410 family members (20, 21). SLC family members have varied biochemical properties, including G-protein coupling receptors, voltage gated ion channels, tyrosine kinase receptors, and various transporters for small molecules or organic anions/cations. Among SLC family members, SLC15, 21 and 22 families are relevant for xenobiotics

transport in the mammary gland. Many of these transporters transfer their substrates bidirectionally by facilitated diffusion down a concentration gradient or by secondary active transport coupled with endogenous ions to exchange or cotransport across cell membranes, but are typically considered as uptake transporters.

The peptide transporters (SLC15) contain 12 TMD, a large extracellular loop between TMD 9 and 10, and intracellular N- and C-terminals. Both *SLC15A1* (PEPT1) and *SLC15A2* (PEPT2) transporters have similar substrate selectivity, but PEPT1 is a low-affinity, high-capacity transporter, while PEPT2 is a high-affinity, low-capacity carrier (22). Both PEPT1 and PEPT2 are expressed in LMEC by RT-PCR analysis. During lactation, mRNA expression of *SLC15A1* is downregulated, while *SLC15A2* increased 28-fold in the LMEC as compared to the MEC (11). In situ hybridization analysis showed that *Slc15a2* mRNA localize at the apical side of rat ductal epithelium (23). The apical localization suggests PEPT2/Pept2 may function as a scavenger system to transport the product of milk protein hydrolysis back into the mammary epithelium driven by an inward-directed proton gradient from breast milk (pH 6.8-7.2 (24)). It may also reuptake some peptide-like drugs such as cephalosporins back into the mammary epithelium, thus reducing the burden of the milk. (23).

Organic anion or cation transport is mediated mostly by solute carrier organic anion transporter family (SLCO) (previously SLC21) and SLC22 families. SLCO family encodes for organic anion transporting polypeptides (rodents: Oatps, human: OATPs). They contain 12 TMD with cytoplasmic N- and C-terminals and a large extracellular loop between TMD 9 and 10 (25). SLC22 family includes organic cation transporters (OCT, *SLC22A1-3*), zwitterion/cation

transporters (OCTN, *SLC22A4-5*), and organic anion transporters (OAT, *SLC22A6-20*). They all consist of 12 TMD with cytoplasmic N- and C-terminals, a large extracellular loop between TMD 1 and 2, and a large intracellular loop between TMD 6 and 7 (26). For organic anion transport, OATs transport relatively small organic anions (generally <400 Da) such as PAH, probenecid and fluorescein, while OATPs transport comparably bulky compounds (generally > 500 Da) such as conjugated steroids, bile acids, thyroid hormone, eicosanoids, peptides, cardiac glycosides (digoxin, ouabain), and numerous drugs (27).

OATPs currently comprise six families (OATP1-6), containing 11 human isoforms and 14 rat isoforms. They transport a wide range of amphipathic compounds generally by a bidirectional, sodium-independent, pH-dependent, electroneutral mechanism (28). *SLCO1A2* (OATP1A2, previously: OATP-A), *SLCO2B1* (OATP2B1, previously: OATP-B), *SLCO3A1* (OATP3A1, previously: OATP-D), and *SLCO4A1* (OATP4A1, previously: OATP-E) mRNA were detected in both LMEC and MEC by RT-PCR or Northern blot analysis (11, 29). During lactation, mRNA expression of both *SLCO1A2* and *SLCO2B1* increases about 1.5-fold in LMEC relative to MEC, whereas *SLCO3A1* and *SLCO4A1* are downregulated. Immunohistochemical analysis showed that OATP2B1 localizes in the contractile myoepithelial cells rather than the luminal secretory cells (29). Interestingly, microarray analysis has shown that *SLCO4C1* (OATP4C1) mRNA expression increases 70-fold in LMEC relative to MEC (30). This suggests a potential role of OATP4C1 in drug transfer into breast milk. The characterization of OATP4C1 is discussed in greater detail in the section D.

*SLC22A1* (OCT1) and *SLC22A3* (OCT3), but not *SLC22A2* (OCT2), mRNA were detected in both LMEC and MEC by RT-PCR analysis (11, 31). During

lactation, mRNA expression of *SLC22A1* increases 7.8-fold in LMEC as compared to MEC, whereas *SLC22A3* is downregulated. OCTN1 (*SLC22A4*) and OCTN2 (*SLC22A5*) were both detected in human mammary tissue by Western blotting, and OCTN2 was detected in the ductal-lobular-alveolar structures, as demonstrated by immunohistochemical analysis (32). During lactation, mRNA expression of *SLC22A4* increases about 6-fold in LMEC relative to MEC, whereas *SLC22A5* is downregulated. *SLC22A6* - 8 (OAT1 - 3) were not detected in lactating or non-lactating human and rat mammary tissue (11, 29, 31).

## **B. Renal physiology**

The kidney plays a critical role in maintaining homeostasis in body fluid composition, conserving essential nutrients, and eliminating natural byproducts, toxins, drugs and drug metabolites from the body. A simple diagram of the structure of the kidney is shown in Figure 1-1. Each kidney is covered by an inelastic capsule, which confines the volume of the kidney despite changes in blood pressure. Each kidney comprises two regions: a dark brown outer region named the cortex, and a pale inner region, which is divided into the medulla and the renal pelvis. The medulla consists of 7 to 18 large conical masses (usually 7 in humans) known as the renal pyramids. The broad base of each pyramid faces the cortex and their apex, papilla, is at renal pelvis. The renal pelvis contains the major renal blood vessels and ureter origin.

Each human kidney contains about 1.25 million functional units, which are called nephrons. Each nephron is composed of a renal corpuscle attached to a long thin convoluted tube and its associated blood supply. The renal corpuscle consists of Bowman's capsule and glomerulus which is a capillary tuft that receives the blood

supply from an afferent arteriole of the renal circulation. The proximal tubule arises directly from Bowman's capsule and connects with the descending loop of Henle. The thin descending limb turns and ascends towards the cortex, and connects to the thick segment. The terminal segment of the thick ascending limb of the loop of Henle and the initial part of the distal tubule contact the afferent arteriole close to the glomerulus and form the juxtaglomerular apparatus, which is responsible for regulation of sodium balance. The distal tubules of a number of nephrons merge via connecting tubules to form collecting ducts and pass through the cortex and medulla to the renal pelvis.

These structures are comprised of epithelial cells, which are rich in mitochondria suggesting a major role in active transport. These cells are joined via tight junctions near the apical surface, which is densely covered by microvilli forming a brush border. The brush border (apical) membrane faces the urine, and the basolateral membrane faces the blood. The renal excretory systems consist of three major processes: glomerular filtration, tubular secretion, and tubular reabsorption. The sum of the three processes for a compound undergoing in the nephrons determines its net renal excretion rate. The glomerular blood pressure provides the driving force to filter water and solute out from the blood to Bowman's capsule. About 20% of the renal blood flow undergoes filtration at the glomerulus and passes along to the proximal tubule. Low molecular weight substances which are not bound to plasma protein (e.g., albumin) are more likely to be filtered. The filtered substances, including glucose, amino acids, sodium, chloride, bicarbonate and exogenous substances (e.g.,  $\beta$ -lactam antibiotics), may be reabsorbed from the glomerular filtrate to the blood. The reabsorption is accompanied by an osmotic equivalent of water so that about two-thirds of the filtered fluid has been reabsorbed by the end of the proximal tubule. In addition to reabsorbing solutes, the proximal tubule actively



secretes some organic anions and cations into the lumen. The homeostasis of endogenous and exogenous substances is achieved by tubular secretion and reabsorption, which are mediated by multiple transporters localized at both sides of the plasma membranes, mainly in the proximal tubular cells. Tubular secretion and reabsorption can occur as a facilitated transport to transfer substances down a concentration gradient or as an active transport requiring energy to move substances against a concentration gradient (33, 34).

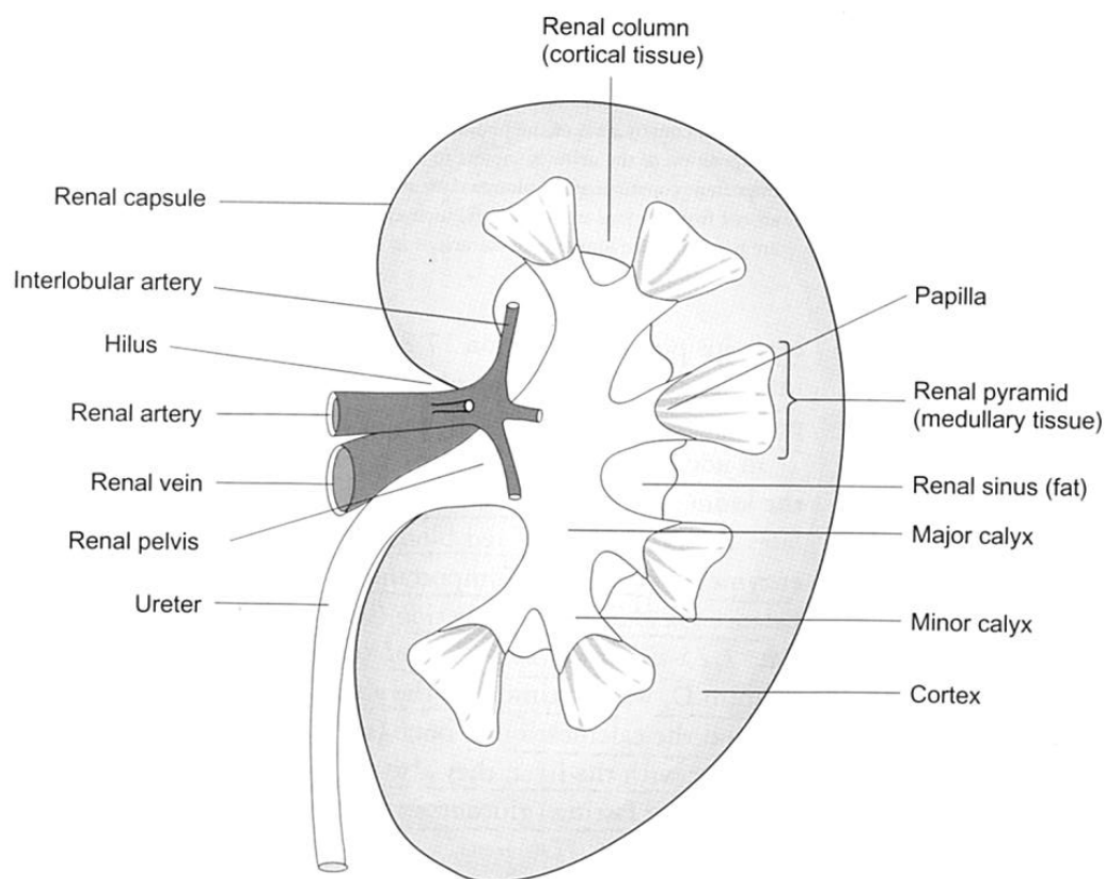


**Figure 1-1: Cross-sectional view of the kidney (34).**

### **C. Drug transporters in the kidney**

The kidney is responsible for homeostasis of endogenous and exogenous substances through tubular secretion and reabsorption. Many of the urinary-eliminated drugs and metabolites are water soluble and cannot easily cross the lipid bilayer of cell membranes. Transporters are needed for selective and efficient transport in renal tubular cells, including the ABC and SLC transporters (Figure 1-2). Several studies have demonstrated that overlapping substrate specificity among uptake and efflux transporters is likely to accelerate the translocation of endogenous and exogenous substances across epithelial or endothelial barriers, and this process is often called vectorial transport (35, 36). Thus, it is important to obtain detailed knowledge regarding transporters expressed in the kidney and their substrates to better understand renal tubular secretion and reabsorption of drugs and/or their metabolites. In the long term, such information will be important in predicting renal drug excretion and transporter-mediated drug-drug interactions. The detailed information of ABC transporter superfamily and SLC superfamily expressed in the kidney is described below.

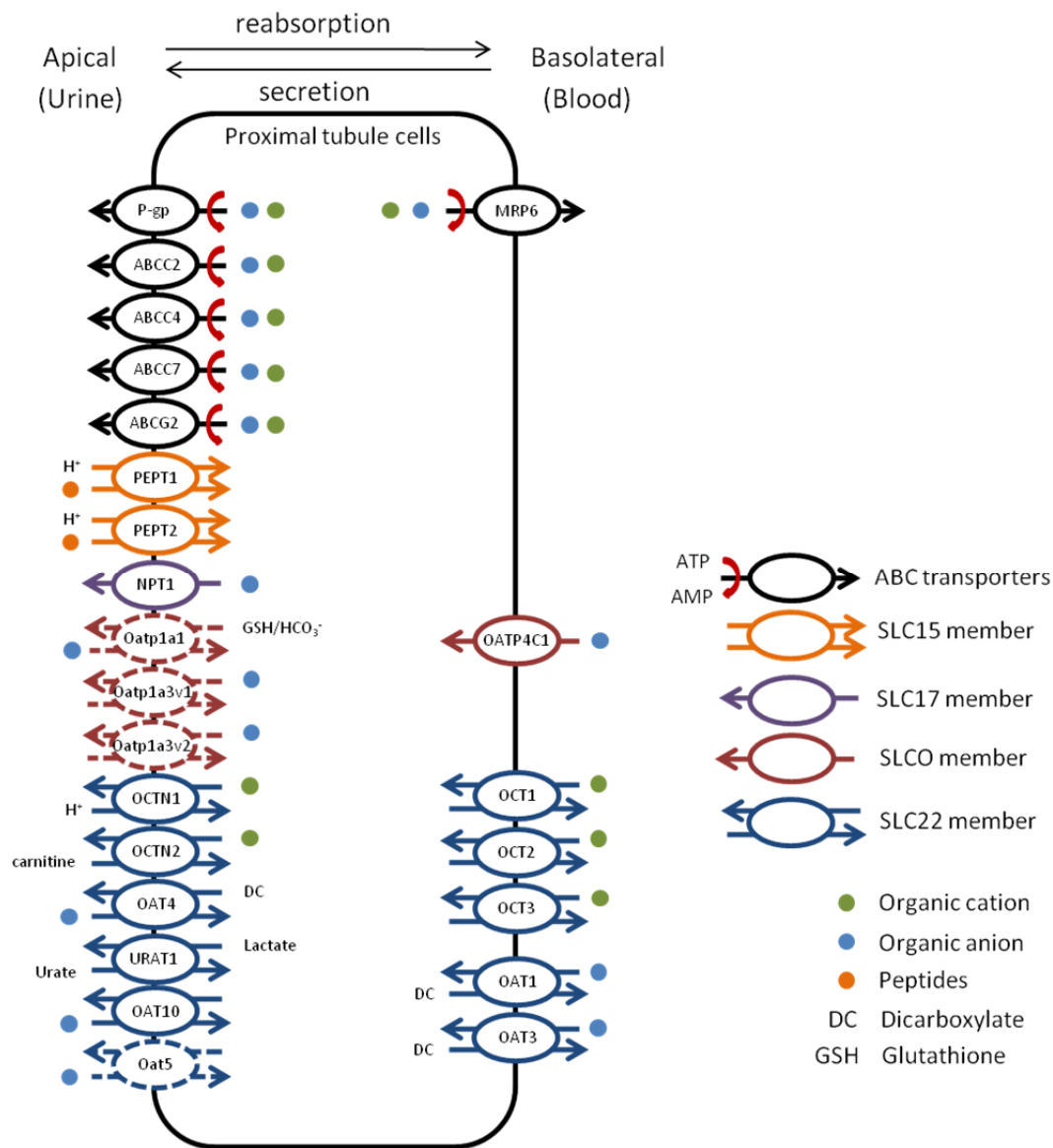


**Figure 1-2: ABC and SLC transporters in proximal tubular cells (adapted from literature (37-39)).**

### 1. ABC transporters

Among ABC transporters, ABCB1, ABCC1-6 and ABCG2 are relevant for xenobiotic transport in the kidney. Because of unidirectional transport, function of ABC transporters in the kidney is determined by their subcellular localization. The

apical transporters are responsible for renal tubular secretion, while the basolateral transporters are important in renal tubular reabsorption.

ABCB1 is expressed at the apical membrane in proximal tubules (40). It plays an important role in tubular secretion of digoxin, and may be responsible for clinically important drug-drug interactions, such as digoxin-quinidine or digoxin-verapamil (41).

ABCC1 localizes at the basolateral membranes of the limb of Henle, distal tubules and collecting ducts, but not proximal tubules in mouse kidney (42). ABCC1 along with an apical uptake transporter may facilitate the tubular reabsorption of substances from fluids in the distal tubules. ABCC1 substrates include a variety of physiological substances such as glutathione, glucuronide and sulfate conjugates as well as xenobiotics, such as methotrexate (MTX), doxorubicin, topotecan and vinblastine (12).

ABCC2 is expressed apically in proximal tubules (43, 44) and plays an important role in tubular secretion of its substrates. ABCC2 shares considerable substrate specificity with ABCC1, but has a distinct function in the body because of different subcellular localization (12). In a patient with a heterozygous ABCC2 mutation, nephrotoxicity was reported due to reduced MTX elimination (45).

ABCC3 localizes at the basolateral membranes in rat distal tubules, thick ascending loop of Henle, and in human proximal tubules (46, 47). ABCC3 may be involved in tubular reabsorption of its substrates, which are similar to ABCC1 (12).

ABCC4 localizes at the apical membrane of renal proximal tubules (48, 49). Studies in Abcc4 knockout mice revealed the importance of this protein in the

tubular secretion of various drugs, such as antivirals (adefovir, tenofovir), diuretics (hydrochlorothiazide, furosemide) and cephalosporin antibiotics (50). ABCC4 may also facilitate the tubular secretion of other substrates, such as cyclic nucleotides, MTX, topotecan, prostaglandins, urate, para-aminohippurate (PAH) and several anionic conjugates (50).

ABCC5 is expressed in the kidney (51, 52), but the localization in the kidney has not been determined yet. Nevertheless, ABCC5 polarizes to basolateral membrane when stably transfected in MDCKII cells, and mediates the transport of nucleotide analogues, such as adefovir, mercaptopurine, thioguanine, cyclic adenosine monophosphate (cAMP) and cyclic guanosine monophosphate (cGMP) (53, 54). The role of ABCC5 in the kidney remains to be investigated.

ABCC6 is highly expressed in kidney and liver and is localized at the basolateral membrane in the proximal tubules (55, 56). It has a limited substrate specificity, which includes the endothelin receptor antagonist BQ123 (cyclo [Trp-Asp-Pro-Val-Leu]), S-(dinitrophenyl)-glutathione and leukotriene C<sub>4</sub>. Its role in renal elimination of its substrates remains to be clarified.

ABCG2 is expressed at the apical membrane in proximal tubules (57, 58). The apical localization suggests its role in facilitating the elimination of its substrates into the urine. ABCG2 transports a wide range of substrates, including uncharged or amphiphilic compounds, particularly anticancer drugs, such as topotecan, MTX, doxorubicin (12).

## 2. SLC transporters

Among SLC family members, SLC15, 17, 21 and 22 families are relevant for xenobiotics transport in the kidney. These transporters are typically considered as uptake transporters. Therefore, the apical SLC transporters are mostly responsible for renal tubular reabsorption, while the basolateral SLC transporters are important in renal tubular secretion.

Pept1 and Pept2 localize at the apical membrane in the S1 segments and S2/S3 segments in the rat proximal tubules, respectively (59). They are proton oligopeptide cotransporters and mediate the renal reabsorption of small anionic peptides and various peptide-like drugs, such as the  $\beta$ -lactam antibiotic cephalosporin (22).

Sodium-dependent phosphate cotransporter 1 (NPT1) (SLC17A1) belongs to type I phosphate/vesicular glutamate transporters (SLC17) containing at least 6 (perhaps 8) TMD (60). It localizes at the apical membrane in all segments of rabbit renal proximal tubules (61), and handles the tubular secretion of urate, PAH and various anionic drugs (62).

Among OATPs, only Oatp1a1, Oatp1a3v1, Oatp1a3v2, Oatp1a5, Oatp2a1, OATP1A2 and Oatp4c1/OATP4C1 have been detected in rodents/human kidney. Oatp1a1 (previously: Oatp1, Oatp) is expressed at the apical membrane of the proximal tubule S3 segment in the outer medulla (63). Oatp1a1 has broad substrate specificity, including anionic, cationic, and neutral compounds. It is expressed predominantly in males and its expression has been related to the longer half-life of perfluorocarboxylates (PFO) as compared to female rats, which indicates an important role in renal reabsorption of PFO (64). The transport mechanisms of Oatp1a1 have been proposed as solute/HCO<sup>3-</sup> exchange and

solute/GSH exchange (65, 66). OATP1A2 (previously: OATP-A) localizes at the apical membrane in human distal tubules (67) and probably participates in the saturable reabsorption of MTX (68). Oatp1a3v1 (previously: OAT-K1) and Oatp1a3v2 (previously: OAT-K2) are expressed exclusively in the kidney (69). Oatp1a3v1 was detected in the brush-border membranes isolated from rat kidney by Western blotting. In addition, both Oatp1a3v1 and Oatp1a3v2 showed a functionally apical uptake or efflux in cell systems (70-72), which suggests that they function as bidirectional organic anion transporters at the apical membrane. Oatp1a3v1 and Oatp1a3v2 have also been implicated as the major excretory route of MTX and may be responsible for the folinic acid rescue for high-dose MTX treatment of acute lymphocytic leukemia by exchanging extracellular folinic acid for intracellular MTX (73, 74). Oatp1a5 (previously: Oatp3) mRNA is highly expressed in rat kidney (75), but its localization has not been determined yet. Endogenous or exogenous substances (e.g., thyroid hormones, E3S, fexofenadine, digoxin) have been reported to interact with rat Oatp1a5 (76, 77), but the role of Oatp1a5 in renal drug elimination remains to be clarified. Oatp2a1 (previously: PGT) localizes at the apical surface of rat collecting ducts, glomerular endothelial and mesangial cells and is responsible for renal reabsorption of prostanoids (78). OATP4C1/Oatp4c1 (previously: OATP-H) was reported to be expressed at the basolateral membrane of the proximal tubules (79). The expression and functional characterization of OATP4C1 is discussed in greater detail in section D.

Oct1, Oct2 and Oct3 all localize at basolateral membrane of rat proximal tubules (80-82). Oct1 is mainly expressed in S1/S2 segments of rat proximal tubules. Oct2 is predominantly expressed in S2/S3 segments of rat proximal tubules, and in all segments of human proximal tubules. OCTs are facilitative and

bidirectional diffusion transporters mediating electrogenic and Na<sup>+</sup>-independent flux of small organic cations with a molecular weight up to about 400-500 Da (83). The transport direction is determined by concentration gradients and the electrical potential across the membrane. OCT1, OCT2 and OCT3 have a broad overlap of substrate and inhibitor specificities. OCTs mediate the renal excretion of neurotransmitters dopamine, epinephrine, and many organic cation drugs such as desipramine, metformin, cimetidine and cisplatin. OCTs also mediate the renal reabsorption of choline (26).

OCTN1 and OCTN2 are strongly expressed at the apical membranes of proximal tubules (84, 85). OCTN1 is a bidirectional proton/organic cation antiporter (86, 87), whereas OCTN2 may function as a unidirectional sodium/L-carnitine cotransporter or a bidirectional sodium-independent organic cation transporter (88, 89). OCTN1 and OCTN2 mediate the renal secretion of organic cations, such as verapamil, choline, whereas OCTN2 can also mediate the reabsorption of L-carnitine following exchange with cationic compounds (26).

OATs are organic anion/dicarboxylate (favorably  $\alpha$ -ketoglutarate) exchangers. OAT1 is predominantly expressed in the kidney (90). It localizes at the basolateral membrane in S2 segment of rat proximal tubules and all segments of human proximal tubules (82, 91). OAT2 is highly expressed in the liver and to a lesser extent in the kidney (90). Its localization in the kidney is controversial. It was detected at the basolateral membrane of human proximal tubules (92), but it has also been reported at the apical surface of rat medullary thick ascending limb of Henle's loop and the collecting ducts (91) or proximal tubule S3 segments (93). Therefore, the role of OAT2 in kidney is still unclear. OAT3 is exclusively expressed in the kidney and its mRNA expression is considerably higher than OAT1 in human kidney (82). OAT3 is expressed at the



basolateral membrane in all segments of rat or human proximal tubules (82, 91, 94). OAT1 and OAT3 mediate the first step of renal tubular excretion of their substrates. They have wide overlapping substrate specificities, including endogenous substrates such as PAH, cyclic nucleotides, prostaglandins, urate, uremic toxins, as well as anionic drugs, such as  $\beta$ -lactam antibiotics, non-steroidal anti-inflammatory drugs (NSAIDs), antiviral drugs, antidiabetic and anticancer drugs. In addition, OAT1 has a larger contribution to low-molecular weight drugs, whereas OAT3 transports more bulky amphipathic anions, such as hepatic hydroxymethylglutaryl –Coenzyme A (HMG-CoA) reductase inhibitors (statins), and even some cationic drugs, including H<sub>2</sub> receptor antagonists (95). OAT4 is highly expressed in the kidney and to a lesser extent in the placenta. It localizes at the apical membrane of the proximal tubules (96, 97), and is involved in renal reabsorption of organic anions, such as E3S, MTX and PAH, driven by an outwardly directed dicarboxylate gradient (84, 98). Urate transporter 1 (URAT1) is mainly expressed in the kidney, and is localized at the apical membrane of proximal tubules (99, 100). OAT4 and URAT1 are urate anion exchangers that play a key role in urate homeostasis via a renal reabsorption mechanism. OAT10 is predominantly expressed in human kidney, and was exclusively detected in the brush-border membrane isolated from the rat kidney. It is responsible for renal reabsorption of nicotinate and urate (101). Oat5 expression is restricted to the kidney, and is localized at the apical membrane in the S2/S3 segment of mouse and rat proximal tubules. It may be involved in renal reabsorption of E3S (102, 103).

#### **D. OATP4C1 (Human: OATP4C1; rodent: Oatp4c1)**

OATP4C1 (*SLCO4C1*) was first isolated from human kidney in 2004 (79). It was initially called OATP-H and renamed as OATP4C1 according to the HUGO Gene Nomenclature Committee (28). It is located on chromosome 5q21, and is about 62 kb long including 13 exons and 12 introns. It consists of 724 amino acids, and the predicted molecular weight is 79 kDa. OATP4C1 was predicted to contain 12 TMD with intracellular N- and C-terminals, by hydrophobicity analysis. There are four putative N-glycosylation sites in the predicted extracellular loop and five potential phosphorylation sites in the intracellular portions. Interestingly, the intracellular loop between TMD 6 and 7 of human OATP4C1 and rat Oatp4c1 contain two and one, respectively, potential ATP binding sites characteristic of the Walker A motif found in ABC transporters but not in other OATP family proteins. The overall homology between human and rat Oatp4c1 is 80.4% at the amino acid level.

Microarray expression studies show that human *SLCO4C1* mRNA is highly expressed in the kidney, neutrophils, liver, moderately in mammary gland, and slightly in lung, skin, peripheral leukocytes and mononuclear cells (104). Rat *Slco4c1* is detected mainly in the kidney and lung, and slightly in the brain by Northern analysis (79), while mouse *Slco4c1* is detected in the kidney and lung by bDNA assay (105). There is no gender difference of *Slco4c1* expression in the rat kidney, but higher *Slco4c1* expression was observed in male mouse kidney as compared to females (79, 105). In addition, *Slco4c1* expression in kidney increases with age in mice(105). RT-PCR from microdissected rat nephron segments showed that rat *Slco4c1* is detected mainly in the proximal convoluted tubule, proximal straight tubule, and slightly in the glomerulus, cortical thick ascending limb and cortical collecting duct. Immunohistochemical analyses has shown that Oatp4c1 localizes at

the basolateral membrane in the rat proximal tubules (79) as well as human OATP4C1 in the transgenic rat harboring human *SLCO4C1* (106). In the 5/6 nephrectomized renal failure model, *Slco4c1* expression was significantly decreased by Northern blot analysis. This may be related to the changes of pharmacokinetics of its substrates in renal failure. Interestingly, microarray analysis showed that *SLCO4C1* is highly expressed in lung tumors and its mRNA expression is 18-fold higher than that in the normal human lung (104). This suggests a potential vital role of OATP4C1 in lung cancer. *SLCO4C1* was also detected in several cancer cell lines, including renal carcinoma cells (ACHN, SN12C), ovarian cancer cells (OVCAR-8, OVCAR-3), leukemia cells (HL-60, RPMI-8226, CCRF-CEM), lung cancer cells (H322M, H23, HOP-62, H460), glioblastoma (SF-539) and breast cancer cells (BT-549) (107).

A promoter analysis showed that *SLCO4C1* promoter region has xenobiotic-responsive element (XRE) motifs, which are generally recognized by aryl hydrocarbon receptors (AhR) and AhR nuclear translocator heterodimer (108). The promoter activities are enhanced by nuclear AhR inducers, 3-methylcholanthrene and HMG-CoA reductase inhibitors (pravastatin, fluvastatin, simvastatin, lovastatin, cerivastatin, itavastatin, mevastatin, atorvastatin, rosuvastatin and pitavastatin). Following pravastatin treatment in ACHN cells, *SLCO4C1* mRNA expression is upregulated 1.73-fold, and uptake of an OATP4C1 substrate, triiodothyronine ( $T_3$ ), is increased 1.4-fold (106).

The reported substrates of OATP4C1 include cardiac glycosides [digoxin ( $K_m$  7.8  $\mu M$ ) and ouabain ( $K_m$  0.38  $\mu M$ )], thyroid hormones [ $T_3$  ( $K_m$  5.9  $\mu M$ ) and thyroxine ( $T_4$ )], cAMP, MTX (79), sitagliptin (109), and E3S (110). The transport direction appears to be unidirectional uptake from outside to inside (79), but the

driving force has not been elucidated. Sodium, chloride, and pH did not affect OATP4C1-mediated uptake, while ATP depletion partially inhibits T<sub>3</sub> uptake to 40% (79). However, Leuthold et al. demonstrated that OATP4C1-mediated E3S or T<sub>4</sub> uptake is significantly higher at extracellular pH 6.5 than pH 8.0 (111). In addition, OATP4C1 has been suggested to possess multiple substrate recognition sites, because digoxin does not inhibit OATP4C1-mediated T<sub>3</sub> (79) or E3S (110) uptake and vice versa, while E3S and T<sub>3</sub> have mutual inhibition.

Furthermore, the physiological role of OATP4C1, reportedly a basolateral uptake transporter, has been postulated to couple with P-glycoprotein, an apical efflux transporter, to facilitate the renal clearance of common substrates, such as digoxin (79) and uremic toxins (106). In studies with transgenic rats harboring human *SLCO4C1*, the hypertension and renal inflammation were ameliorated in renal failure models. The decreased plasma concentrations of uremic toxins (guanidino succinate, asymmetric dimethylarginine, and *trans*-aconitate) suggest that OATP4C1 may facilitate the excretion of uremic toxins in renal failure models and, by extension, in patients with chronic kidney disease. The enhancement of the uremic toxins excretion and the amelioration of end-organ damage were also observed by pravastatin-induced *Slco4c1* up-regulation in rat renal failure models (106). However, direct evidence that these toxins are OATP4C1 substrates is lacking.

## **E. Summary**

The well documented benefits of breastfeeding and the limited data regarding drug transfer into breast milk, make it difficult for patients and their doctors to weigh the benefits and risks between maternal treatment and infant drug exposure. For

most of the drugs that have been studied, the exposure risks can be predicted by passive diffusion using mathematical models that incorporate easily measured parameters such as drug protein binding, ionization, and fat partitioning. However, several reports showed that certain drugs accumulate in breast milk at substantially higher levels than predicted by passive diffusion and in particular, drugs that are substrates for xenobiotic transporters. A comprehensive microarray analysis was performed to measure the expression of 55 xenobiotic transporter genes in LMEC isolated from human breast milk and MEC isolated from reduction mammoplasty specimens and to identify the genes that are upregulated during lactation (30). In accord with a previous study (10), ABCG2 expression was upregulated during lactation by 164-fold in LMEC relative to MEC. A novel finding showed a 70-fold increase of *SLCO4C1* expression in LMEC as compared to MEC, suggesting a potential role in drug transfer into the milk.

Human OATP4C1 and rat Oatp4c1 have been demonstrated to localize at the basolateral membrane in the kidney (79, 106). Therefore, we hypothesized that OATP4C1/Oatp4c1 localizes at the basolateral membrane in the mammary gland and couples with ABCG2/Abcg2, an apical efflux transporter, to facilitate the transfer of common substrates into breast milk. To study the role of Oatp4c1 in drug disposition, we sought to generate stably transfected cell lines expressing rat Oatp4c1. Initial attempts to generate Oatp4c1-expressing MDCKII cells produced unexpected results as the transporter localized at the apical rather than the basolateral membranes.

This dissertation work aims to validate the subcellular localization of OATP4C1/Oatp4c1 in the *in vitro* models and in human/rat tissues and to explore their transport characteristics. We used a comprehensive approach, including multiple antibodies amenable to immunohistochemistry, immunofluorescence, and

immunoblotting to probe the expression of Oatp4c1 in intact tissues and cells as well as biochemically separated and enriched apical and basolateral membranes isolated from polarized cells and rat renal proximal tubules. Furthermore, proteomic analysis was used to qualitatively validate the specificity of these antibodies. Functional activity of Oatp4c1 in MDCKII-Oatp4c1 was probed with E3S and MTX. The expression and subcellular localization of human OATP4C1 in the *in vitro* model, human kidney, lung tumor specimens and cancer cells were also examined. Functional activity of OATP4C1 in MDCKII-OATP4C1 and Sf9-OATP4C1 was probed with ouabain and E3S.

## CHAPTER 2 : PLAN OF WORK

**Hypothesis 1:** Oatp4c1 is upregulated in mammary gland during lactation. It functions as a basolateral uptake transporter, and couples with apically-expressed efflux transporter Abcg2 to facilitate the transfer of common substrates into the milk.

Specific Aim 1a: To develop and validate rat Oatp4c1 antibodies amenable for immunoblotting, immunohistochemistry and immunofluorescence.

Specific Aim 1b: To create and validate a stably transfected rat Oatp4c1-expressing cell line with appropriate characteristics for uptake studies.

Specific Aim 1c: To determine the expression and subcellular localization of Oatp4c1 in rat tissues (liver, kidney, lactating and non-lactating mammary gland).

To explore the xenobiotic transporters responsible for drug transport into the milk, a microarray study was performed by Dr. Philip Empey and showed a 70-fold increase of *SLCO4C1* mRNA expression in human lactating mammary epithelial cells relative to non-lactating mammary epithelial cells (30). The upregulation of *SLCO4C1* expression during lactation suggested a potential role of OATP4C1 in drug transfer into the milk. To determine the subcellular localization of Oatp4c1 in mammary epithelium, rat Oatp4c1 antibodies will be developed in Specific Aim 1a. The antibody specificities will be validated using a stably transfected rat Oatp4c1-expressing cell line established in Specific Aim 1b by Western blotting, immunohistochemistry and immunofluorescence. To investigate the role of Oatp4c1 in drug disposition, a single clone with the highest Oatp4c1 expression will be obtained and will be used in Specific Aim 3a and 3b. Specific Aim 1c will investigate the expression and subcellular localization of Oatp4c1 in rat liver, kidney, lactating and non-lactating mammary gland by Western blotting and immunochemical analysis.

**Hypothesis 2:** Oatp4c1 localizes at the apical membrane in the rat kidney cortex.

Specific Aim 2a: To verify the apical localization of Oatp4c1 in the rat kidney cortex by proteomic analysis in the isolated brush-border membrane (BBM) and basolateral membrane (BLM).

Specific Aim 2b: To determine the precise expression pattern of Oatp4c1 at the organ and nephron level.

A previous study reported that Oatp4c1 localizes to the basolateral membrane in the rat kidney cortex (79). However, results from Specific Aim 1c showed that Oatp4c1 localizes at the apical membrane of polarized epithelial cells grown *in vitro*. In Specific Aim 2a we will isolate BBM and BLM from rat kidney cortex to elucidate these contradictory results. The proteins in BBM and BLM preparations will be analyzed by Western blotting and LC-MS/MS to validate the localization of Oatp4c1 in rat kidney. Specific Aim 2b will determine the precise location of Oatp4c1 at the organ and nephron level by double immunofluorescence with proximal tubule marker or distal tubule marker. Double immunofluorescence staining will also be used to access the location of Oatp4c1 relative to major apical efflux transporters in the rat kidney.

**Hypothesis 3:** Oatp4c1 functions as an uptake transporter involved in renal tubular reabsorption. The *in vitro* cell systems can be used to identify potential substrates and explore the physiological role of Oatp4c1.

Specific Aim 3a: To investigate Oatp4c1 transport characteristics and driving force.



Specific Aim 3b: To identify potential Oatp4c1 substrates.

The kidney is responsible for homeostasis of endogenous and exogenous substances through tubular secretion and reabsorption, which in part is mediated by various membrane transporters, including those in the SLC superfamily. The results from Specific Aim 1c showed that Oatp4c1 localizes at the apical membrane in rat kidney inner cortex, suggesting a potential role in renal reabsorption of its substrates. To have a better understanding of the physiological role of Oatp4c1, its substrates and transport characteristics will be explored. In Specific Aim 3a we will verify E3S, a human OATP4C1 substrate (110, 111), as a rat Oatp4c1 substrate and will investigate the transport kinetic and driving force of Oatp4c1-mediated E3S transport using the Oatp4c1-expressing cells developed in Specific Aim 1a. In Specific Aim 3b we will determine the interaction of Oatp4c1 with potential physiological substrates by studying their capacity to inhibit transport of E3S.

**Hypothesis 4:** OATP4C1 is localized at the apical membrane in the *in vitro* cell systems and human kidney, and is highly expressed in lung cancer. The *in vitro* cell systems can be used to study the role of OATP4C1 in drug disposition.

Specific Aim 4a: To develop and validate human OATP4C1 antibodies amenable for immunoblotting, immunohistochemistry and immunofluorescence.

Specific Aim 4b: To create and validate human OATP4C1-expressing cells with appropriate characteristics for functional studies.

Specific Aim 4c: To determine the expression and subcellular localization of OATP4C1 in the human kidney.

Specific Aim 4d: To determine the expression of OATP4C1 in cancer cells.

The subcellular localization of membrane transporters determines their physiological function. The novel finding of the apical localization of rat Oatp4c1 in this project suggests its physiological role is tubular reabsorption not tubular secretion. To validate the subcellular localization of OATP4C1 in human kidney, human OATP4C1 antibodies will be developed in Specific 4a. The antibody specificities will be validated in a stably transfected OATP4C1-expressing cell line established in Specific Aim 4b by Western blotting, immunohistochemistry and immunofluorescence. The functional activity of OATP4C1 in the transfected cell line will also be validated using ouabain and E3S as substrates in uptake studies. OATP4C1 will also be overexpressed in insect cells for substrate screening and its functional activity will be probed with ouabain and E3S. In Specific Aim 4c we will determine the subcellular localization of OATP4C1 in human kidney. In Specific Aim 4d we will examine *SLCO4C1*/OATP4C1 expression in several cancer cell lines, lung tumor and adjacent normal lung tissue sections.

## CHAPTER 3 : MATERIALS AND METHODS

### A. Materials

Madin-Darby canine kidney II (MDCKII) cells were purchased from European Collection of Cell Cultures (Salisbury, UK). LLC-PK1 cells (porcine kidney proximal tubule epithelial cells) were purchased from American Type Culture Collection (ATCC, Manassas, VA).

Transwells #3414, and snapwells #3407 were obtained from Corning Costar (Cambridge, MA). All cell culture media were purchased from Mediatech (Manassas, VA). Fetal bovine serum was from Atlanta Biologicals (Lawrenceville, GA). Penicillin-streptomycin, blasticidin, geneticin were obtained from Invitrogen (Carlsbad, CA).

RNeasy Kit, Qiashredder columns, RNase-free DNase set, and QIAprep Spin Miniprep Kit were obtained from Qiagen (Valencia, CA). ThermoScript™ RT-PCR kit, LR Clonase™ II Enzyme Mix, Tag-On-Demand™ Suppressor System and ethidium bromide were purchased from Invitrogen. RecoverALL™ Total nucleic acid isolation kit was from Invitrogen Ambion. XL1-Blue Supercompetent cell was from Stratagene (Santa Clara, CA). Zymoclean™ Gel DNA Recovery kit was from Zymo Research (Irvine, CA). Phusion High-Fidelity PCR kit, restriction enzymes (KpnI, SspI, EcoRV, Sall), and PNGase F were purchased from New England Biolabs (Ipswich, MA). The SYBR® Green PCR Core Reagents kit was obtained from Applied Biosystems (Foster City, CA). All primers were purchased from Integrated DNA Technologies (Coralville, IA). Fluorescein calibration dye was obtained from Bio-Rad (Hercules, CA). Sea-Kem LE agarose was from Cambrex (Rockland, ME). FuGENE 6 transfection reagent and Complete Mini EDTA-free protease inhibitor

tablets were obtained from Roche Diagnostics (Indianapolis, IN). Sodium butyrate was from Sigma-Aldrich (St. Louis, MO).

LDS sample buffer, Magic Mark™ XP protein ladder, Prolong Gold antifade reagent containing DAPI were purchased from Invitrogen. Polyvinylidene difluoride membrane was from Millipore (Billerica, MA). HistoGel™ was obtained from Thermo Scientific. Richard-Allan Scientific (Kalamazoo, MI). Sulfo-NHS-SS-Biotin, streptavidin agarose beads, BCA Protein Assay kit and Supersignal West Pico chemiluminescent kit were obtained from Thermo Scientific Pierce (Rockford, IL). Avidin/biotin blocking kit, normal goat serum, NovaRED kit, hematoxylin, and Vecta Mount were purchased from Vector Laboratories (Burlingame, CA). Streptavidin-HRP reagent was from Dako (Carpinteria, CA).

Rat monoclonal antibody against E-cadherin (DECMA-1), mouse monoclonal antibodies against calbindin-D<sub>28k</sub> (CB-955) and aquaporin 1 (1/22) were obtained from Abcam (Cambridge, MA). Mouse monoclonal antibody against Zo-1 (zo1-1A12), Alexa Fluor® 488 goat anti-mouse IgG (H+L) and Alexa Fluor® 568 goat anti-rabbit IgG (H+L), Alexa Fluor® 488 goat anti-rabbit IgG (H+L), and Alexa Fluor® 568 goat anti-rat IgG (H+L) were from Invitrogen. Mouse monoclonal antibody against  $\beta$ -actin (AC-15) was from Sigma-Aldrich. Mouse monoclonal antibody against P-gp (C219) was from Signet (Dedham, MA). Mouse monoclonal antibody against human BCRP (BXP-21), rat monoclonal antibody against rat Abcg2 (BXP-53) and Mrp4 (M<sub>4</sub>I-10) were from Kamiya (Seattle, WA). Rabbit polyclonal antibody against Na<sup>+</sup>/K<sup>+</sup>-ATPase (#3010) was obtained from Cell Signaling (Danvers, MA). HRP-conjugated goat anti-mouse IgG (H+L), HRP-conjugated goat anti-rabbit IgG (H+L), HRP-conjugated goat anti-rat IgG (H+L) were purchased from Thermo Scientific Pierce (Rockford, IL).

[<sup>3</sup>H]-E3S (45.6 Ci/mmol) was purchased from Perkin Elmer (Waltham, MA) and [<sup>3</sup>H]-MTX (40 Ci/mmol) from American Radiolabeled Chemicals (St. Louis, MO). Bio-safe<sup>®</sup> II scintillation cocktail was obtained from Research Products International (Mount Prospect, IL). GF120918 was a gift from GlaxoSmithKline (Research Triangle Park, NC). Hoechst 33342 was obtained from Invitrogen. OE67 membrane filters were from Millipore Corporation (Bedford, MA). RC55 membrane filters were from Schleicher and Schuell (Keene, NJ).

## **B. Creation and validation of a rat Oatp4c1-expressing cell line**

### **1. Development of rat Oatp4c1 antibody**

Rabbit polyclonal antibodies against rat Oatp4c1 were generated using an extracellular loop [SPDFEARAGKC (PA1556) (79)], two amino-terminus [KGVENPAFVPSSPDTPRR (PA1254); QPRESED PQKSTEPS (F3608)], and two carboxyl-terminus [STITVEEDLNKIENEG (PA1343); TVEEDLNKIENEG (PA1562)] sequence peptides (Figure 3-1). The antigen sequence specificities were confirmed with NCBI's BLAST. The antigen preparation, immunization and serum collection were performed by Open Biosystems (Rockford, IL). The rabbits were immunized with 0.5 mg of antigen on Day 1 and boosted with 0.25 mg of antigen on Days 14, 28 and 42. The terminal sera were collected on Day 90. The antibody specificities were validated by Western blotting, immunohistochemical analysis and immunofluorescence as described in Section B-8, Section B-9 and Section B-10. PA1343 was affinity-purified.

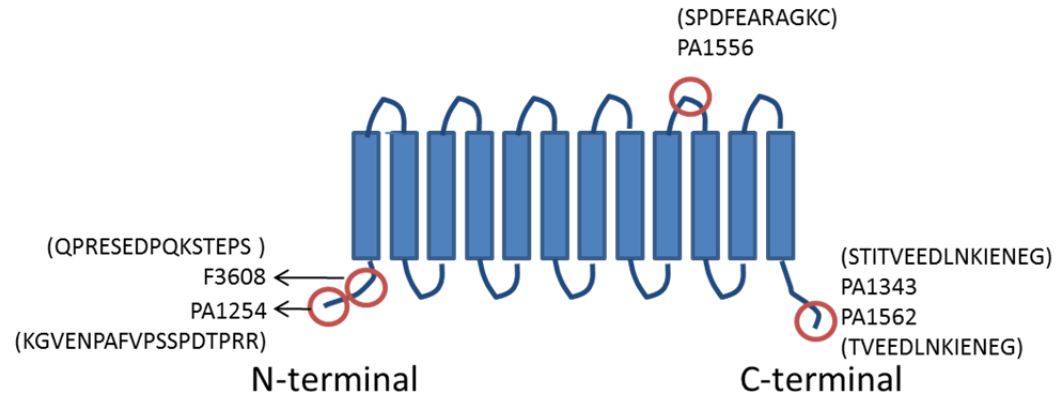


**Figure 3-1: Rat Oatp4c1 antibody antigen peptide sequence and location.**

## 2. Construction of plasmid vector

Total RNA was isolated from a frozen kidney of a Sprague-Dawley rat using RNeasy Kit as directed by the manufacture with sample disruption using Qiashredder and on-column DNA digestion. Total RNA concentration was determined by the measurement of optical density at 260 nm with a UV-Vis Spectrophotometer (ND-1000, NanoDrop, Wilmington, DE). Total RNA quality was verified by an OD260/OD280 absorption ratio greater than 2.0. Reverse-transcription of 1 µg RNA to cDNA was performed with reverse ThermoScript™ RT-PCR kit with oligo (dT)<sub>20</sub> primers using Peltier Thermal Cycler (Waltham, MA). Rat Slco4c1 cDNA was amplified using Phusion High-Fidelity PCR kit with forward (5'-CACCATGCAGGGTTCCAAGGGAG-3') and reverse (5'-CTATCCTTCGTTCTCTATTTTGTG-3') primers. The amplification protocol included an initial denaturation (98 °C for 1 min) followed by 40 cycles of a denaturation step (98 °C for 10 sec), an annealing step (64 °C for 30 sec) and an extension step (72 °C for 35 sec), and a final extension step (72 °C for 10 min).

To confirm the amplified fragment was of appropriate size, amplification products were separated by 0.8% agarose gel electrophoresis in 1 x TBE running buffer (89 mM Tris-Borate, 2 mM EDTA, pH 8.0) for 1 hr at 80 V. The gel was visualized by staining with 0.5 µg/ml ethidium bromide, and imaged on an Image Station 2000 MM (Eastman Kodak, New Haven, CT). The single band at appropriate size was cut from the gel on a UV lamp transilluminator (Fisher Scientific, Pittsburgh, PA) and purified using Zymoclean™ Gel DNA Recovery kit following the manufacturer's protocol. The subsequent sequence (*Slco4c1*) was cloned into the vector pENTR using pENTR Directional TOPO Cloning kit and the construct was transformed into competent One Shot TOP10 *E. coli*. The competent cells were grown in an agar plate with 50 µg/ml kanamycin. The plasmid DNA was isolated from positive transformants using QIAprep Spin Miniprep Kit according to the manufacturer's protocol. The plasmid construct (500 ng) was validated by EcoRV, Sall or KpnI restriction enzyme digestion for 2 hr at 37°C and 0.8% agarose gel electrophoresis. The sequence was confirmed (Davis sequencing, Davis, CA) to share 100% identity with rat *Slco4c1* sequence (GeneBank accession number NM\_001002024). The plasmid DNA (150 ng, pENTR/*Slco4c1*) was then subcloned into the multiple cloning site of the mammalian expression vector pcDNA6.2/GFP-DEST using Gateway® LR Clonase® II enzyme mix as directed by the manufacturer's protocol. The construct was transformed into XL1-Blue Supercompetent cells and the competent cells were grown in an agar plate with 100 µg/ml carbenicillin. The plasmid DNA (pcDNA6.2/GFP-DEST/*Slco4c1*, Figure 3-2) from positive transformants was validated by EcoRV, SspI and KpnI restriction enzyme digestion for 2 hr at 37°C and 0.8% agarose gel electrophoresis.

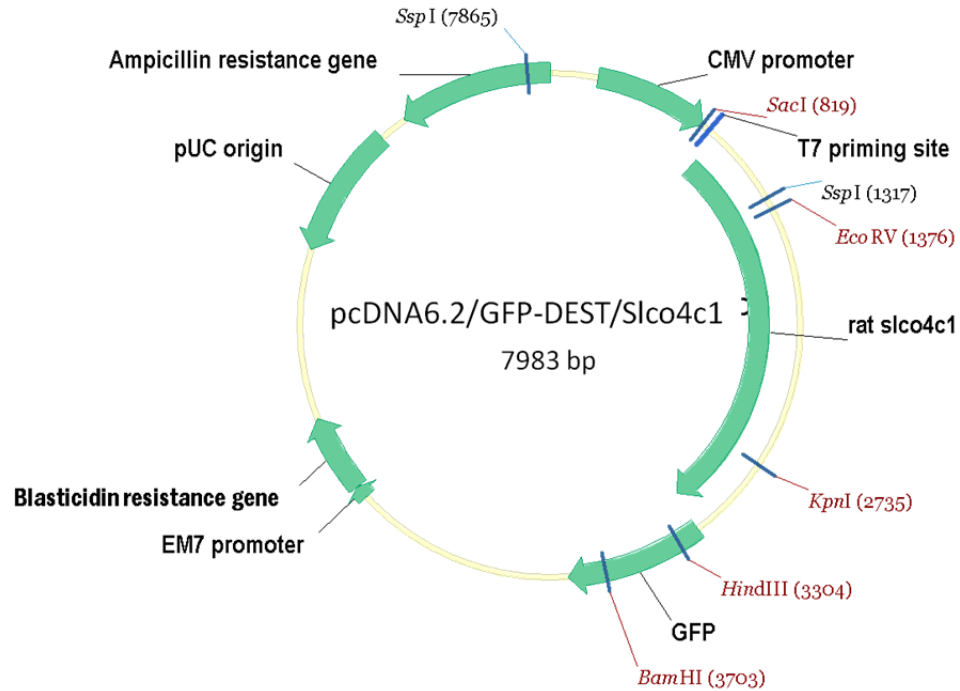


**Figure 3-2: pcDNA6.2/GFP-DEST/ Slco4c1 plasmid construct.**

### 3. Cell culture and transfection

MDCKII cells were cultured in minimum essential medium (MEM) supplemented with 5% fetal bovine serum, 100 U/ml penicillin, and 100 µg/ml streptomycin at 37°C in a humidified incubator with 5% CO<sub>2</sub>. LLC-PK1 cells were cultured in Dulbecco's modified Eagle's medium (DMEM) supplemented with 10% fetal bovine serum, 100 U/ml penicillin, and 100 µg/ml streptomycin. The pcDNA6.2/GFP-DEST/Slco4c1 and pcDNA6.2/GFP-DEST (vector) were transfected into MDCKII and LLC-PK1 cells at 50% confluence with the lipid-based FuGENE 6 transfection reagent at a 3:1 ratio as directed by manufacturer's protocol. The transfected cells were selected with 5 µg/ml of blasticidin. Success of transfection was evaluated by Western blot analysis of cell



lysates and immunohistochemical analysis of paraformaldehyde-fixed paraffin-embedded cell pellet sections for rat Oatp4c1 following procedures described in Section B-8 Western blot and Section B-9 Immunohistochemistry. The subcellular localization in pooled cells was examined by confocal microscopy and surface protein biotinylation assay as described in Section B-10 Immunofluorescence microscopy and Section B-11 Surface protein biotinylation assay.

4. Single clone selection by fluorescence-activated cell sorting (FACS) with transiently expressed C-terminal-tagged green fluorescent protein (GFP)

MDCKII-Oatp4c1 ( $1 \times 10^6$  cells/well) were grown in a 6-well plate and allowed to become 90% confluent overnight. Cells were treated with Tag-On-Demand™ Suppressor System for 6 hr at 37°C, and then replaced with fresh growth medium. After 48 hr, cells were trypsinized, pelleted by centrifugation at 300 g for 5 min, resuspended in growth medium and filtered with a 35 µm cell strainer to remove cell clumps and debris. FACS analyses were performed at UK Flow Cytometry Core Facility. Cells were sorted into individual wells in 96-well plates with excitation at 478 nm and emission at 507 nm using FACSCalibur cytofluorimeter (BD Biosciences, San Jose, CA) and MoFlo™ High-Performance Cell Sorter (DakoCytomation, Fort Collins, CO). Cells in 96-well plates were immediately transferred to the incubator. Cell medium was replaced every three days. Upon confluence, cells were transferred to 24-well plate, 12-well plate, 6-well plate, T-25 and T-75 serially. Oatp4c1 expression was evaluated by immunofluorescence staining as described in Section B-10 Immunofluorescence microscopy.

5. Single clone selection by immunofluorescence labeling and FACS

The immunofluorescence labeling of viable cells was according to procedures described by Cunningham with some modifications (112). MDCKII-Oatp4c1 cells ( $1 \times 10^6$  cells) were trypsinized, pelleted by centrifugation at 300 g for 5 min, resuspended in 10% BSA/PBS containing 110 µg/ml PA1343 (for rat Oatp4c1) and incubated for 1 hr at room temperature. Cells were washed with PBS and centrifuged twice. Cell pellets were labeled with 4 µg/ml Alexa Fluor 488 goat anti-rabbit IgG in 10% BSA/PBS for 30 min at 4°C. Following two washes with PBS and centrifugation, cells were resuspended in growth medium. At UK Flow Cytometry Core Facility, cells were sorted into individual wells in 96-well plates with excitation at 495 nm and emission at 519 nm. Cells in 96-well plates were immediately transferred to the incubator. Cell medium was replaced every three days. Upon confluence, cells were transferred to 24-well plates, 12-well plates, 6-well plates, T-25 and T-75 flasks serially. Oatp4c1 expression was evaluated by immunofluorescence staining as described in Section B-10 Immunofluorescence microscopy.

6. Single clone selection by serial dilution

MDCKII-Oatp4c1 cells were plated in 96-well plates as shown in Figure 3-3. Cells were trypsinized, centrifuged, resuspended in growth medium. Cell suspension ( $5 \times 10^3$  cells/ml; 200 µl) was added in A1 and growth medium (100 µl) was added to all the other wells. Cell suspension (100 µl) was transferred from A1 to B1 and mixed by gently pipetting and repeated down the entire

column. Cell suspension (100  $\mu$ l) from H1 was discarded to have the same volume as the wells above it. Growth medium (100  $\mu$ l) was added to the first column to achieve final volume of 200  $\mu$ l. Cell suspension (100  $\mu$ l) was transferred from the first column to the second column and mixed by gently pipetting and repeated across entire plate. Cell suspension (100  $\mu$ l) from each well in the last column was discarded. The final volume was brought to 200  $\mu$ l by adding 100  $\mu$ l of growth medium. Cell medium was replaced every three days. Upon confluence, cells were transferred to 24-well plates, 12-well plates, 6-well plates, T-25 and T-75 flasks serially. Oatp4c1 expression was evaluated by immunofluorescence staining as described in Section B-10 Immunofluorescence microscopy.

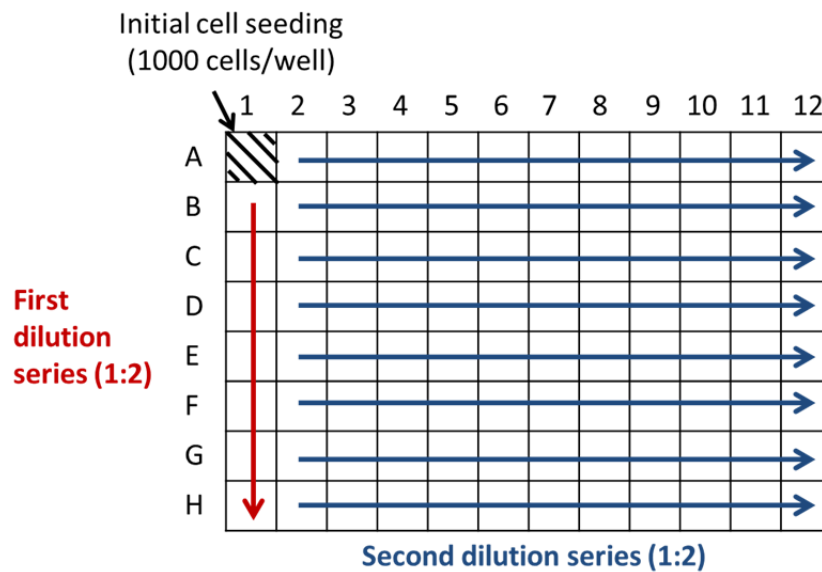


**Figure 3-3: Plate setup for serial dilution.**

7. Regulation of Oatp4c1 expression by sodium butyrate, blasticidin, simvastatin, glycerol, and MG132

MDCKII-Oatp4c1 cells were grown in 6-well plates ( $5 \times 10^5$  cells/well) or Lab-Tek™ 8-well chamber slides ( $1.4 \times 10^4$  cells/well, Thermo Scientific Nunc, Rochester, NY) allowed to become 50% confluent overnight, and then incubated with 0.1 - 5 mM of sodium butyrate for 24 hr. Cells grown in 6-well plates were washed with ice-cold PBS, scraped with cell scrapers and centrifuged at 300 g for 5 min. Cell lysates were prepared and subjected to Western blot to evaluate Oatp4c1 expression as described in Section B-8 Western blot. Total RNA was isolated from cell pellets and subjected to qRT-PCR analysis to assess *Sico4c1* mRNA expression as described in Section C-1 Quantitative real time polymerase chain reaction (qRT-PCR). Cells grown in chamber slides were stained for immunofluorescence analysis to evaluate Oatp4c1 expression as described in Section B-10 Immunofluorescence microscopy.

Cells were also grown in 10 and 30 µg/ml of blasticidin for two passages or treated with 10 and 20 µM simvastatin for 24 hr, 0 – 1.5 M glycerol for 48 hr, or 0.1 and 10 µM MG132 for 12 and 24 hr, respectively, to evaluate their effects on *Sico4c1*/Oatp4c1 expression in MDCKII-Oatp4c1 cells.

8. Western blot

MDCKII-Oatp4c1 and MDCK-pcDNA cells were grown in a T-75 flask to confluence. Following a wash with ice-cold PBS, cells were scraped and pelleted by centrifugation at 300 g for 5 min. Cell pellets were resuspended in RIPA buffer (50 mM Tris, 150 mM NaCl, 1% Nonidet P-40, 0.5% deoxycholate, 1 mM EDTA,

0.1% SDS, pH 8.0) with protease inhibitor cocktail (Complete Mini tablets) and shaken at 4°C for 30 minutes. Cell lysates were stored at -80°C until use.

Cell lysates were mixed with NuPAGE LDS sample buffer and 0.1 M dithiothreitol (DTT) before heating to 70°C for 10 min. Proteins were separated on a 10% SDS-polyacrylamide gel with 5% stacking gel and Tris-Glycine SDS running buffers (25 mM Tris, 192 mM glycine, 0.1% SDS) and transferred to a polyvinylidene difluoride membrane with transfer buffer (25 mM Tris, 192 mM glycine) at 200 mA for 2 hr at 4°C. Following blocking with 5% skimmed milk in PBST (10 mM phosphate buffer pH 7.6, 150 mM NaCl, 0.05% Tween-20) for 3 hr at room temperature, the membranes were incubated with 55 µg/ml anti-Oatp4c1 polyclonal antibody (PA1343) or 14.5 µg/ml anti-β-actin in 5% skimmed milk in PBST at 4°C. After three 10 min washes with PBST, the membranes were incubated with 0.04 µg/ml HRP conjugated goat anti-rabbit (for Oatp4c1) or anti-mouse IgG (for β-actin) in 5% skimmed milk in PBST for 1 hr at room temperature. Following three 10 min PBST washes, the membranes were visualized by Supersignal<sup>®</sup> West Pico chemiluminescent kit and imaged on an Image Station 2000 MM (Eastman Kodak).

## 9. Immunohistochemistry

MDCKII-Oatp4c1 and MDCKII-pcDNA cells were grown in two T-75 flasks to confluence. Following a wash with PBS, cells were scraped and centrifuged at 300 g for 5 min. Cell pellets were encapsulated with HistoGel<sup>™</sup> and then fixed in 4% paraformaldehyde for 6 hr at room temperature. The cell pellets were embedded in paraffin at UK Histology Laboratory of the Imaging Facility, and cut as 6 µm-thick sections using Microm HM325 microtome (Thermo Scientific).

Sections were heated at 60°C on Barnstead Lab-Line slide warmer (Dubuque, IA) to affix the tissues on the slides. Sections were deparaffinized with 3 changes of xylene for 5 min each, and rehydrated with 3 changes of 100% ethanol, 1 change of 95% ethanol, and 1 change of 70% ethanol for 2 min each. Then, the antigen was retrieved by pressure-cooking in 10 mM citrate buffer, pH 6.0. Sections were blocked with 3% H<sub>2</sub>O<sub>2</sub> in PBS for 5 min, avidin and biotin blocking reagent for 15 min each, 2% normal goat serum in PBST for 30 min, and subsequently incubated with PA1343 (for Oatp4c1, 220 µg/ml) for 24 hr at room temperature. Following three 5 min washes with PBST, sections were incubated with 5 µg/ml biotinylated goat anti-rabbit IgG for 30 min at room temperature. Sections were washed with PBST for 5 min four times, and incubated with streptavidin-HRP reagent for 20 min. After five more 5 min PBST washes, sections were incubated with NovaRED chromogen substrate for 5 min for visualization. Sections were then washed with H<sub>2</sub>O for 5 min three times, and counterstained with hematoxylin to visualize nuclei. After washing with running tap water for 5 min, sections were dehydrated with 1 change of 70% ethanol, 1 change of 95% ethanol, 3 changes of 100% ethanol for 2 min each. Glass coverslips were then mounted onto the glass slides with Vecta Mount.

#### 10. Immunofluorescence microscopy

Oatp4c1-expressing and vector-transfected MDCKII and LLC-PK1 cells (5 x 10<sup>5</sup> cells/well) were seeded on polycarbonate #3407 snapwell (0.4 µm pore size, 1.12 cm<sup>2</sup> growth area) and grown for 4 days to allow for polarization. Transepithelial electrical resistance (TEER) was measured every day with a

Millicell ohmmeter and a Millicell-ERS probe (Millipore, Bedford, MA) until  $> 200 \Omega \cdot \text{cm}^2$  was achieved.

Cell containing inserts were washed with ice-cold PBS. Filter membranes were then cut and transferred to 24 well plates for staining. Cells were fixed with -20°C methanol for 10 min, rehydrated with room temperature PBS for 5 min, permeabilized with 0.2% Triton X-100/PBS for 15 min, blocked with 10% goat serum for 1 hr, and then incubated with PA1343 (for Oatp4c1, 110 µg/ml) and anti-Zo-1 (5 µg/ml) for 2 hr at room temperature. Following three 5 min washes with 0.2% Triton X-100/PBS, cells were incubated with 4 µg/ml Alexa Fluor 568 anti-rabbit IgG and Alexa Fluor 488 anti-mouse IgG in blocking solution for 1 hr at room temperature. Cells were washed with 0.2% Triton X-100/PBS three times and mounted on glass slides with Prolong Gold containing DAPI solution to visualize nuclei. The fluorescence emission was visualized using Axiovert 200M confocal microscope (Carl Zeiss, Thornwood, NY).

#### 11. Surface protein biotinylation assay

MDCKII-Oatp4c1 and MDCKII-pcDNA cells ( $1 \times 10^6$  cells/well) were grown on polycarbonate #3414 transwell (3 µm pore size, 4.67 cm<sup>2</sup> growth area) for 4 days to achieve TEER  $> 200 \Omega \cdot \text{cm}^2$ . Cells were washed with ice-cold PBS-Mg/Ca buffer (PBS buffer containing 0.1 mM CaCl<sub>2</sub> and 1.0 mM MgCl<sub>2</sub>). Freshly prepared Sulfo-NHS-SS-Biotin (1 mg/ml in PBS-Mg/Ca) was added to either the apical or basolateral chamber and incubated with slow rocking at 4°C for 20 min. Cells were then washed and incubated with quenching buffer (5 mM glycine in PBS-Mg/Ca) with slow rocking at 4°C for 20 min to remove unreacted biotin.

Following washing with PBS-Mg/Ca, the cells were lysed with 700  $\mu$ l lysis buffer (10 mM Tris, 150 mM NaCl, 1 mM EDTA, 0.1% SDS, 1% Triton X-100, pH 7.4) with the protease inhibitor cocktail for 30 min at 4°C with shaking. Cell lysates were centrifuged at 10,000 g for 2 min at 4°C, and the supernatants were incubated with streptavidin agarose beads with end-over-end rotation for 1 hr at 4°C. Samples were washed three times with lysis buffer, and incubated with 50  $\mu$ l 2X Laemmli Buffer (125 mM Tris, 10% glycerol, 2% SDS, 5% 2- $\beta$ -mercaptoethanol, pH 6.8) for 30 min at room temperature. 2- $\beta$ -mercaptoethanol was used to break the disulfide (SS) bond between the biotin and the protein reactive group, releasing the biotinylated membrane proteins from the beads. The samples were centrifuged at 10,000 g for 2 min, and the supernatants were subjected to Western blot analysis as described in Section B-8 Western blot.

### **C. Determination of Oatp4c1 expression and subcellular localization in rat tissues**

#### **1. Quantitative real time polymerase chain reaction (qRT-PCR)**

RNA isolation from rat tissues and reverse-transcription were performed as described in Section B-2 Construction of plasmid vector. Quantification of the expression level of Slco4c1 and the house-keeping gene 18s rRNA was performed using the qRT-PCR on the iCycler Multicolor Real-Time PCR Detection System (Bio-Rad, Hercules, CA). Slco4c1 primer sequences were obtained from published literature (79), and 18s rRNA primers were designed using reference sequences deposited in NCBI's Entrez Gene with the software assistance of PrimerQuest (Integrated DNA Technologies, Coralville, IA). Reference accession numbers, primer sequences, and product sizes are



provided in Table 3-1. PCR reaction master mixes (50 µL) were made using the SYBR® Green PCR Core Reagents kit and contained 200 nM of each primer, 1.25 mM dNTPs, 1x SYBR Green buffer, 0.025 U/µl Taq polymerase, and 4 mM MgCl<sub>2</sub>, 20 nM fluorescein. Amplification conditions were as follows: 95°C (5 min), [95°C (45 sec), 61.6°C (1 min), 72°C (1 min)] × 50 cycles. No-template (water) reaction mixtures were prepared as negative control. To confirm the generation of a single product of appropriate size, all amplification products were separated by 3% agarose gel electrophoresis in 1 x TBE running buffer for 50 min at 150 V. The gel was visualized by staining with ethidium bromide, and imaged on an Image Station 2000 MM (Eastman Kodak). Relative copy number of each gene in the samples was determined in triplicate and normalized to relative copy number of the housekeeping gene 18s rRNA within each sample. The fold change in *Slco4c1* expression relative to reference tissue (FC) was calculated with 2<sup>-ΔΔCt</sup> method using the following equation:

$$FC = 2^{-[(Ct_{Slco4c1} - Ct_{18s})_{target} - (Ct_{Slco4c1} - Ct_{18s})_{reference}]} \quad \text{Equation 3-1}$$

The error propagation was as follows:

$$S_{dCT} = S_{Ct_{Slco4c1} - Ct_{18s}} = \sqrt{S_{Ct_{Slco4c1}}^2 + S_{Ct_{18s}}^2} \quad \text{Equation 3-2}$$

$$S_{ddCT} = \sqrt{S_{dCT, target}^2 + S_{dCT, reference}^2} \quad \text{Equation 3-3}$$

$$S_{FC} = \ln 2 \times S_{ddCT} \times FC \quad \text{Equation 3-4}$$

**Table 3-1: Slco4c1 and 18s rRNA primers information.**

Gene	Reference sequence	Forward primer (5' → 3')	Product size (bp)	Ref.
		Reverse primer (5' → 3')		
Slco4c1	NM_001002024	GCAAGGTATTGTAGTAAATGGCCTAG	127	(79)
		AGACAACACGCAAAAGGAGATGT		
18s rRNA	X03205.1	CGCCGCTAGAGGTGAAATTCTT	101	
		CGAACCTCCGACTTTCGTTCTT		

## 2. Western blot

Crude membrane fractions were prepared from Sprague-Dawley female rat tissues (kidney, liver, lactating and non-lactating MG). The tissues were disrupted in Dounce Buffer (10 mM Tris, pH 7.6, 0.5 mM MgCl<sub>2</sub> with protease inhibitor cocktail) with brief pulses of sonication using a probe ultrasonic processor (Thermo Fisher Scientific) at 4°C and the tonicity was restored to 150 mM with sodium chloride. Following 300 g centrifugation for 5 min, EDTA was added to the supernatant to a final concentration of 5 mM. The samples were centrifuged at 100,000 g for 1 hr at 4°C. Pellets were resuspended in Resuspension Buffer (0.2 M mannitol, 0.07 M sucrose, 50 µM Tris HCl, 1 µM EDTA). Protein concentrations were measured using the BCA Protein Assay Kit. Crude membrane fractions were stored at -80°C until use. Procedures for Western blot

analysis of Oatp4c1 expression in rat tissues were the same as those described in Section B-8 Western blot.

### 3. Immunohistochemistry

Female Sprague-Dawley rat liver, kidney and MG were isolated and fixed in 4% paraformaldehyde for 6 hr at room temperature. The tissues were embedded in paraffin at UK Histology Laboratory of the Imaging Facility, and cut as 6 µm-thick sections. Procedures for immunohistochemical analysis of Oatp4c1 localization in rat tissues were as described in Section B-9 Immunohistochemistry.

To further study the localization of Oatp4c1, rat tissue sections were double stained with anti-Oatp4c1 antibody (PA1343, 110 µg/ml) and the following antibodies: anti-E-cadherin (2 µg/ml), anti-AQP1 (10 µg/ml), and anti-calbindin-D<sub>28k</sub> (40 µg/ml), anti-Abcg2 (BXP-53, 12.5 µg/ml), anti-Mrp4 (3 µg/ml), anti-P-gp (2.5 µg/ml). For visualization, the sections were incubated with fluorescence conjugated secondary antibodies for 30 min at room temperature and mounted with glass coverslips using Prolong Gold containing DAPI solution. Fluorescence was visualized using Axiovert 200M confocal microscope (Carl Zeiss).

### 4. BBM (brush-border membrane) and BLM (basolateral membrane) isolation

The BBM and BLM were isolated by Percoll density gradient centrifugation according to procedures described by Goldinger et al. with some modifications (113). Briefly, two male Sprague-Dawley rats were anesthetized with isoflurane

and euthanized by cervical dislocation. The kidneys were excised and frozen immediately. Kidney cortex tissues were excised and homogenized in sucrose buffer (250 mM sucrose, 10 mM triethanolamine, pH 7.4, protease inhibitor cocktail) with a motorized homogenizer. Samples were centrifuged at 2,500 g for 15 min at 4°C. The resultant supernatant was centrifuged at 20,000 g for 20 min at 4°C. The less dense top layer of the pellet was collected and the lower dark segment of the pellet was discarded. The pellet was resuspended in 26.5 ml sucrose buffer with 10 strokes of a tight plunger in a Dounce homogenizer. Following addition of 3.5 ml Percoll, the suspension was mixed by inversion and centrifuged at 48,000 g for 30 min at 4°C. Two distinct bands were formed and carefully isolated. The upper band was BLM and the lower one was BBM (113). An equal volume of sucrose buffer was added to each fraction, and the Percoll was removed by centrifuging at 93,000 g for 1 hr at 4°C. The single band of membrane proteins was collected and the glassy Percoll pellet was discarded. The BLM was resuspended in mannitol buffer (150 mM mannitol, 2.5 mM EGTA, 6 mM HEPES, pH 7.4). The BBM pellet was further purified by magnesium precipitation (114). Briefly, following resuspension of the BBM pellet in a buffer (100 mM mannitol, 1.6 mM EGTA, 0.3 mM PMSF, 0.3 mM sodium orthovanadate, 4 mM HEPES, pH 7.4),  $\text{MgCl}_2$  was added to yield a final concentration of 12 mM. The mixture was incubated on ice for 15 min with intermittent and gentle mixing. Remaining cellular debris were removed by centrifuging at 3,000 g for 10 min at 4°C, and the resultant supernatant was centrifuged at 30,000 g for 40 min at 4°C to isolate membrane proteins. The BBM pellet was resuspended in mannitol buffer and again precipitated by addition of 12 mM  $\text{MgCl}_2$  as described above. The final pellet was resuspended in mannitol buffer. The BBM and BLM were stored at -80°C until use.

Separation efficiency was evaluated by Western blot analysis following procedures described in Section B-8 Western blot. Procedures were the same but with different antibodies. Na<sup>+</sup>/K<sup>+</sup>-ATPase was used as a basolateral marker and was labeled with anti-Na<sup>+</sup>/K<sup>+</sup>-ATPase (1:1000). Mrp4 and Abcg2 served as apical markers and were labeled with anti-Mrp4 (3 µg/ml) and rabbit polyclonal anti-Abcg2 (150 µg/ml), respectively. The rabbit polyclonal anti-Abcg2 antibodies were generated (Open Biosystems) against Walker A peptide (GKSSLLDVLAARKD) of rat Abcg2 (115).

#### 5. Protein trypsin digestion and LC-MS/MS analysis

Approximately 100 µg of proteins from the BBM and BLM were subjected to 10% SDS-PAGE separation. The protein gel bands at 65-100 and 100-150 kDa were excised and underwent DTT reduction, iodoacetamide (IAA) alkylation, and in-gel trypsin digestion using a standard protocol as previously reported (116, 117). The resulting tryptic peptides were extracted, and concentrated to 15 µl each using a SpeedVac, and 5 µl was injected for nano-LC-MS/MS analysis. LC-MS/MS data were acquired on an LTQ Velos Orbitrap mass spectrometer (Thermo Fisher Scientific) coupled with a Nano-LC Ultra/cHiPLC-nanoflex HPLC system (Eksigent) through a nano-electrospray ionization source. The tryptic peptides sample was injected by an autosampler, desalted on a trap column, and subsequently separated by reverse phase C18 column (75 µm i.d. x 150 mm) at a flow rate of 250 nl/min. The HPLC gradient was linear from 5% to 60% mobile phase B for 30 min using mobile phase A (H<sub>2</sub>O, 0.1% formic acid) and mobile B (90% acetonitrile, 0.1% formic acid). Eluted peptides were analyzed using data-dependent acquisition: peptide mass spectrometry was obtained by Orbitrap with

a resolution of 100,000. The seven most abundant peptides were subjected to collision induced dissociation (CID) and MS/MS analysis in LTQ linear trap. The LC-MS/MS data were submitted to a local MASCOT server for MS/MS protein identification search via the ProteomeDiscoverer software. The mass error tolerance was 5 ppm for peptide MS and 0.8 Da for MS/MS. All peptides were required to have an ion score greater than 30 ( $P < 0.05$ ). The false discovery rate (FDR) in each LC-MS/MS analysis was set to be less than 1%.

#### **D. Functional characterization of Oatp4c1 in MDCKII-Oatp4c1 cells**

##### **1. [<sup>3</sup>H]-E3S uptake and inhibition studies**

MDCKII-Oatp4c1 and MDCKII-pcDNA cells ( $5 \times 10^5$  cells/well) were grown in 6-well plates. The cell culture medium was replaced with that containing 5 mM sodium butyrate to induce transporter expression 24 hr prior to uptake. The uptake buffer used in all transport experiments contained 118 mM NaCl, 23.8 mM NaHCO<sub>3</sub>, 4.83 mM KCl, 0.96 mM KH<sub>2</sub>PO<sub>4</sub>, 1.20 mM MgSO<sub>4</sub>, 5.0 mM glucose and 1.53 mM CaCl<sub>2</sub>. Buffer pH was adjusted to 7.4 by supplementation with 12.5 mM HEPES and pH adjustment with 1M Tris-base. Alternatively, the buffer was supplemented with 12.5 mM 2-(N-morpholino)ethanesulfonic acid (MES) and pH was adjusted to 4.5 or 5.5 with 1M Tris-base. Before the study, cells were washed once and pre-incubated with uptake buffer for 15 min at 37°C. Uptake was initiated by replacing the uptake buffer with that containing [<sup>3</sup>H]-E3S. After incubation for designated time at 37°C, cells were washed three times with ice-cold PBS, lysed with 0.5 ml of 0.5 N NaOH and neutralized with 0.1 ml of 2.5 N HCl. The intracellular radioactivity was determined by transferring 0.5 ml of lysate

into scintillation cocktail for liquid scintillation counting with a Packard 2200CA Tri-Carb (PerkinElmer, Waltham, MA) liquid scintillation counter. Protein concentrations were measured using the BCA Protein Assay Kit. Net uptake was calculated as the difference between [<sup>3</sup>H]-E3S uptake into MDCKII-Oatp4c1 cells and uptake into MDCKII-pcDNA cells. For [<sup>3</sup>H]-E3S uptake under ATP-depletion conditions, cells were pre-incubated for 20 min prior to the experiment and during the experiment (1 min) with uptake buffer containing 20 mM 2-deoxy-D-glucose and 10 mM NaN<sub>3</sub> without D-glucose (69). For the inhibition study, cells were pre-incubated for 15 min prior to and during the experiment with 100 µM of various compounds (T<sub>3</sub>, T<sub>4</sub>, digoxin, ouabain, MTX, kynurenic acid, indoxyl sulfate, hippuric acid and *trans*-aconitic acid, uric acid, citric acid, and riboflavin) compounds at pH 5.5 or 7.4. Based on model fitting criteria, transport parameters were estimated using a sigmoid-E<sub>max</sub> equation:

$$v = T_{max} \times S^n / (S_{50}^n + S^n) \quad \text{Equation 3-5}$$

Where, V, S, T<sub>max</sub>, S<sub>50</sub>, and n represent the initial uptake velocity, substrate concentration, maximum uptake velocity, Michaelis-Menten constant equivalent, and Hill slope, respectively. The model was fitted to the data (obtained in triplicate) by nonlinear regression using GraphPad Prism (GraphPad Software, San Diego, CA).

Values are presented as means ± S.D. Statistical analysis was performed by an unpaired Student's t-test or two-way ANOVA and Bonferroni post-hoc test for multiple comparisons as indicated with p < 0.05 as the criterion of significance. The software program GraphPad Prism was used for statistical analysis (GraphPad Software, San Diego, CA)

## 2. [<sup>3</sup>H]-MTX uptake and inhibition studies

Time dependent 1  $\mu$ M [<sup>3</sup>H]-MTX uptake studies as well as the inhibition studies at pH 5.5 or pH 7.4 were performed. Procedures were the same as described above in [<sup>3</sup>H]-E3S uptake and inhibition studies.

## E. Creation and validation of human OATP4C1-expressing cell lines

### 1. MDCKII cells

#### i. Plasmid vector construction and transfection

Human SLCO4C1 DNA purchased from OriGene (Rockville, MD) was amplified by PCR using Phusion High-Fidelity PCR kit with forward (5'-CACCATGAAGAGCGCCAAAGGTATTG- 3') and reverse (5'-CTACCCTTCTTTTACTATTTTGTTGAG-3') primers. Amplification conditions were as follows: 98°C (1 min), [98°C (10 sec), 63°C (30 sec), 72°C (40 sec)] × 25 cycles, 72°C (10 min). The amplified fragment of appropriate size was examined on 1% agarose gel, and further purified. The subsequent sequence was cloned into pENTR vector and transformed into competent One Shot TOP10 *E. coli*. The competent cells were grown in an agar plate with 50  $\mu$ g/ml kanamycin. The plasmid DNA (pENTR/SLCO4C1) from positive transformants was validated by EcoRI restriction enzyme digestion and by PCR with M13 forward (5'-GTTTTCCAGTCACGAC-3') and M13 reverse (5'-CAGGAAACAGCTATGAC-3') primers with following amplification conditions: 98°C (1 min), [98°C (10 sec), 52°C (30 sec), 72°C (45 sec)] × 25 cycles, 72°C



(5 min). The restriction enzyme product and PCR product were examined on 0.8% agarose gel. The plasmid DNA sequence was also confirmed (Davis sequencing) to share 100% identity with human *SLCO4C1* sequence (GeneBank accession number NM\_180991). The plasmid DNA was subcloned into pcDNA6.2/EmGFP-Bsd/V5-DEST vector. The construct was transformed into XL1-Blue Supercompetent cells and the competent cells were grown in an agar plate with 100 µg/ml carbenicillin. The plasmid construct (pcDNA6.2/EmGFP-Bsd/V5-DEST/*SLCO4C1*, Figure 3-4) was validated by PCR with T7 forward (5'-TAATACGACTCACTATAGGG-3') and *SLCO4C1* reverse (5'-CTACCCTTCTTTTACTATTTTGTTGAG-3') primers with following amplification conditions: 98°C (1 min), [98°C (10 sec), 53°C (30 sec), 72°C (30 sec)] × 25 cycles, 72°C (10 min). The PCR product was examined on 0.8% agarose gel. The detailed procedures are described in Section Chapter 3B2 Construction of plasmid vector. The plasmid construct (pcDNA6.2/EmGFP-Bsd/V5-DEST/*SLCO4C1*) and vector (pcDNA6.2/EmGFP-Bsd/V5-DEST) were transfected into MDCKII cells as described in Section Chapter 3B3 Cell culture and transfection.

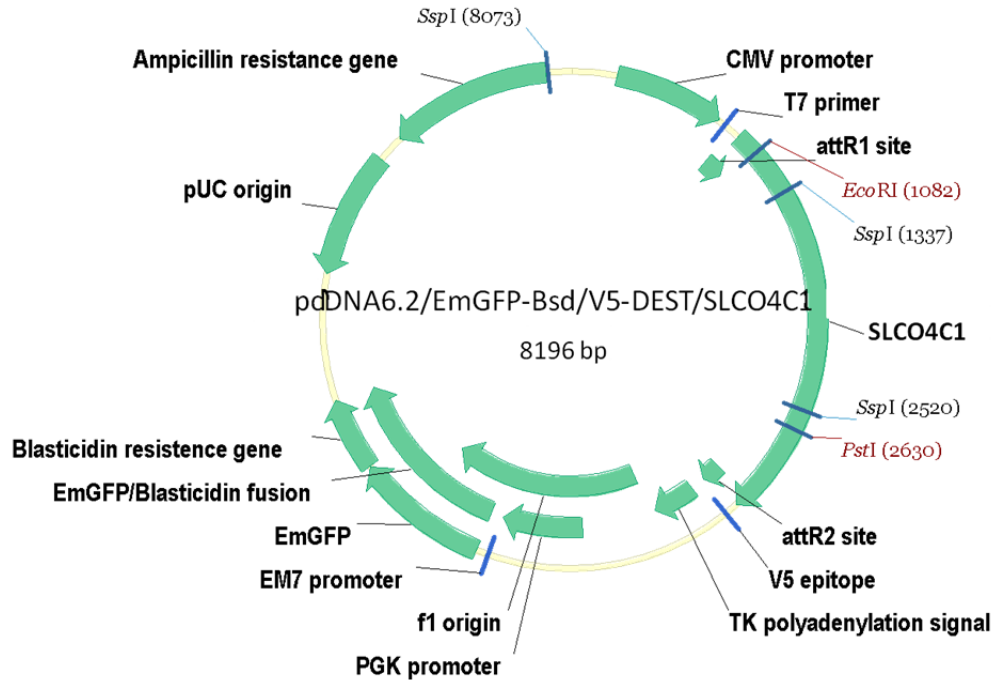


**Figure 3-4: pcDNA6.2/EmGFP-Bsd/V5-DEST/SLCO4C1 plasmid construct.**

## ii. Validation of OATP4C1 expression and subcellular localization

Transfection efficiency was evaluated by Western blot analysis and immunohistochemistry following procedures described in Section Chapter 3B8 Western blot and Section B9 Immunohistochemistry, respectively. Subcellular localization of OATP4C1 in MDCKII-OATP4C1 cells was assessed by immunofluorescence microscopy and surface protein biotinylation assay as described in Section B10 Immunofluorescence microscopy and Section B11 Surface protein biotinylation assay, respectively. Procedures were the same but with different antibodies: rabbit polyclonal antibodies against human OATP4C1 generated against amino-terminus [DPQRENSQPQELQKPQEPQK (PA1243)] and carboxyl-terminus [VLAEQDLNKIVKEG (PA1245)] sequence

peptides (Figure 3-5). Antibodies development was as described in Section B1  
Development of rat Oatp4c1 antibody.

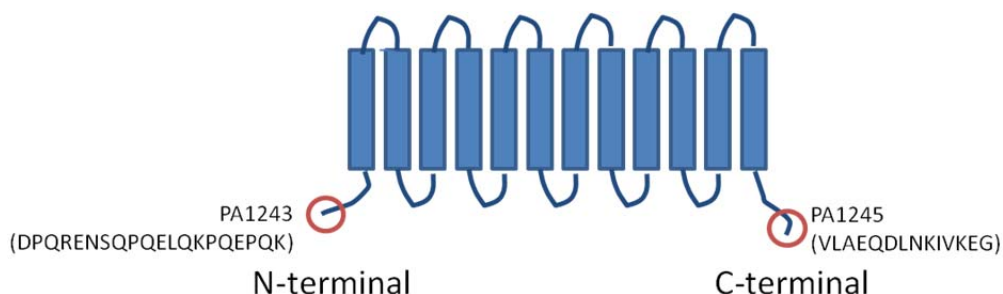


**Figure 3-5: Human OATP4C1 antibody antigen peptide sequence and location.**

iii. Validation of OATP4C1 function in MDCKII-OATP4C1 cells

OATP4C1 function was evaluated with [ $^3\text{H}$ ]-ouabain or [ $^3\text{H}$ ]-E3S uptake studies. Procedures were the same as described in Section D1 [ $^3\text{H}$ ]-E3S uptake and inhibition studies.

2. *Spodoptera frugiperda* (Sf9) insect cells

i. Plasmid vector construction

The construction of pENTR/SLCO4C1 was described in Section . Plasmid vector construction and transfection. The plasmid construct was cloned into pDEST8 vector and transformed into XL1-Blue Supercompetent cells. The competent cells were grown in an agar plate with 100  $\mu\text{g/ml}$  carbenicillin. The plasmid construct (pDEST8/SLCO4C1, Figure 3-6) was

validated by Bsu361 restriction enzyme digestion and 0.8% agarose gel electrophoresis. The plasmid DNA was then recombined in MAX Efficiency<sup>®</sup> DH10Bac<sup>™</sup> competent *E. Coli* containing baculovirus genome. The competent cells were grown in an agar plate with 100 µg/ml carbenicillin. For background control, the empty vector (pDEST8) was also recombined as above. The plasmid DNA from positive transformants was verified by PCR with M13 forward (5'-GTTTTCCCAGTCACGAC-3') and M13 reverse (5'-CAGGAAACAGCTATGAC-3') primers with the following amplification conditions: 94°C (1 min), [94°C (30 sec), 54°C (30 sec), 68°C (1 min)] × 30 cycles, 68°C (10 min). The PCR product was examined on 0.8% agarose gel.

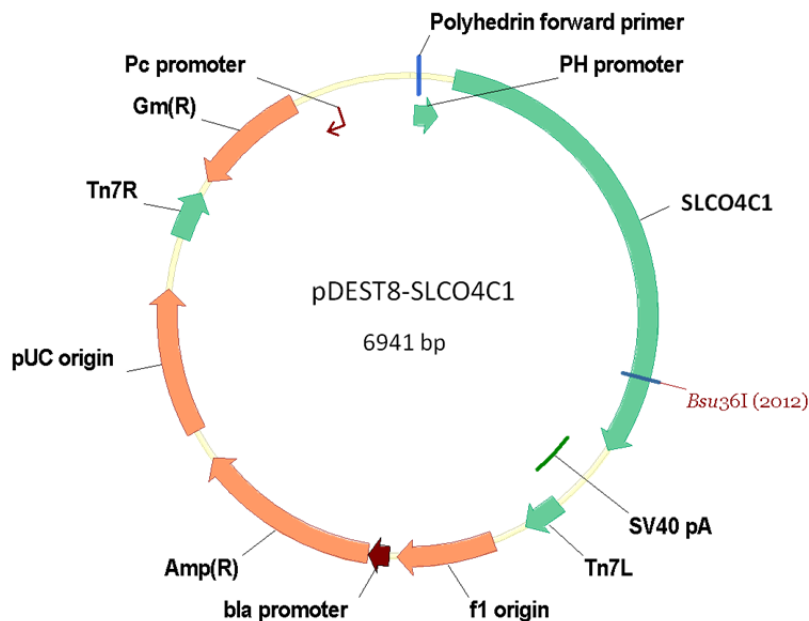


**Figure 3-6: pDEST8/SLCO4C1 plasmid construct.**

## ii. Cell culture, transfection and infection

Sf9 cell suspensions were grown in Sf-900 II SFM medium supplemented with 100 U/ml penicillin and 100 µg/ml streptomycin at 27°C with constant shaking in Barnstead® MaxQ™ 4000 incubated shaker (Dubuque, IA). Sf9 cells ( $9 \times 10^5$  cells/well) were seeded in a 6-well plate and incubated at 27°C for 1 hr for cells to be attached. The recombinant bacmids (pDEST8/SLCO4C1 and pDEST8) were transfected into Sf9 cells with Cellfectin reagent as directed by manufacturer's protocol. After 48 hr, cells were scraped and centrifuged at 500 g for 5 min. The supernatant containing the recombinant baculovirus (P1 viral stock) was harvested.

To minimize experimental variability from protein expression and inside-out ratio of membrane vesicles, a large batch of membranes was prepared for all subsequent transport studies. The recombinant baculovirus stock was amplified by infecting Sf9 cell suspensions ( $1 \times 10^6$  cells/ml, log phase) with P1 viral stock at a 1:4 (v/v ; viral stock: Sf9 cell suspensions) at 27°C for 48 hr with constant shaking. The supernatant (P2 viral stock) was harvested by centrifugation at 500 g for 5 min. Sf9 cells were infected with P2 viral stock at 27°C for 48 hr and again with P3 viral stock as described above. After incubation at 27°C for 48 hr, cells were centrifuged at 500 g for 5 min. The supernatant (P4 viral stock) was dispensed in aliquots and stored at -80°C until use. Cell pellets for membrane vesicle preparation were stored at -80°C until use.

### iii. Membrane vesicle preparation

The cell pellets were thawed on ice and resuspended in ice-cold hypotonic buffer (0.5 mM Na<sub>2</sub>HPO<sub>4</sub>, 0.1 mM EDTA, pH 7.4) supplemented with protease inhibitor cocktails and incubated for 90 min at 4°C. The suspension was centrifuged at 100,000 g for 40 min at 4°C, and the pellet was homogenized in ice-cold TS buffer (50 mM Tris-HCl, 250 mM sucrose, 0.25 mM CaCl<sub>2</sub>, pH 7.4) using a tight-fitting Dounce homogenizer. After centrifugation at 500 g at 4°C for 10 min, the supernatant was centrifuged at 100,000 g for 40 min at 4°C. The pellet was resuspended in TS buffer and passed through a 27-gauge needle 25 times. The vesicles were dispensed in aliquots and stored at -80°C until use. The membrane protein concentrations were determined by BCA Protein Assay Kit. OATP4C1 expression was determined by Western blotting as described in Section Chapter 3E1.ii. Validation of OATP4C1 expression and subcellular localization.

### iv. Vesicular transport assay

Sf9 membrane vesicles (40 µg) containing OATP4C1 or vector were incubated with the indicated concentrations of [<sup>3</sup>H]-ouabain in 50 µl of TS buffer supplemented with 10 mM creatine phosphate, 0.1 mg/ml of creatine phosphokinase, 10 mM MgCl<sub>2</sub> and 4 mM ATP at 37°C. At the designated time, the reaction was stopped by adding 1.5 ml of ice-cold stop buffer (10 mM Tris-HCl, 250 mM sucrose, 100 mM NaCl, pH7.4) and immediately vacuum filtered onto a cellulose acetate filter (0.45-µm pore size, OE67). The filter was washed twice with 1.5 ml of ice-cold stop buffer, and the radioactivity retained on the filter was measured by liquid scintillation

counting. Procedures for [ $^3\text{H}$ ]-E3S were the same as described above but with regenerated cellulose filters (0.45- $\mu\text{m}$  pore size, RC55). The filters were selected due to their minimal binding of ouabain or E3S. OATP4C1-mediated uptake was calculated after subtraction of nonspecific uptake by vector membrane vesicle.

## **F. Validation of OATP4C1 expression in human kidney and cancer cells**

### **1. Immunohistochemical analysis in human kidney sections**

De-identified human kidney sections were obtained from Markey Cancer Center Biospecimen Core (IRB#05-0155-X1G). Subcellular localization of OATP4C1 was assessed by immunohistochemical analysis as described in Section Chapter 3B9 Immunohistochemistry. Procedures were the same but with a different antibody. MRP4 was served as a positive control and was labeled with 3  $\mu\text{g}/\text{ml}$  of  $\text{M}_4\text{I}_{10}$ . OATP4C1 was detected with 550  $\mu\text{g}/\text{ml}$  of PA1243 or PA1245.

### **2. qRT-PCR analysis for *SLCO4C1* expression in cancer cells**

Prostate cancer cell lines (LnCap, DU145, PC3) and lung cancer cell line H1299 were cultured in RPMI 1640 medium supplemented with 10% fetal bovine serum, 100 U/ml penicillin, and 100  $\mu\text{g}/\text{ml}$  streptomycin. Lung cancer cell lines (A549, H460), breast cancer cell line MCF7 and glioblastoma cell line U118 were cultured in Dulbecco's modified Eagle's medium (DMEM) supplemented with 10% fetal bovine serum, 100 U/ml penicillin, and 100  $\mu\text{g}/\text{ml}$  streptomycin. Breast cancer cell line MDA-MB-231 and melanoma cell line MDA-MB-435 were

cultured in Improved Minimum Essential Medium (IMEM) with 10% fetal bovine serum, 100 U/ml penicillin, and 100 µg/ml streptomycin.

Cancer cell lines were grown in a T-25 flask to confluence. Cells were trypsinized and pelleted by centrifugation at 300 g for 5 min. RNA isolation from cell pellets and reverse-transcription were performed as described in Section Chapter 3B2 Construction of plasmid vector. Procedures for qRT-PCR were the same as described in Section Chapter 3C1 Quantitative real time polymerase chain reaction (qRT-PCR) with different primers (Table 3-2).

**Table 3-2: SLCO4C1 and 18s rRNA primers information.**

Gene	Reference sequence	Forward primer (5' → 3')	Product size (bp)
		Reverse primer (5' → 3')	
SLCO4C1	NM_180991	GAGAAGCTCCGGTCACTGTC	149
		ACTACAATACCTTGCGTGAC	
18s rRNA	X03205.1	CGCCGCTAGAGGTGAAATTCTT	101
		CGAACCTCCGACTTTCGTTCTT	



3. OATP4C1/SLCO4C1 expression in lung tumor and adjacent normal lung tissue sections

i. qRT-PCR

Human lung tumor and adjacent normal lung tissue sections were obtained from the Markey Cancer Center Biospecimen Core (IRB#05-0155-X1G). The tissues were rinsed with 20 µl of xylene, scraped from the slides with blades and transferred to microcentrifuge tubes for RNA isolation. RNA isolation was performed with RecoverALL™ total nucleic acid isolation kit as directed by manufacture's protocol. Total RNA quality was verified by an OD260/OD280 absorption ratio within a range of 1.8-2.1. Reverse-transcription of 100 ng RNA to cDNA was performed with reverse ThermoScript™ RT-PCR kit with oligo (dT)<sub>20</sub> primers using Peltier Thermal Cycler. PCR was conducted using TaqMan® Gene Expression Assay (Table 3-3) and TaqMan® Universal PCR Master mix in a total volume of 20 µl using ABI PRISM® 7000 sequence detection system (Applied Biosystems, Foster city, CA). Amplification conditions were as follows: 50°C (2 min), 95°C (10 min), [95°C (15 sec), 60°C (1 min)] × 40 cycles. No-template (water) reaction mixtures were prepared as negative control.

**Table 3-3: TaqMan® Gene Expression Assay for SLCO4C1 and 18s rRNA.**

Gene	Reference sequence	Assay ID	Exon Boundary	Amplicon length (bp)
SLCO4C1	NM_180991	Hs00698884_m1	4-5	77
		Hs01030668_m1	7-8	58
		Hs01030660_m1	10-11	64
18s rRNA	X03205.1	Hs03003631_g1	-	69

ii. Immunohistochemistry

Procedures were as described in Section Chapter 3B9 Immunohistochemistry. OATP4C1 was detected with 110 µg/ml of PA1243 or PA1245.

## CHAPTER 4 : RESULTS

### A. Creation and validation of a rat Oatp4c1-expressing cell line

1. Specific Aim 1a: To develop and validate rat Oatp4c1 antibodies amenable for immunoblotting, immunohistochemistry and immunofluorescence.

To investigate the expression and subcellular localization of rat Oatp4c1 in the *in vitro* cell models or rat tissues, four rabbit polyclonal antibodies were generated against either amino-terminus or carboxyl-terminus of rat Oatp4c1. The antibody specificities were determined by Western blotting, immunohistochemical analysis, and immunofluorescence staining in the *in vitro* cell models developed in Specific Aim 1b. Among the four antibodies, PA1343 was affinity-purified and used for subsequent experiments.

2. Specific Aim 1b: To create and validate a stably transfected rat Oatp4c1-expressing cell line with appropriate characteristics for uptake studies.

To study the role of rat Oatp4c1 in drug disposition, we generated rat Oatp4c1-expressing MDCKII cells. Rat Slco4c1 mRNA was isolated from rat kidney and amplified by PCR. The amplified fragment of appropriate size was examined by agarose gel electrophoresis. As shown in Figure 4-1 A, rat Slco4c1 mRNA was successfully isolated from rat kidney. The amplification product was further purified and cloned into pENTR vector. The plasmid construct was validated by KpnI, Sall and EcoRV restriction enzyme digestion (Figure 4-1 B) and DNA sequencing which had 100% identity with the published rat Slco4c1 sequence (GeneBank accession number NM\_001002024). The plasmid DNA

was then subcloned into pcDNA6.2/GFP-DEST vector and was validated by EcoRV, Sspl and KpnI restriction enzyme digestion (Figure 4-1 C).

The plasmid DNA (pcDNA6.2/GFP-DEST/Slco4c1) and vector (pcDNA6.2/GFP-DEST) were transfected into MDCKII and LLC-PK1 cells. Transfection efficiency was examined by Western blotting using the antibody generated in Specific Aim 1a (PA1343) (Figure 4-2 A). Oatp4c1 expression was detectable as a band at ~80 kDa in MDCKII-Oatp4c1 cells, but not in MDCKII-pcDNA (empty vector) cells. Expression was also confirmed in paraformaldehyde-fixed paraffin-embedded cell pellet sections by immunohistochemical analysis (Figure 4-2 B). Oatp4c1 was observed on the cell membrane (Figure 4-2 B, inset) in the MDCKII-Oatp4c1 cells, and no staining was observed in the negative control (rabbit IgG) or in the MDCKII-pcDNA cells. This demonstrated that the transfection was successful and that the antibody was specific.

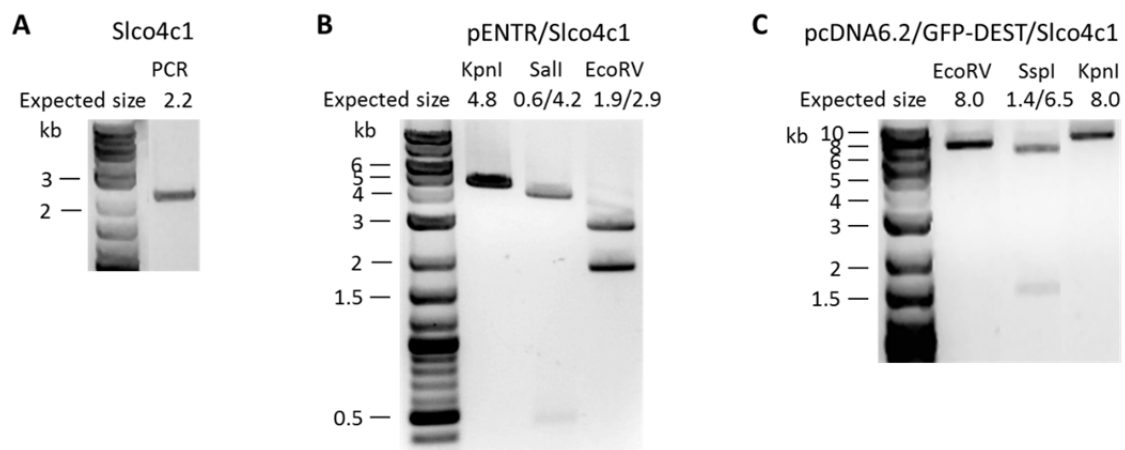


**Figure 4-1: Validation of Slco4c1 plasmid constructs.**

PCR products of Slco4c1 isolated from rat kidney and the restriction enzyme digestion products of the plasmid construct were examined by agarose gel electrophoresis.

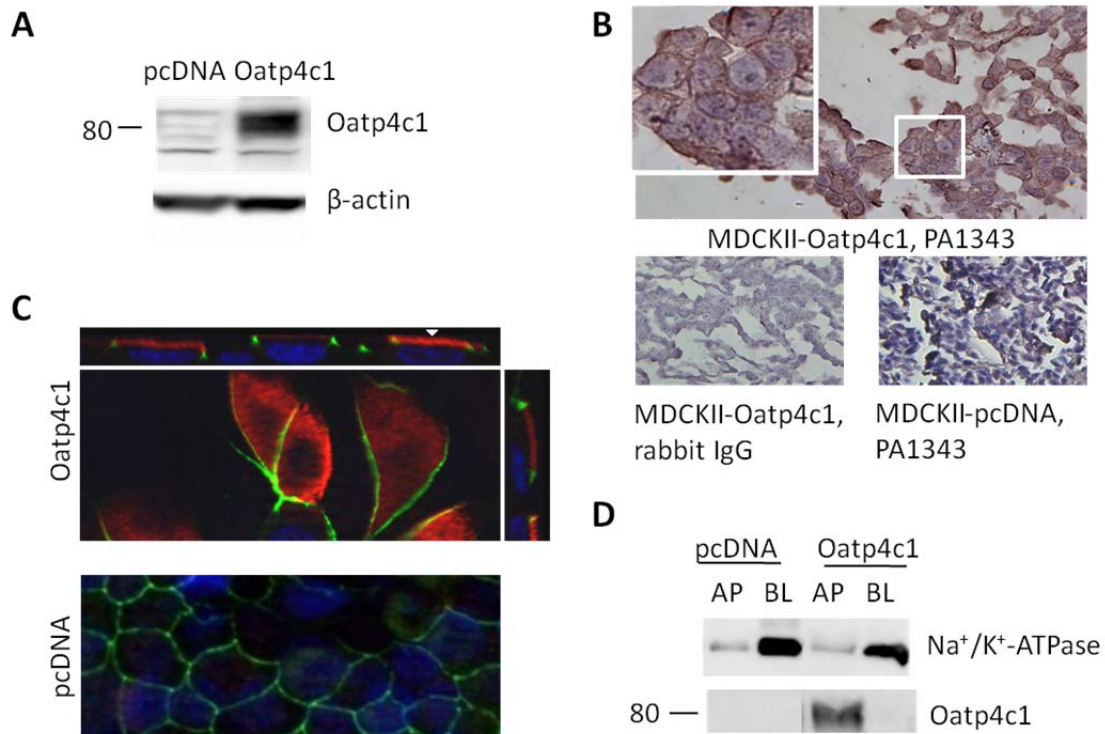


**Figure 4-2: Validation of Oatp4c1 expression and subcellular localization in MDCKII-Oatp4c1 cells.**

(A) Western blot of Oatp4c1 (~ 80 kDa) and  $\beta$ -actin (~42 kDa) in 50  $\mu$ g cell lysates. (B) Immunohistochemical analysis of Oatp4c1 expression in paraformaldehyde-fixed paraffin-embedded cell sections. (C) Confocal microscopy of Oatp4c1 (red) expression and localization in polarized MDCKII cells. Center image in the Oatp4c1 panel is a single optical section of the x-y plane while top and right images represent x-z and y-z planes, respectively, reconstructed from image stacks. The apical and basal sides can be demarcated by Zo-1 (green) and the nuclei (DAPI, blue), respectively, in both x-z and y-z sections. (D) Western blot of Oatp4c1 in proteins isolated from either the apical (AP) or basolateral (BL) membranes of polarized MDCKII cells. Na<sup>+</sup>/K<sup>+</sup>-ATPase served as a BL marker to demonstrate the relative efficiency of AP and BL membrane separation.

Subsequently, we sought to determine the subcellular localization of Oatp4c1 in polarized cell monolayers by confocal immunofluorescence laser scanning microscopy (Figure 4-2 C). A tight-junction protein, Zo-1, was used as an apical marker. As shown in Figure 4-2 C, Oatp4c1 localized at the apical membrane, along with Zo-1, in MDCKII-Oatp4c1 cells. This result was also confirmed by the surface membrane protein biotinylation method. The surface proteins on either apical or basolateral membranes of polarized MDCKII-Oatp4c1 cells were labeled with biotin and isolated from streptavidin agarose beads. Western blot analysis of a basolateral marker  $\text{Na}^+/\text{K}^+$ -ATPase demonstrated the efficient separation of the apical and basolateral membranes. Western blot analysis of Oatp4c1 demonstrated that the transporter was enriched in the apical membrane fraction, but not in the basolateral membrane (Figure 4-2 D). Collectively, these data verified the apical expression of the transporter in Oatp4c1-expressing MDCKII cells. However, there is precedent showing that a transporter can mislocalize in MDCKII cells. Expression studies in MRP4-transfected MDCKII cells show that MRP4 traffics to the basolateral membrane due to low expression of an adaptor protein,  $\text{Na}^+/\text{H}^+$  exchanger regulatory factor 1 (NHERF1), in these cells (118, 119). However, MRP4 polarized correctly in NHERF1 expressing LLC-PK1 cells. While the adaptor proteins facilitating Oatp4c1 trafficking are not known, we transfected LLC-PK1 with pcDNA6.2-Oatp4c1 and determined its polarity. As observed in MDCKII cells, Oatp4c1 also localized to the apical membrane in LLC-PK1 cells (Figure 4-3)

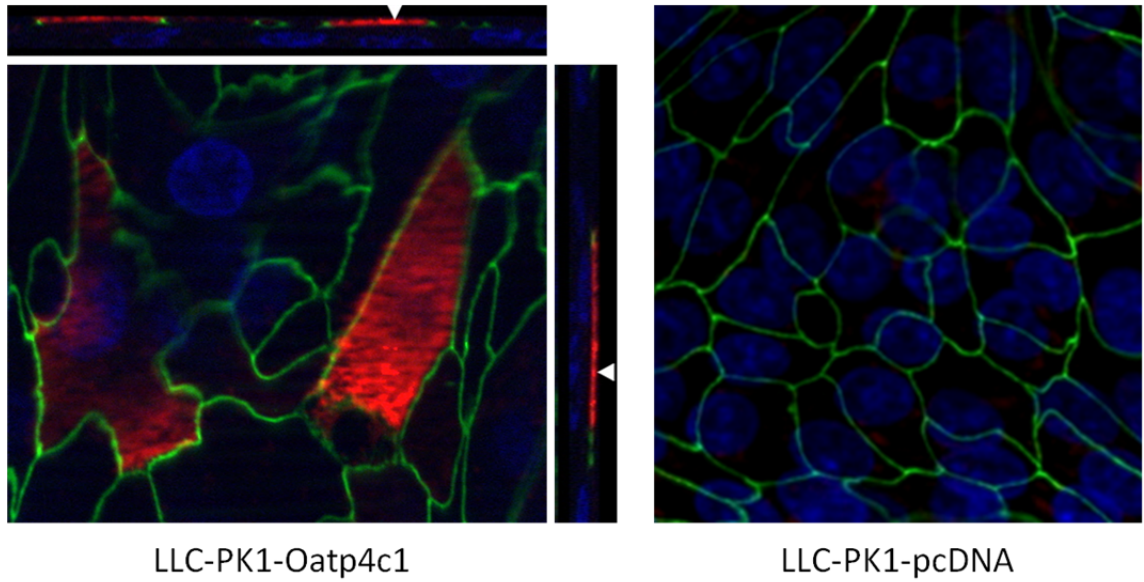


**Figure 4-3: Confocal microscopy of Oatp4c1 expression and subcellular localization in LLC-PK1-Oatp4c1 cells.**

Center image in the Oatp4c1 (red) panel is a single optical section of the x-y plane while top and right images represent x-z and y-z planes, respectively, reconstructed from image stacks. The apical and basal sides can be demarcated by Zo-1 (green) and the nuclei (DAPI, blue), respectively, in both x-z and y-z sections.



Despite successful transfection, our immunofluorescence studies showed that expression was not detectable in at least 97% of the cells (Figure 4-4). Therefore, we attempted to generate a single clone with homogenous high Oatp4c1 expression. Our initial attempt was to sort individual live cells into a 96-well plate by FACS analysis with transient C-terminal-tagged GFP. MDCKII-Oatp4c1 cells were treated with Tag-On-Demand™ Suppressor Supernatant, which decodes the stop codon as serine, allows translation to continue through the downstream reading frame and produces transient C-terminal tagged GFP fusion protein. In this initial attempt, 70 clones were obtained. However, immunofluorescence staining showed none of them exhibited Oatp4c1 expression.

The second attempt was to sort the cells by immunofluorescence labeling. Oatp4c1-expressing cells were labeled with PA1343 (rabbit polyclonal anti-Oatp4c1) and Alexa Fluor 488 goat anti-rabbit IgG, and then sorted with Alexa Fluor 488 fluorescence by FACS analysis. However, none of 110 clones showed Oatp4c1 expression by immunofluorescence staining. The third attempt was to randomly seed individual live cells in 96-well plates. Unfortunately, none of 220 clones showed Oatp4c1 expression by immunofluorescence staining. It has previously been demonstrated that the expression of foreign protein in recombinant cells decreases the cell proliferation rate (120, 121). Expressing foreign protein utilizes host cell's resources and imposes a metabolic burden (metabolic load) on the host cells, which may change the physiology and biochemistry of the cells. This led us to hypothesize that the expression of Oatp4c1 decreases the cell proliferation rate and this effect is magnified when expanding from a single cell. In this case, single cells expressing the protein were perhaps not dividing during the time we were expanding the single clones.

Therefore, the fourth attempt was to generate the clones starting from more than one cell using the serial dilution method. Finally, out of 100 clones, 15 showed Oatp4c1 expression by immunofluorescence staining. Among them, clone 94 (c94) had more cells exhibiting Oatp4c1 expression as compared to the pooled cells (Figure 4-4). This clone was selected to use for uptake studies in Specific Aim 3a and Specific Aim 3b.

Despite multiple efforts and approaches to generate this single clone of Oatp4c1-expressing MDCKII cells (c94), immunofluorescence staining showed that expression was detectable in only ~11% of the cells determined by manual counting. To increase Oatp4c1 expression, we sought to treat the cells with sodium butyrate, simvastatin, glycerol, MG132 or increase the concentration of the selection antibiotic, blasticidin. Oatp4c1 expression was determined by PCR, Western blotting and immunofluorescence staining.

Sodium butyrate is commonly used to induce protein expression (122, 123). In this study, MDCKII-pcDNA and MDCKII-Oatp4c1 pooled cells were treated with 0.1 - 5 mM sodium butyrate for 24 hr. Oatp4c1 expression was increased by sodium butyrate in a concentration-dependent manner at mRNA (Figure 4-5 A) and protein (Figure 4-5 B) levels. However, the number of cells exhibiting Oatp4c1 expression was not remarkably increased with sodium butyrate treatment (Figure 4-5 C). In addition, since sodium butyrate was reported to disrupt basolateral localization of overexpressed Na<sup>+</sup>/K<sup>+</sup>-ATPase  $\beta_1$ - and  $\beta_2$  subunits in MDCK I cells (124), we wanted to ensure that induced expression did not interfere with the subcellular localization of Oatp4c1. Immunofluorescence staining was performed and demonstrated that the apical polarity was maintained (Figure 4-5 D).

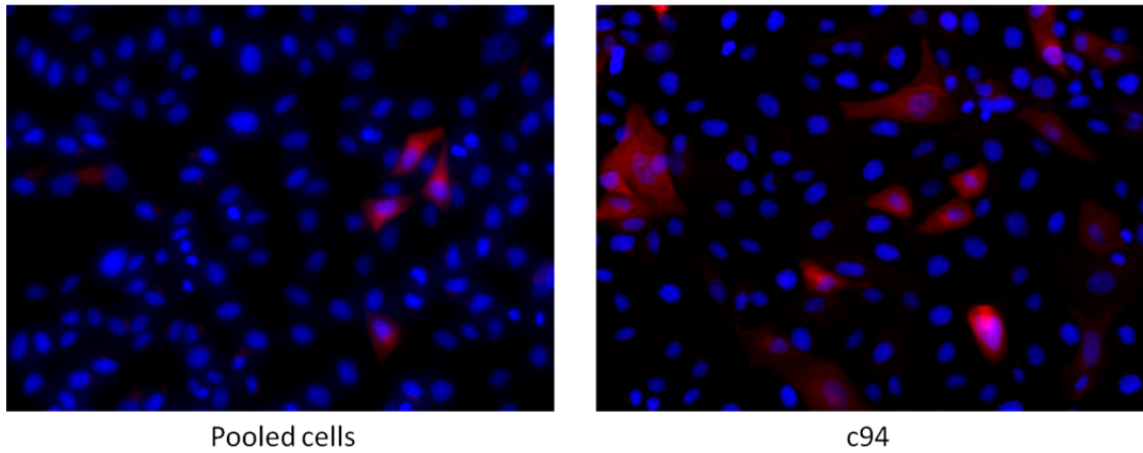


**Figure 4-4: Immunofluorescence staining for Oatp4c1 expression in MDCKII-Oatp4c1 pooled cells and c94.**

Oatp4c1 and nuclei were stained with PA1343 (red) and DAPI (blue), respectively.

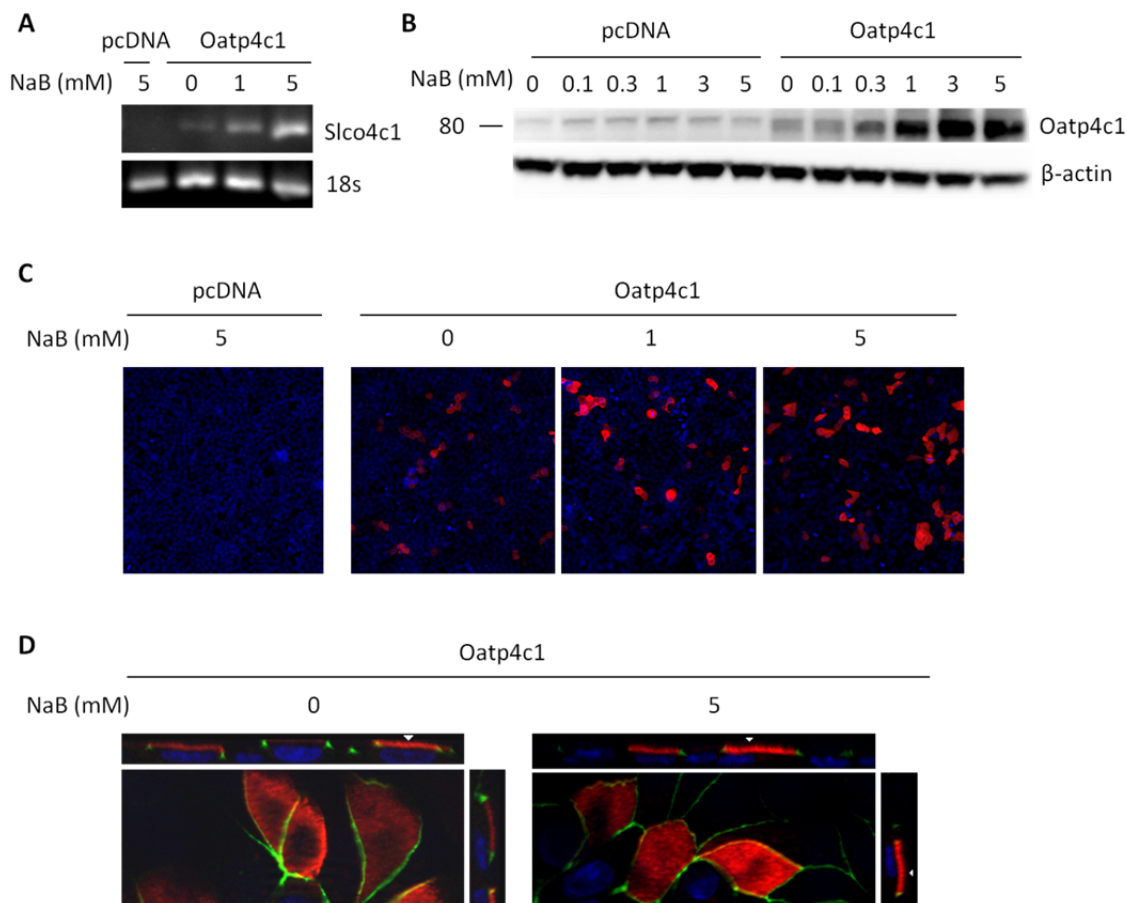


**Figure 4-5: Effect of 24 hr sodium butyrate (NaB) treatment on Oatp4c1 expression and subcellular localization in MDCKII-Oatp4c1 pooled cells.**

(A) PCR and agarose gel electrophoresis of Slco4c1 and 18s rRNA (loading control). (B) Western blot of Oatp4c1 (~80 kDa) and β-actin (~42 kDa) in cell lysates (40 μg protein). (C) Immunofluorescence staining for Oatp4c1 expression (red). (D) Confocal microscopy of Oatp4c1 (red) expression and localization in polarized cells. Center image in the Oatp4c1 panel is a single optical section of the x-y plane while top and right images represent x-z and y-z planes, respectively, reconstructed from image stacks. The apical and basal sides can be demarcated by Zo-1 (green) and the nuclei (DAPI, blue), respectively, in both x-z and y-z sections.

The second approach to enhance Oatp4c1 expression was to increase the selection antibiotic, blasticidin, concentration from 5 µg/ml to 10 or 30 µg/ml. MDCKII-pcDNA and MDCKII-Oatp4c1 cells were grown in designated concentration of blasticidin for 2 passages. Oatp4c1 expression was higher in the cells grown in 10 or 30 µg/ml blasticidin than those in 5 µg/ml blasticidin at mRNA (Figure 4-6 A) and protein (Figure 4-6 B) levels, and achieved a maximum at 10 µg/ml. The number of cells exhibiting Oatp4c1 expression was slightly enhanced with increasing blasticidin concentration (Figure 4-6 C).

A promoter analysis showed *SLCO4C1* promoter region has xenobiotic-responsive element (XRE) motifs (106), which are generally recognized by aryl hydrocarbon receptors (AhR) and AhR nuclear translocator heterodimer (108). Simvastatin, an inducer of nuclear AhR, can enhance promoter activity and upregulate *SLCO4C1* expression (106). MDCKII-pcDNA and MDCKII-Oatp4c1 cells were treated with 10 or 20 µM of simvastatin for 24 hr. *Slco4c1* mRNA expression was increased by simvastatin in a concentration-dependent manner (Figure 4-7 A), but this did not lead to changes in protein expression (Figure 4-7 B). Additionally, the number of cells exhibiting Oatp4c1 expression was not changed with simvastatin treatment (Figure 4-7 C).

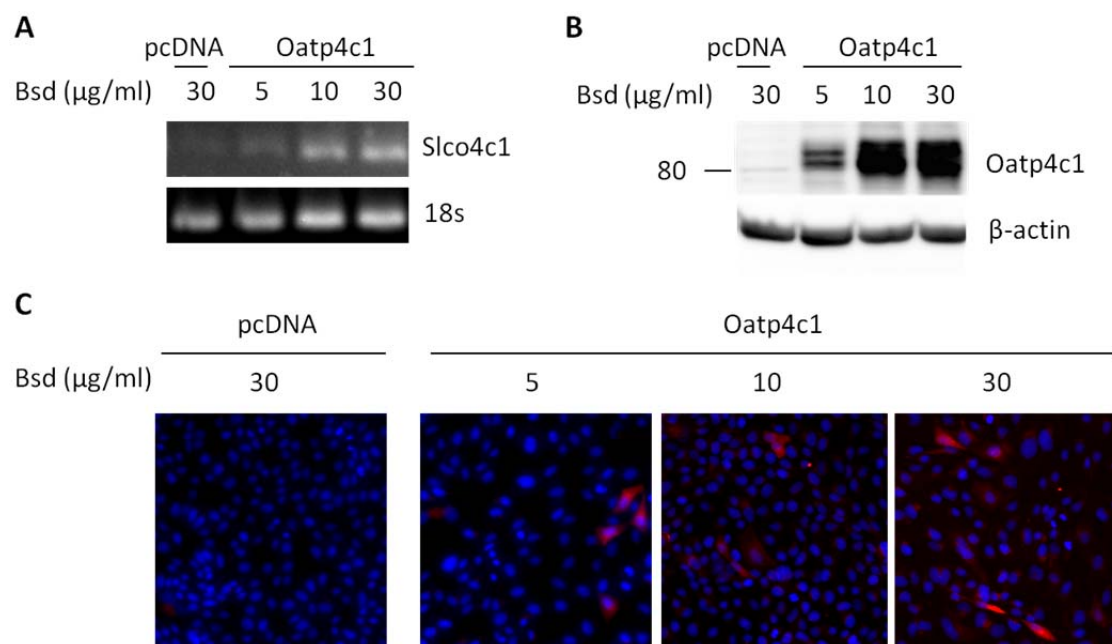


**Figure 4-6: Effect of increasing blasticidin (Bsd) concentration for two passages on Oatp4c1 expression in MDCKII-Oatp4c1 pooled cells.**

(A) PCR and agarose gel electrophoresis of Slco4c1 and 18s rRNA (loading control). (B) Western blot of Oatp4c1 (~80 kDa) and β-actin (~42 kDa) in cell lysates (40 μg protein). (C) Immunofluorescence staining for Oatp4c1 expression (red).

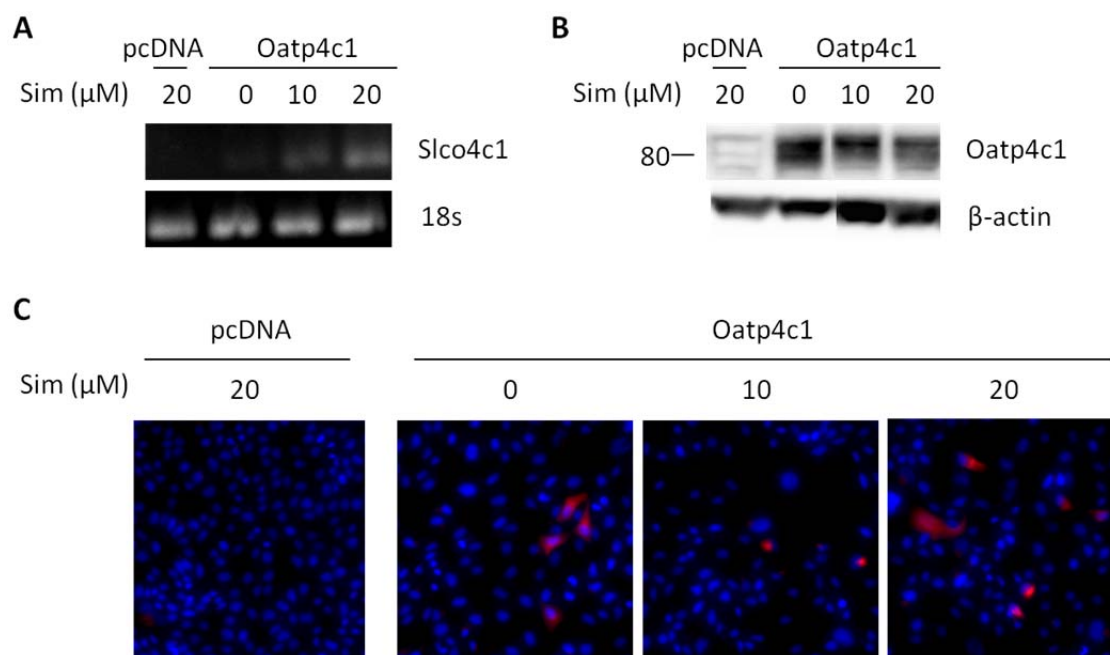


**Figure 4-7: Effect of 24 hr simvastatin (Sim) treatment on Oatp4c1 expression in MDCKII-Oatp4c1 pooled cells.**

(A) PCR and agarose gel electrophoresis of Slco4c1 and 18s rRNA (loading control). (B) Western blot of Oatp4c1 (~80 kDa) and  $\beta$ -actin (~42 kDa) in cell lysates (40  $\mu$ g protein). (C) Immunofluorescence staining for Oatp4c1 expression (red).

Primary amino acid sequence of rat Oatp4c1 showed a considerably higher number of cysteine residues (27 cysteine/724 amino acids) as compared with other transporters, such as ABCG2 (12 cysteine/655 amino acids), p-glycoprotein (7 cysteine/1279 amino acids) or MRP4 (11 cysteine/859 amino acids). Disulfide bonds between cysteine residues in proteins play a key role in protein folding. More cysteine residues may cause more turns or folding, and the protein may be more difficult to be properly folded. Therefore, we hypothesized that most of Oatp4c1 in the transfected MDCKII cells is misfolded so that scarce number of cells exhibit Oatp4c1 expression. Misfolded proteins fail to traffic from endoplasmic reticulum (ER) via the Golgi apparatus to plasma membrane, and are targeted for degradation via the ubiquitin/proteasome-dependent pathway. In an attempt to rescue misfolded proteins, we treated the cells with the chemical chaperone, glycerol or the proteasome inhibitor, MG132.

Glycerol is a chemical chaperone, and stabilizes misfolded proteins into conformations that are not targeted for degradation and can escape the ER (125, 126). In this study, MDCKII-pcDNA and MDCKII-Oatp4c1 cells were treated with 0.5 - 1.5 M glycerol for 48 hr. However, glycerol decreased Oatp4c1 expression, and did not change the number of cells exhibiting Oatp4c1 expression (Figure 4-8).

N-benzoyloxycarbonyl (Z)-Leu-Leu-leucinal (MG132) is a proteasome inhibitor, and can prevent misfolded proteins, which are retained in the ER from being targeted for premature proteolysis. In this study, MDCKII-pcDNA and MDCKII-Oatp4c1 cells were treated with MG132 (0.1  $\mu$ M for 24 hr or 10  $\mu$ M for 12 hr). However, MG132 decreased Oatp4c1 expression, and did not change the number of cells exhibiting Oatp4c1 expression (Figure 4-9).



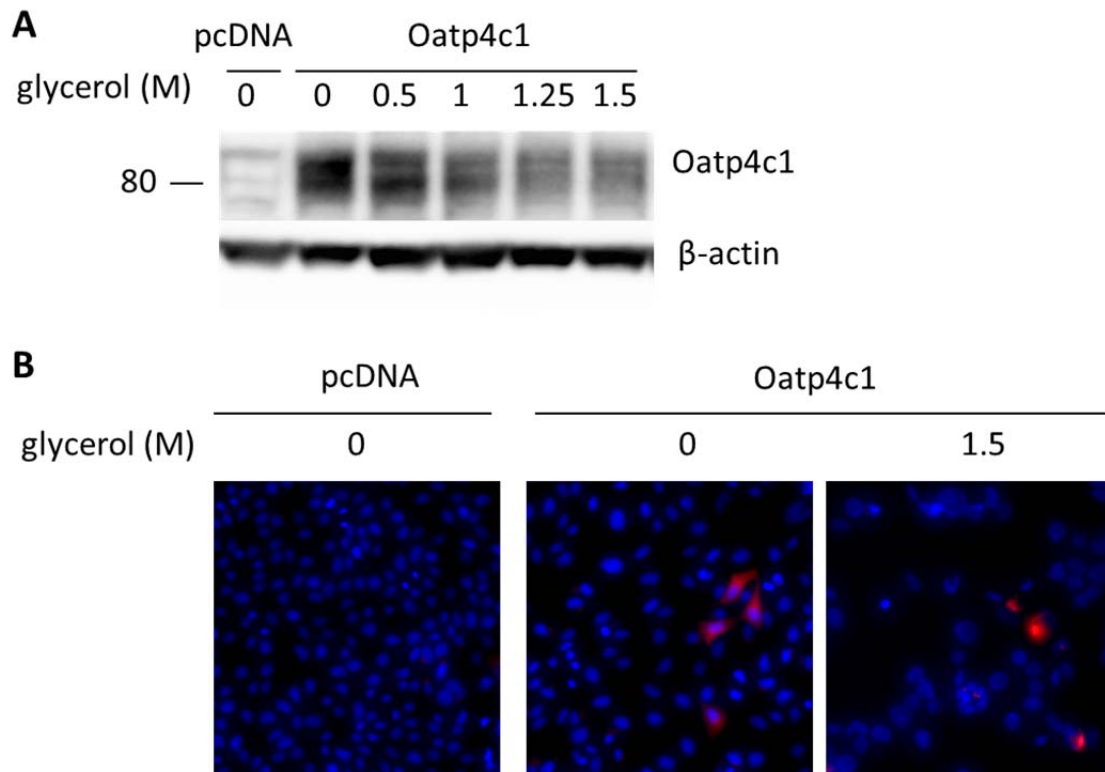


**Figure 4-8: Effect of 48 hr glycerol treatment on Oatp4c1 expression in MDCKII-Oatp4c1 pooled cells.**

(A) Western blot of Oatp4c1 (~80 kDa) and  $\beta$ -actin (~42 kDa) in cell lysates (40  $\mu$ g protein). (B) Immunofluorescence staining for Oatp4c1 expression (red).

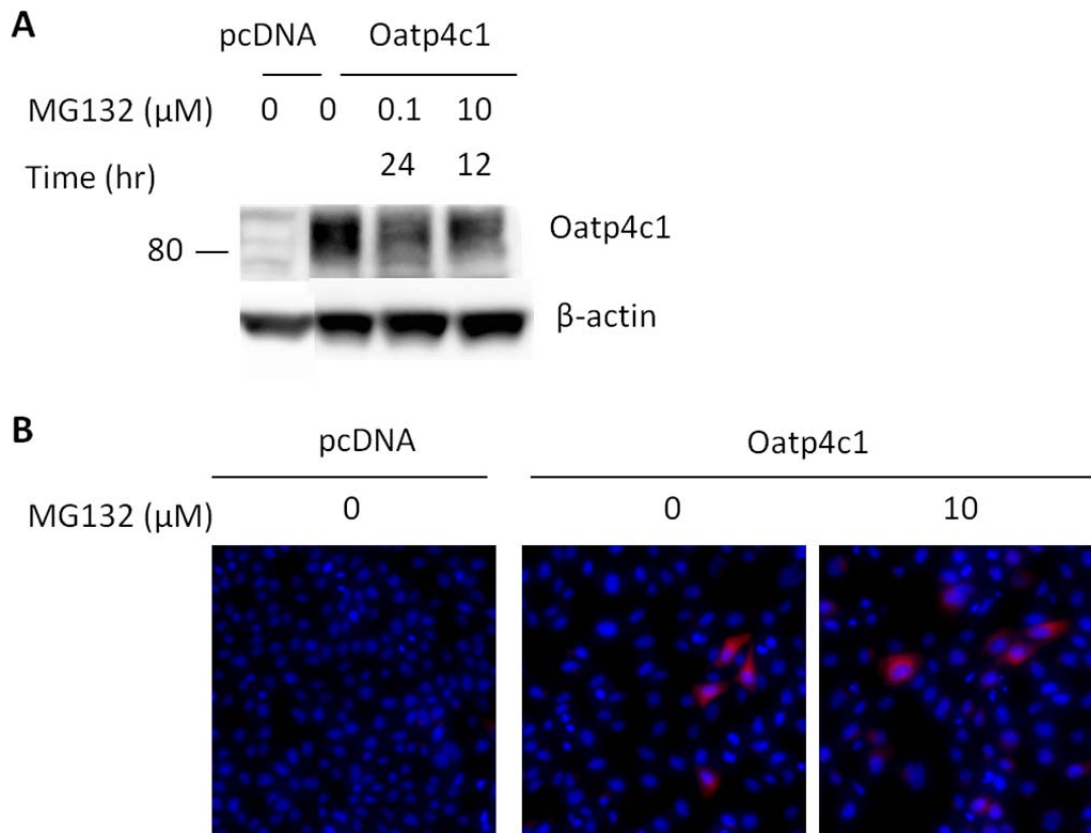


**Figure 4-9: Effect of MG132 treatment on Oatp4c1 expression in MDCKII-Oatp4c1 pooled cells.**

(A) Western blot of Oatp4c1 (~80 kDa) and  $\beta$ -actin (~42 kDa) in cell lysates (40  $\mu$ g protein). (B) Immunofluorescence staining for Oatp4c1 expression (red).

In summary, Oatp4c1 expression was enhanced by sodium butyrate treatment or increasing blasticidin concentration, but not by simvastatin, glycerol or MG132 treatment. To optimize growth conditions to obtain the highest Oatp4c1 expression, MDCKII-Oatp4c1 pooled cells and c94 were treated with 5 mM sodium butyrate or 30 µg/ml blasticidin or both. As shown in Figure 4-10, the impact of sodium butyrate on inducing Oatp4c1 expression was substantial, so that the effect of blasticidin was negligible. The substantially higher Oatp4c1 expression in c94 than in pooled cells was also demonstrated. Finally, after multiple efforts and approaches, as compared with the pooled cells, the number of cells exhibiting Oatp4c1 expression in c94 with sodium butyrate treatment was substantially higher (Figure 4-11). Therefore, to achieve the highest Oatp4c1 expression, c94 prior treated with sodium butyrate were applied for the following uptake studies described in Specific Aim 3a and Specific Aim 3b.

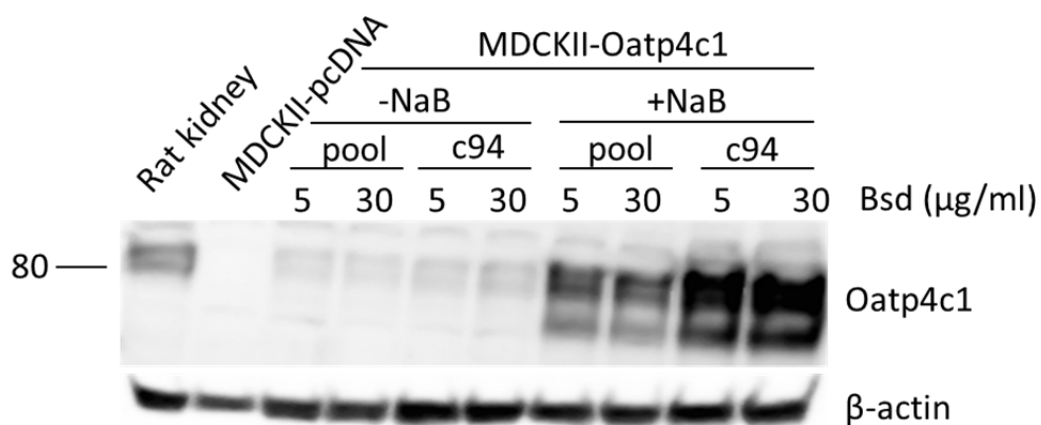


**Figure 4-10: Effect of sodium butyrate (NaB, 5 mM) and blasticidin (Bsd, 30 μg/ml) on Oatp4c1 expression in MDCKII-Oatp4c1 pooled cells and c94.**

Western blot of Oatp4c1 (~80 kDa) and β-actin (~42 kDa) in cell lysates (40 μg protein).

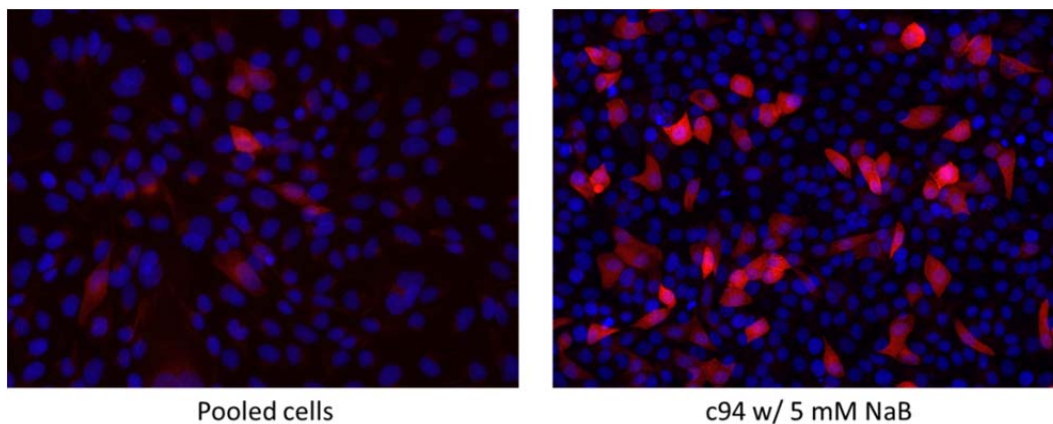


**Figure 4-11: Immunofluorescence staining for Oatp4c1 expression in MDCKII-Oatp4c1 pooled cells and sodium butyrate (NaB) treated c94.**

Oatp4c1 and nuclei were stained with PA1343 (red) and DAPI (blue), respectively.

## B. Determination of Oatp4c1 expression and subcellular localization in rat tissues

1. Specific Aim 1c: To determine the expression and subcellular localization of Oatp4c1 in the rat tissues (liver, kidney, lactating and non-lactating mammary gland).

Microarray analysis of various transporters expressed in lactating MEC isolated from breast milk and non-lactating MEC isolated from surgical reduction mammoplasty specimen showed that human *SLCO4C1* is increased 70-fold in lactating MEC relative to non-lactating MEC. The upregulation of *SLCO4C1* expression during lactation has been confirmed by qRT-PCR (30). This phenomenon was also confirmed in rats by qRT-PCR (Figure 4-12 A) and Western blotting (Figure 4-12 B). Liver and kidney served as a negative and positive control, respectively, and has been demonstrated by Northern analysis (79). Oatp4c1 was expressed in the rat kidney and lactating MG, but not in the rat liver and non-lactating MG. This result was confirmed by Western blotting (Figure 4-12 B). A single band was detected at ~80 kDa in the rat kidney, and at a slightly lower molecular weight in the rat MG, and both of the bands were reduced to ~65 kDa after deglycosylation. In accord with the mRNA expression, no protein band was detected in the rat liver and non-lactating MG. The specific band reactivity was confirmed by pre-absorbing the antibody with antigen peptide (STITVEEDLNKIENEG) prior to use. The bands were abolished after antigen peptide blocking (Figure 4-12 C).

In addition, the ontogeny of Oatp4c1 in rat kidney (Figure 4-13) and liver (Figure 4-14) was investigated. In rat kidney, *Slco4c1* mRNA expression was minimal at birth and then gradually increases to adult levels (Figure 4-13 A), and

this was confirmed by Western blotting (Figure 4-13 B). This phenomenon was consistent with the ontogenic expression of *Slco4c1* in mouse kidney (52). In addition, higher Oatp4c1 expression was observed in non-lactating female rat kidney as compared with males at both mRNA and protein levels, but it was inconsistent with the previous finding showing no gender differences of *Slco4c1* mRNA expression in the rat kidney (79). Neither *Slco4c1* mRNA (Figure 4-14 A) nor Oatp4c1 protein (Figure 4-14 B) were detected in rat livers of pups or adults across the ages.

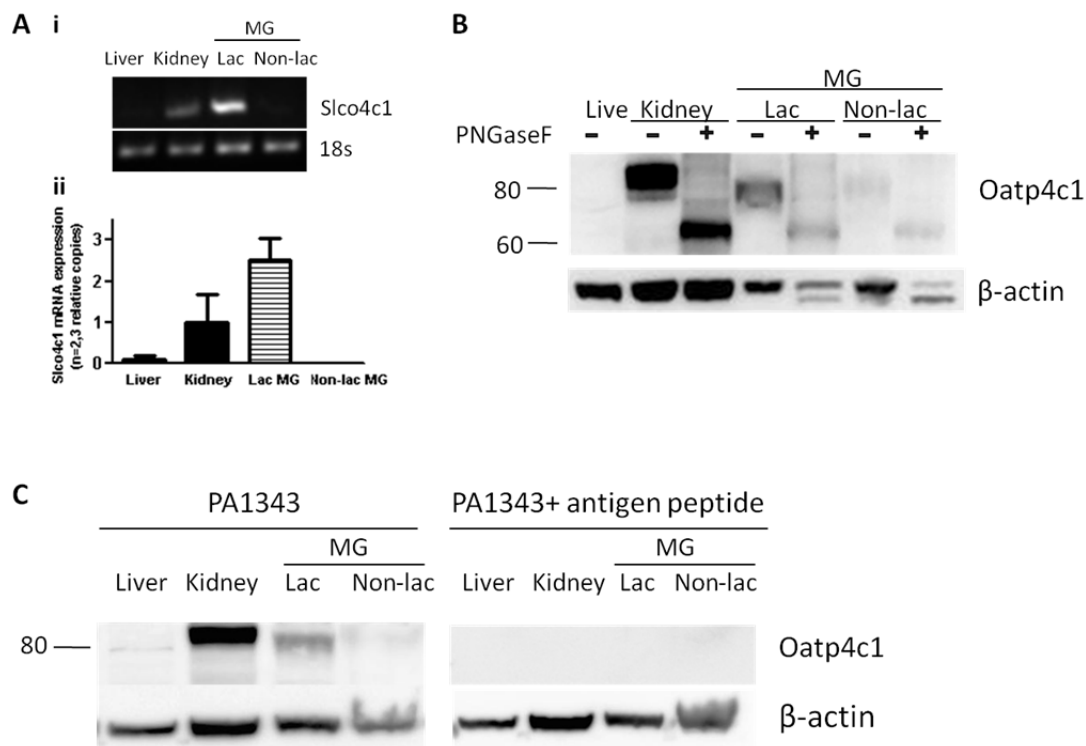


**Figure 4-12: Oatp4c1 expression in female adult rat liver, kidney, lactating and non-lactating MG.**

(A) i. qRT-PCR and agarose gel electrophoresis analysis for *Slco4c1* mRNA and 18s rRNA (loading control) expression in rat tissues. ii. Relative *Slco4c1* mRNA expression normalized with 18s rRNA. Each bar represents the mean  $\pm$  S.D (n=2 (liver) or 3). (B) Western blot of native (~80 kDa), deglycosylated (~60 kDa) Oatp4c1 and  $\beta$ -actin (~42 kDa) in rat tissue crude membrane fractions (40  $\mu$ g protein). PNGaseF was used for deglycosylation. (C) Western blot of Oatp4c1 and  $\beta$ -actin in rat tissue crude membrane fractions (40  $\mu$ g protein) with and without antigen peptide blocking. Lac: lactating, Non-lac: non-lactating

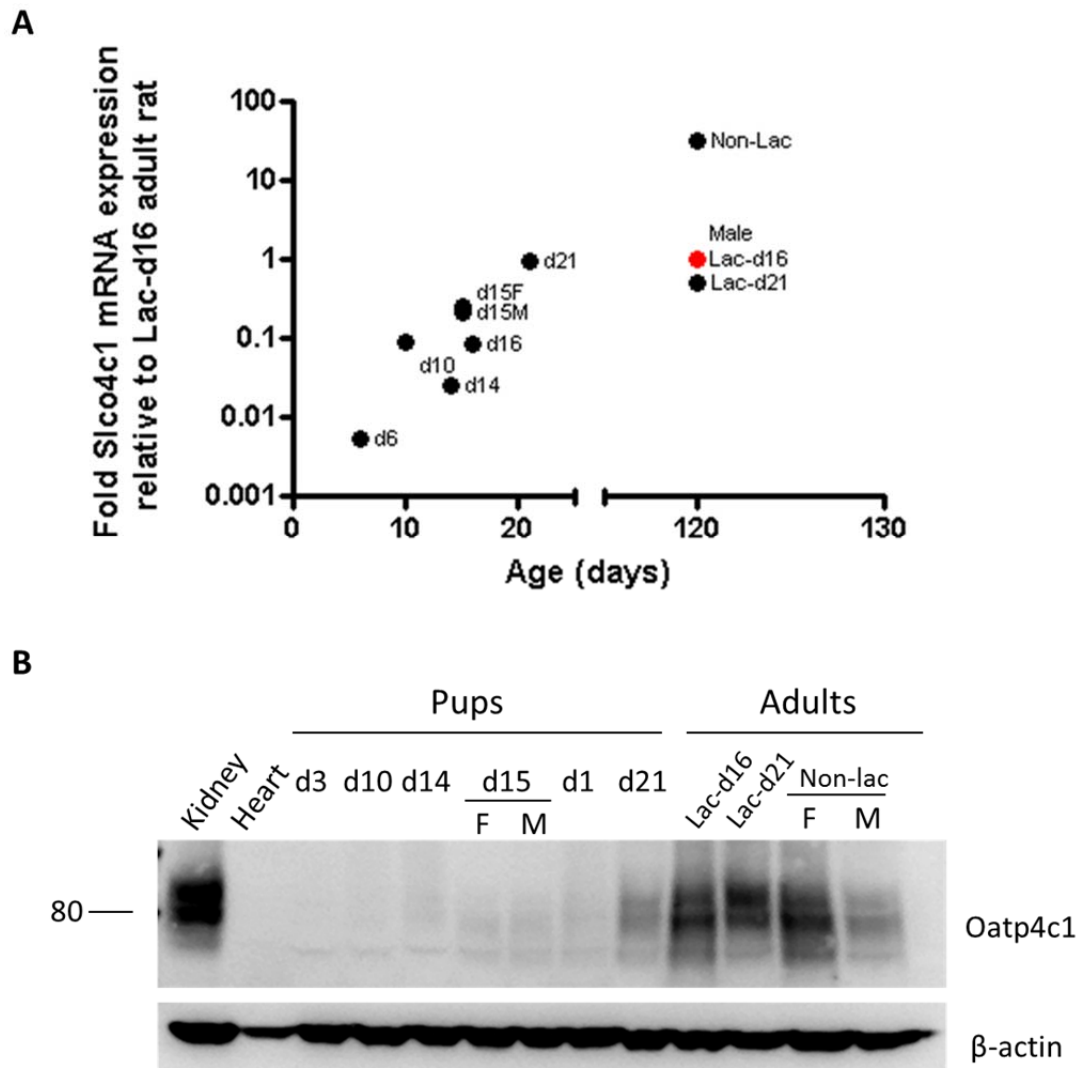


**Figure 4-13: Ontogeny of Oatp4c1 in rat kidney.**

(A) Relative *Slco4c1* mRNA expression calculated with  $2^{-\Delta\Delta C_t}$  method. Relative copy number of *SLCO4C1* in the samples was normalized to 18s rRNA within each sample and values were then normalized with those in lac-d16 kidney. Each dot represents the mean of three determinations from one rat. (B) Western blot of Oatp4c1 (~80 kDa) and  $\beta$ -actin (~42 kDa) in rat tissue crude membrane fractions (40  $\mu$ g protein). Lac-d16: rats had been lactating for 16 days, Lac-d21: rats had been lactating for 21 days, Non-lac: non-lactating, F: female, M; male



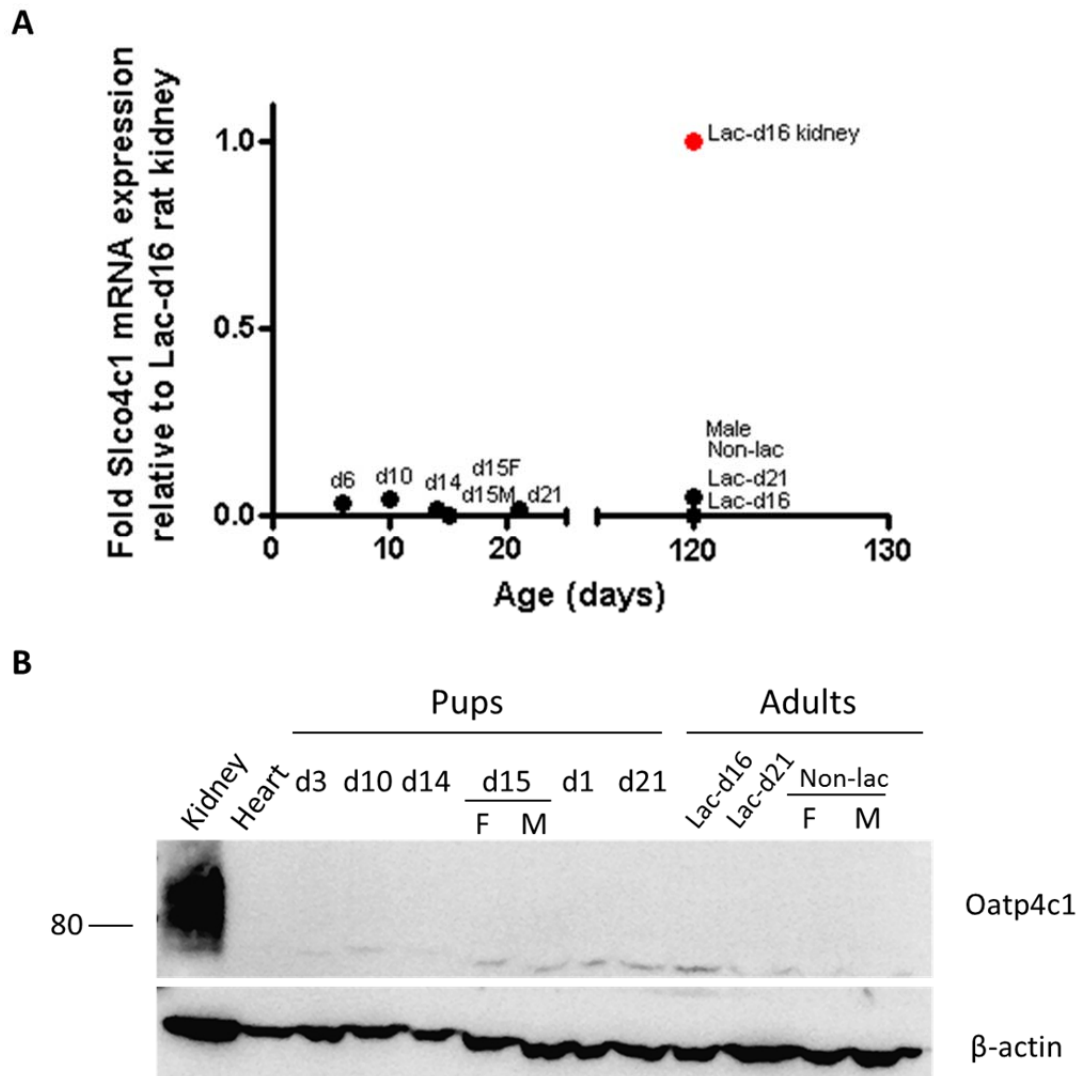


**Figure 4-14: Ontogeny of Oatp4c1 in rat liver.**

(A) Relative *Slco4c1* mRNA expression calculated with  $2^{-\Delta\Delta C_t}$  method. Relative copy number of *SLCO4C1* in the samples was normalized to 18s rRNA within each sample and values were then normalized with those in lac-d16 kidney. Each dot represents the mean of three determinations from one rat. (B) Western blot of Oatp4c1 (~80 kDa) and  $\beta$ -actin (~42 kDa) in rat tissue crude membrane fractions (40  $\mu$ g protein). Lac-d16: rats had been lactating for 16 days, Lac-d21: rats had been lactating for 21 days, Non-lac: non-lactating, F: female, M: male.

The subcellular localization of Oatp4c1 was then assessed by immunohistochemical analysis in paraformaldehyde-fixed paraffin-embedded liver, kidney and MG tissue sections. To assure the quality of the tissue specimens, the rat liver and MG sections were stained with anti-Abcg2 antibody, and the rat kidney sections were stained with anti-Mrp4 antibody. All tissues showed specific staining. Consistent with the PCR and Western blot results (Figure 4-12 A, B), Oatp4c1 was not detected in the rat liver, but Oatp4c1 stained strongly in apical membranes of kidney tubules and MG (Figure 4-15). No staining was observed in tissue sections exposed to rabbit IgG, instead of primary antibody, and Oatp4c1 staining was abolished when probing with antibody that was pre-adsorbed with antigen peptide (Figure 4-16). The distinct apical expression of Oatp4c1 in rat kidney was also demonstrated using dual staining for a basolateral marker E-cadherin (127) and Oatp4c1 (Figure 4-17).

Because these results were in contrast to the reported expression pattern of Oatp4c1 in the rat kidney, we developed additional antibodies, including the polyclonal antibody reported previously (79). As shown in Figure 4-16, apical expression was confirmed using three different antibodies (PA1254, F3608 and PA1562), however, we were not able to observe any staining, above background levels, with the antibody reported previously (79).

In rat MG, the apical expression of Oatp4c1 was demonstrated by colocalization of Oatp4c1 and an apical marker Abcg2 (10) and distinct localization of Oatp4c1 and a basolateral marker E-cadherin (128) (Figure 4-18).

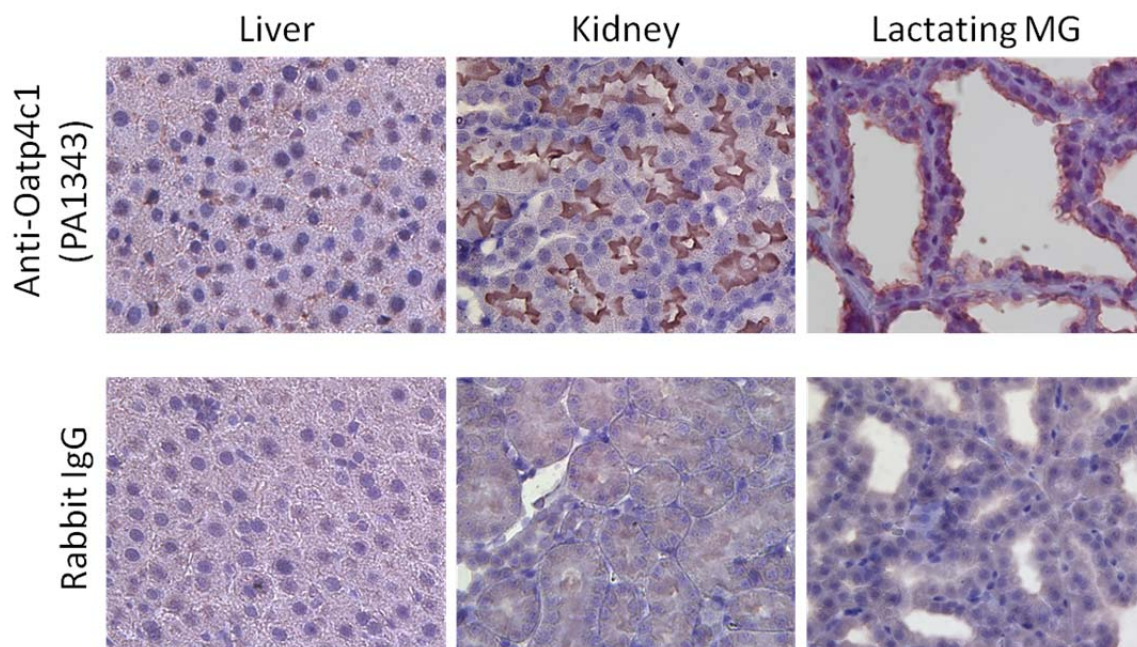


**Figure 4-15: Oatp4c1 localization in rat liver, kidney and lactating MG.**

Immunohistochemical analysis for Oatp4c1 subcellular localization in paraformaldehyde-fixed paraffin-embedded rat tissue sections. Oatp4c1 was detected with PA1343. Rabbit IgG was used as a negative control. Magnification: 40x.

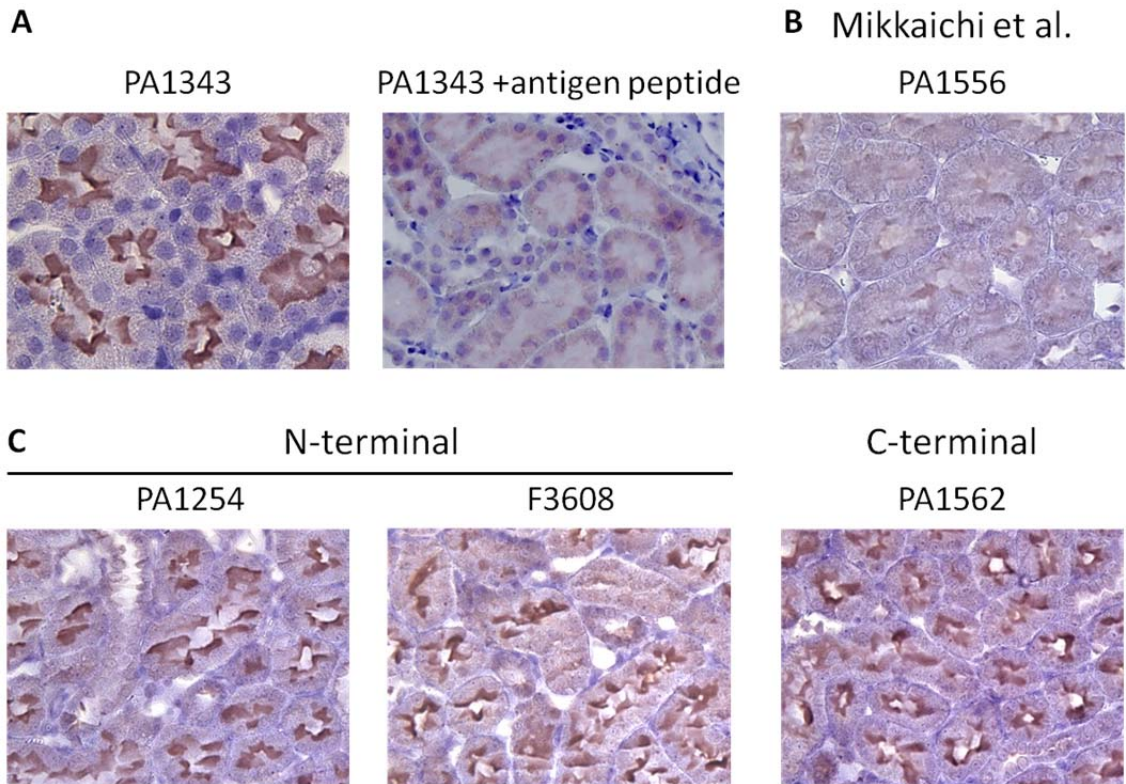


**Figure 4-16: Verification of apical Oatp4c1 localization in rat renal tubules by four different antibodies.**

Immunohistochemical analysis for Oatp4c1 subcellular localization in paraformaldehyde-fixed paraffin-embedded rat kidney sections with rabbit polyclonal anti-Oatp4c1 antibodies as indicated. A. Antibody specificity (PA1343) was demonstrated by pre-absorbing PA1343 with antigen peptide (STITVEEDLNKIENEG) overnight at 4°C prior to use. Magnification: 40x.

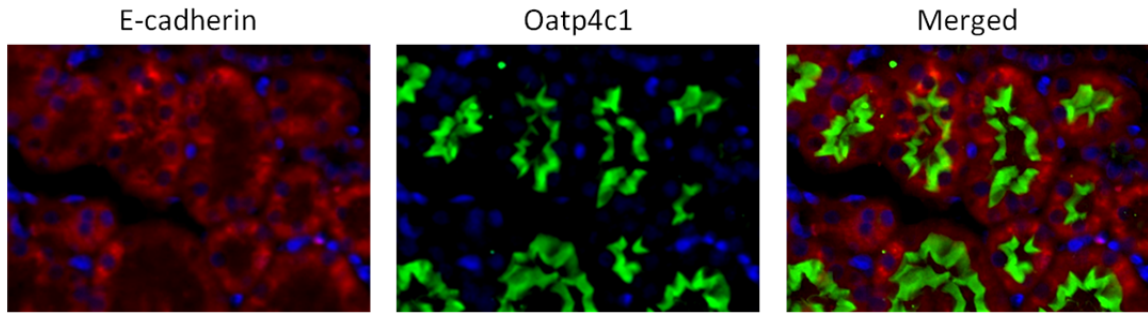


**Figure 4-17: Double immunofluorescence staining for Oatp4c1 (green) and E-cadherin (red) in rat kidney.**

E-cadherin served as a basolateral marker. Magnification: 40x.

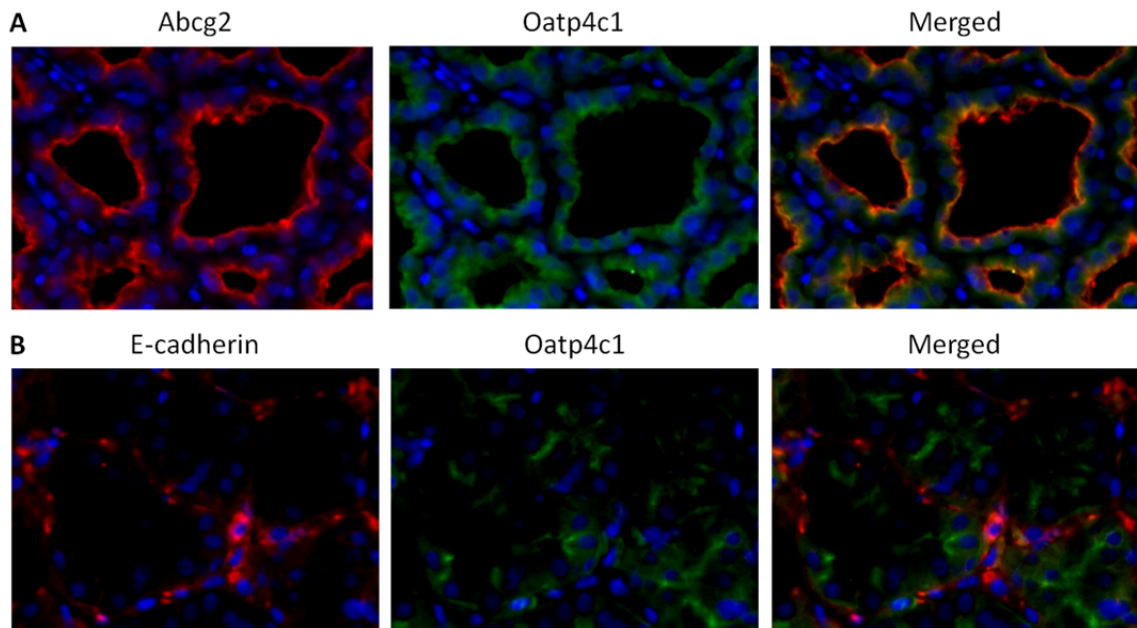


**Figure 4-18: A. Double immunofluorescence staining for Oatp4c1 (green) and Abcg2 (A, red) or E-cadherin (B, red) in rat lactating MG.**

Abcg2 and E-cadherin served as apical and basolateral marker, respectively. Magnification: 40x.

2. Specific Aim 2a: To verify the apical localization of Oatp4c1 in the rat kidney cortex by proteomic analysis in the isolated brush-border membrane (BBM) and basolateral membrane (BLM).

Concurrently with the studies outlined in Figure 4-16, we wanted to definitively demonstrate the specificity of our PA1343 antibody used for Western blot and immunolocalization of Oatp4c1. Proteomic analysis was performed on proteins collected from BBM and BLM, which were isolated from rat kidney cortex by Percoll density gradient. Western blotting (Figure 4-19 A) and proteomic analysis (Figure 4-19 B) were applied to analyze the proteins in these two fractions. Abcg2 and Mrp4 were used as apical markers, which were enriched in BBM. Na<sup>+</sup>/K<sup>+</sup>-ATPase, a basolateral marker (127), was detectable in both membrane fractions, but more so in BLM than BBM. Oatp4c1 was detected in BBM but not in BLM (Figure 4-19 A), which was consistent with immunohistochemistry results (Figure 4-15).

To validate the specificities of our antibodies, the proteome in BBM and BLM were each analyzed by LC-MS/MS following separation by SDS-PAGE. The gel bands of proteins eluting at 65-100 and 100-150 kDa were excised, and underwent reduction, alkylation, and in-gel trypsin digestion (116, 117). The abundance of the identified proteins was determined by the total number of spectra identified from a protein (spectral counts, SC) (129, 130), and SC > 2 was used as the cutoff. The proteins with molecular weight less than 65 kDa or more than 150 kDa were excluded. The LC-MS/MS analysis identified 6 proteins unique to the BBM, 19 proteins unique to the BLM, and 56 proteins were either enriched in one membrane or equally distributed in both membrane preparations. Among them, the spectral counts of the SLC and ABC family with reported



localization, along with the apical marker (meprin) and basolateral marker ( $\text{Na}^+/\text{K}^+$ -ATPase) are shown in Figure 4-19 B. Eleven apical proteins were predominantly in the BBM, four basolateral proteins were enriched in the BLM, and three proteins with previously reported apical localization were found in both fractions (ambiguous). Four unique peptides of Oatp4c1 (GVENPAFVPSSPDTPRR; RASASPSQVEVSAVASR; TSQTHQNNSTSFQHMDENFGK; KVDITSTAXSPDFEAR) were found only in the BBM and not in the BLM. These qualitative data provide additional and conclusive evidence that Oatp4c1 localizes at the apical membrane in the rat kidney cortex.

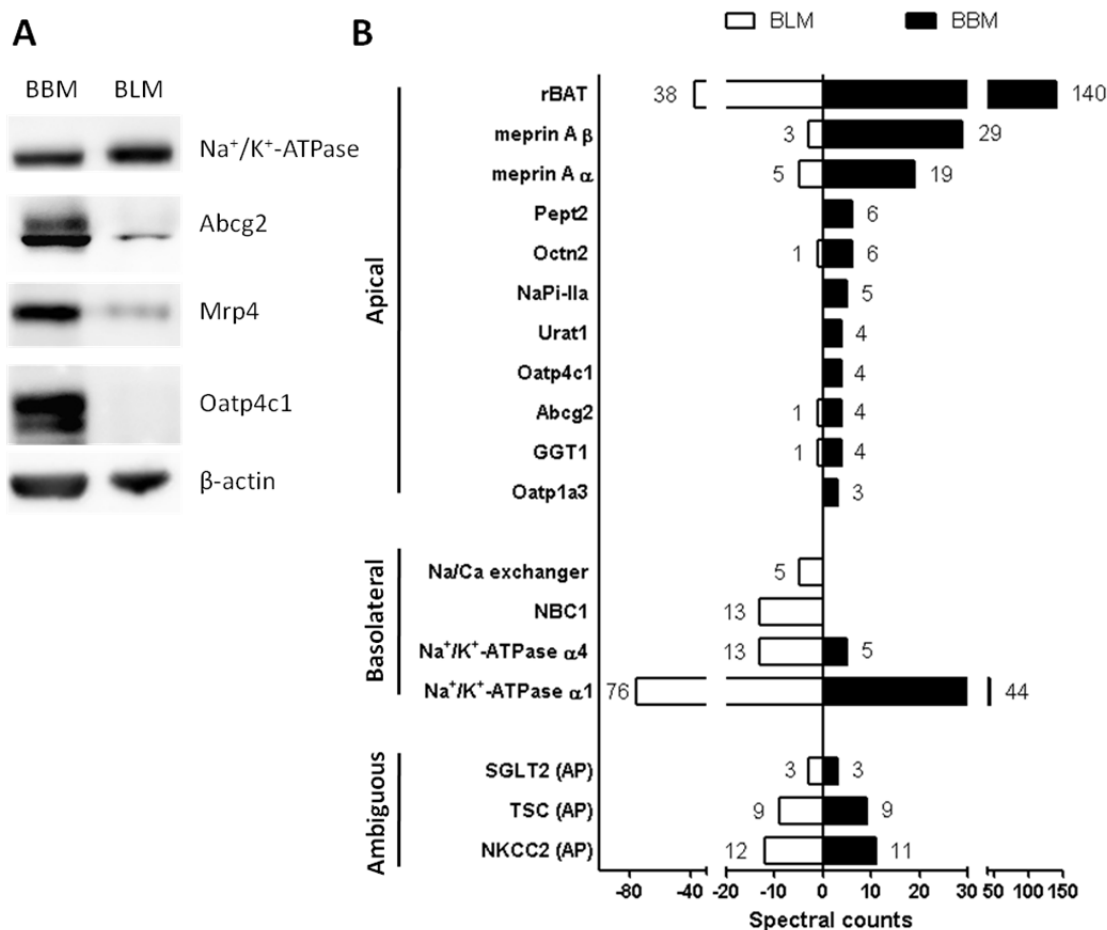


**Figure 4-19: Expression of Oatp4c1 in isolated kidney brush border membrane (BBM) and basolateral membrane (BLM) fractions.**

(A) Western blot of Oatp4c1 in BBM and BLM fractions (20 µg protein) isolated from rat kidney cortex. Na<sup>+</sup>/K<sup>+</sup>-ATPase α 1 was used as a basolateral marker. Abcg2 and Mrp4 served as apical markers. Oatp4c1 was detected with PA1343. (B) Spectral counts detected in protein digests obtained from ~65-150 kDa sections excised from the SDS-PAGE gel. Proteins with 3 or more spectral counts in one fraction are presented as “Apical” or “Basolateral” based on previously published literature. Spectral counts indicate the number of unique peptides detected in each fraction.



3. Specific Aim 2b: To determine the precise expression pattern of Oatp4c1 at the organ and nephron level.

To further gain insight on the potential physiological role of Oatp4c1, we assessed its precise expression pattern at the organ and nephron level. Immunohistochemical analysis (Figure 4-20) showed that Oatp4c1 is expressed densely in the renal tubules located in the juxtamedullary cortex. To ascertain its location within the tubule, we used double immunofluorescence to stain for Oatp4c1 and the proximal tubule marker, aquaporin 1 (AQP1) (131), or a distal tubule marker, calbindin-D<sub>28K</sub> (132). As shown in Figure 4-21, Oatp4c1 colocalized with AQP1, but not with calbindin-D<sub>28K</sub>. Therefore, Oatp4c1 is expressed in the proximal tubule within the juxtamedullary cortex, which suggests that it localizes in the proximal straight tubules (S3). Double immunofluorescence staining was also used to access the location of Oatp4c1 relative to major apical efflux transporters in the rat kidney. As shown in Figure 4-22, Mrp4 was expressed in the superficial cortex (S1, S2) and did not colocalize with Oatp4c1. P-gp was expressed in the juxtamedullary cortex (S3) and colocalized with Oatp4c1. Abcg2 was expressed in the whole cortex (S1, S2, S3) and partially colocalized with Oatp4c1.

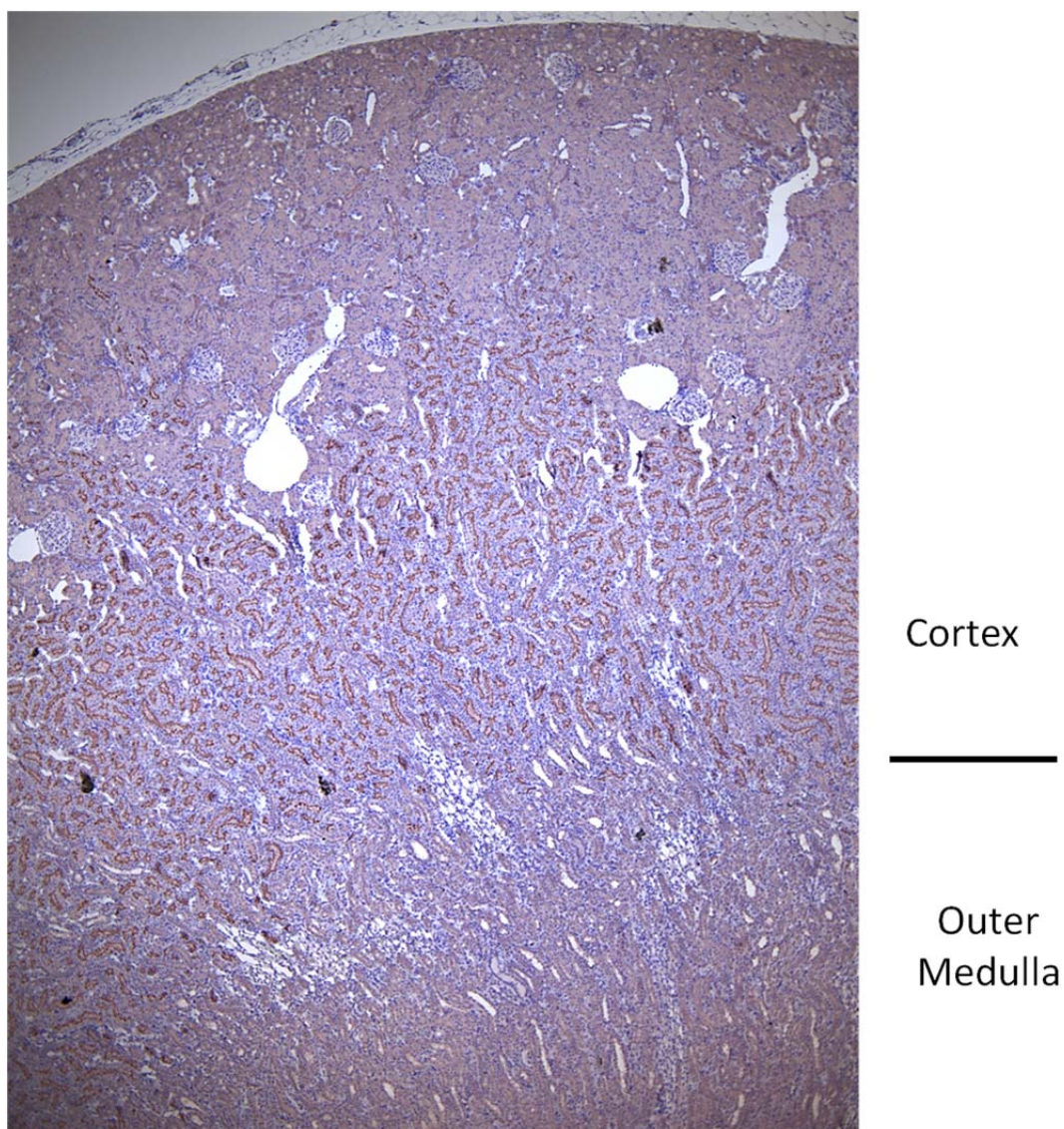


**Figure 4-20: Oatp4c1 location in rat kidney.**

Immunohistochemical analysis for Oatp4c1 (red) location in paraformaldehyde-fixed paraffin-embedded rat kidney sections with PA1343. Magnification: 4x.

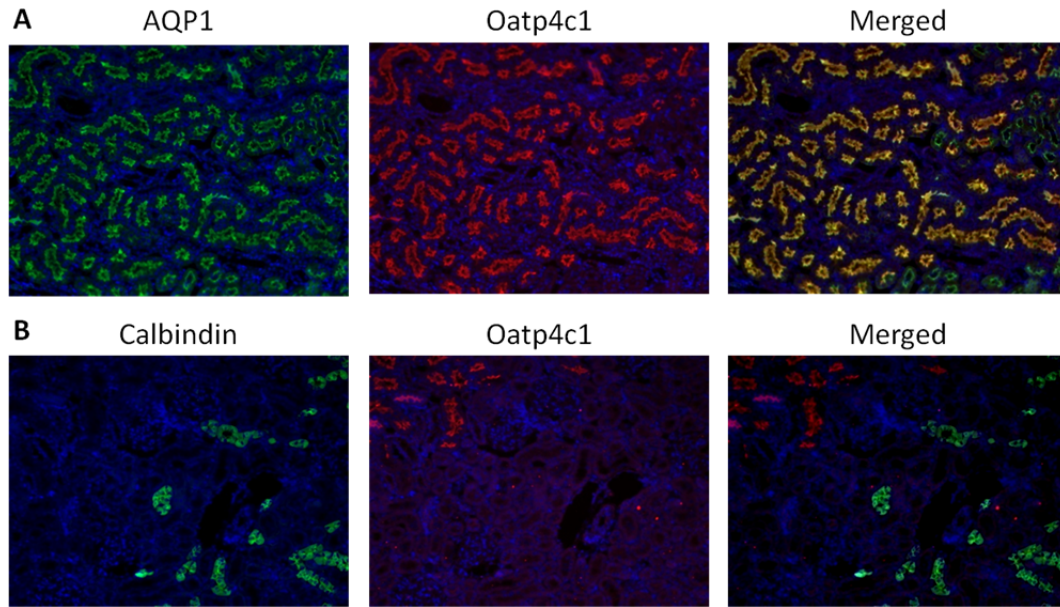


**Figure 4-21: Double immunofluorescence staining for Oatp4c1 (red) and the proximal tubule marker AQP1 (A, green) or the distal tubule marker calbindin-D<sub>28K</sub> (B, green).**

Yellow color in merged panels indicates colocalization. Nuclei (blue) were stained with DAPI. Magnification: 10x.

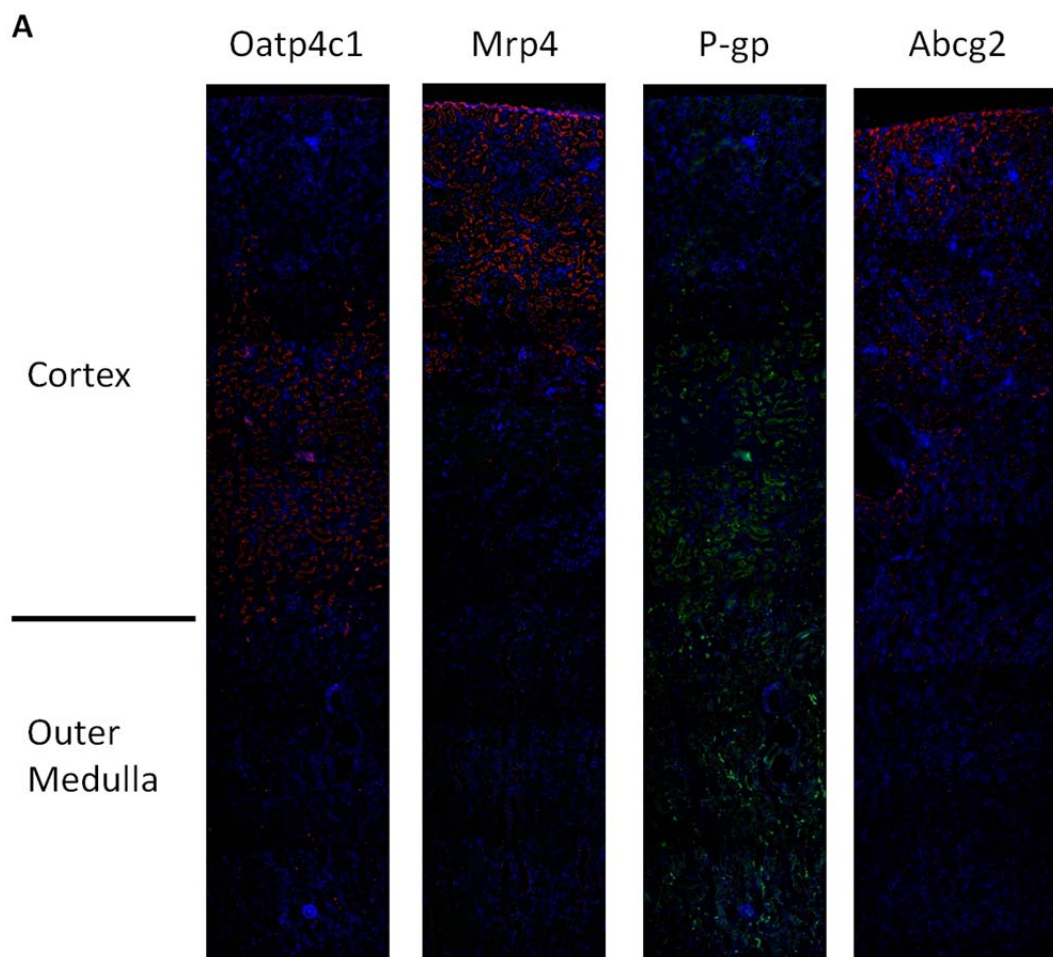


**Figure 4-22 (part 1 of 2): Oatp4c1 colocalization with major efflux transporters in the kidney cortex.**

(A) Paraformaldehyde-fixed paraffin-embedded rat kidney sections were stained for Oatp4c1 (red), Mrp4 (red), P-gp (green), and Abcg2 (red). The images were stitched from six individual images using Image J with Fiji plug-in (National Institute Health, Bethesda, MD). Magnification: 4x.



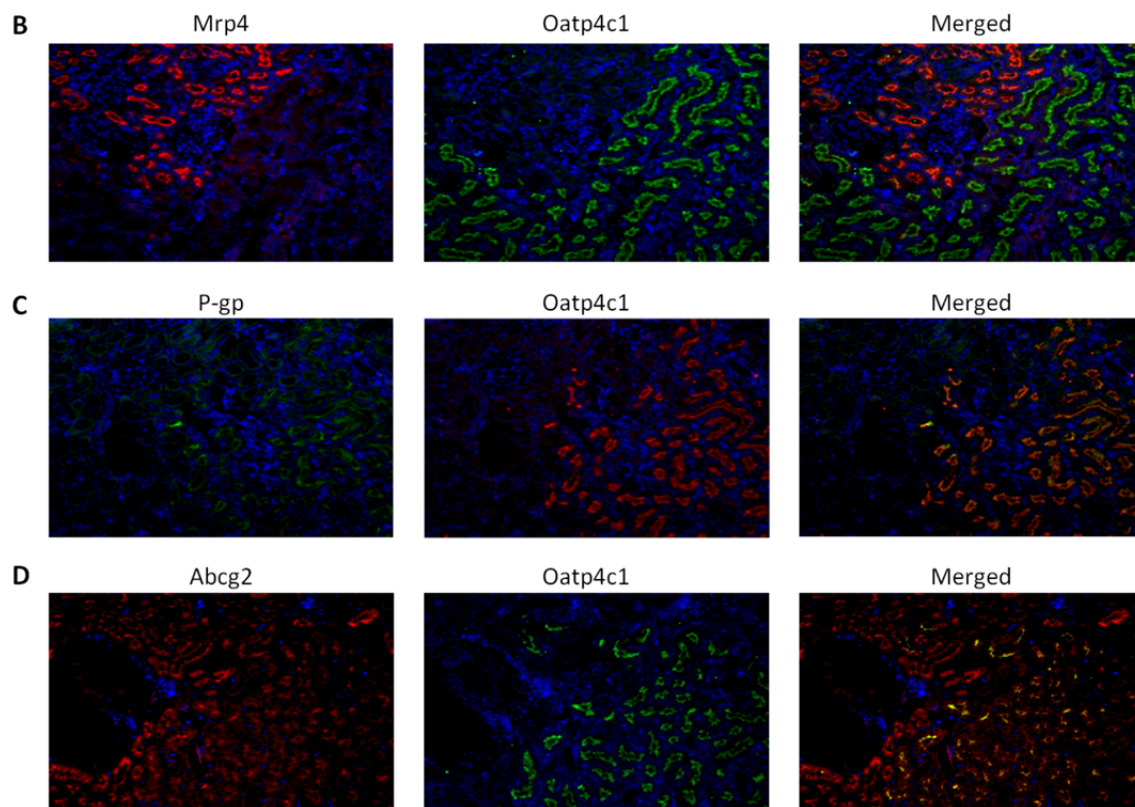


**Figure 4-22 (part 2 of 2) Oatp4c1 colocalization with major efflux transporters in the kidney cortex.**

(B-D) Sections were double stained for Mrp4 (red) and Oatp4c1 (green) (B); P-gp (green) and Oatp4c1 (red) (C); Abcg2 (red) and Oatp4c1 (green) (D). Yellow/orange color in merged panels indicates colocalization. Nuclei (blue) were stained with DAPI. Magnification: 10x (B-D).

### C. Functional characterization of Oatp4c1 in MDCKII-Oatp4c1 cells

1. Specific Aim 3a: To investigate Oatp4c1 transport characteristics and driving force.

To validate the functional activity of rat Oatp4c1 in MDCKII cells generated in Specific Aim 1b and to gain further insight on its role in the transport of physiological substrates, we performed uptake and inhibition studies using E3S, which was previously shown to be a human OATP4C1 substrate (110, 111). In preliminary studies, MDCKII-pcDNA and MDCKII-Oatp4c1 c94 cells were incubated with 0.5  $\mu\text{M}$  [ $^3\text{H}$ ]-E3S in the absence (control) and presence of 100  $\mu\text{M}$  unlabeled E3S for 1 min at pH 5.5 and pH 7.4. As shown in Figure 4-23, the uptake of [ $^3\text{H}$ ]-E3S in MDCKII-Oatp4c1 c94 cells was susceptible to inhibition by 100  $\mu\text{M}$  unlabeled E3S and transport appeared to be more efficient in cells exposed to media with pH 5.5 than pH 7.4. These data demonstrated the functionality of the *in vitro* model and provided evidence that E3S is also a substrate of rat Oatp4c1.

The transport kinetics of [ $^3\text{H}$ ]-E3S in MDCKII-Oatp4c1 (c94) cells were studied further to determine the pH dependent differences in transport. From a physiological perspective, relating to the expression of Oatp4c1 in the kidney, this could be important as the pH in urine is in the acidic range under normal conditions, but can be basic (pH > 7) under pathological conditions. The time dependent uptake of [ $^3\text{H}$ ]-E3S (0.5  $\mu\text{M}$ ) was more efficient in Oatp4c1 cells as compared to vector-transfected cells at pH 4.5, 5.5 and 7.4 (Figure 4-24 A). Oatp4c1-mediated uptake, obtained by subtracting transport in vector-transfected cells, was more efficient at pH 4.5 and 5.5 than at pH 7.4 (Figure 4-24 B).

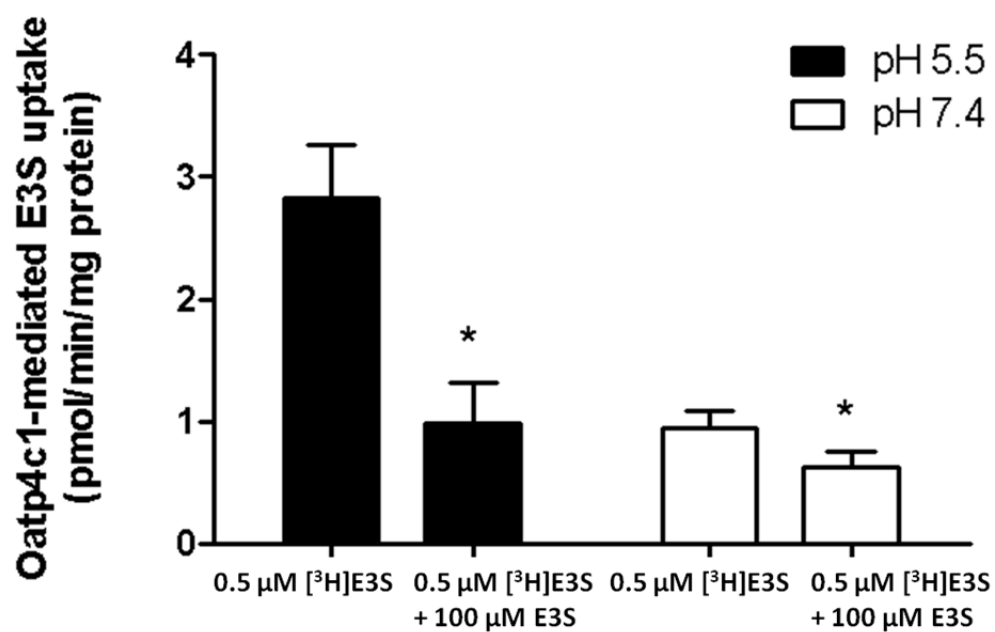


**Figure 4-23: Inhibition of Oatp4c1-mediated 0.5  $\mu$ M [ $^3$ H]-E3S uptake by 100  $\mu$ M E3S at 1 min at pH 5.5 and pH 7.4.**

Oatp4c1-mediated uptake was calculated after subtraction of nonspecific uptake by pcDNA cells. Each column represents the mean  $\pm$  S.D. of triplicate determinations from one representative experiment. Statistical analysis was performed by unpaired student's t-test. \*  $p < 0.05$ , significant differences from control.

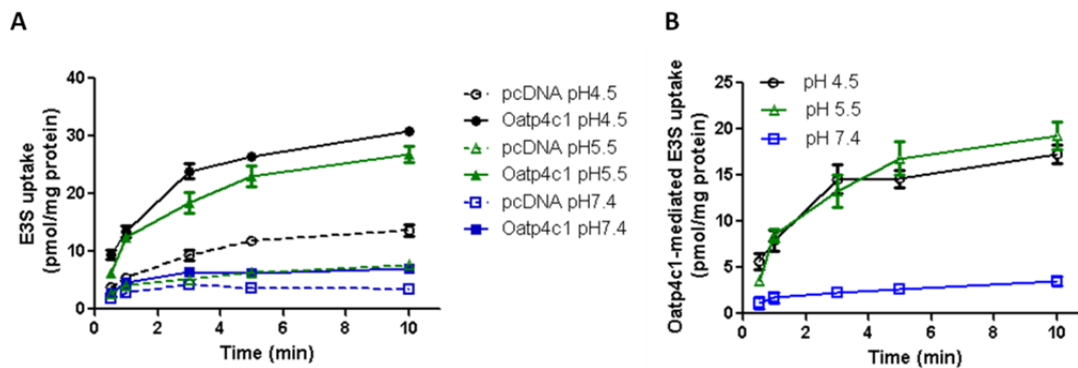


**Figure 4-24: Time-dependent Oatp4c1-mediated  $[^3\text{H}]$ -E3S (0.5  $\mu\text{M}$ ) transport in MDCKII-Oatp4c1 c94 cells at pH 4.5, pH 5.5 and pH 7.4.**

(A)  $[^3\text{H}]$ -E3S intracellular concentration in MDCKII-pcDNA and MDCKII-Oatp4c1 c94 cells. (B) Oatp4c1-mediated uptake was calculated after subtraction of nonspecific uptake by pcDNA cells. Each point represents the mean  $\pm$  S.D. of triplicate determinations from one representative experiment.



To obtain quantitative estimates of the pH dependent differences in transport, we examined the concentration dependent uptake of 1 - 150  $\mu\text{M}$  [ $^3\text{H}$ ]-E3S, and estimated transport kinetic parameters under conditions of linearity with respect to time (1 min). [ $^3\text{H}$ ]-E3S uptake in MDCKII-Oatp4c1 c94 and MDCKII-pcDNA cells at pH 4.5, pH 5.5 and pH 7.4 is shown in Figure 4-25 A, and the net uptake is shown in Figure 4-25 B. A Michaelis-Menten or a modified Michaelis-Menten model, incorporating Hill slope, (Sigmoid- $E_{\text{max}}$ ) was fitted to the net Oatp4c1 transport data, and Sigmoid- $E_{\text{max}}$  model was selected because of lower AIC (Table 4-1). Transport kinetic parameters were estimated by nonlinear regression (Table 4-2). The Michaelis-Menten  $K_{\text{m}}$ -equivalent parameter,  $S_{50}$ , at pH 7.4 ( $21.5 \pm 3.6 \mu\text{M}$ ) was comparable to the reported  $K_{\text{m}}$  ( $26.6 \pm 4.9 \mu\text{M}$ ) for human OATP4C1 at pH 7.4 (110). There was a trend toward increasing  $S_{50}$  with a decrease in pH. Similarly, the estimated  $T_{\text{max}}$  was 5- and 4-fold higher at pH 4.5 and pH 5.5, respectively, than the  $T_{\text{max}}$  estimate at pH 7.4. Accordingly, increased E3S transport activity at acidic extracellular pH could be ascribed to the increased maximum transport rate. In addition, the estimated Hill slope value of 2.6 at pH 7.4 suggests positive cooperativity.

Using the estimated transport parameters we then determined the uptake transport clearance as a function of [ $^3\text{H}$ ]-E3S concentration. As shown in Figure 4-26, the uptake transport clearance ( $v/S$ ) was constant at concentrations below the  $S_{50}$  value, but decreased rapidly as the substrate concentration saturated the transporter. This analysis also demonstrated that the transporter uptake clearance was 10-20 fold higher at acidic pH conditions.

The relationship between proton concentration and E3S uptake velocity was also examined. E3S uptake velocity was estimated from the parameter

estimates in Table 4-2. In a log-log scale, the function of  $y = ax^b$  appears as a straight line, in which  $b$  is the slope. At 0.3  $\mu\text{M}$  E3S, the slope was 1, indicating E3S uptake velocity was linear with proton concentration (Figure 4-27). At higher concentrations of E3S, the slope was less than 1, indicating that E3S uptake velocity reached a plateau faster with increasing proton concentration, suggesting that proton concentration plays a role in Oatp4c1-mediated E3S uptake.

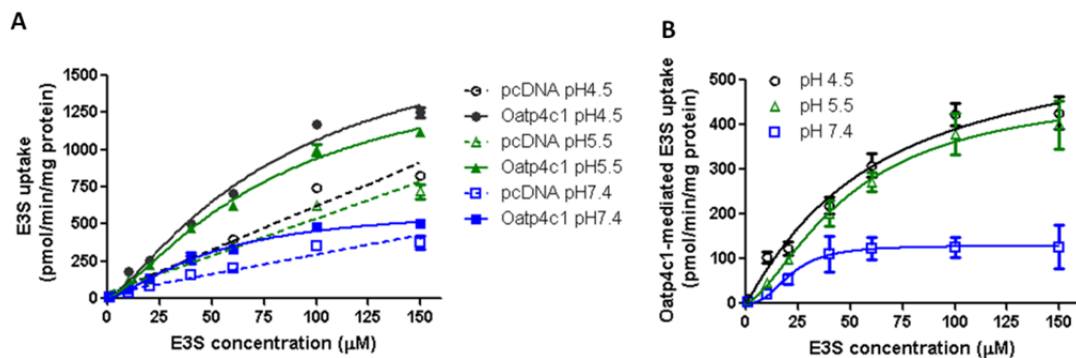


**Figure 4-25: Concentration-dependent Oatp4c1-mediated  $[^3\text{H}]\text{-E3S}$  transport in MDCKII-Oatp4c1 c94 cells at pH 4.5, pH 5.5 and pH 7.4.**

(A)  $[^3\text{H}]\text{-E3S}$  intracellular concentration in MDCKII-pcDNA and MDCKII-Oatp4c1 c94 cells at 1 min. (B) Oatp4c1-mediated uptake was calculated after subtraction of nonspecific uptake by pcDNA cells. Each point represents the mean  $\pm$  S.D. of triplicate determinations from one representative experiment.

**Table 4-1: Akaike Information Criterion (AIC) of model selection for transport kinetic parameter estimation of Oatp4c1-mediated E3S transport at pH 4.5, 5.5 and 7.4.**

Model selection was performed using WinNonlin.

	pH 4.5	pH 5.5	pH 7.4
Michaelis-Menten	62.3	57.3	53.2
Sigmoid- $E_{\text{max}}$	60.5	49.8	37.4

**Table 4-2: Transport kinetic parameters of Oatp4c1-mediated E3S transport at pH 4.5, 5.5 and 7.4 (mean  $\pm$  S.E.).**

The parameters were estimated by fitting a Sigmoid- $E_{\max}$  to the data by GraphPad. Statistical analysis was performed by two-way ANOVA with Bonferroni post-hoc test for all pairwise comparisons. \*, \*\*, \*\*\*  $p < 0.05$  indicate significant differences between pH 4.5 and 5.5, pH 4.5 and 7.4, and pH 5.5 and 7.4, respectively.

	pH 4.5	pH 5.5	pH 7.4
$T_{\max}$ (pmol/mg protein/min)	612.6 $\pm$ 109.7*	484.0 $\pm$ 50.4***	129.3 $\pm$ 11.0**
$S_{50}$ ( $\mu$ M)	60.5 $\pm$ 22.7	49.3 $\pm$ 8.8	21.5 $\pm$ 3.6
Hill Slope	1.1 $\pm$ 0.2	1.5 $\pm$ 0.2	2.6 $\pm$ 1.0

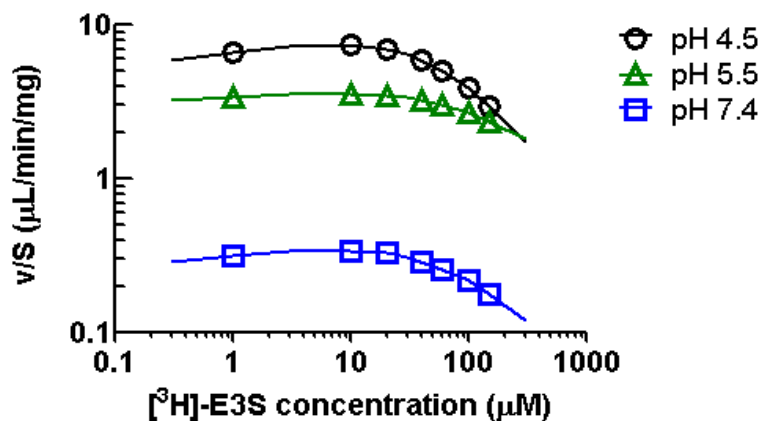


**Figure 4-26: The effect of pH on uptake transport clearance.**

The uptake clearance  $v/S$  was simulated using the parameter estimates in Table 4-2. The solid lines show the best fit to the data using  $v/S = V_{\max} \times S^{n-1} / (S_{50}^n + S^n)$  obtained from  $[^3\text{H}]\text{-E3S}$  uptake.

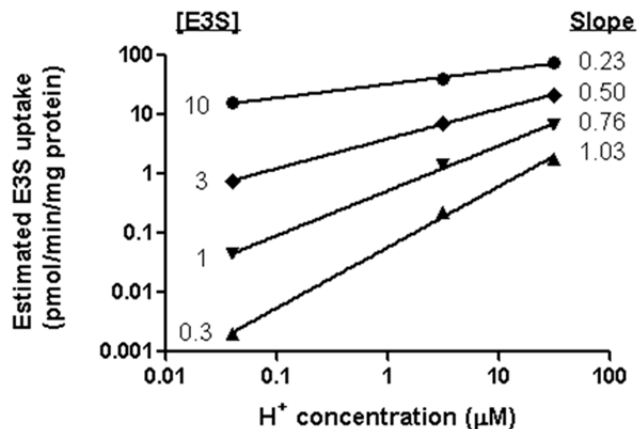


**Figure 4-27: The relationship between proton concentration and E3S uptake.**

E3S uptake velocity was simulated at 0.3, 1, 3 and 10  $\mu\text{M}$  using the parameter estimates in Table 4-2. The solid lines show the best fit to the data using  $V = aH^s$ , where  $V$ ,  $H$  and  $s$  represent E3S uptake velocity, proton concentration, and slope, respectively.

Examination of the reported Oatp4c1 and OATP4C1 primary amino acid sequences had revealed the presence of a potential ATP binding site (Walker A motif) (79). However, an ATP-depletion assay revealed that OATP4C1 mediated transport of  $T_3$  was not ATP-dependent at pH 7.4 (79). To examine whether Oatp4c1-mediated [ $^3$ H]-E3S transport was ATP-dependent, the effect of ATP depletion on its accumulation was assessed. Twenty minutes prior to the transport experiment, and for the duration (1 min) of transport, cells were incubated with either uptake buffer or buffer lacking glucose, but supplemented with 20 mM 2-deoxy-D-glucose and 10 mM  $\text{NaN}_3$  at pH 5.5 and pH 7.4. Oatp4c1-mediated [ $^3$ H]-E3S (0.5  $\mu\text{M}$ ) uptake did not change under ATP-depleted condition at both pH 5.5 and pH 7.4 (Figure 4-28 B). In addition, [ $^3$ H]-E3S intracellular concentrations in Oatp4c1-expressing and vector-transfected MDCKII cells were higher under ATP-depleted condition at pH 5.5 (Figure 4-28 A), suggesting the presence of an endogenous ATP-dependent efflux transporter in the MDCKII cells.

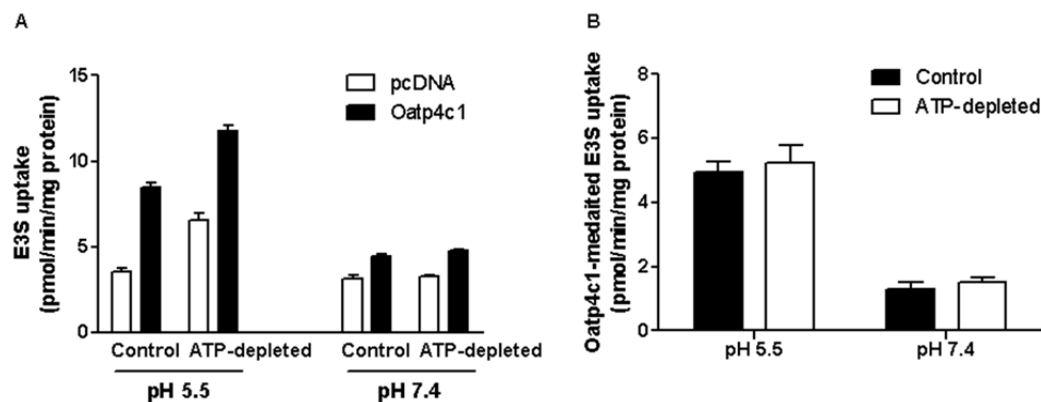


**Figure 4-28: Effect of ATP depletion on [ $^3\text{H}$ ]-E3S uptake (0.5  $\mu\text{M}$ ) via Oatp4c1.**

(A) [ $^3\text{H}$ ]-E3S intracellular concentration in MDCKII-pcDNA and MDCKII-Oatp4c1 c94 cells. ATP-depletion was achieved by incubating the cells in uptake buffer containing 20 mM 2-deoxy-D-glucose and 10 mM  $\text{NaN}_3$  without D-glucose at pH 5.5 and pH 7.4. (B) Oatp4c1-mediated uptake was calculated after subtraction of nonspecific uptake by pcDNA cells. Each column represents the mean  $\pm$  S.D. of triplicate determinations from one representative experiment.

2. Specific Aim 3b: To identify potential Oatp4c1 substrates.

Having validated E3S as an Oatp4c1 substrate, we next attempted to determine the interaction of Oatp4c1 with potential physiological substrates by studying their capacity to inhibit transport of this prototypical substrate. OATP4C1 was reported to transport T<sub>3</sub>, T<sub>4</sub>, ouabain, digoxin and MTX (79). In addition, *in vivo* studies suggested that OATP4C1/Oatp4c1 is involved in the elimination of uremic toxins (106). [<sup>3</sup>H]-E3S (0.5 μM) uptake was determined in the absence and presence of 100 μM of putative substrates for 1 min at pH 5.5 (Figure 4-29 A, B) or pH 7.4 (Figure 4-29 C, D). Oatp4c1-mediated [<sup>3</sup>H]-E3S uptake was significantly inhibited by T<sub>4</sub> at pH 5.5, and significantly stimulated in the presence of T<sub>3</sub> at both pH 5.5 and pH 7.4 (Figure 4-29 B, D). In addition, [<sup>3</sup>H]-E3S accumulation was significantly higher in the presence of T<sub>3</sub> in both Oatp4c1-expressing and vector-transfected cells (Figure 4-29 A, C). Neither reported OATP4C1 substrates (digoxin, ouabain, MTX), nor putative substrates (kynurenic acid, indoxyl sulfate, hippuric acid and *trans*-aconitic acid, uric acid, citric acid, riboflavin) affected Oatp4c1-mediated E3S uptake at either pH 5.5 or pH 7.4.



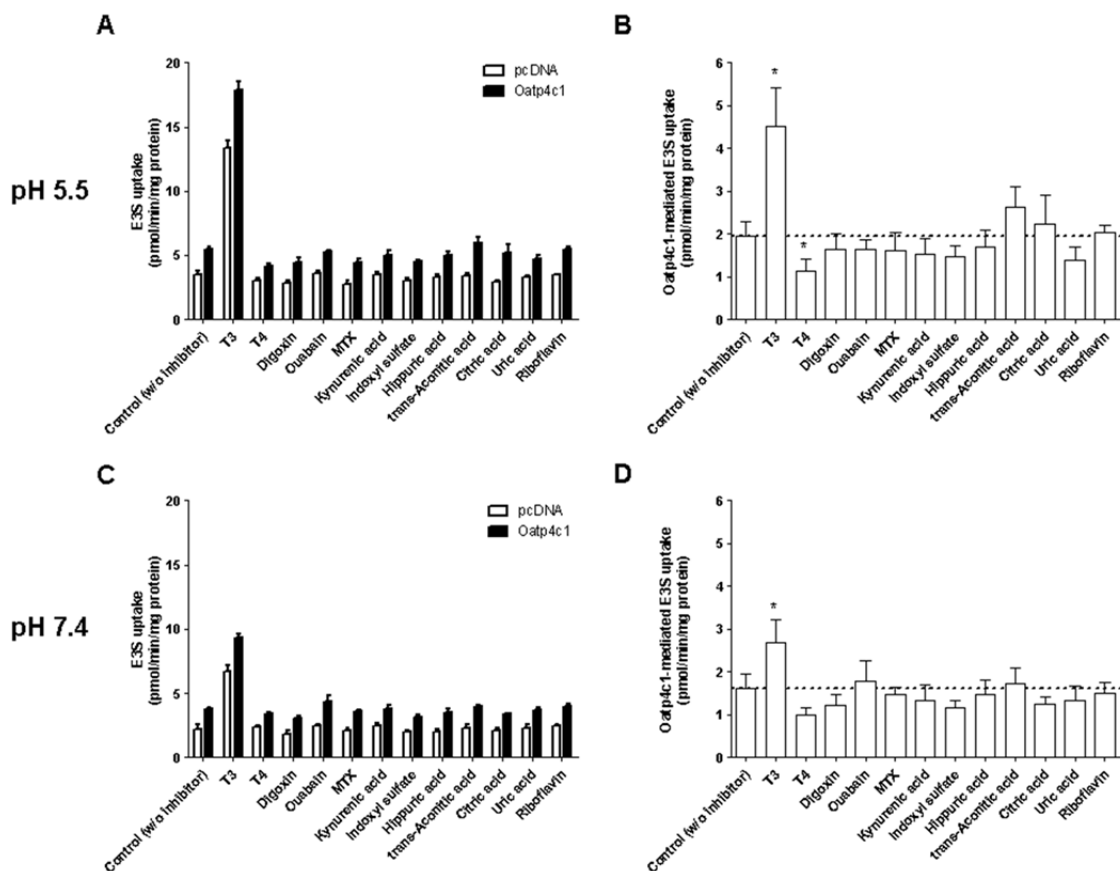


**Figure 4-29: Effect of putative substrates on [<sup>3</sup>H]-E3S uptake at pH 5.5 and 7.4.**

MDCKII-pcDNA and MDCKII-Oatp4c1 c94 cells were incubated with 0.5  $\mu$ M [<sup>3</sup>H]-E3S in the absence (control) and presence of various compounds (100  $\mu$ M) for 1 min at pH5.5 (A, B) and 7.4 (C, D). Oatp4c1-mediated uptake was estimated after subtracting the nonspecific uptake measured in pcDNA cells (B, D). Each bar represents the mean  $\pm$  S.D. of triplicate determinations from one representative experiment. Statistical analysis was performed by two-way ANOVA with Bonferroni post-hoc test compared with control.\*  $p < 0.05$ , significant differences from control.

Human OATP4C1 has been proposed to possess multiple substrate recognition sites. In accord with a previous report demonstrated in MDCKII-OATP4C1 cells (110), Oatp4c1-mediated E3S uptake was not inhibited by digoxin and ouabain. Therefore, Oatp4c1 may also have multiple substrate binding sites. If so, the unchanged Oatp4c1-mediated E3S uptake by putative substrates (Figure 4-29) may be because they interact with a different site than that of E3S. To verify these putative substrates, we used another reported OATP4C1 substrate, MTX (79), as a prototype substrate. As shown in Figure 4-30 A, time dependent uptake of [ $^3$ H]-MTX (1  $\mu$ M) was more efficient in Oatp4c1 cells as compared to vector-transfected cells at pH 5.5 and pH 7.4, suggesting MTX is Oatp4c1 substrate. However, Oatp4c1-mediated MTX uptake was comparable at pH 5.5 and pH 7.4 (Figure 4-30 B), which is unlike the pH effect observed with E3S uptake.

The capacity of the putative substrates to inhibit MTX transport was examined. [ $^3$ H]-MTX (1  $\mu$ M) uptake was determined in the absence and presence of 100  $\mu$ M various compounds for 1 min at pH 5.5 (Figure 4-31 A, B) or pH 7.4 (Figure 4-31 C, D). Oatp4c1-mediated [ $^3$ H]-MTX uptake was significantly stimulated by the presence of *trans*-aconitic acid and uric acid at pH 5.5 (Figure 4-31 B). Oatp4c1-mediated [ $^3$ H]-MTX uptake was significantly inhibited by T<sub>3</sub> at pH 7.4. (Figure 4-31 D). Additionally, as observed in [ $^3$ H]-E3S inhibition studies, [ $^3$ H]-MTX accumulation was significantly higher in the presence of T<sub>3</sub> in both Oatp4c1-expressing and vector-transfected cells (Figure 4-31 A, C). Neither reported OATP4C1 substrates (T<sub>4</sub>, digoxin, ouabain, and E3S), nor putative substrates (kynurenic acid, indoxyl sulfate, riboflavin) changed Oatp4c1-mediated MTX uptake at either pH 5.5 or pH 7.4.

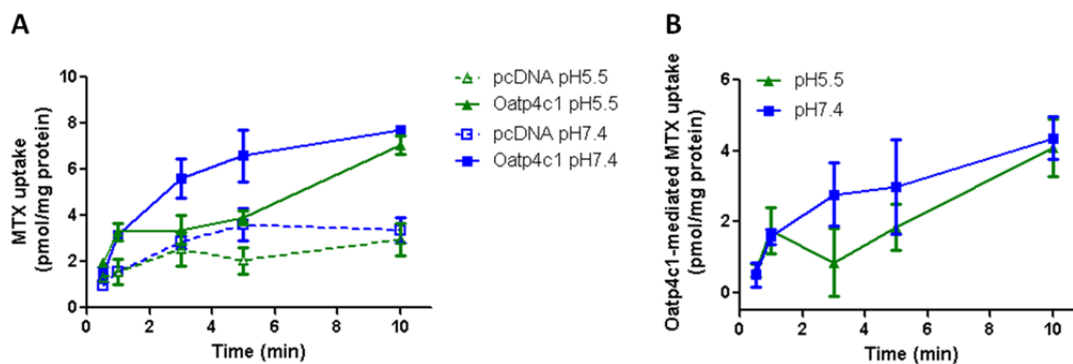


**Figure 4-30: Time-dependent Oatp4c1-mediated [ $^3\text{H}$ ]-MTX (1  $\mu\text{M}$ ) transport in MDCKII-Oatp4c1 c94 cells at pH 5.5 and pH 7.4.**

(A) [ $^3\text{H}$ ]-MTX intracellular concentration in MDCKII-pcDNA and MDCKII-Oatp4c1 c94 cells. (B) Oatp4c1-mediated uptake was calculated after subtraction of nonspecific uptake by pcDNA cells. Each point represents the mean  $\pm$  S.D. of triplicate determinations from one representative experiment.

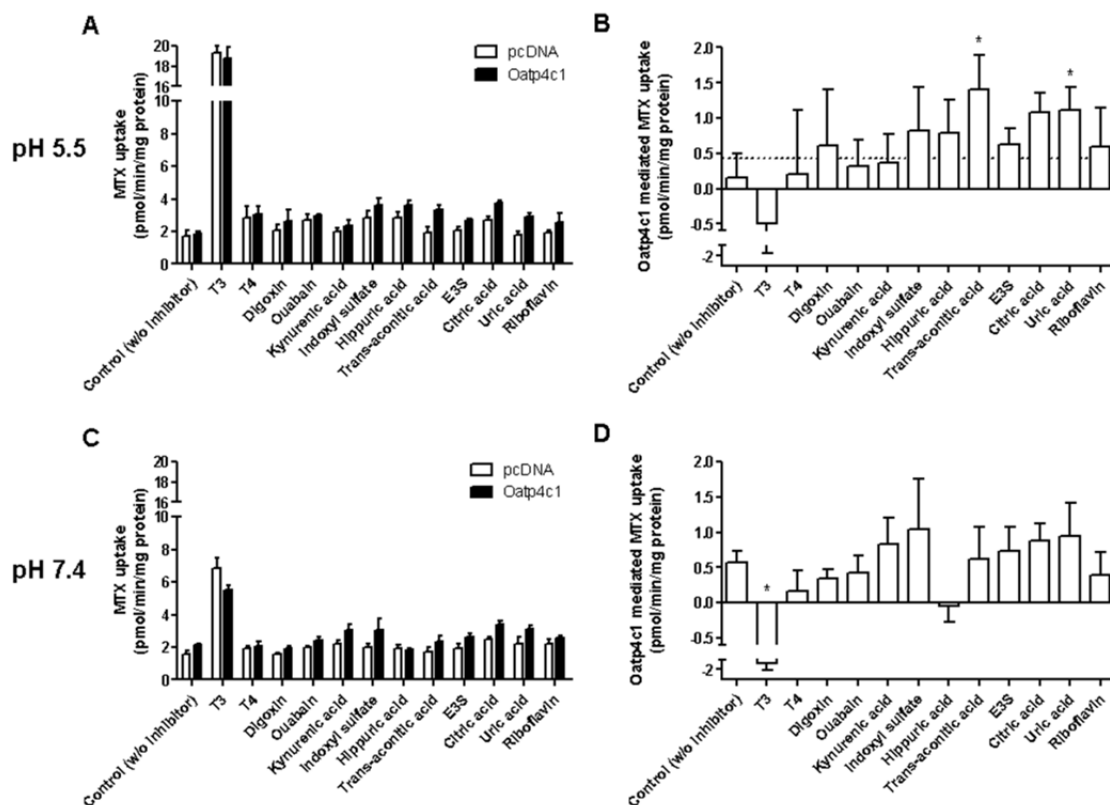


**Figure 4-31: Effect of putative substrates on [<sup>3</sup>H]-MTX uptake at pH 5.5 and 7.4.**

MDCKII-pcDNA and MDCKII-Oatp4c1 c94 cells were incubated with 1  $\mu$ M [<sup>3</sup>H]-MTX in the absence (control) and presence of various compounds (100  $\mu$ M) for 1 min at pH5.5 (A, B) and 7.4 (C, D). Oatp4c1-mediated uptake was estimated after subtracting the nonspecific uptake measured in pcDNA cells (B, D). Statistical analysis was performed by two-way ANOVA with Bonferroni post-hoc test compared with control. Each bar represents the mean  $\pm$  S.D. of triplicate determinations from one representative experiment. \*  $p < 0.05$ , significant differences from control.

#### D. Creation and validation of human OATP4C1-expressing cell lines

1. Specific Aim 4a: To develop and validate human OATP4C1 antibodies amenable for immunoblotting, immunohistochemistry and immunofluorescence.

To investigate the expression and subcellular localization of human OATP4C1 in the *in vitro* cell models and human tissues, two rabbit polyclonal antibodies were generated against either amino-terminus (PA1243) or carboxyl-terminus (PA1245) of human OATP4C1. The antibodies specificities were validated by Western blotting, immunohistochemical analysis, and immunofluorescence staining in the *in vitro* cell models developed in Specific Aim 4b.

2. Specific Aim 4b: To create and validate human OATP4C1-expressing cells with appropriate characteristics for functional studies.

To study the role of human OATP4C1 in drug disposition, we generated OATP4C1-expressing MDCKII cells and OATP4C1-expressing Sf9 cells. Human *SLCO4C1* DNA purchased from OriGene was amplified by PCR reaction. The amplified fragment of appropriate size was confirmed by agarose gel electrophoresis (Figure 4-32 A). The amplification product was purified and cloned into pENTR vector. The plasmid construct was verified by EcoRI restriction enzyme digestion and by PCR with M13 forward and M13 reverse primers, which bound to ~110 bp upstream and ~150 bp downstream of the gene insertion site, respectively, in the pENTR vector (Figure 4-32 B). This sequence was confirmed with 100% identity as compared to the published human *SLCO4C1* sequence (GeneBank accession number NM\_180991). The plasmid

DNA was then subcloned into pcDNA6.2/EmGFP-Bsd/V5-DEST vector and was verified by PCR with T7 forward primer, which bound to 50 bp upstream of gene insertion site in the vector, and SLCO4C1 reverse primers (Figure 4-32 C).

The SLCO4C1 plasmid DNA (pcDNA6.2/EmGFP-Bsd/V5-DEST/SLCO4C1) and empty plasmid DNA (pcDNA6.2/EmGFP-Bsd/V5-DEST) were transfected into MDCKII cells. Transfection efficiency was examined by Western blotting using the antibody generated in Specific Aim 4a (PA1245) (Figure 4-33 A). OATP4C1 expression was detectable as a band at ~60 kDa in MDCKII-OATP4C1 cells, but not in MDCKII-pcDNA (empty vector) cells. Human kidney served as a positive control with a band detected at ~70 kDa. OATP4C1 was also detectable as a broad band at 60-70 kDa in OATP4C1-expressing Sf9 cells, which will be described later. In addition, validation of antibody PA1243 for Western blotting is shown in Figure 4-33 B. OATP4C1 was detected at ~60 and 80 kDa in human kidney and at ~60 kDa in Sf9-OATP4C1 cells, but not in Sf9-vector cells. After antigen peptide blocking, the specific bands in human kidney (~80 kDa) and Sf9-OATP4C1 cells (~60 kDa) were abolished, demonstrating the antibody specificity.

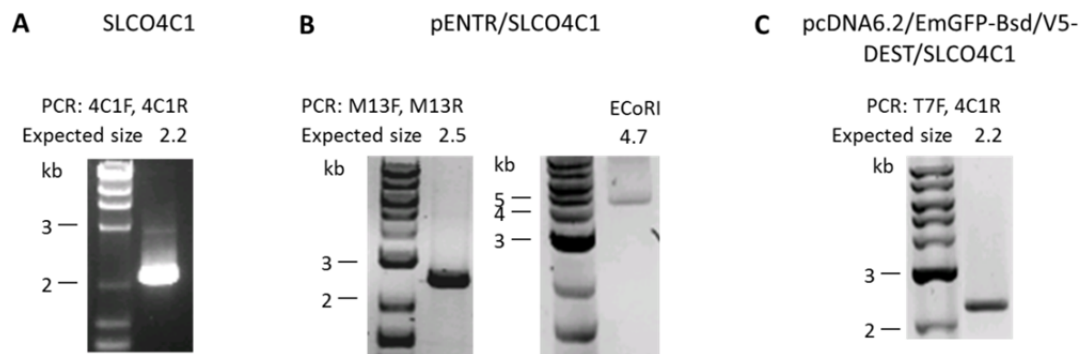


**Figure 4-32: Validation of SLCO4C1 plasmid constructs.**

PCR products and the restriction enzyme digestion products of SLCO4C1 and plasmid DNA were examined by agarose gel electrophoresis.

OATP4C1 expression in MDCKII-OATP4C1 cells was also confirmed in paraformaldehyde-fixed paraffin-embedded cell pellet sections by immunohistochemical analysis using antibody PA1243 (Figure 4-33 C). OATP4C1 was observed on the cell membrane in the MDCKII-OATP4C1 cells, and the staining was abolished when probed with antibody that was pre-adsorbed with antigen peptide. Despite some background staining detected in the negative control (rabbit IgG), no staining was observed in the MDCKII-pcDNA cells. This demonstrated that the transfection was successful and that the antibody was specific.

The subcellular localization of OATP4C1 in polarized cell monolayers was assessed by confocal immunofluorescence laser scanning microscopy (Figure 4-33 D) and surface protein biotinylation assay (Figure 4-33 E). As observed for rat *Oatp4c1*, OATP4C1 localized at the apical membrane in MDCKII-OATP4C1 cells (Figure 4-33 D). As shown in Figure 4-33 E, surface biotinylation assay demonstrated that OATP4C1 was enriched in the apical membrane fraction as compared to the basolateral membrane. Collectively, these data verified the apical localization of the transporter in OATP4C1-expressing MDCKII cells.



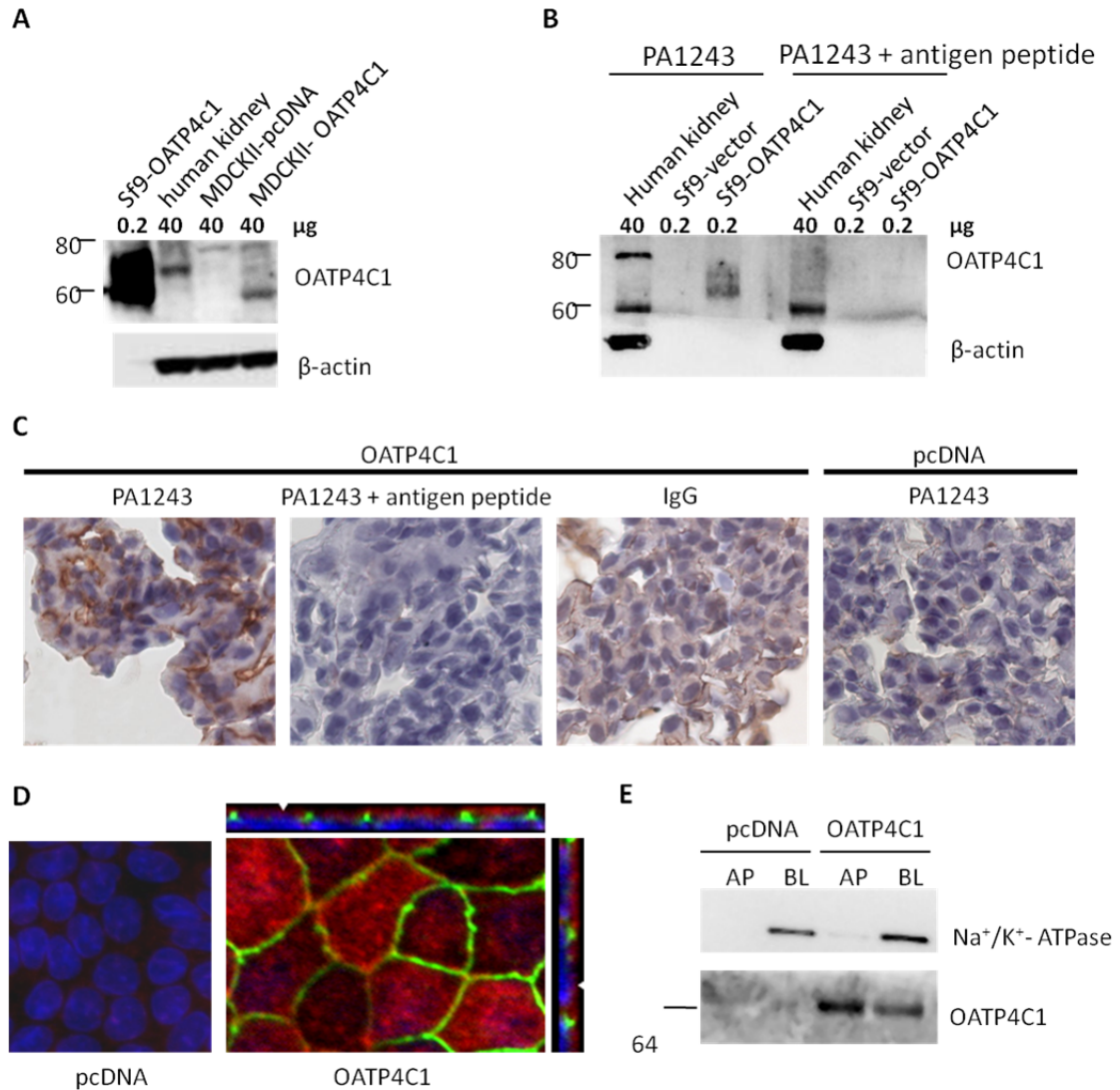


**Figure 4-33: Validation of OATP4C1 expression and subcellular localization in MDCKII-OATP4C1 cells.**

(A) Western blot of OATP4C1 and  $\beta$ -actin. OATP4C1 was detected with PA1245. (B) Western blot of OATP4C1 and  $\beta$ -actin with and without antigen peptide blocking. OATP4C1 was detected with PA1243. (C) Immunohistochemical analysis of OATP4C1 expression in paraformaldehyde-fixed paraffin-embedded cell sections. OATP4C1 was detected with PA1243. (D) Confocal microscopy of OATP4C1 (red) expression and localization in polarized MDCKII cells. Center image is a single optical section of the x-y plane while top and right images represent x-z and y-z planes, respectively, reconstructed from image stacks. The apical and basal sides can be demarcated by Zo-

1 (green) and the nuclei (DAPI, blue), respectively, in both x-z and y-z sections. OATP4C1 was detected with PA1245. (E) Western blot of OATP4C1 in proteins isolated from either the apical (AP) or basolateral (BL) membranes of polarized MDCKII cells. Na<sup>+</sup>/K<sup>+</sup>-ATPase served as a BL marker to demonstrate the relative efficiency of AP and BL membrane separation. OATP4C1 was detected with PA1245.

To validate the functional activity of OATP4C1 in MDCKII cells, the uptake studies of reported OATP4C1 substrates, ouabain and E3S (79, 110, 111), was performed. Ouabain transport kinetics were determined by [<sup>3</sup>H]-ouabain uptake for concentrations ranging from 1 to 150  $\mu$ M at 5 min. OATP4C1-mediated uptake (net) was calculated after subtraction of nonspecific uptake by pcDNA cells. As shown in Figure 4-34, [<sup>3</sup>H]-ouabain uptake was higher in MDCKII-OATP4C1 as compared to MDCKII-pcDNA cells, and a saturable concentration-dependent OATP4C1-mediated ouabain uptake was observed. It confirmed ouabain as an OATP4C1 substrate and showed the functional activity of OATP4C1 in the transfected cells. Michaelis-Menten and sigmoid- $E_{\max}$  were fitted to the net OATP4C1 transport data. The transport kinetic parameters were estimated by nonlinear regression (

Table 4-3). The AIC for the two models were comparable. Therefore, the simpler Michaelis-Menten model was selected. The estimated  $S_{50}$  ( $0.19 \pm 0.09$   $\mu$ M) was in the similar range of the reported  $K_m$  ( $0.38 \pm 0.1$   $\mu$ M) (79).

The functional activity of OATP4C1 in MDCKII cells was also validated with E3S. [<sup>3</sup>H]-E3S uptake was determined at 0.5 and 1  $\mu$ M for 5 min. As shown in Figure 4-35, [<sup>3</sup>H]-E3S uptake was higher in MDCKII-OATP4C1 than that in MDCKII-pcDNA cells, and the net uptake was increased with concentration. Despite that the concentrations were not high enough to reach saturation, the data suggest that E3S is an OATP4C1 substrate.

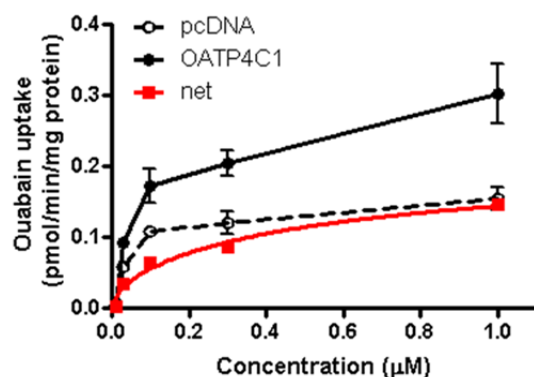


**Figure 4-34: Concentration-dependent OATP4C1-mediated [ $^3\text{H}$ ]-ouabain transport in MDCKII-OATP4C1 cells at pH 7.4.**

[ $^3\text{H}$ ]-ouabain intracellular concentration (5 min) in MDCKII-pcDNA and MDCKII-OATP4C1 cells. OATP4C1-mediated uptake (net) was calculated after subtraction of nonspecific uptake by pcDNA cells. Each point represents the mean  $\pm$  S.D. of triplicate determinations from one representative experiment.

**Table 4-3: Transport kinetic parameters of OATP4C1-mediated [ $^3\text{H}$ ]-ouabain transport at pH 7.4 (mean  $\pm$  S.E.).**

The transport parameters were estimated by GraphPad, and AIC for model selection was estimated by WinNonlin.

	Michaelis-Menten	Sigmoid- $E_{\max}$
$T_{\max}$ (pmol/min/mg protein)	$0.17 \pm 0.03$	$0.26 \pm 0.24$
$S_{50}$ ( $\mu\text{M}$ )	$0.19 \pm 0.09$	$0.70 \pm 2.02$
Hill Slope	-	$0.67 \pm 0.36$
AIC	-34.00	-34.23

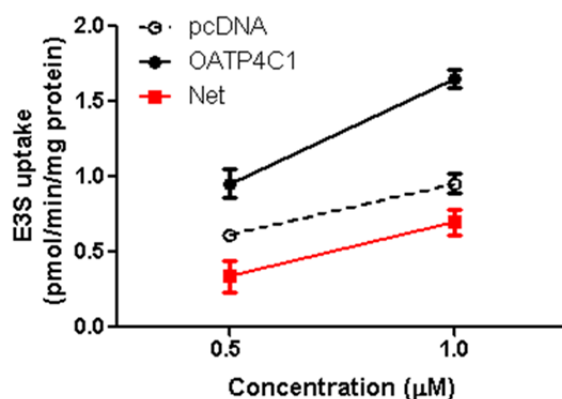


**Figure 4-35: Concentration-dependent OATP4C1-mediated [<sup>3</sup>H]-E3S transport in MDCKII-OATP4C1 cells at pH 7.4.**

[<sup>3</sup>H]-E3S intracellular concentration (5 min) in MDCKII-pcDNA and MDCKII-OATP4C1 cells. OATP4C1-mediated uptake (net) was calculated after subtraction of nonspecific uptake by pcDNA cells. Each point represents the mean ± S.D. of triplicate determinations from one representative experiment.

In addition to MDCKII cells, we also overexpressed OATP4C1 in Sf9 cells. Sf9 can express higher level of recombinant protein and is easily scaled up for substrate screening to study the role of human OATP4C1 in drug disposition. pENTR/SLCO4C1 construct was generated as previously described in developing OATP4C1-expressing MDCKII cells, and was subcloned into pDEST8 vector. The size of the plasmid construct was confirmed by Bsu361 restriction enzyme digestion (Figure 4-36 A). The plasmid DNA was then recombined in DH10Bac<sup>TM</sup> competent *E. Coli.* containing baculovirus genome. For background control, the empty vector (pDEST8) was also recombined as above. Recombinant bacmid DNA was verified by PCR with M13 forward and M13 reverse primers (Figure 4-36 B).

The recombinant bacmids (pDEST8/SLCO4C1 and pDEST8) were transfected into Sf9 cells, and the supernatant containing recombinant baculovirus stock was harvested after 48 hr. The viral stock was amplified by infecting a large volume of Sf9 cell suspensions. The infected Sf9 cells were centrifuged to collect cell pellets for membrane vesicle preparation. Successful infection was confirmed by Western blotting for OATP4C1 expression in the membrane vesicles. As shown in Figure 4-37, OATP4C1 was detected in Sf9-OATP4C1 membrane vesicles but not in Sf9-vector.

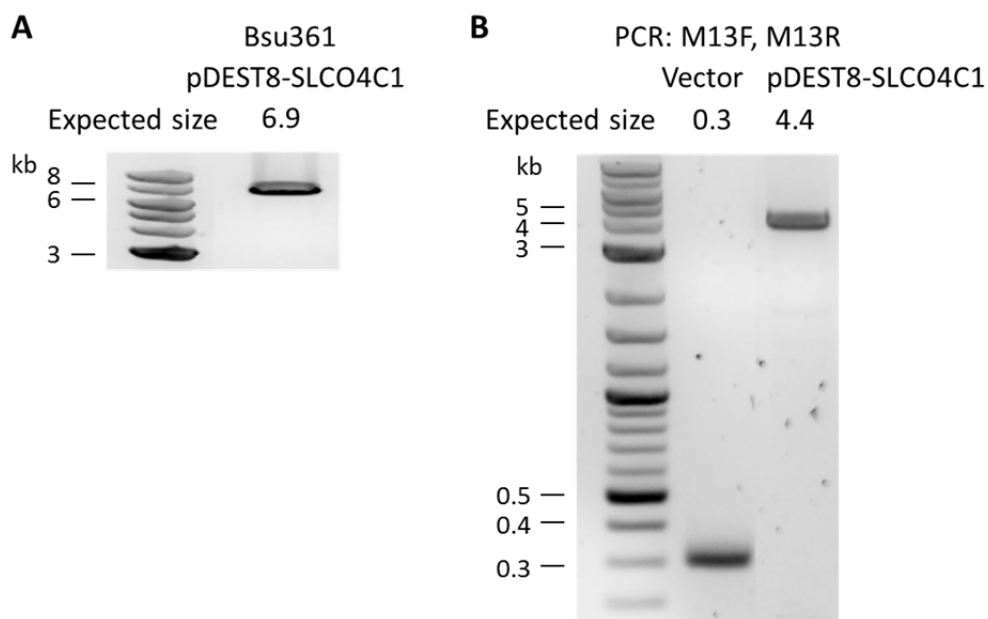


**Figure 4-36: Validation of pDEST8-SLCO4C1 plasmid construct.**

Restriction enzyme digestion products and PCR products of pDEST8-SLCO4C1 were examined by agarose gel electrophoresis.

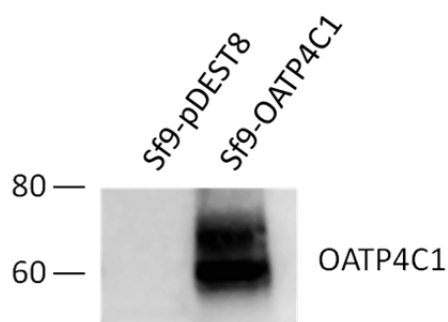


**Figure 4-37: Validation of OATP4C1 expression in Sf9-OATP4C1 membrane vesicles.**

Western blot analysis for OATP4C1 expression in Sf9-pDEST8 and Sf9-OATP4C1 membrane vesicles (0.2  $\mu$ g protein). OATP4C1 was detected with PA1245.

To validate the functional activity of OATP4C1 in Sf9 cells, vesicular transport studies of [ $^3\text{H}$ ]-ouabain and [ $^3\text{H}$ ]-E3S were performed. As shown in Figure 4-38, the time dependent uptake of [ $^3\text{H}$ ]-ouabain (0.5  $\mu\text{M}$ ) was higher in Sf9-OATP4C1 as compared to Sf9-pDEST8 membrane vesicles at pH 7.4. Based on this result, the 3 min time point was chosen to determine the initial rate. To evaluate [ $^3\text{H}$ ]-ouabain transport kinetics, the initial rate of [ $^3\text{H}$ ]-ouabain uptake were determined for concentrations ranging from 0.01 to 1  $\mu\text{M}$  (Figure 4-39 A and B). However, the nonspecific adsorption determined by incubation in cold uptake buffer was substantial. At 1  $\mu\text{M}$ , the nonspecific adsorption was 55% of the total radioactivity remaining on the filter. After subtracting the nonspecific adsorption, [ $^3\text{H}$ ]-ouabain uptake in Sf9-pDEST8 showed saturation transport kinetics, indicating the presence of an endogenous uptake transporter (Figure 4-39 B). OATP4C1-mediated ouabain uptake was calculated after subtraction of nonspecific uptake in Sf9-pDEST8. Michaelis-Menten and sigmoid- $E_{\text{max}}$  models were fitted to the net OATP4C1 transport data. The transport kinetic parameters were estimated by nonlinear regression (Table 4-4). The simpler Michaelis-Menten model was selected because the AIC of the two models were comparable. The estimated  $S_{50}$  ( $0.18 \pm 0.09 \mu\text{M}$ ) was comparable with the  $S_{50}$  estimated from MDCKII-OATP4C1 cells ( $0.19 \pm 0.09 \mu\text{M}$ ) and was in the similar range of the reported  $K_m$  ( $0.38 \pm 0.1 \mu\text{M}$ ) (79). However, the high nonspecific adsorption decreased the sensitivity, therefore another substrate with low adsorption was needed to study OATP4C1 function.



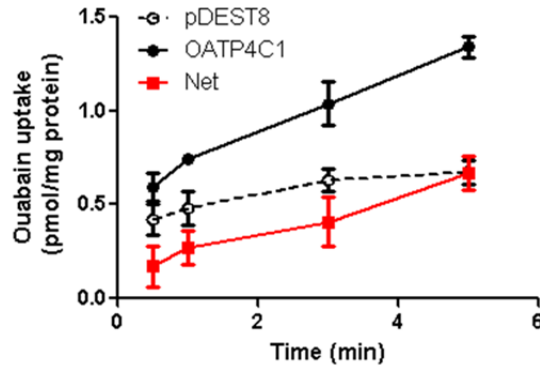


**Figure 4-38: Time-dependent OATP4C1-mediated [ $^3\text{H}$ ]-ouabain (0.5  $\mu\text{M}$ ) transport in Sf9-OATP4C1 membrane vesicles at pH 7.4.**

[ $^3\text{H}$ ]-ouabain accumulation in Sf9-pDEST8 and Sf9-OATP4C1 membrane vesicles. OATP4C1-mediated uptake was calculated after subtraction of nonspecific uptake by Sf9-pDEST8. Each point represents the mean  $\pm$  S.D. of triplicate determinations from one representative experiment.

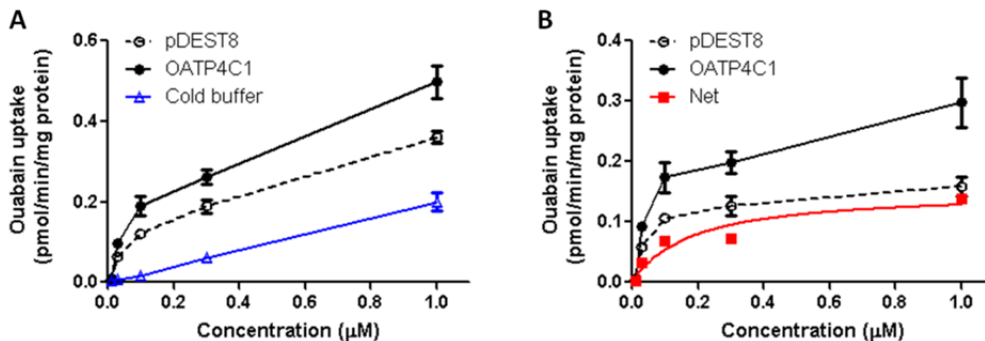


**Figure 4-39: Concentration-dependent OATP4C1-mediated [ $^3\text{H}$ ]-ouabain transport in Sf9-OATP4C1 membrane vesicles at pH 7.4.**

(A) [ $^3\text{H}$ ]-ouabain accumulation (3 min) in Sf9-pDEST8 and Sf9-OATP4C1 membrane vesicles. Nonspecific adsorption on the filter was measured by incubation in cold buffer. (B) Data from panel A with nonspecific adsorption subtraction. OATP4C1-mediated uptake was calculated after subtraction of nonspecific uptake by Sf9-pDEST8. Each point represents the mean  $\pm$  S.D. of triplicate determinations from one representative experiment.

**Table 4-4: Transport kinetic parameters of OATP4C1-mediated [<sup>3</sup>H]-ouabain transport in Sf9-OATP4C1 membrane vesicles at pH 7.4 (mean ± S.E.).**

The transport parameters were estimated by GraphPad, and AIC for model selection was estimated by WinNonlin.

	Michaelis-Menten	Sigmoid-E <sub>max</sub>
T <sub>max</sub> (pmol/min/mg protein)	0.15 ± 0.02	0.37 ± 0.90
S <sub>50</sub> (μM)	0.18 ± 0.09	2.76 ± 20.80
Hill Slope	-	0.55 ± 0.39
AIC	-30.83	-30.70

Because of the high nonspecific adsorption on the filter membrane of ouabain, which interfered with data interpretation, another substrate, E3S, was used to investigate OATP4C1 transport characteristics. Preliminary studies showed that nonspecific adsorption of E3S was only 0.3% of the total radioactivity. The time dependent uptake of [ $^3$ H]-E3S (30  $\mu$ M) was higher in Sf9-OATP4C1 as compared to Sf9-pDEST8 membrane vesicles at pH 7.4, and the 5 min time point was chosen to determine the initial rate (Figure 4-40 A). To evaluate [ $^3$ H]-E3S transport kinetics, the initial rate of [ $^3$ H]-E3S uptake was determined for concentrations ranging from 1 to 30  $\mu$ M (Figure 4-40 B). The net uptake was increased with concentration, but did not reach a plateau, implying that the transporter was not saturated at these concentrations. In addition, the pH effect on OATP4C1-mediated E3S transport was examined. [ $^3$ H]-E3S (20  $\mu$ M) accumulation in Sf9-pDEST8 and Sf9-OATP4C1 for 5 min at pH 6.5 and pH 7.4 was determined (Figure 4-41 A). As shown in Figure 4-41 B, there was a trend toward increasing net uptake with a decrease in pH.

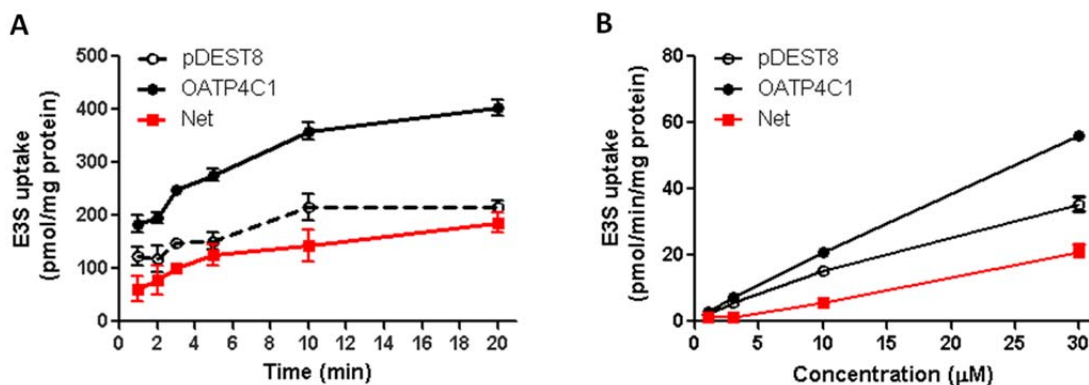


**Figure 4-40: Time-dependent and concentration-dependent OATP4C1-mediated [ $^3$ H]-E3S transport in Sf9-OATP4C1 membrane vesicles at pH 7.4.**

(A) Time-dependent 30  $\mu$ M [ $^3$ H]-E3S accumulation in Sf9-pDEST8 and Sf9-OATP4C1 membrane vesicles. (B) Concentration-dependent [ $^3$ H]-E3S accumulation in Sf9-pDEST8 and Sf9-OATP4C1 membrane vesicles at 5 min. Nonspecific adsorption on the filter was measured by incubation in cold buffer and was subtracted as background. OATP4C1-mediated (net) uptake was calculated after subtraction of nonspecific uptake by Sf9-pDEST8. Each point represents the mean  $\pm$  S.D. of triplicate determinations from one representative experiment.

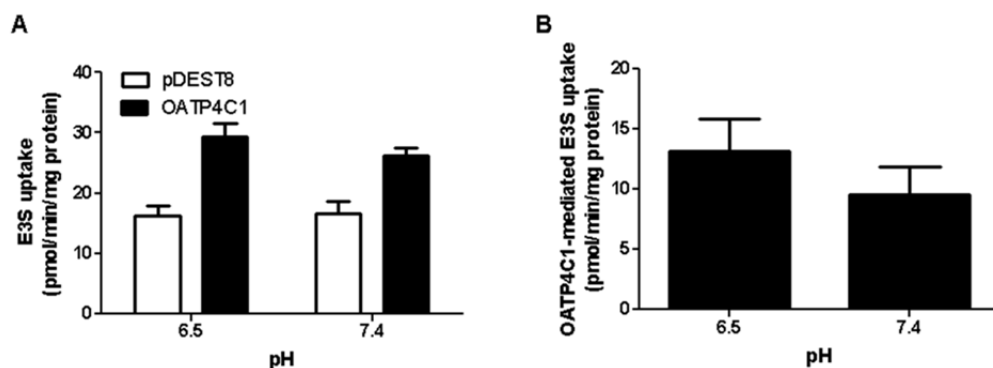


**Figure 4-41: Effect of pH on OATP4C1-mediated [ $^3\text{H}$ ]-E3S transport in Sf9-OATP4C1 membrane vesicles.**

(A) [ $^3\text{H}$ ]-E3S (20  $\mu\text{M}$ ) accumulation in Sf9-pDEST8 and Sf9-OATP4C1 membrane vesicles for 5 min at pH 6.5 and pH 7.4. (B) OATP4C1-mediated uptake was calculated after subtraction of nonspecific uptake by Sf9-pDEST8. Each point represents the mean  $\pm$  S.D. of triplicate from one representative experiment.

## **E. Validation of OATP4C1 expression in human kidney and cancer cells**

1. Specific Aim 4c: To determine the expression and subcellular localization of OATP4C1 in the human kidney.

OATP4C1 expression in human kidney by Western blotting was shown in Figure 4-33 A and B. The subcellular localization of OATP4C1 was then assessed by immunohistochemical analysis in paraformaldehyde-fixed paraffin-embedded human kidney tissue sections. To assure the quality of the kidney specimens, sections were stained with anti-MRP4 antibody (clone M4I<sub>10</sub>), which showed specific staining (Figure 4-42). However, no staining was observed using the PA1243 and PA1245 anti-OATP4C1 antibodies, despite several attempts to improve antigen recovery and to maximize reaction time (prolonged incubations).

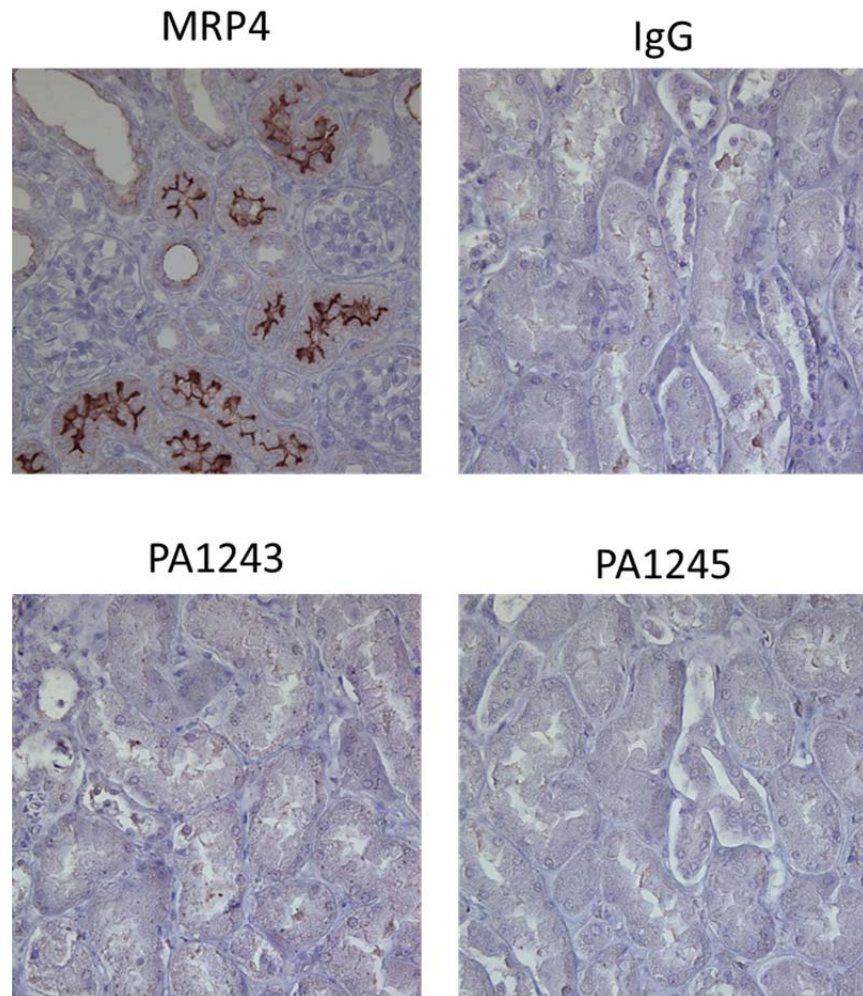


**Figure 4-42: Immunohistochemical analysis for OATP4C1 subcellular localization in human kidney sections.**

OATP4C1 was detected with rabbit polyclonal anti-OATP4C1 antibodies as indicated. Rabbit IgG was used as a negative control. MRP4, a positive control, was detected with M<sub>4</sub>I<sub>10</sub>. Magnification: 40x.

2. Specific Aim 4d: To determine the expression of OATP4C1 in cancer cells.

Microarray analysis showed a 18-fold increase of *SLCO4C1* expression in lung tumor relative to normal lung (104). In addition, *SLCO4C1* expression in lung tumor was 2-fold higher than that in human kidney. To screen *SLCO4C1* expression in different type of cancer cells, qRT-PCR was performed in 10 cancer cell lines, including prostate cancer, glioblastoma, breast cancer and melanoma cells. As shown in Figure 4-43, *SLCO4C1* expression in H1299 (non-small cell lung cancer cells) was 20-fold higher than that in human kidney, whereas *SLCO4C1* expression in other cell lines was not significantly different from that in human kidney.

*SLCO4C1* was also observed in human formalin fixed paraffin embedded lung cancer specimens. *SLCO4C1*/OATP4C1 expression in these tissues was determined by qRT-PCR and immunohistochemical analysis. Because tissue fixation and storage typically cause nucleic acid fragmentation and chemical modification, three primers were used in qRT-PCR to prevent false negative interpretation from unsuccessful amplification. 18s rRNA was used as an internal control, and relative *SLCO4C1* expression was normalized with normal lung tissue from the same patient calculated by the  $2^{-\Delta\Delta C_t}$  method. Compared with adjacent normal lung tissue, *SLCO4C1* expression was higher in the tumor for five patients (2451, 2492, 2506, 2508 and 2509), but lower for four patients (2493, 2497, 2507 and 2534) (Figure 4-44). Two patients from each group were chosen for immunohistochemical analysis to confirm OATP4C1 expression in tumor and normal lung tissue. Unlike the qRT-PCR results, OATP4C1 staining was stronger in the tumor than in the normal lung in all of four patients (Figure 4-45). Despite this discrepancy between immunohistochemistry and qRT-PCR



results, these data collectively suggested that OATP4C1 is highly expressed in lung tumors.

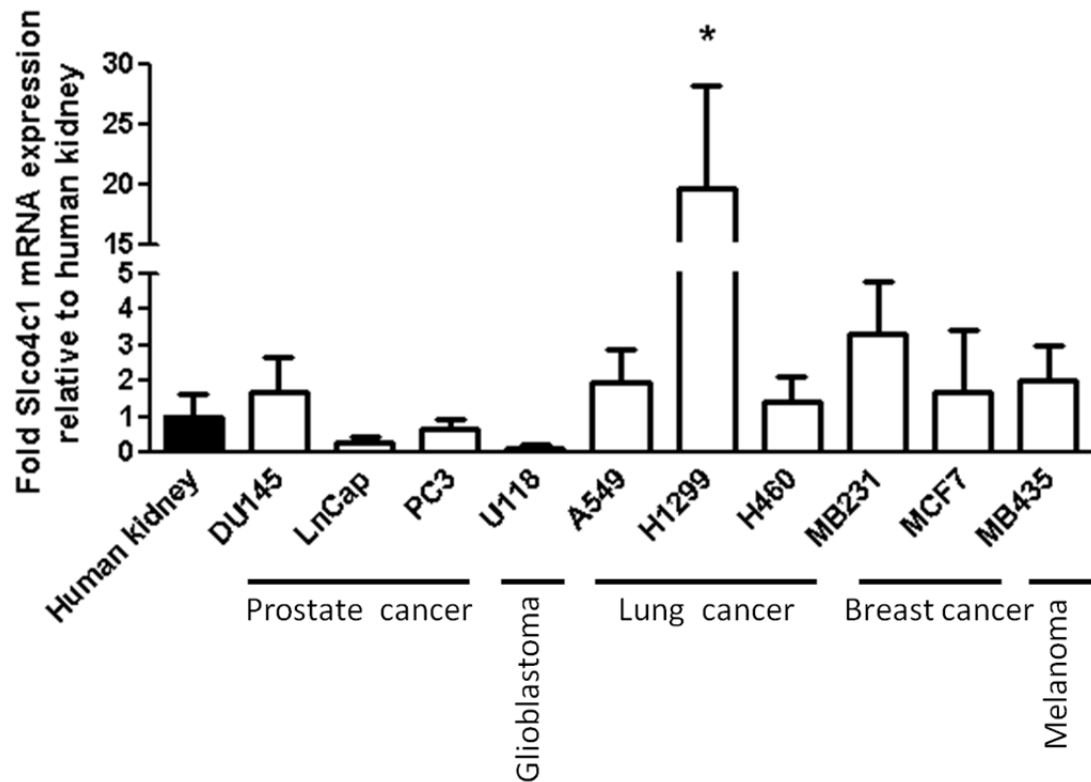


**Figure 4-43: Relative *SLCO4C1* expression in cancer cells calculated with the  $2^{-\Delta\Delta C_t}$  method.**

Relative copy number of *SLCO4C1* in the samples was normalized to 18s rRNA within each sample and values were then normalized with those in human kidney. Each bar represents mean of triplicate determinations. Statistical analysis was performed by one-way ANOVA with Dunnett's test. \*  $p < 0.05$ , significant difference from control (human kidney).

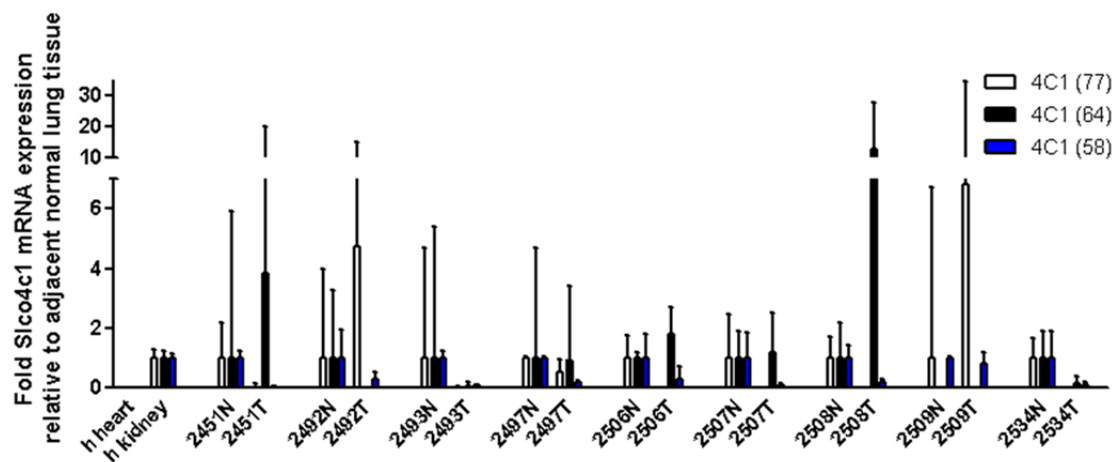


**Figure 4-44: Relative *SLCO4C1* expression in lung tumor and adjacent normal lung tissue of 9 patients calculated with the  $2^{-\Delta\Delta C_t}$  method.**

Relative copy number of *SLCO4C1* in the samples was normalized to 18s rRNA within each sample and values were then normalized with those in adjacent normal lung tissue of each patient. Each bar represents mean of triplicate determinations. The amplicon length of the primer is denoted in the parentheses. Four patients selected for immunohistochemical analysis are indicated by the blue underline.

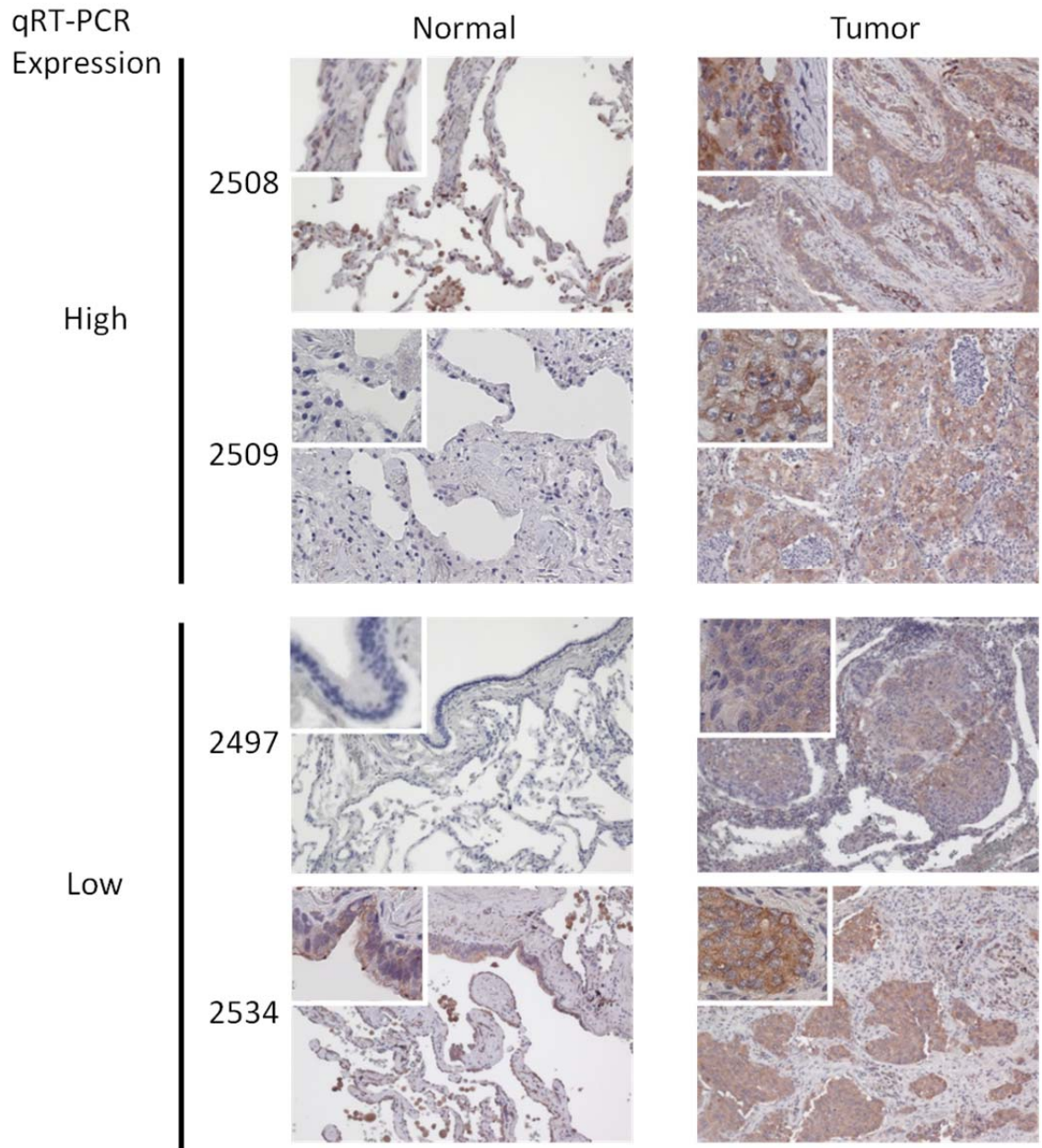


**Figure 4-45: OATP4C1 expression in the lung tumor and adjacent normal lung tissue of 4 patients.**

Immunohistochemical analysis of OATP4C1 expression in paraformaldehyde-fixed paraffin-embedded lung tumor and adjacent normal lung tissue slides. OATP4C1 was detected with PA1243. Magnification: 10x (inset 40x).

## CHAPTER 5 : DISCUSSION

### A. Creation and validation of a rat Oatp4c1-expressing cell line

Despite the well documented benefits of breastfeeding, limited data regarding the risk of drug transfer into breast milk and the possibility of exposing infants to drugs poses a dilemma for lactating mothers and their physicians. To identify the transporters involved in drug transfer into the milk, a comprehensive microarray analysis examining xenobiotic transporter genes regulation during lactation was performed and demonstrated that *SLCO4C1* expression was upregulated 70-fold in LMEC as compared to MEC. This suggests its potential role in drug transfer into the milk. In accord with the published literature, ABCG2 expression was upregulated during lactation 164-fold (10). OATP4C1/Oatp4c1 had been demonstrated to localize at the basolateral membrane in the kidney (79, 106). Therefore, we hypothesized that OATP4C1/Oatp4c1 localized at the basolateral membrane in the mammary gland and coupled with ABCG2/Abcg2, an apical efflux transporter, to facilitate the transfer of their common substrates into breast milk.

To examine the expression and subcellular localization of rat Oatp4c1 in the cells and tissues, antibodies amenable to immunohistochemistry, immunofluorescence, and immunoblotting were generated and validated. Rat Oatp4c1-expressing MDCKII cell lines were generated to study the role of Oatp4c1 in drug disposition. The MDCKII cell line was selected because of its extensive use in the published literature, ease of transfection and subsequent selection, ability to form a polarized monolayer and tight junctions. The successful transfection was demonstrated by a distinct band at appropriate molecular weight by Western blotting and specific membrane localization by immunohistochemical analysis. Unexpected results from immunofluorescence confocal

microscopy and surface protein biotinylation assay both showed that the transporter localized at the apical rather than the basolateral membranes (Figure 4-2). Although this result was unexpected, it is not without precedent, as others demonstrated that apical/basolateral sorting depends on the host cell (35). Previous results by Lai and Tan showed that MRP4 localized in the basolateral membrane of MDCKII cells (118). However, MRP4 localizes at the apical membrane of human and rodent renal proximal tubules (133). This discrepancy was later attributed to species differences in NHERF1 expression, an adaptor protein that determines the trafficking of MRP4 (119). Therefore, Oatp4c1-expressing LLC-PK1 cells were generated to confirm the subcellular localization of Oatp4c1. As observed in MDCKII cells, Oatp4c1 also localized at the apical membrane in LLC-PK1 cells (Figure 4-3).

Apical/basolateral sorting of newly synthesized proteins typically occurs in the *trans*-Golgi network, where apical and basolateral components are selectively packaged into specific transport vesicles mediated by sorting signals (134, 135). Apical sorting signals localized to all the portions of apical proteins (extracellular, transmembrane and cytoplasmic domain) include the glycosylphosphatidylinositol (GPI) anchor or N- and O-linked protein glycosylation. Basolateral sorting signals usually located in the cytoplasmic tail of basolateral proteins include tyrosine-based YXXØ, NPXY motifs (where X can be any amino acid and Ø is a bulky hydrophobic residue) and dileucine-based motifs. The trafficking of basolateral proteins containing the tyrosine-based or dileucine-based sorting signals is via adaptor proteins. AP1-μ1B is a well-characterized adaptor protein associated with basolateral sorting. It is expressed in various polarized epithelial cell lines, including MDCKII, Caco-2, but not in LLC-PK1 cells. Lack of AP1-μ1B in LLC-PK1 cells results in missorting of many basolateral proteins to the apical membrane, but stable expression of AP1-μ1B restores the basolateral trafficking (136).

Although Oatp4c1 localized at the apical membrane in both of MDCKII and LLC-PK1 cells, we can not rule out the possibility that the adaptor protein for Oatp4c1 trafficking is lacking in both cells. Therefore, it was necessary to determine the subcellular localization of Oatp4c1 in the kidney to confirm this result.

Although transfection led to detectable protein by Western blot, immunofluorescence studies showed that the transfection efficiency was very low (~ 3%) in MDCKII cells (Figure 4-4). Therefore, we attempted to obtain a single clone with homogenous high Oatp4c1 expression. Our initial attempt was to sort individual live cells into a 96-well plate by FACS analysis with transient C-terminal-tagged GFP, which was produced by adding Tag-On-Demand™ Suppressor Supernatant. However, none of the subsequent clones showed Oatp4c1 expression. Tag-On-Demand™ Suppressor Supernatant is a replication-incompetent adenovirus containing human tRNA<sup>ser</sup> suppressor, which has been mutated to recognize the TAG stop codon and decode it as serine. Translation is thereby continued through the downstream reading frame and produces a transient C-terminal tagged GFP fusion protein. The sorting gate (fluorescence channel boundaries) was set based on the fluorescence intensity, which was determined by the efficiency of Tag-On-Demand™ Suppressor Supernatant. Observed low GFP intensity was probably due to low efficiency of Tag-On-Demand™ Suppressor Supernatant, and resulted in a wide sorting gate which may have compromised the purity of sorted cells. Therefore, some of the sorted cells may not have contained the *Slco4c1* gene.

The second attempt was to sort the cells by immunofluorescence labeling. Oatp4c1 was labeled with rabbit polyclonal antibody PA1343 and Alexa 488 anti-rabbit IgG. Individual live cells were then sorted into a 96-well plate by FACS analysis with Alexa 488 fluorescence. However, none of the subsequent clones exhibited Oatp4c1

expression. The labeling of Oatp4c1 needs the C-terminal primary antibody and the secondary antibody to penetrate into the cells, and that may be difficult to achieve without permeabilization agent, Triton-X 100. Therefore, low fluorescence intensity was observed and resulted in a wide sorting gate, which compromised the purity of sorted cells.

The third attempt was to randomly seed individual live cells in 96-well plates. Unfortunately, none of the subsequent clones showed Oatp4c1 expression. These failures lead us to hypothesize that the expression of Oatp4c1 decreases the cell proliferation rate and this effect is magnified when expanding from a single cell. The decreased cell proliferation rate is probably because of the metabolic burden created from expressing a foreign protein in recombinant host cells (121). Therefore, the fourth attempt was to generate the clones starting from more than one cell using the serial dilution method. Although the homogeneity of Oatp4c1 expression was compromised, but we finally obtained one clone (c94) that showed higher Oatp4c1 expression by Western blotting (Figure 4-10) and more cells exhibiting Oatp4c1 expression as compared to the pooled cells (11% vs. 3%) by immunofluorescence staining (Figure 4-4).

To increase Oatp4c1 expression, we sought to treat the cells with sodium butyrate, simvastatin, glycerol, MG132, or to increase the selection antibiotic, blasticidin, concentration. Sodium butyrate is commonly used to induce protein expression (122, 123). It is a short-chain fatty acid that has been recognized to function as a transcription activator due to its ability to influence chromatin structure via inhibition of histone deacetylase activity (137). However, sodium butyrate was reported to disrupt the protein trafficking in Na<sup>+</sup>/K<sup>+</sup>-ATPase  $\beta_1$ - and  $\beta_2$  subunits-overexpressed MDCK-I cells (124). A concentration-dependent upregulation of Oatp4c1 expression was observed at mRNA



and protein levels, while apical polarity was maintained (Figure 4-5). The upregulation of Oatp4c1 expression, as well as increased number of cells exhibiting Oatp4c1 expression, were also observed in high concentrations of selection antibiotic, blasticidin (Figure 4-6). However, the effect of blasticidin was negligible when co-treating Oatp4c1-expressing MDCKII c94 cells with sodium butyrate and blasticidin (Figure 4-10).

Several HMG-CoA reductase inhibitors (statins) have been shown to enhance *SLCO4C1* promoter activity by inducing nuclear AhR, which binds to the XRE motifs on *SLCO4C1* promoter region. However, our data showed that simvastatin induced *Slco4c1* mRNA expression, but this did not result in increased protein expression in the MDCKII-Oatp4c1 cells (Figure 4-7). This is inconsistent with a previous report, which showed that pravastatin/fluvastatin increased *SLCO4C1* expression as well as protein function,  $T_3$  uptake, in ACHN cells (renal carcinoma cells) (106). However, other transporters expressed in ACHN cells (107), which transport  $T_3$ , may also be regulated by pravastatin/fluvastatin and thereby increase  $T_3$  uptake. Although a direct relationship between mRNA and protein levels is often expected, several reports have demonstrated weak correlation between mRNA and protein levels (138, 139). This may be the result of differences in regulatory controls, translation rates, posttranslational modification and protein degradation. In fact, simvastatin was shown to decrease androgen receptor protein expression, while its mRNA expression was not changed (140). Whether the discrepancies in Oatp4c1 mRNA and protein expression by simvastatin treatment are due to protein degradation will have to be investigated further.

The primary amino acid sequence of rat Oatp4c1 contains a high number of cysteine residues as compared to other transporters, such as ABCG2, P-gp, and MRP4. Disulfide bonds between cysteine residues play a key role in protein folding, which is important for protein trafficking and function. The high number of cysteine residues in

Oatp4c1 may lead to a higher degree of folding, which may not be possible in the MDCKII cells. In turn, misfolded proteins fail to traffic out of the endoplasmic reticulum (ER) via the Golgi apparatus to the plasma membrane, and are targeted for degradation via the ubiquitin/proteasome-dependent pathway. Glycerol is a chemical chaperone, and has protein-stabilizing properties in vitro, due to its ability to increase protein hydration (126). Glycerol has been shown to stabilize misfolded  $\Delta F508$  cystic fibrosis transmembrane conductance regulator protein (CFTR) mutant protein into conformations that are not targeted for degradation and can escape ER and degradation (125). Treatment of  $\Delta F508$  CFTR-expressing cells with high concentrations (1 - 1.25 M) of glycerol for 2 or 3 days increased the stability of fully glycosylated matured form of CFTR on Western blotting and restored the ability of forskolin-dependent (cAMP-activated) chloride transport (141). MG132 is a proteasome inhibitor that can prevent misfolded proteins, which are retained in ER, from being targeted for premature proteolysis. Its effect on misfolded protein rescue has been demonstrated in ABCG2 mutant C592G- or C608G-expressing Flp-In-293 cells. MG132 increased the expression of the fully glycosylated mature form of ABCG2 mutant by Western blotting, membrane localization by immunofluorescence staining, and also protein function as cellular resistance to ABCG2 substrate, SN-38 (142). However, treatment with glycerol or MG132 did not increase Oatp4c1 expression (Figure 4-8, Figure 4-9). This suggests that Oatp4c1 was properly folded in MDCKII cells and the low number of cells exhibiting Oatp4c1 expression (~11%) was not due to misfolded proteins. The potential cause for low Oatp4c1-expressing cells is that Oatp4c1 expression decreases the cell proliferation rate, and therefore the majority of the cell population doesn't express Oatp4c1. The slow growth rate of Oatp4c1-expressing cells is possibly due to the metabolic burden created from expressing foreign protein or protein toxicity caused from overexpressing proteins at levels higher than the physiological level (121). Recombinant protein expression

introducing a foreign protein in host cells utilizes host cell's resources, such as ATP or amino acids, imposes a metabolic burden on the host cells, and may decrease the growth rate of the host cells. The recombinant protein expression is usually significantly higher than that in physiological environment, which may not need for the host cells and cause toxicity in the host cells. In addition, Oatp4c1 functions as an uptake transporter, which may increase intracellular concentrations of substances that slow the growth rate or cause cell death.

Overall, although the number of cells exhibiting Oatp4c1 expression is low, we believe that Oatp4c1 expression with sodium butyrate induction is adequate to study Oatp4c1 function.

## **B. Determination of Oatp4c1 expression and subcellular localization in rat tissues**

The upregulation of human *SLCO4C1* expression in MG during lactation was also observed in rats by RT-PCR analysis, and protein upregulation was confirmed by Western blotting (Figure 4-12). In accord with the published literature, *Slco4c1*/Oatp4c1 was expressed in the kidney, but not in the liver (79). The expression of *Slco4c1* in rat kidney was lower than that in rat MG at the mRNA level, but was higher at the protein level. The discrepancies in *Slco4c1* mRNA and protein expression in kidney and MG may be due to tissue-dependent regulatory controls and/or posttranslational modification. An ontogenic study showed that *Slco4c1* mRNA expression in rat kidney increases with age, whereas liver expression was absent in rats of all ages (Figure 4-13, Figure 4-14). However, our observation is inconsistent with the previous findings that showed no gender differences of *Slco4c1* mRNA expression in the rat kidney (79). In terms of gender differences, higher Oatp4c1 expression was observed in non-lactating

female rat kidney as compared with males at both mRNA and protein levels (Figure 4-13). The expression of *Slco4c1* in non-lactating female rat kidney was higher than that in lactating female rat kidney at the mRNA level, but was the same at the protein level. The discrepancies may be due to differences in regulatory controls and/or posttranslational modification during lactation. However, these results were not conclusive because of the small sample size (one).

The subcellular localization of Oatp4c1 in rat tissues was determined by immunohistochemical analysis and showed apical localization in both rat kidney and MG (Figure 4-15), which was inconsistent with a previous report showing that Oatp4c1 localized at the basolateral membrane in the rat proximal tubule (79). The immunohistochemistry result was verified with four different antibodies, which were raised against unique C- and N-terminal peptides (Figure 4-16). The apical localization was also demonstrated by distinct localization of Oatp4c1 and a basolateral marker E-cadherin (Figure 4-17), and colocalization of Oatp4c1 and an apical marker p-glycoprotein (Figure 4-22 C). In addition, biochemical separation of BBM and BLM from proximal rat kidney tubules confirmed the location of Oatp4c1 at the apical/brush border membranes by Western blot and proteomic analyses (Figure 4-19). Furthermore, the proteomic analyses provide additional validation for the Oatp4c1 antibody specificity.

This extensive validation of the in vitro and in vivo subcellular localization was deemed necessary as our results were not in accordance with previous reports, which showed that Oatp4c1 localizes at the basolateral membrane in the rat proximal tubule (79), as did human OATP4C1 in the transgenic rat harboring human SLCO4C1 (106). These authors hypothesized that basolateral expression of Oatp4c1 worked in tandem with an apical efflux transporter to efficiently transport substrates across the kidney epithelium and into the urine (79, 106). The contradictory finding in the original report by

Mikkaichi and colleagues may have been a result of limited validation performed with the antibody used in that study. Our attempt to develop this polyclonal antibody (79), using the reported 11 amino acid peptide antigen, did not yield a reagent that was amenable to immunohistochemistry (Figure 4-16). The results of the transgenic OATP4C1 expression pattern reported by Toyohara et al., however, are more difficult to reconcile (106). In their publication, they present evidence that OATP4C1 localizes in the basolateral membrane of renal tubule epithelium in transgenic rats. Provided that the anti-OATP4C1 antibody recognized the correct transgenic protein, one potential explanation for the observed differences in the subcellular localization could be abnormal trafficking of the human OATP4C1 protein in the transgenic rat.

It is not without precedent that antibodies used to detect transporter proteins result in controversial findings. For instance while both BXP-9 and BXP-21 are well-validated antibodies, ABCG2 was only recently detected in human kidney using BXP-9 (57), but not with BXP-21 (143). Similarly, numerous examples can be found in the literature demonstrating the cross-reactivity of several P-glycoprotein antibodies including the C219 antibody used in this study (144). In fact, close examination of the P-gp staining obtained in Figure 4-22 A showed that both membrane and intracellular expression pattern. However, the knowledge that P-gp is expressed on the membrane allows for the correct interpretation of its expression across the kidney structures. To avoid potential misinterpretation of results due to antibody immunoreactivity, we also applied two-dimensional LC/MS-MS analysis to identify the proteome in BBM and BLM isolated from the rat kidney cortex and indirectly validate our Western blot results. Methods for separation of the BBM from the BLM have been developed based on the fact that these membranes have distinct lipid and carbohydrate compositions, so that their density and net charge are different (145). Density gradient centrifugation (146), phase partitioning,

differential centrifugation (147), and free flow electrophoresis (148) have all been described to separate BBM from BLM. In this study, differential and density gradient centrifugation were applied for the separation, and BBM were further purified by magnesium precipitation. Some of the most abundant proteins, such as Na<sup>+</sup>/K<sup>+</sup>-ATPase or rBat, SGLT2, TSC or NKCC2, were detectable in both membrane fractions, showing lack of absolute efficiency in the separation of the two membrane fractions. Cross-contamination between the two fractions was also observed in previous reports using the same method (145, 149, 150). However, these proteins were sufficiently enriched in the appropriate fraction, suggesting adequate separation of basolateral and apical membranes. In all, the LC-MS/MS analyses detected 81 proteins in both the apical and basolateral membranes. Among those, eighteen were either in the SLC or ABC transporter families (Figure 4-19 B). Based on the literature, fourteen of these proteins, not including Oatp4c1, were enriched or uniquely identified in the appropriate fraction (apical or basolateral) and three proteins (ambiguous) were equally present in both preparations. Four unique Oatp4c1 sequence peptides were found only in BBM but not in BLM. These results are in agreement with the findings from Western blotting and immunohistochemical analyses and definitively demonstrate that Oatp4c1 localized at the apical membrane in the rat proximal tubule.

The expression of Oatp4c1 at the apical membrane in the kidney suggests its potential role in renal reabsorption of its substrates as other apically expressed organic anion transporters (OATs or OATPs) do. As examples, Oatp1a1 expressed at the apical membrane of rat proximal straight tubule in the outer medulla is responsible for renal reabsorption of perfluorocarboxylates (PFO) (63, 64). Oatp2a1 localized at the apical surface of rat collecting ducts is responsible for renal reabsorption of prostanoids (78). OAT4 expressed at the apical membrane in the proximal tubule is involved in E3S and

urate reabsorption (97, 98). URAT1 expressed at the apical membrane in the proximal tubule plays a key role in urate homeostasis via a renal reabsorption mechanism (99). OATP1A2 expressed at the apical membrane in the distal tubule may participate in the saturable reabsorption of MTX (67).

The upregulation of Oatp4c1 in MG during lactation indicates that Oatp4c1 may play a role in determining the final concentrations of endogenous and exogenous substances into milk. The apical localization of Oatp4c1 in rat MG was demonstrated by immunohistochemical analysis (Figure 4-15) and confirmed further by the distinct localization of Oatp4c1 and the basolateral marker E-cadherin, and colocalization of Oatp4c1 with the apical marker Abcg2 (Figure 4-18). The apical localization of Oatp4c1 suggests that it is involved in xenobiotic reuptake from the milk to reduce exposure to the suckling infants, or that it functions as a scavenger system, as Pept2 does. Pept2 is expressed at the apical membrane in MG and has been suggested to transport the hydrolyzed milk protein product, as well as some peptide-like drugs, such as cephalosporins, back into the mammary epithelium (23).

### **C. Functional characterization of Oatp4c1 in MDCKII-Oatp4c1 cells**

The apical localization of Oatp4c1 in the proximal straight tubule suggests its potential role in renal reabsorption of its substrates. Several human OATP4C1 substrates have been reported, including cardiac glycosides (digoxin, ouabain), thyroid hormones ( $T_3$ ,  $T_4$ ), cAMP, MTX, sitagliptin and E3S (79, 109, 110). To explore the physiological role of Oatp4c1, several uptake studies and inhibition studies were performed in MDCKII-Oatp4c1 cells. In agreement with previous studies with OATP4C1 (110, 111), we showed that E3S is an Oatp4c1 substrate (Figure 4-23, Figure 4-24 and Figure 4-25). Oatp4c1-mediated E3S uptake was inhibited by  $T_4$  and enhanced by  $T_3$

(Figure 4-29 B and D), suggesting that  $T_4$  is a substrate/inhibitor and  $T_3$  is an enhancer. However, a previous report showed that OATP4C1-mediated E3S transport was decreased by  $T_3$  at pH 7.4 (110). The discrepancies may be attributable to differences between the rat Oatp4c1 and human OATP4C1, which share 80.4% homology. It is interesting to note that E3S accumulation was significantly higher in the presence of  $T_3$  in both Oatp4c1-expressing and vector-transfected cells (Figure 4-29 A and C). This suggests the presence of a  $T_3$ -inhibitable endogenous transporter involved in E3S efflux in the MDCKII cells.

OATP4C1 has been suggested to possess multiple substrate recognition sites. In a previous study it was shown that digoxin does not inhibit OATP4C1-mediated  $T_3$  (79) or E3S (110) uptake and vice versa, while E3S and  $T_3$  have mutual inhibition. Consistent with that report (110), our results showed that digoxin and ouabain did not change Oatp4c1-mediated E3S uptake, nor did MTX (Figure 4-29). These data provide initial evidence that Oatp4c1 possess multiple substrate recognition sites. One interacts with E3S/ $T_4$ , and another with digoxin/ouabain, and possibly MTX. Therefore, to verify putative substrates, multiple prototypical substrates recognized by different binding sites need to be used for future inhibition studies. In addition to E3S, the capacity of putative substrates to inhibit MTX transport was examined. MTX was shown to be an Oatp4c1 substrate (Figure 4-30). However, neither digoxin nor ouabain inhibited Oatp4c1-mediated MTX uptake (Figure 4-31 B and D), suggesting that they do not share the same binding site. In contrast, Oatp4c1-mediated MTX uptake was inhibited by  $T_3$ , which was suggested to be an enhancer for E3S uptake (Figure 4-29). Both MTX and  $T_3$  may bind to the same site to modulate Oatp4c1 function, but the affinity of MTX was too low to change Oatp4c1-mediated E3S uptake. In addition, MTX accumulation was also significantly higher in the presence of  $T_3$  in both Oatp4c1-expressing and vector-



transfected cells (Figure 4-31 A and C). This suggests the presence of a T<sub>3</sub>-inhibitable endogenous transporter involved in MTX efflux in the MDCKII cells. However, the low value/percentage of the net MTX uptake (0.2-0.5 pmol/min/mg protein corresponding to 0.0002-0.0005 %) indicated that Oatp4c1 transported MTX at a low efficiency as compared to E3S (~0.074 %). Therefore, additional inhibition studies with digoxin as a model substrate and by direct measurement of putative substrates, such as uremic toxins, are needed to definitively determine if these are substrates and/or inhibitors of Oatp4c1. These studies are necessary so that physiological role of Oatp4c1, as well as its function in the renal disposition of drugs and/or their metabolites, can be understood. Overall, we demonstrated that Oatp4c1 transports E3S and MTX. Both molecules are known to be reabsorbed in the tubules (151, 152), and this process is possibly mediated by Oatp4c1. The increased uremic toxin plasma concentrations observed in wild-type rats in the 5/6 nephrectomy renal failure model were reduced in OATP4C1 transgenic rats (106), consistent with a model of basolateral uptake by OATP4C1 and apical efflux by another transporter. However, our data demonstrated that Oatp4c1 was expressed at the apical membranes and functions as an uptake transporter, thereby implying a function in renal reabsorption, not tubular secretion. Therefore, there may be other basolateral uptake or apical efflux transporters involved in renal elimination of uremic toxins. Oat1 and Oat3, which are expressed at the basolateral membrane in the proximal tubule (91), have been shown to be responsible for indoxyl sulfate and hippuric acid uptake from blood into tubular cells (153). Moreover, the down-regulation of Oat1 and Oat3 expression in a chronic renal failure model may result in the uremic toxin accumulation (154). As for apical efflux transporters, hippuric acid, indoxyl sulfate and kynurenic acid have been shown to inhibit MRP4-mediated MTX uptake and ABCG2-mediated E3S uptake in inverted membrane vesicles (155). Furthermore, ABCG2-mediated transport is more efficient under acidic conditions (156, 157), which are likely

to prevail under normal physiological conditions in the proximal tubules. Thus, impaired efflux by an ABC transporter may also provide an explanation for increased uremic toxin accumulation in the blood of animals in the renal failure models. Clearly, more studies are required to elucidate the role of different transporters in human kidney pathophysiology and in the animal models of renal failure.

The driving force responsible for Oatp4c1 mediated transport is not fully understood. Mikkaichi et al. showed that pH did not affect OATP4C1-mediated uptake (79), while Leuthold et al. showed that E3S and T<sub>3</sub> uptake were significantly higher at extracellular pH 6.5 than pH 8.0 in *Xenopus laevis* oocytes expressing OATP4C1 (111). The pH-dependent transport has been also demonstrated in rat Oatp1a1, Oatp1a4, Oatp1a5, Oatp1b2 and human OATP1A2, OATP1B1, OATP1B3, OATP2B1, OATP3A1\_v1, OATP3A2\_v2, OATP4A1 (111, 158-160). In this study, we demonstrated that Oatp4c1-mediated E3S uptake was pH dependent. In our estimates,  $V_{\max}$  and transport uptake clearance ( $v/S$ ) were 4- and 10-fold higher, respectively, at pH 5.5 than at pH 7.4 (Figure 4-25 B, Figure 4-26, Table 4-2). The observed pH-dependent Oatp4c1-mediated uptake may be a consequence of changed intrinsic transport activity at different pH and/or altered ionization state of the substrate molecules and thus different substrate-transporter protein interaction. With a pKa of 2 (156), in our experiments (pH 4.5, 5.5 and 7.5) the ionization state of E3S is essentially constant. Therefore, any changes in E3S uptake from pH 7.4 to 4.5 could be a result of pH gradient as the driving force or changes in the protein structure. As shown in Figure 4-27, Oatp4c1-mediated E3S uptake reached a plateau with increasing H<sup>+</sup>, suggesting that H<sup>+</sup> plays a role in E3S transport, either directly by E3S/H<sup>+</sup> cotransport mechanism, or indirectly by E3S/HCO<sub>3</sub><sup>-</sup> exchange mechanism. The increasing extracellular H<sup>+</sup> concentration leads to a conversion of HCO<sub>3</sub><sup>-</sup> and H<sup>+</sup> into H<sub>2</sub>O and CO<sub>2</sub>, causing an outwardly directed HCO<sub>3</sub><sup>-</sup>

gradient across cell membranes. The outwardly  $\text{HCO}_3^-$  gradient facilitates the substrate uptake, which suggests that Oatp4c1 may be a  $\text{HCO}_3^-$  exchanger as are other OATPs (Oatp1a1, OATP1B3 and OATP2B1 (111)). Further studies examining substrate uptake in  $\text{HCO}_3^-$  replete and depleted conditions are needed to confirm a potential organic anion/ $\text{HCO}_3^-$  exchange mechanism. In addition, the pH in renal proximal tubules of rats is acidic (6.68-6.87 (161-164)) and may provide the driving force for Oatp4c1 function. Furthermore, pH-dependent changes in the protein structure may also be important for substrate transport (111, 156). A conserved histidine amino acid in the third TMD has been proposed to be critical for pH dependent transport by OATPs/Oatps. However, this histidine is only present in rat and mouse Oatp4c1, but not in human OATP4C1, which showed pH-dependent E3S and  $\text{T}_4$  uptake (111). Therefore, this histidine in the rodent proteins may not be important for Oatp4c1-mediated transport.

Interestingly, the primary amino acid sequence of rat Oatp4c1 and human OATP4C1 contain one and two potential ATP binding sites, respectively, characteristic of the Walker A motif found in ABC transporters, but not in OATP family proteins (79). Upon investigation, Mikkaichi et al. showed that ATP depletion by sodium azide and 2-deoxyglucose decreases, but does not significantly affect  $\text{T}_3$  transport in MDCKII-OATP4C1 cells (79). Similarly, our results showed that ATP depletion did not affect E3S transport in MDCKII-Oatp4c1 cells, suggesting that ATP is not involved in Oatp4c1-mediated transport (Figure 4-28). In addition, E3S accumulation in Oatp4c1-expressing and vector-transfected MDCKII cells were higher under ATP-depleted condition at pH 5.5 but not at pH 7.4 (Figure 4-28 A), suggesting the presence of an endogenous ATP-dependent efflux transporter, which has increased transport activity at pH 5.5 in MDCKII cells. Interestingly, increased E3S accumulation in Abcg2-expressing and vector-transfected MDCKII cells was also observed after GF120918 treatment at pH 5.5 but not

pH 7.4 (Figure A-1), suggesting the existence of a GF120918-inhibitable endogenous efflux transporter, which has increased transport activity at pH 5.5 in MDCKII cells. The indicated endogenous transporters may be the same. There are three endogenous ABC transporters identified in MDCKII cells: p-glycoprotein, Mrp1 and Mrp2 (165). P-glycoprotein is inhibitable by GF120918, but there is no evidence that it transports E3S (166, 167). Mrp1 can transport E3S, but is not inhibitable by GF120918 (168-170). Mrp2 can transport E3S, but its inhibition by GF120918 is controversial (43, 165, 167, 169, 171). Therefore, there may be other GF120918-inhibitable ATP-dependent endogenous transporter present in MDCKII cells or these two phenomena are governed by different transporters.

Most of the OATPs/Oatps are bidirectional transporters. However, a previous report showed that OATP4C1-mediated  $T_3$  transport is unidirectional from outside to inside (79). To investigate the transport direction of Oatp4c1, further studies examining E3S efflux in E3S pre-loaded cells or examining E3S flux from apical to basolateral or from basolateral to apical in a polarized monolayer are needed.

#### **D. Creation and validation of human OATP4C1-expressing cell lines**

Although the primary sequence homology between human and rat Oatp4c1 is 80.4%, it is possible that species differences exist in subcellular localization. Human OAT2 and rat Oat2 share 79% homology, but human OAT2 localizes at the basolateral membrane of proximal tubules (92), whereas rat Oat2 localizes at the apical surface of proximal tubule S3 segments, medullary thick ascending limb of Henle's loop and the collecting ducts (91, 93). To examine the expression and subcellular localization of human OATP4C1 in cells and tissues, two antibodies amenable to immunohistochemistry, immunofluorescence, and immunoblotting were generated and

validated. To study the role of OATP4C1 in drug disposition, two human OATP4C1-expressing cell lines were generated. The MDCKII cell line was selected because of its ability to form a polarized monolayer and tight junctions for directional transport study. Sf9 cells were selected because of their higher expression level of recombinant proteins and ease of scaling up for substrate screening. The successful transfection in MDCKII cells was demonstrated as a distinct band at ~60 kDa in MDCKII-OATP4C1 cells but not in MDCKII-pcDNA cells by Western blotting (Figure 4-33 A). The apparent molecular weight was lower than the calculated molecular weight (79 kDa) which may be attributable to absent glycosylation or misfolded truncated protein. The successful transfection was also verified by immunohistochemical analysis showing specific membrane localization in OATP4C1-expressing cells, but not in vector-transfected cells. The specific staining was abolished when probing with antibody that was pre-absorbed with antigen peptide, but some background staining was observed in sections exposed to rabbit IgG instead of primary antibody (Figure 4-33 C). As observed in rat *Oatp4c1*, OATP4C1 localized at the apical membrane in MDCKII-OATP4C1 cells (Figure 4-33 D). Surface biotinylation assay demonstrated that OATP4C1 was enriched in the apical membrane fraction as compared with the basolateral membrane (Figure 4-33 E). Although efficient separation between apical and basolateral membrane was demonstrated by  $\text{Na}^+/\text{K}^+$ -ATPase, the membrane fractions may be contaminated with cytosol, which contains partially processed or misfolded OATP4C1 in the ER/Golgi system. Functional activity of OATP4C1 in MDCKII-OATP4C1 cells was probed with ouabain and E3S by uptake studies. A saturable concentration-dependent OATP4C1-mediated ouabain uptake was observed and the transport parameters were estimated (Figure 4-34, Table 4-3). The estimated  $K_m$  ( $0.19 \pm 0.09 \mu\text{M}$ ) was in the similar range of the reported  $K_m$  ( $0.38 \pm 0.1 \mu\text{M}$ ) (79). In addition, a concentration-dependent OATP4C1-mediated E3S uptake was observed, despite the concentrations we used were not high

enough to show saturation kinetics (Figure 4-35). Further studies with higher concentrations are needed to show saturation kinetics and obtain transport parameters. These data confirmed that ouabain and E3S were OATP4C1 substrates (79, 110) and showed the functional activity of OATP4C1 in MDCKII-OATP4C1 cells, although its apparent molecular weight was lower than the calculated one. Collectively, OATP4C1 expression and function were validated in MDCKII-OATP4C1 cells which can be used to investigate the driving force and transport direction of OATP4C1-mediated transport and explore the potential substrates and the role of OATP4C1 in drug disposition.

In addition to MDCKII cells, OATP4C1 was overexpressed in Sf9 cells with a baculovirus expression system. The successful infection was demonstrated as a broad band at ~60 kDa as observed in MDCKII-OATP4C1 cells (Figure 4-37). The recombinant protein expressed in Sf9 cells commonly appears as a deglycosylated form, however, no reports indicate any functional consequence of different glycosylation patterns (172, 173). Functional activity of OATP4C1 in Sf9-OATP4C1 cells was probed with ouabain and E3S by vesicular transport assay. Selecting membrane filters with minimal drug adsorption is important for this assay. High background adsorption may decrease the sensitivity and interfere with data interpretation. This was the case with ouabain studies using the OE67 filter membrane. Although the estimated  $K_m$  ( $0.18 \pm 0.09 \mu\text{M}$ ) of OATP4C1-mediated ouabain uptake was comparable with the  $K_m$  estimated from MDCKII-OATP4C1 cells ( $0.19 \pm 0.09 \mu\text{M}$ ) and in the similar range of the reported  $K_m$  ( $0.38 \pm 0.1 \mu\text{M}$ ) (79) (Figure 4-39, Table 4-4), the high background adsorption may decrease the sensitivity of the capacity to be inhibited for substrate screening during inhibition studies. The nonspecific adsorption of E3S on RC55 filter membrane was relatively low (~0.3%). A concentration-dependent OATP4C1-mediated E3S uptake was observed, but the concentrations we used were not high enough to saturate the

transporter (Figure 4-40 B). Further studies with higher concentrations are needed to show saturation kinetics and obtain transport parameters. The pH effect on OATP4C1-mediated E3S transport was also examined (Figure 4-41). There was a trend toward increasing net uptake with a decrease in pH. Additional studies at more than two pH conditions are needed to confirm the pH-dependency of OATP4C1-mediated E3S transport. Vesicular transport assay is a good tool to study ATP-dependent transport for efflux transporters, but not for uptake transporters such as OATP4C1. Extracellular ATP is not able to penetrate into cells and bind to the intracellular ATP-binding site of OATP4C1 to function. Therefore, to examine if ATP is the driving force for OATP4C1, determining E3S uptake in the presence and absence of a cell-permeable ATP-analogue, formycin A (174, 175), is needed. Collectively, OATP4C1 expression and function were validated in Sf9-OATP4C1 cells and the system can be used to further investigate the role of OATP4C1 in drug disposition.

#### **E. Validation of OATP4C1 expression in human kidney and cancer cells**

OATP4C1/Oatp4c1 was isolated from human/rat kidney (79) and its basolateral localization in the renal proximal tubules was determined in the transgenic rat harboring human SLCO4C1 and in the rat (79, 106). However, we have definitively demonstrated that rat Oatp4c1 localized at the apical membrane in the kidney, and thereby its physiological function implies a role in renal reabsorption, not tubular secretion. We also attempted to determine OATP4C1 subcellular localization in human kidney by immunohistochemical analysis. Despite multiple approaches and efforts, no staining was observed using our anti-OATP4C1 antibodies, whereas the quality of tissue specimens was verified with MRP4 expression (Figure 4-42) and the amenability of our anti-

OATP4C1 antibodies in immunohistochemistry was validated in MDCKII-OATP4C1 cells (Figure 4-33 C) and in lung tumor specimens (Figure 4-45). It is not without precedent that well-validated antibodies failed to detect transporter proteins in tissues which were later detected by other antibodies. For instance, ABCG2 was not detected in human kidney with BXP-21 (143), but was recently detected with BXP-9 (57). In addition, the antibodies used in immunohistochemical analysis of OATP4C1 in human kidney may have been degraded because it was performed one year later than that in MDCKII-OATP4C1 cells and in lung tumor specimens. Further studies with different antibodies or performing Western blot analysis on isolation BBM and BLM from human kidney are needed to verify the subcellular localization in human kidney.

Microarray analysis has shown that *SLCO4C1* was highly expressed in lung tumor, and its expression in lung tumor was 18- and 2- fold higher than in normal lung, and normal kidney, respectively (104). *SLCO4C1* was also detected in several cancer cell lines, including renal carcinoma cells (ACHN, SN12C), ovarian cancer cells (OVCAR-8, OVCAR-3), leukemia cells (HL-60, RPMI-8226, CCRF-CEM), lung cancer cells (H322M, H23, HOP-62, H460), glioblastoma (SF-539) and breast cancer cells (BT-549) (107). The high *SLCO4C1* expression in lung tumor was confirmed in non-small cell lung cancer cells H1299 and in lung tumor specimens. Our data demonstrated a 20-fold increase of *SLCO4C1* expression in H1299 cells relative to human kidney (Figure 4-43). Further studies need to confirm this message with Western blotting.

RT-PCR and immunohistochemical analysis were performed in the lung tumor and adjacent normal lung tissue specimen isolated from patients. Total RNA isolated from formaldehyde-fixed paraffin-embedded (FFPE) slides is typically fragmented and chemically modified. During tissue fixation process, formaldehyde reacts with the nitrogen atoms of lysine, arginine, and histidine, resulting in extensive cross-linking of



the proteins within each cell. Nucleic acids are subsequently trapped and modified by extensive protein-protein and protein-nucleic acid crosslinks. Even after protease treatment, some of the nucleic acid bases are still crosslinked, which cannot be recognized as templates and be amplified by polymerases. During storage, atmospheric oxygen, water and light cause nucleic acid degradation and fragmentation over time. Samples that have been stored over five years typically yield nucleic acids with only ~100 nt (176-178). Therefore, successful amplification is limited to small fragments and less sensitivities in template detection. Our samples were stored for over 2.5 years so that the isolated RNA was possibly fragmented. To prevent false negative interpretation from unsuccessful amplification due to fragmented and chemically modified RNA, three primers were utilized in RT-PCR analysis. Results from only one of three primers demonstrated higher *SLCO4C1* expression in the tumor than in the adjacent lung tissue in five out of nine patients (Figure 4-44). Two patients with either higher or lower *SLCO4C1* expression in tumor relative to adjacent normal lung were selected to examine OATP4C1 expression by immunohistochemical analysis. All of four patients showed stronger OATP4C1 staining in the tumor than in the adjacent normal lung tissue (Figure 4-45). The discrepancies from RT-PCR and immunohistochemistry results may be due to unsuccessful amplification of the fragmented RNA. Collectively, these data demonstrated highly OATP4C1 expression in lung tumor and possibly higher than in normal lung. The high OATP4C1 expression in the lung tumor may facilitate the uptake of physiological substrates that facilitate tumor cell survival but may also uptake anticancer drugs, such as MTX, and these functions may have implications in cancer therapy. Clearly, more studies are required to elucidate the role of OATP4C1 in the treatment for lung cancer.

## CHAPTER 6 : CONCLUSIONS

This dissertation focused on validation of the subcellular localization of OATP4C1/Oatp4c1 in *in vitro* models and in human/rat tissues and on its transport characteristics. Multiple antibodies amenable to immunohistochemistry, immunofluorescence, and immunoblotting were developed and validated with OATP4C1/Oatp4c1-expressing *in vitro* models. The expression of *Slco4c1*/Oatp4c1 in Oatp4c1-expressing MDCKII cells was increased with sodium butyrate or blasticidin treatment, but was not changed with glycerol or MG132 treatment. Simvastatin enhanced Oatp4c1 expression only at the mRNA level, but not at the protein level. A single clone with highest Oatp4c1 expression (c94) was obtained by serial dilution method. The effect of blasticidin on increasing Oatp4c1 expression was negligible when co-treating sodium butyrate and blasticidin in c94 cells. Therefore, for *in vitro* functional studies, c94 cells were first treated with sodium butyrate to induce Oatp4c1 expression.

Oatp4c1 expression in rat kidney was increased with age, while it was not detected in rat liver at any age. Higher *Slco4c1*/Oatp4c1 expression was observed in female rat kidney as compared with males. To determine the subcellular localization of Oatp4c1 in the *in vitro* models and in rat tissues, a comprehensive approach was undertaken, and these studies definitively demonstrated that Oatp4c1 is expressed at the apical membrane in the rat proximal tubule and mammary epithelium. Our approach included a variety of complementary methods to verify this observation. Western blotting demonstrated that the antibody used recognized a protein of appropriate molecular weight. Immunofluorescence and immunohistochemical analysis revealed that the protein localizes at the apical membrane of polarized epithelium *in vitro* (Oatp4c1-expressing MDCKII, LLC-PK1 cells) and *in vivo* (rat kidney, MG). The immunohistochemistry results were verified with four different antibodies, which were

raised against unique C- and N-terminal peptides, and also confirmed by double immunofluorescence staining with apical or basolateral markers. In addition, biochemical separation of apical and basolateral membranes from polarized cells *in vitro* and proximal rat kidney tubules confirmed the location of Oatp4c1 at the brush border membranes by Western blot and proteomic analyses. Furthermore, the proteomic analyses provide additional validation for the Oatp4c1 antibody specificity. In addition, double immunofluorescence staining and immunohistochemical analysis showed that Oatp4c1 localized in the proximal straight tubule (S3 segment) in the juxtamedullary cortex, and colocalized with P-gp and Abcg2, but not with Mrp4.

The apical localization of rat Oatp4c1 in the kidney suggests its potential role in tubular reabsorption of its substrates. Although we did not perform extensive studies to identify potential Oatp4c1 substrates, we demonstrated that most human OATP4C1 substrates were rat Oatp4c1 substrates, including E3S, MTX and possibly T<sub>4</sub> (79, 110). T<sub>3</sub> was an enhancer for Oatp4c1-mediated E3S uptake, but was an inhibitor for Oatp4c1-mediated MTX uptake. This suggests that T<sub>3</sub> and MTX shared the same binding site while the affinity of MTX was too low to change Oatp4c1-mediated E3S uptake. In accord with the previous finding of OATP4C1 (110), ouabain and digoxin did not inhibit Oatp4c1-mediated E3S uptake, which provides corroborating evidence that Oatp4c1 possesses multiple binding sites. In addition, previously purported uremic toxin substrates failed to inhibit Oatp4c1-mediated E3S uptake, suggesting that they were not substrates or that they interact with a different binding site. The Oatp4c1-mediated E3S uptake was ATP-independent and pH-dependent, suggesting that the pH gradient is the driving force for Oatp4c1-mediated transport. The increased E3S transport activity at acidic extracellular pH was ascribed to the increased maximum transport rate ( $V_{max}$ ). In addition, our data indicated the presence of an ATP-dependent and/or GF120918-

inhibitable endogenous E3S efflux transporter with increased transport activity at acidic pH in MDCKII cells.

In accord with previous microarray data demonstrating that human *SLCO4C1* expression was upregulated during lactation, rat *Slco4c1*/Oatp4c1 expression was increased in lactating MG as compared with non-lactating MG, indicating a potential role of Oatp4c1 in endogenous or exogenous substances transport into the milk. The apical localization of Oatp4c1 suggests that it is involved in reuptake of xenobiotic from the milk, resulting in their reduced exposure to the suckling infants, or that it functions as a scavenger system.

Human OATP4C1 was demonstrated to localize at the apical membrane in the *in vitro* model (MDCKII cells). However, the determination of the subcellular localization of OATP4C1 in human kidney was not possible, even though that the antibody we developed was amenable for immunohistochemistry and the quality of tissue specimens was verified. Further studies with different antibodies or performing Western blot analysis on isolation BBM and BLM from human kidney are needed to verify the subcellular localization in human kidney. Uptake study in MDCKII-OATP4C1 cells and vesicular transport study in Sf9-OATP4C1 cells confirmed that ouabain and E3S were OATP4C1 substrates (79, 110). In addition, our data demonstrated that OATP4C1 was highly expressed in lung cancer cells (H1299) and lung tumor specimens by RT-PCR and immunohistochemical analysis, respectively.

For future studies, generating OATP4C1-knockout mice will be useful to gain more insight of the physiological role of OATP4C1 and its impact on the pharmacokinetics of drugs. Metabolomic analysis of urine from OATP4C1-knockout mice will be applied in an attempt to identify endogenous substrates without prior knowledge of transport studies.

In addition, to determine the role of OATP4C1 in lung cancer cells, cell viability will be first examined in the OATP4C1-transfected cells or in the SLCO4C1 siRNA-silencing lung cancer cells (H1299) with treatment of anticancer drugs which are also OATP4C1 substrates, such as MTX. To examine if OATP4C1 confers cell death through apoptotic pathways, the apoptotic outcome will be examined by terminal deoxynucleotidyl transferase-mediated deoxyuridine triphosphate nick end-labeling (TUNEL) assay or Annexin V assay.

Overall, the apical localization of Oatp4c1 in the rat kidney and MG is a highly novel finding of this study, and thereby implies its physiological role in renal reabsorption, not tubular secretion. Further studies to identify Oatp4c1 substrates will explore the physiological role and significance of Oatp4c1.

## APPENDICES

### Appendix 1: Lists of abbreviations

CFTR	Cystic fibrosis transmembrane conductance regulator protein
ER	Endoplasmic reticulum
A→B	From apical to basolateral
ABC	ATP-binding cassette
AE	Apical efflux
AhR	Aryl hydrocarbon receptors
AIC	Akaike Information Criterion
ANOVA	Analysis of variance
AP	Apical
AQP1	Aquaporin 1
ATP	Adenosine triphosphate
AU	Apical uptake
B→A	From basolateral to apical
BBM	Brush-border membrane
BCRP	Breast cancer resistance protein
BL	Basolateral
BLM	Basolateral membrane
Bsd	Blasticidin
C	Substrate concentration
c94	Clone 94
cAMP	Cyclic adenosine monophosphate
cGMP	Cyclic guanosine monophosphate
D	Diffusion
DMEM	Dulbecco's modified Eagle's medium
dNTP	Deoxyribonucleotide triphosphate
DTT	Dithiothreitol
E3S	Estrone-3-sulfate
FACS	Fluorescence-activated cell sorting
GF	GF120918
GFP	Green fluorescent protein

HMG-CoA	Hydroxymethylglutaryl–CoA
HRP	Horseradish peroxidase
IgG	Immunoglobulin G
K <sub>m</sub>	Michaelis-Menten constant
LMEC	Lactating mammary epithelial cells
MDCKII	Madin-Darby canine kidney II
MDR	Multidrug resistance protein
MEC	Non-lactating mammary epithelial cells
MEM	Minimum essential medium
MG	Mammary gland
MG132	N-benzoyloxycarbonyl (Z)-Leu-Leu-leucinal
MRP	Multidrug resistance-associated protein
MTX	Methotrexate
n	Hill slope
NaB	Sodium butyrate
NBD	Nucleotide binding domains
NHERF1	Na <sup>+</sup> /H <sup>+</sup> exchanger regulatory factor 1
NSAIDs	Non-steroidal anti-inflammatory drugs
OAT	Organic anion transporter
OATP	Organic anion transporting polypeptide
OCT	Organic cation transporter
OCTN	Zwitterion/cation transporters
PAH	Para-aminohippurate
PC	Paracellular transport
PEPT	Peptide transporter
PFO	Perfluorocarboxylates
P-gp	P-glycoprotein
PS	Permeability-surface area product
RT-PCR	Real-time polymerase chain reaction
S <sub>50</sub>	Michaelis-Menten constant equivalent
SC	Spectral counts
SDS-PAGE	Sodium dodecyl sulfate polyacrylamide gel electrophoresis
Sim	Simvastatin
SLC	Solute carrier

SLCO	Solute carrier organic anion transporter
T3	Triiodothyronine
T4	Thyroxine
TEER	Transepithelial electrical resistance
$T_{\max}$	Maximum uptake velocity
TMD	Transmembrane domains
URAT	Urate transporter
V	Initial uptake velocity
V <sub>max</sub>	Maximum transport rate
XRE	Xenobiotic-responsive element



## **Appendix 2: Identification of Abcg2 as a potential transporter of uremic toxins**

### Introduction:

OATP4C1 has been proposed to be involved in the elimination of uremic toxins and its expression in a transgenic rat model was shown to decrease the concentration of uremic toxins in a 5/6 nephrectomy renal failure model (106). However, we demonstrated that Oatp4c1 is expressed at the apical membrane in the kidney, which suggests that Oatp4c1 is involved in renal reabsorption but not tubular secretion as previously suggested (79, 106, 110). Lack of E3S transport inhibition by uremic toxins led us to probe the interaction of uremic toxins with other transporters as a way to reconcile previous observations in a renal failure model (106). Recent evidence suggests that human ABCG2 and MRP4 may also transport uremic toxins (155). Therefore, we hypothesized that impaired uremic toxin clearance could result from impaired transport by an efflux pump in the renal tubules. This hypothesis is consistent with previous work demonstrating that the function of ABCG2 is less efficient at pH 7.4 than in acidic pH, while the urine pH ranges in the acidic range under normal conditions, but can be basic (> pH 7) under pathological situations. (156, 157). In this study, the capacity of uremic toxins to inhibit Abcg2 –mediated Hoechst 33342 efflux was determined by at pH 5.5 and pH 7.4.

### Methods:

Rat Abcg2- and pcDNA3.1 (vector)-transfected MDCKII cells generously provided by Dr. McNamara's lab (13) were grown in MEM supplemented with 5% fetal bovine serum, 100 U/ml penicillin, 100 µg/ml streptomycin, and 500 µg/ml geneticin.

Functional activity of Abcg2 in MDCKII-Abcg2 cells was preliminary assessed by [<sup>3</sup>H]-E3S uptake studies in the presence and absence of 10 µM GF120918 at pH 5.5 and pH 7.4. The procedures were the same as described in Chapter 3 -D -1 [<sup>3</sup>H]-E3S uptake and inhibition studies.

Functional activity of Abcg2 in MDCKII-Abcg2 cells was also assessed by Hoechst 33342 efflux. MDCKII-pcDNA and MDCKII-Abcg2 cells were grown in 6-well plates (1 x 10<sup>6</sup> cells/well) and allowed to become confluent overnight. Cells were washed once and pre-incubated in OptiMEM in the presence and absence of 10 µM GF120918, 2 mM MTX, and 1 mM uremic toxins (kynurenic acid, indoxyl sulfate, hippuric acid and trans-aconitic acid) for 15 min and during the duration of the Hoechst 33342 incubation. The experiment was initiated by incubating cells with 2 µM Hoechst 33342 for 45 min at 37°C. Cells were washed twice with ice-cold PBS and lysed with 500 µl of 10 mM HEPES (pH 7.4) containing 0.2% SDS for 30 min. Lysates (200 µl) were transferred to a 96-well plate and the fluorescence of Hoechst 33342 was determined in a microplate reader (SpectraMax M5, Molecular Devices, Sunnyvale, CA) at excitation and emission wavelengths of 360 and 460 nm, respectively. Protein concentration in cell lysates was measured by BCA Protein Assay Kit, and used to normalize the fluorescence readings.

### Results and Discussion:

To evaluate functional activity of Abcg2 in MDCKII-Abcg2 cells, the uptake studies of ABCG2 substrate, E3S (179), was performed in the presence and absence of Abcg2 inhibitor GF120918 (13) at pH 5.5 and pH 7.4. As shown in Figure A-1, there was no significant difference between [<sup>3</sup>H]-E3S accumulation in MDCKII-Abcg2 and MDCKII-pcDNA cells at both pH values, suggesting that E3S was not a rat Abcg2 substrate or

E3S intracellular concentration was not high enough to show a significant Abcg2-mediated transport. In addition, [ $^3\text{H}$ ]-E3S accumulation in both MDCKII-Abcg2 and MDCKII-pcDNA cells were substantially higher in the presence of GF120918 at pH 5.5 but not at pH 7.4, suggesting the presence of a GF120918-inhibitable endogenous efflux transporter in MDCKII cells. This endogenous efflux transporter may interfere Abcg2-mediated E3S transport.

Therefore, another ABCG2 substrate, Hoechst 33342 (180), was then used to access Abcg2 function. Intracellular fluorescence after 45 min incubation with Hoechst 33342 was determined in the absence and presence of GF120918 at pH 5.5 and 7.4 (Figure A-2 A). Abcg2-mediated Hoechst 33342 efflux was calculated by subtracting the accumulation in Abcg2-expressing cells from that in vector-transfected cells. Transport specificity was demonstrated by GF120918 inhibition. As shown in Figure A-2 B, Abcg2-mediated Hoechst 33342 effluxes were both reduced with GF120918 addition at both pH values. At pH 7.4, the decreased net accumulation was resulted from the increased accumulation in MDCKII-Abcg2 cells as GF120918 inhibiting Abcg2-mediated efflux. However, at pH 5.5, the decreased net accumulation was resulted from the decreased accumulation in MDCKII-pcDNA cells while the accumulation in MDCKII-Abcg2 cells was not changed (Figure A-2 A). The decreased accumulation in MDCKII-pcDNA cells in the presence of GF120918 was probably because of the presence of a GF120918-inhibitable endogenous uptake transporter functioned at pH 5.5. In addition, inconsistent with previous reports showing ABCG2 function was less efficient at pH 7.4 than in acidic pH (156, 157). Abcg2-mediated Hoechst 33342 efflux was higher at pH 7.4 than at pH 5.5. The discrepancy was probably because of different assay system. Inverted membrane vesicles were used in previous reports, whereas intact cells were used in this study which required the substrates penetrated into the cells before being efflux. In

addition, the endogenous uptake transporter functioned at pH 5.5 may also interfere Abcg2-mediated Hoechst 33342 transport.

The capacity of uremic toxins to inhibit Hoechst 33342 efflux was also examined. Among the uremic toxins tested, indoxyl sulfate and *trans*-aconitic acid inhibited Abcg2-mediated Hoechst 33342 efflux at pH 5.5, but not at pH 7.4. This suggests that Abcg2 may transport these uremic toxins only at normal condition (acidic pH) but not at pathological conditions (pH >7), and therefore, the uremic toxin plasma concentrations is increased in renal failure model (106). With a predicted pKa of 17.0, the ionization states of indoxyl sulfate at pH 5.5 and 7.4 are constant. Therefore, the pH-dependent inhibitory effect was resulted from the drug-protein interactions. However, the predicted pKa for *trans*-aconitic acid is 2.8 and 4.46. The unionization ratio is 8.4% and 0.1% at pH 5.5 and pH 7.4, respectively, indicating that the unionized form of 1 mM *trans*-aconitic acid is 84  $\mu$ M and 1  $\mu$ M at pH 5.5 and pH 7.4, respectively. Therefore, the pH-dependent inhibitory effect was probably resulted from different amount of unionized drug diffused into the cells. More studies using inverted membrane vesicles or different model substrates were required to elucidate the role of Abcg2 or other renal transporters in uremic toxins disposition.

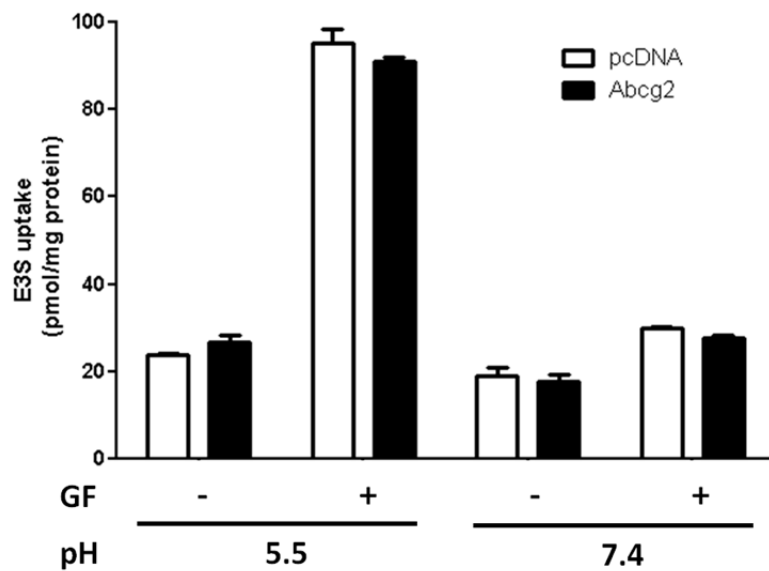


**Figure A-1: The effect of GF120918 on [ $^3$ H]-E3S uptake in MDCKII-Abcg2 cells at pH 5.5 and 7.4.**

MDCKII-pcDNA and MDCKII-Abcg2 cells were incubated with 5  $\mu$ M [ $^3$ H]-E3S in the absence and presence of 10  $\mu$ M GF120918 for 15 min at pH 5.5 and 7.4. Each bar represents the mean  $\pm$  S.D. of triplicate determinations from one representative experiment.

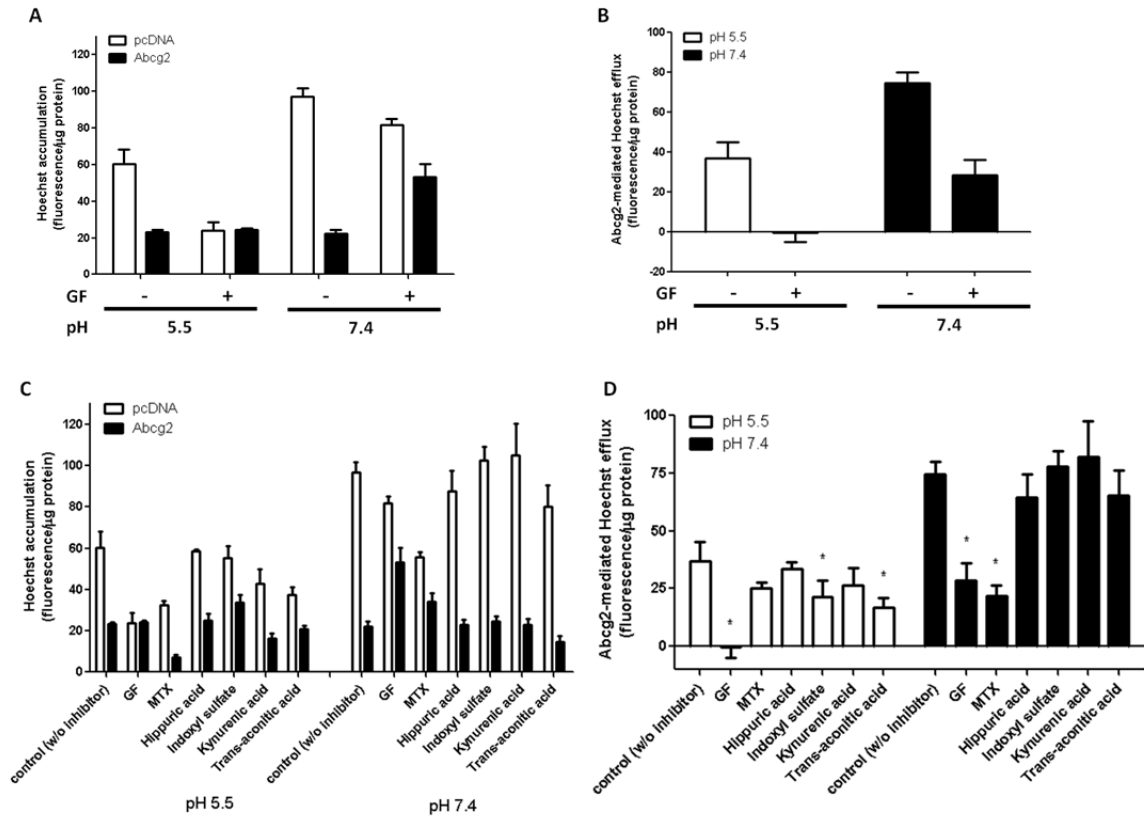


**Figure A-2: Inhibition of Hoechst 33342 efflux by various compounds in MDCKII-Abcg2 cells at pH 5.5 and 7.4.**

MDCKII-pcDNA and MDCKII-Abcg2 cells were incubated with 2  $\mu$ M Hoechst 33342 in the absence (control) and presence of 10  $\mu$ M GF120918 (GF), 2 mM MTX, and 1 mM uremic toxins (kynurenic acid, indoxyl sulfate, hippuric acid and *trans*-aconitic acid) for 45 min at pH5.5 and 7.4. Abcg2-mediated efflux was calculated by subtracting the accumulation in Abcg2-expressing cells from that in vector-transfected cells (B, D). Each bar represents the mean  $\pm$  S.D. of triplicate determinations from one representative experiment. Statistical analysis was performed by two-way ANOVA with Bonferroni post-hoc test comparing with control.\*  $p < 0.05$ , significant differences from control.

### **Appendix 3: Creation and validation of human ABCG2-expressing Sf9 cells**

#### Introduction:

ABCG2 also known as breast cancer resistance protein (BCRP) is a half-transporter containing only 6 TMD, and forms a homodimer to acquire transport activity. ABCG2 is expressed at the apical membrane in multiple tissues, including liver, intestine, placenta, blood-brain-barrier, lung, mammary gland and kidney proximal tubule (57, 58). It limits the entry of its substrates into the tissues and facilitates the elimination of its substrates to the bile and urine. In addition, it is important in nutrients as well as xenobiotic accumulation in the milk (10). ABCG2 transports a wide range of substrates including uncharged or amphiphilic compounds, such as MTX, mitoxantrone and cimetidine (12). To study the role of ABCG2 in drug disposition, ABCG2-expressing Sf9 cells were developed for substrate screening.

#### Methods:

pFastBac1-ABCG2 plasmid vector construct (Figure A-3) was generated previously in our lab. Detail procedures for pFastBac1-ABCG2 plasmid vector construct were as described in Chapter 3-E-2-i. Plasmid vector construction. Briefly, ABCG2 was cloned into pFastBac1 and recombined in MAX Efficiency<sup>®</sup> DH10Bac<sup>™</sup> competent *E. Coli*. containing baculovirus genome. The bacmid DNA from positive transformants was verified by PCR with M13 forward (5'-GTTTTCCCAGTCACGAC-3') and M13 reverse (5'-CAGGAAACAGCTATGAC-3') primers and agarose gel electrophoresis.

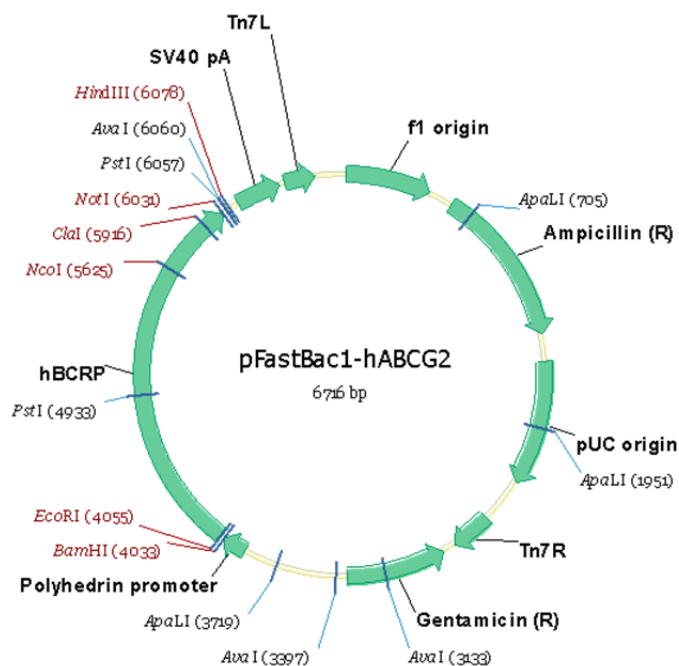


**Figure A-3: pFastBac1-ABCG2 plasmid construct.**

Procedures for Sf9 cell culture, transfection, infection, membrane vesicle preparation and vesicular transport assay were the same as described in Chapter 3-E-2 *Spodoptera frugiperda* (Sf9) insect cells. The successful infection of ABCG2 was detected with 0.25 µg/ml BXP-21.

MDCKII-ABCG2 c40 cells generously provided by Dr. McNamara's lab (30) were grown in MEM supplemented with 5% fetal bovine serum, 100 U/ml penicillin, 100 µg/ml streptomycin, and 500 µg/ml geneticin.



### Results and Discussion:

pFastBac1-ABCG2 plasmid vector construct and recombinant bacmid DNA were generated previously in our lab. Recombinant bacmids were verified by PCR with M13 forward and M13 reverse primers (Figure A-4).

The recombinant bacmids (pFastBac1-ABCG2 and pFastBac1) were transfected into Sf9 cells, and the supernatant containing recombinant baculovirus stock was harvested after 48 hr. The viral stock was amplified by infecting a large volume of Sf9 cell suspensions. The infected Sf9 cells were centrifuged to collect cell pellets for membrane vesicle preparation. Successful infection was validated by Western blotting for ABCG2 expression in the membrane vesicles. As shown in Figure A-5, ABCG2 was detected in Sf9-ABCG2 membrane vesicles but not in Sf9-vector. In addition, in accord with previous reports (172), as compared with the protein band in MDCKII-ABCG2 c40 cells with PNGase F deglycosylation, the overexpressed ABCG2 in Sf9 cells was unglycosylated.

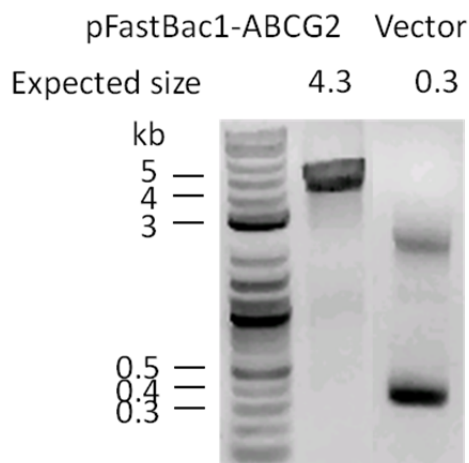


**Figure A-4: Validation of the pFastBac1-ABCG2 plasmid construct.**

PCR product of pFastBac1-ABCG2 with M13 forward and M13 reverse primers by agarose gel electrophoresis.

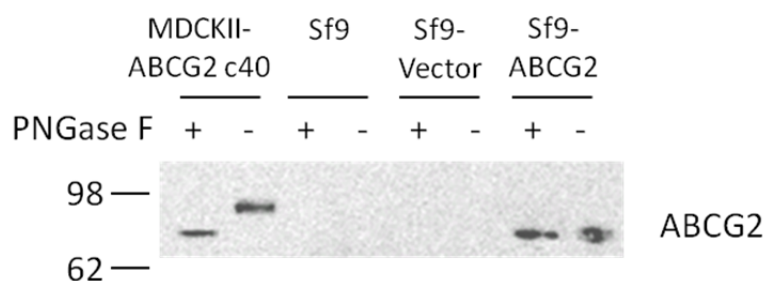


**Figure A-5: Validation of ABCG2 expression in ABCG2-expressing Sf9 membrane vesicles.**

Western blot analysis for ABCG2 expression in 1  $\mu$ g MDCKII-ABCG2 c40 cell membrane fractions, Sf9-vector and Sf9-ABCG2 membrane vesicles. ABCG2 was detected with BXP-21. PNGase F was used for deglycosylation.

Functional activity of ABCG2 in Sf9-ABCG2 membrane vesicles was validated with MTX by vesicular transport assay. MTX transport kinetics were determined by [ $^3\text{H}$ ]-MTX uptake for concentrations ranging from 500 to 3000  $\mu\text{M}$  at 5 min. ATP-dependent uptake was calculated by subtracting values obtained in the presence of AMP from those in the presence of ATP. The difference between ATP-dependent uptake in Sf9-vector and in Sf9-ABCG2 membrane vesicles was ABCG2-mediated uptake. As shown in Figure A-6, ATP-dependent MTX uptake in Sf9-ABCG2 membrane vesicles was saturable, while that in Sf9-vector membrane vesicle was a flat line. It confirmed that MTX is an ABCG2 substrate (181). A sigmoid- $E_{\text{max}}$  was fitted to the net ABCG2 transport data. The transport kinetic parameters were estimated by nonlinear regression (Table A-1). The estimated  $K_m$  ( $1191 \pm 380.7$ ) was comparable with the reported  $K_m$  ( $\sim 1000 \mu\text{M}$ ) (181). In addition, the estimated Hill coefficient value of 1.8 suggests positive transport cooperativity. The transport specificity was demonstrated by ABCG2 inhibitor, GF120918, inhibition (182). As shown in Figure A-7, ATP-dependent MTX uptake in Sf9-ABCG2 membrane vesicles was substantially reduced in the presence of GF120918, while that in Sf9-vector membrane vesicles was unaltered. Collectively, the expression and functional activity of ABCG2 in Sf9-ABCG2 membrane vesicles were validated, and the membrane vesicles can be used for substrate screening to study the role of ABCG2 in drug disposition.

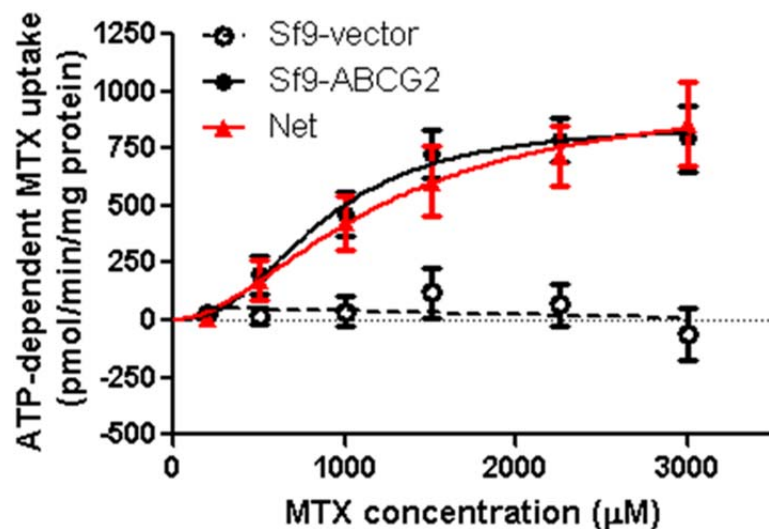


**Figure A-6: Concentration-dependent ABCG2-mediated [<sup>3</sup>H]-MTX transport in Sf9-ABCG2 membrane vesicles at pH 7.4.**

[<sup>3</sup>H]-MTX accumulation (5 min) in Sf9-vector and Sf9-ABCG2 membrane vesicles. ATP-dependent uptake was calculated by subtracting values obtained in the presence of AMP from those in the presence of ATP. ABCG2-mediated uptake was the difference between ATP-dependent uptake in Sf9-vector and in Sf9-ABCG2 membrane vesicles. Each point represents the mean  $\pm$  S.D. of triplicate determinations from one representative experiment.

**Table A-1: Transport kinetic parameters of ABCG2-mediated MTX uptake at pH 7.4 (mean  $\pm$  S.E.).**

The transport parameters were estimated by GraphPad.

$T_{\max}$ (pmol/min/mg protein)	$994.8 \pm 220.7$
$S_{50}$ (μM)	$1191 \pm 380.7$
Hill Slope	$1.8 \pm 0.7$

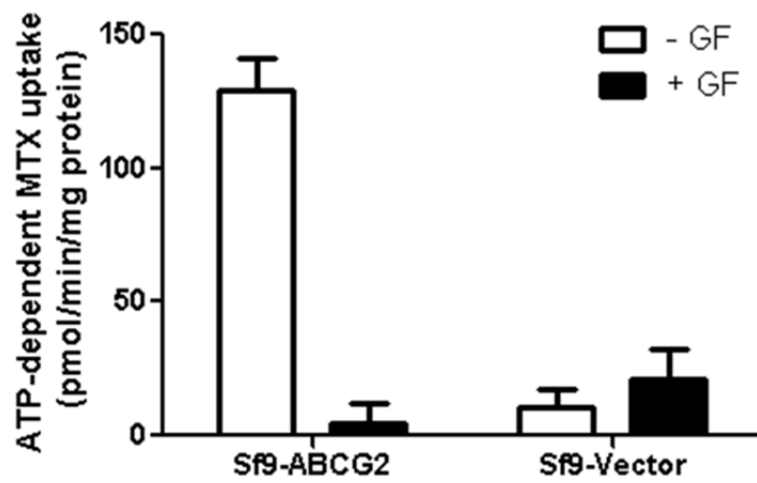


**Figure A-7: Inhibition of GF120918 on ATP-dependent [ $^3$ H]-MTX uptake in Sf9-ABCG2 membrane vesicles at pH 7.4.**

ATP-dependent 500  $\mu$ M [ $^3$ H]-MTX uptake (5 min) were determined in the absence and presence of 100  $\mu$ M GF120918 (GF) in Sf9-ABCG2 and Sf9-vector membrane vesicles at pH 7.4. ATP-dependent uptake was calculated by subtracting values obtained in the presence of AMP from those in the presence of ATP. Each bar represents the mean  $\pm$  S.D. of triplicate determinations from one representative experiment.

## Appendix 4: Development of a mathematical model to simulate the transport of common substrate of apical uptake and apical efflux transporters across the renal proximal tubular cells

### Introduction

Double immunofluorescence staining showed that Oatp4c1, as an uptake transporter, were colocalized with efflux transporters, Abcg2 and p-glycoprotein, at the apical membrane in rat proximal straight tubule (Figure 4-22 D). For their common substrates, such as digoxin (Oatp4c1 and p-glycoprotein substrate (183)) and E3S (Oatp4c1 and Abcg2 substrate (179)), a three compartment mathematical model was developed to simulate their transport in the renal proximal tubular cells.

### Methods

This three compartment system incorporates four transport processes including apical uptake (AU), apical efflux (AE), paracellular transport between the cells (PC), passive diffusion across the apical and basolateral membranes in proximal tubule epithelial cell (D) (Figure A-8). AU and AE were calculated saturable Michaelis-Menten type transport kinetics.

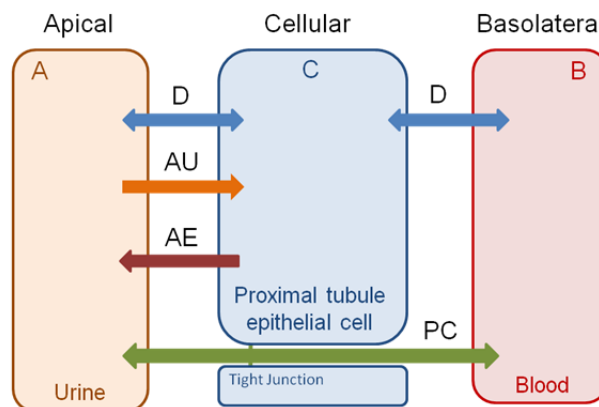


**Figure A-8: A schematic representation of the transport model for flux across renal proximal tubule monolayer.**

Passive diffusion is assumed to be equal for the apical and basolateral membranes, and the drug transfer across basolateral membrane is only by passive diffusion. The kinetic model was simulated using STELLA (Isee systems, Lebanon, NH) (Figure A-9).

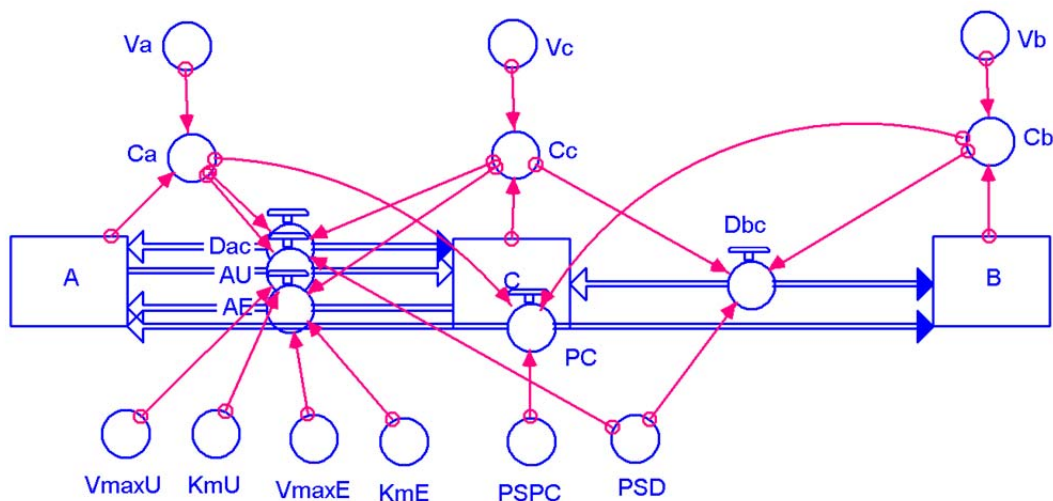


**Figure A-9: Schematic representation of the mathematical model for flux across renal proximal tubule monolayer built by STELLA.**

Squares, circles and “pipes” represent compartments, parameters, and transport processes, respectively. Blue arrows demonstrate the transport direction. Red arrows signify the determinants of each compartment and transport processes.

The equations and parameter settings were as follows:

$$A(t) = A(t - dt) + (D_{AC} + AE + PC - AU)dt \quad \text{Equation A-1}$$

$$C(t) = C(t - dt) + (D_{BC} + AU - D_{AC} - AE)dt \quad \text{Equation A-2}$$

$$B(t) = B(t - dt) + (-D_{BC} - PC)dt \quad \text{Equation A-3}$$

$$AU = PSAU \times C_A = \frac{V_{max}U \times C_A}{K_mU + C_A}; AE = PSAE \times C_C = \frac{V_{max}E \times C_C}{K_mE + C_C};$$

$$V_{max}U = V_{max}E = 15000 \text{ pmol/hr}, K_mU = K_mE = 30 \text{ } \mu\text{M} \quad \text{Equation A-4}$$

$$D_{AC} = PSD(C_C - C_A); D_{BC} = PSD(C_B - C_C); PSD = 100 \text{ ml/hr} \quad \text{Equation A-5}$$

$$PC = PSPC(C_B - C_A); PSPC = 1 \text{ ml/hr} \quad \text{Equation A-6}$$

$$C_A = A/V_A; C_B = B/V_B; C_C = C/V_C; V_A = V_B = 2000 \text{ } \mu\text{l}; V_C = 20 \text{ } \mu\text{l} \quad \text{Equation A-7}$$

where A, B, and C represent apical (urine), basolateral (blood), and cellular (proximal tubule epithelial cells) compartments, respectively;  $C_A$ ,  $C_B$ , and  $C_C$ , represent the substrate concentrations in each compartment; and  $V_A$ ,  $V_B$ , and  $V_C$ , represent the volume of each compartment. AU, AE,  $D_{AC}$ ,  $D_{BC}$ , PC represent apical uptake, apical efflux, passive diffusion across apical membrane, passive diffusion across basolateral membrane, and paracellular transport between the cells, respectively. PSAU, PSE, PSD, PSPC represent permeability-surface area product (PS) of apical uptake, apical efflux, passive diffusion, paracellular transport, respectively.  $K_mU$ ,  $V_{max}U$ ,  $K_mE$ ,  $V_{max}E$  represent the  $K_m$  and  $V_{max}$  of uptake and efflux transporters, respectively.

The flux from  $B \rightarrow A$  and  $A \rightarrow B$  at 10 min (initial rate) were simulated for the concentrations ranging from 0.1 to 100000  $\mu\text{M}$ . PS were calculated by the following equation:

$$PS = \frac{A}{T \times C_0 \times SA} \quad \text{Equation A-8}$$

where A, T,  $C_0$ , and SA represents amount of substrate in recipient compartment (pmol), time (hr), initial concentration ( $\mu\text{M}$ ) and surface area ( $\text{cm}^2$ ), respectively. The  $K_m$  and  $V_{max}$  of uptake transporter and efflux transporter were changed one at a time to evaluate the effect of each parameter on transport direction.



## Results and Discussion

In this model, four transport processes were included: apical uptake (AU), apical efflux (AE), passive diffusion across the apical and basolateral membrane ( $D_{AC}$ ,  $D_{BC}$ ), and paracellular transport between the cells (PC). The substrate flux in each compartment and the initial rate of  $B \rightarrow A$  and  $A \rightarrow B$  are derived as follows:

$$\frac{dx_A}{dt} = PS_D(C_C - C_A) - PS_{AU}C_A + PS_{AE}C_C + PS_{PC}(C_B - C_A) \quad \text{Equation A-9}$$

$$\frac{dx_B}{dt} = PS_D(C_C - C_B) + PS_{PC}(C_A - C_B) \quad \text{Equation A-10}$$

$$\frac{dx_C}{dt} = PS_D(C_A - C_C) + PS_D(C_B - C_C) + PS_{AU}C_A - PS_{AE}C_C \quad \text{Equation A-11}$$

*Initial rate  $B \rightarrow A$  (represents tubular secretion):* assuming initial substrate concentration in apical compartment is zero ( $C_A = 0$ ), Equation 5-1 becomes:

$$\frac{dx_{A,B \rightarrow A}}{dt} = PS_D C_C + PS_{AE} C_C + PS_{PC} C_B \quad \text{Equation A-12}$$

and rapid equilibration between the B and C compartments such that  $dx_C/dt = 0$ , Equation A-11 can be rearranged as:

$$C_C = \frac{PS_D C_B}{2PS_D + PS_{AE}} \quad \text{Equation A-13}$$

Substitution of Equation A-13 into Equation A-12 yields:

$$\frac{dx_{A,B \rightarrow A}}{dt} = C_B \left[ \frac{PS_D(PS_D + PS_{AE})}{2PS_D + PS_{AE}} + PS_{PC} \right] \quad \text{Equation A-14}$$

The permeability surface area product (PS) becomes:

$$PS_{B \rightarrow A} = \frac{\frac{dx_{A,B \rightarrow A}}{dt}}{C_B \text{Area}} = \frac{PS_D(PS_D + PS_{AE})}{2PS_D + PS_{AE}} + PS_{PC} = \frac{PS_D + PS_{AE}}{2 + \frac{PS_{AE}}{PS_D}} + \frac{PS_{PC}}{PS_D} \quad \text{Equation A-15}$$

$$\text{while } PS_{AE} = \frac{V_{max}E}{K_mE + C_c}$$

*Initial rate A → B (represents renal reabsorption):* assuming initial substrate concentration in basolateral compartment is zero ( $C_B = 0$ ), Equation A-10 becomes:

$$\frac{dX_{B,A \rightarrow B}}{dt} = PS_D C_c + PS_{PC} C_A \quad \text{Equation A-16}$$

and rapid equilibration between the A and C compartments such that  $dX_C/dt = 0$ , Equation A-11 can be rearranged as:

$$C_C = \frac{C_A(PS_D + PS_{AU})}{2PS_D + PS_{AE}} \quad \text{Equation A-17}$$

Substitution of Equation A-13 into Equation A-12 yields:

$$\frac{dX_{B,A \rightarrow B}}{dt} = C_A \left[ \frac{PS_D(PS_D + PS_{AU})}{2PS_D + PS_{AE}} + PS_{PC} \right] \quad \text{Equation A-18}$$

The PS becomes:

$$PS_{A \rightarrow B} = \frac{\frac{dX_{B,A \rightarrow B}}{dt}}{C_A \text{Area}} = \frac{PS_D(PS_D + PS_{AU})}{2PS_D + PS_{AE}} + PS_{PC} = \frac{PS_D + PS_{AU}}{2 + \frac{PS_{AE}}{PS_D}} + \frac{PS_{PC}}{PS_D} \quad \text{Equation A-19}$$

$$\text{while } PS_{AE} = \frac{V_{max}E}{K_mE + C_c}, \quad PS_{AU} = \frac{V_{max}U}{K_mU + C_A}$$

As shown in Equation A-15, apical uptake (AU) transporter played no role in  $PS_{B \rightarrow A}$ . This was demonstrated in Figure A-10 D and Figure A-11 D showing that the changes of  $K_m$  or  $V_{max}$  of AU transporter did not alter  $PS_{B \rightarrow A}$ . Equation 1-11 showed  $PS_{A \rightarrow B}$  was influenced by both  $PS_{AU}$  and  $PS_{AE}$  (panels E in Figure A-10, Figure A-11, Figure A-12 and Figure A-13), and  $PS_{max,A \rightarrow B}$  was more sensitive to  $PS_{AU}$  than  $PS_{AE}$ , because the effect of  $PS_{AE}$  is attenuated by its scaling by  $PS_D$  (Equation A-19).

Intuitively, transporter mediated flux of a substrate is determined by the predominant intrinsic clearance ( $V_{max}/K_m$ ) of the AU or AE transporters. Flux from A → B

and  $B \rightarrow A$  is neutralized if the intrinsic transporter clearances of AU and AE transporters are the same. Flux from  $A \rightarrow B$  is predominant if the intrinsic transporter clearance of the AU transporter is higher than that of AE transporter and vice versa. However, that is only true at low concentrations (panels A, B and C in Figure A-10, Figure A-11, Figure A-12 and Figure A-13). As shown in Equation A-15 and Equation A-19, the only difference between  $PS_{B \rightarrow A}$  and  $PS_{A \rightarrow B}$  is the numerator,  $PS_D + PS_{AE}$  and  $PS_D + PS_{AU}$ , respectively. At low concentrations ( $C_C \ll K_mE$  or  $C_A \ll K_mU$ ),  $PS_{AE}$  and  $PS_{AU}$  approximately equals to intrinsic clearance ( $V_{max}/K_m$ ). Therefore, the predominance of  $PS_{B \rightarrow A}$  or  $PS_{A \rightarrow B}$  is determined by the intrinsic clearance ( $V_{max}/K_m$ ) of the AU or AE transporters. At concentration near the  $K_m$ ,  $C_C$  and  $C_A$  is unignorable. For  $PS_{B \rightarrow A}$ , substrates cross basolateral membrane into the cells by passive diffusion down the concentration gradient. Therefore,  $C_C$  is lower than the donor concentration, and, supposedly, lower than  $C_A$  which is the donor concentration for  $PS_{A \rightarrow B}$ . When the  $K_m$  or  $V_{max}$  of AU and AE transporters are equal,  $PS_{AE}$  is thereby higher than  $PS_{AU}$ , and  $PS_{B \rightarrow A}$  is higher than  $PS_{A \rightarrow B}$  (panels B in Figure A-10, Figure A-11, Figure A-12 and Figure A-13). At high concentrations, transporters become saturated, and  $PS_{B \rightarrow A}$  and  $PS_{A \rightarrow B}$  gradually decrease to the same value as passive diffusion (panels A, B and C in Figure A-10, Figure A-11, Figure A-12 and Figure A-13).

In conclusion, at low concentrations ( $C \ll K_m$ ), transporter mediated flux of a substrate is determined by the predominant intrinsic clearance ( $V_{max}/K_m$ ) of the AU or AE transporters. At concentrations near the  $K_m$ , flux from  $B \rightarrow A$ , indicating tubular secretion, is predominant, despite the intrinsic clearance of AU transporter is higher than that of AE transporter.

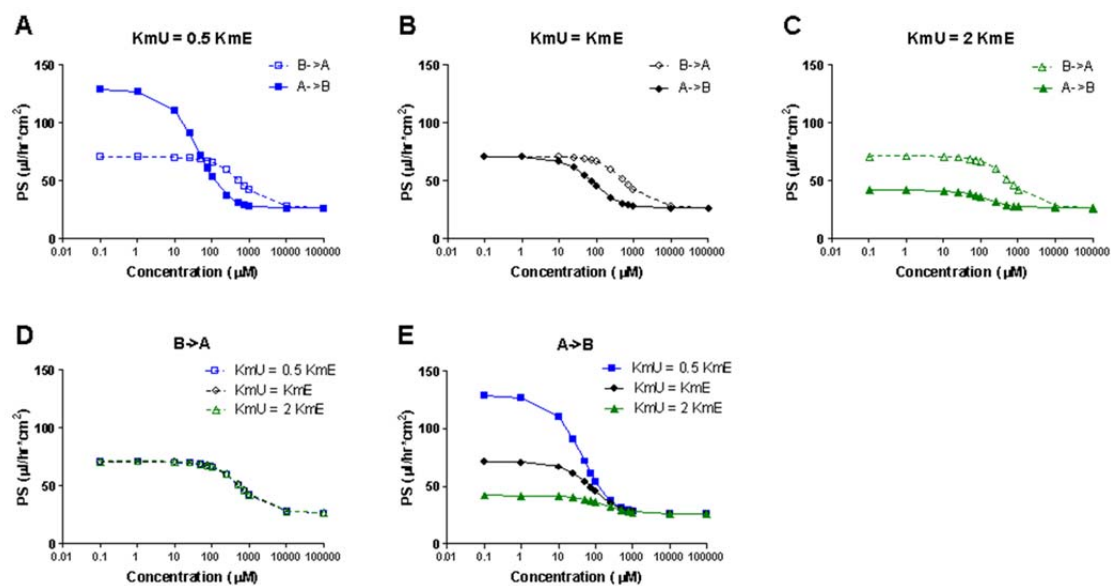


**Figure A-10: The influence of  $K_mU$  on flux of  $B \rightarrow A$  and  $A \rightarrow B$ .**

$V_{max}U = V_{max}E = 15000 \text{ pmol/hr}$ ,  $K_mE = 30 \mu M$ ,  $K_mU = 15$  (A), 30 (B), 60 (C)  $\mu M$

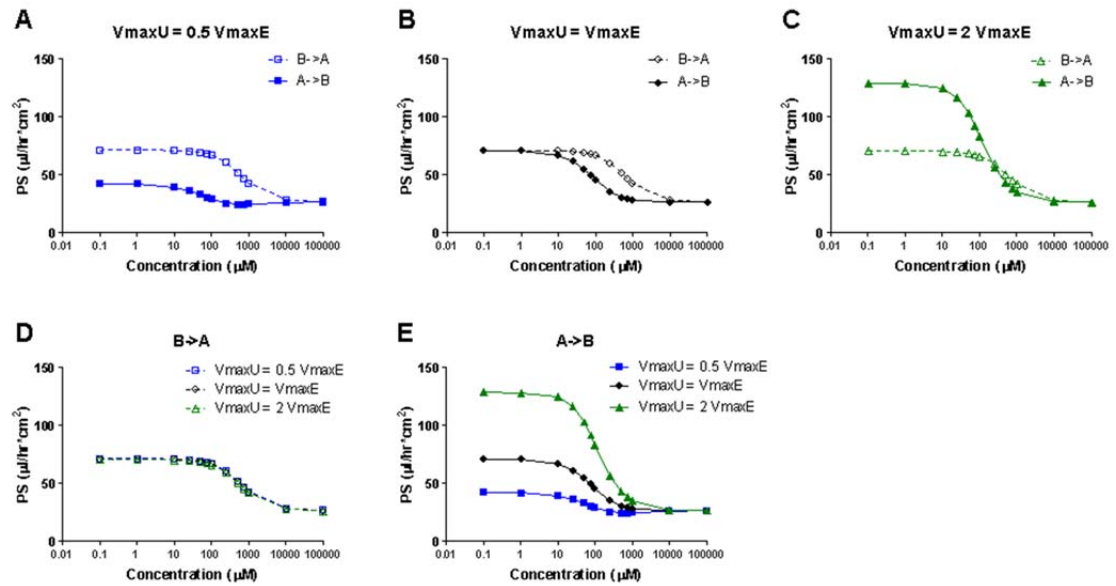


**Figure A-11: The influence of  $V_{\max}U$  on flux of  $B \rightarrow A$  and  $A \rightarrow B$ .**

$K_mU = K_mE = 30 \mu\text{M}$ ,  $V_{\max}E = 15000 \text{ pmol/hr}$ ,  $V_{\max}U = 7500$  (A), 15000 (B), 30000 (C)  $\text{pmol/hr}$

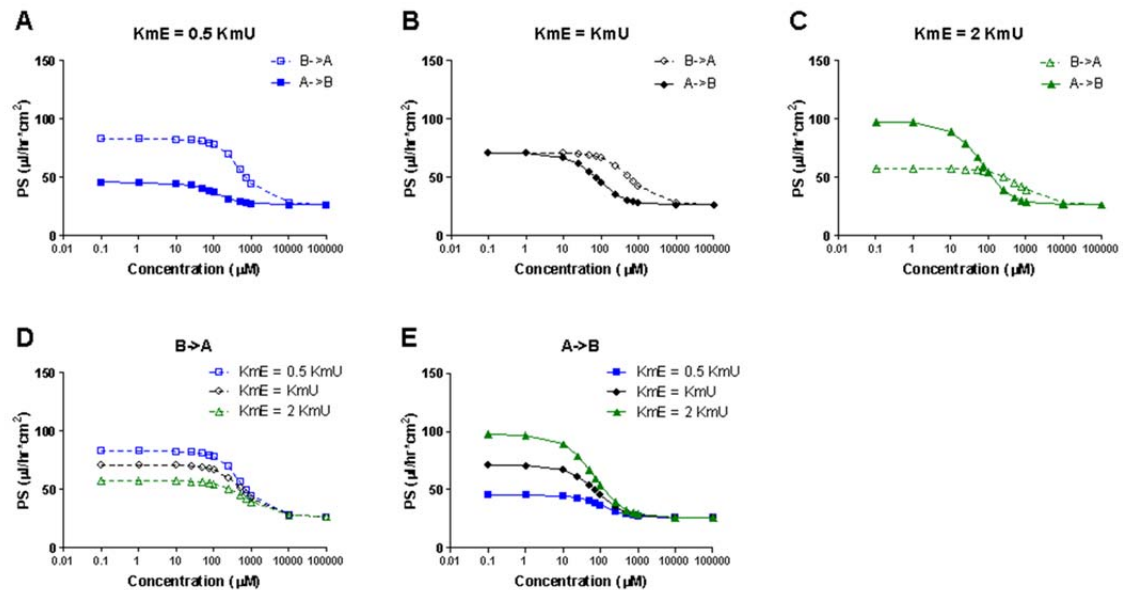


**Figure A-12: The influence of  $K_mE$  on flux of  $B \rightarrow A$  and  $A \rightarrow B$ .**

$V_{\max}U = V_{\max}E = 15000 \text{ pmol/hr}$ ,  $K_mU = 30 \mu\text{M}$ ,  $K_mE = 15$  (A), 30 (B), 60 (C)  $\mu\text{M}$

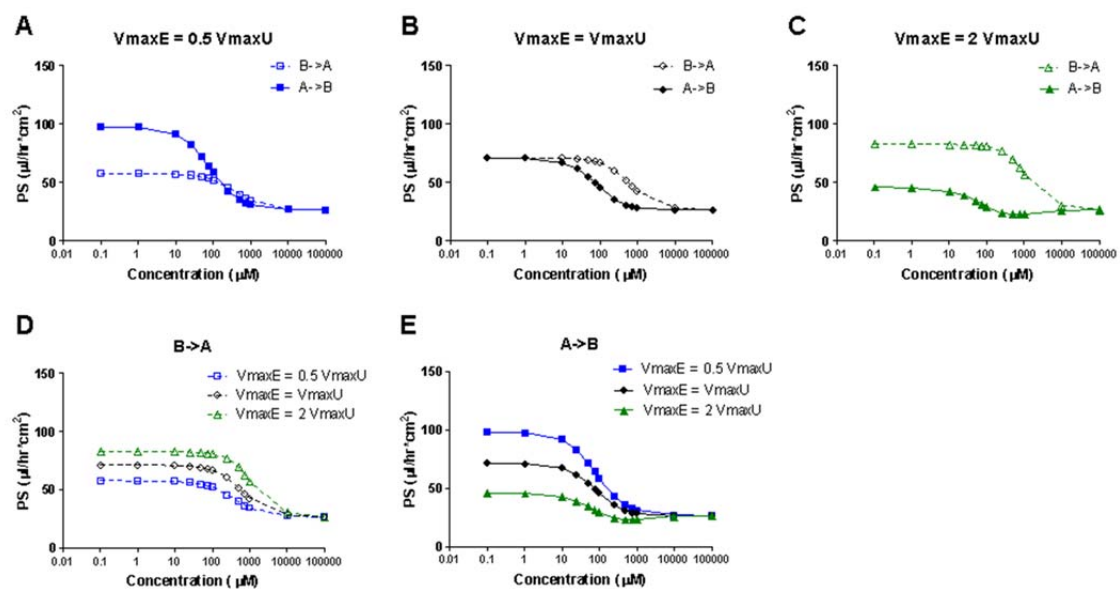


**Figure A-13: The influence of  $V_{\max}E$  on flux of  $B \rightarrow A$  and  $A \rightarrow B$ .**

$K_mU = K_mE = 30 \mu M$ ,  $V_{\max}U = 15000 \text{ pmol/hr}$ ,  $V_{\max}E = 7500$  (A),  $15000$  (B),  $30000$  (C)  $\text{pmol/hr}$

## REFERENCES

1. Breastfeeding, S. o. (2005) Breastfeeding and the Use of Human Milk, *Pediatrics* 115, 496-506.
2. Ito, S., and Lee, A. (2003) Drug excretion into breast milk—Overview, *Advanced Drug Delivery Reviews* 55, 617-627.
3. Hennighausen, L., and Robinson, G. W. (2005) Information networks in the mammary gland, *Nat Rev Mol Cell Biol* 6, 715-725.
4. Neville, M. C., McFadden, T. B., and Forsyth, I. (2002) Hormonal Regulation of Mammary Differentiation and Milk Secretion, *Journal of Mammary Gland Biology and Neoplasia* 7, 49-66.
5. Fleishaker, J. C., Desai, N., and McNamara, P. J. (1987) Factors affecting the milk-to-plasma drug concentration ratio in lactating women: physical interactions with protein and fat, *J Pharm Sci* 76, 189-193.
6. Fleishaker, J. C., and McNamara, P. J. (1988) Effect of altered serum protein binding on propranolol distribution into milk in the lactating rabbit, *Journal of Pharmacology and Experimental Therapeutics* 244, 925-928.
7. Dean, M., Hamon, Y., and Chimini, G. (2001) The human ATP-binding cassette (ABC) transporter superfamily, *Journal of Lipid Research* 42, 1007-1017.
8. Cordon-Cardo, C., O'Brien, J. P., Boccia, J., Casals, D., Bertino, J. R., and Melamed, M. R. (1990) Expression of the multidrug resistance gene product (P-glycoprotein) in human normal and tumor tissues, *Journal of Histochemistry & Cytochemistry* 38, 1277-1287.
9. van der Valk, P., van Kalken, C. K., Ketelaars, H., Broxterman, H. J., Scheffer, G., Kuiper, C. M., Tsuruo, T., Lankelma, J., Meijer, C. J., Pinedo, H. M., and et al. (1990) Distribution of multi-drug resistance-associated P-glycoprotein in normal and neoplastic human tissues. Analysis with 3 monoclonal antibodies recognizing different epitopes of the P-glycoprotein molecule, *Ann Oncol* 1, 56-64.
10. Jonker, J. W., Merino, G., Musters, S., van Herwaarden, A. E., Bolscher, E., Wagenaar, E., Mesman, E., Dale, T. C., and Schinkel, A. H. (2005) The breast cancer resistance protein BCRP (ABCG2) concentrates drugs and carcinogenic xenotoxins into milk, *Nat Med* 11, 127-129.
11. Alcorn, J., Lu, X., Moscow, J. A., and McNamara, P. J. (2002) Transporter Gene Expression in Lactating and Nonlactating Human Mammary Epithelial Cells

- Using Real-Time Reverse Transcription-Polymerase Chain Reaction, *Journal of Pharmacology and Experimental Therapeutics* 303, 487-496.
12. Choudhuri, S., and Klaassen, C. D. (2006) Structure, function, expression, genomic organization, and single nucleotide polymorphisms of human ABCB1 (MDR1), ABCC (MRP), and ABCG2 (BCRP) efflux transporters, *Int J Toxicol* 25, 231-259.
  13. Wang, L., Leggas, M., Goswami, M., Empey, P. E., and McNamara, P. J. (2008) N-(4-[2-(1,2,3,4-Tetrahydro-6,7-dimethoxy-2-isoquinoliny)ethyl]-phenyl)-9,10-dihydro-5-methoxy-9-oxo-4-acridine Carboxamide (GF120918) As a Chemical ATP-Binding Cassette Transporter Family G Member 2 (Abcg2) Knockout Model to Study Nitrofurantoin Transfer into Milk, *Drug Metabolism and Disposition* 36, 2591-2596.
  14. van Herwaarden, A. E., Wagenaar, E., Merino, G., Jonker, J. W., Rosing, H., Beijnen, J. H., and Schinkel, A. H. (2007) Multidrug Transporter ABCG2/Breast Cancer Resistance Protein Secretes Riboflavin (Vitamin B2) into Milk, *Molecular and Cellular Biology* 27, 1247-1253.
  15. Merino, G., Jonker, J. W., Wagenaar, E., van Herwaarden, A. E., and Schinkel, A. H. (2005) The Breast Cancer Resistance Protein (BCRP/ABCG2) Affects Pharmacokinetics, Hepatobiliary Excretion, and Milk Secretion of the Antibiotic Nitrofurantoin, *Molecular Pharmacology* 67, 1758-1764.
  16. van Herwaarden, A. E., and Schinkel, A. H. (2006) The function of breast cancer resistance protein in epithelial barriers, stem cells and milk secretion of drugs and xenotoxins, *Trends in Pharmacological Sciences* 27, 10-16.
  17. Merino, G., Álvarez, A. I., Pulido, M. M., Molina, A. J., Schinkel, A. H., and Prieto, J. G. (2006) BREAST CANCER RESISTANCE PROTEIN (BCRP/ABCG2) TRANSPORTS FLUOROQUINOLONE ANTIBIOTICS AND AFFECTS THEIR ORAL AVAILABILITY, PHARMACOKINETICS, AND MILK SECRETION, *Drug Metabolism and Disposition* 34, 690-695.
  18. Gerk, P. M., Kuhn, R. J., Desai, N. S., and McNamara, P. J. (2001) Active transport of nitrofurantoin into human milk, *Pharmacotherapy* 21, 669-675.
  19. Oo, C. Y., Kuhn, R. J., Desai, N., and McNamara, P. J. (1995) Active transport of cimetidine into human milk, *Clin Pharmacol Ther* 58, 548-555.
  20. Fredriksson, R., Nordström, K. J. V., Stephansson, O., Hägglund, M. G. A., and Schiöth, H. B. (2008) The solute carrier (SLC) complement of the human



- genome: Phylogenetic classification reveals four major families, *FEBS Letters* 582, 3811-3816.
21. Schinkel, A. H., and Jonker, J. W. (2003) Mammalian drug efflux transporters of the ATP binding cassette (ABC) family: an overview, *Adv Drug Deliv Rev* 55, 3-29.
  22. Rubio-Aliaga, I., and Daniel, H. (2008) Peptide transporters and their roles in physiological processes and drug disposition, *Xenobiotica* 38, 1022-1042.
  23. Groneberg, D. A., Döring, F., Theis, S., Nickolaus, M., Fischer, A., and Daniel, H. (2002) Peptide transport in the mammary gland: expression and distribution of PEPT2 mRNA and protein, *American Journal of Physiology - Endocrinology And Metabolism* 282, E1172-E1179.
  24. Ito, S., and Alcorn, J. (2003) Xenobiotic transporter expression and function in the human mammary gland, *Advanced Drug Delivery Reviews* 55, 653-665.
  25. Hagenbuch, B., and Gui, C. (2008) Xenobiotic transporters of the human organic anion transporting polypeptides (OATP) family, *Xenobiotica* 38, 778-801.
  26. Koepsell, H., and Endou, H. (2004) The SLC22 drug transporter family, *Pflügers Archiv European Journal of Physiology* 447, 666-676.
  27. Sekine, T., Cha, S. H., and Endou, H. (2000) The multispecific organic anion transporter (OAT) family, *Pflügers Archiv European Journal of Physiology* 440, 337-350.
  28. Hagenbuch, B., and Meier, P. J. (2004) Organic anion transporting polypeptides of the OATP/ SLC21 family: phylogenetic classification as OATP/ SLCO superfamily, new nomenclature and molecular/functional properties, *Pflügers Arch* 447, 653-665.
  29. Pizzagalli, F., Varga, Z., Huber, R. D., Folkers, G., Meier, P. J., and St-Pierre, M. V. (2003) Identification of Steroid Sulfate Transport Processes in the Human Mammary Gland, *Journal of Clinical Endocrinology & Metabolism* 88, 3902-3912.
  30. Empey, P. E. (2007) Xenobiotic transporters in lactating mammary epithelial cells: predictions for drug accumulation in breast milk
  31. Gerk, P. M., Oo, C. Y., Paxton, E. W., Moscow, J. A., and McNamara, P. J. (2001) Interactions between Cimetidine, Nitrofurantoin, and Probenecid Active Transport into Rat Milk, *Journal of Pharmacology and Experimental Therapeutics* 296, 175-180.

32. Kwok, B., Yamauchi, A., Rajesan, R., Chan, L., Dhillon, U., Gao, W., Xu, H., Wang, B., Takahashi, S., Semple, J., Tamai, I., Nezu, J., Tsuji, A., Harper, P., and Ito, S. (2006) Carnitine/xenobiotics transporters in the human mammary gland epithelia, MCF12A, *Am J Physiol Regul Integr Comp Physiol* 290, R793-802.
33. Inui, K. I., Masuda, S., and Saito, H. (2000) Cellular and molecular aspects of drug transport in the kidney, *Kidney Int* 58, 944-958.
34. Gillian Pocock, C. D. R. (2004) *Human Physiology - The Basis of Medicine*, 2 ed., Oxford University Press.
35. Ito, K., Suzuki, H., Horie, T., and Sugiyama, Y. (2005) Apical/basolateral surface expression of drug transporters and its role in vectorial drug transport, *Pharm Res* 22, 1559-1577.
36. Nies, A. T., Schwab, M., and Keppler, D. (2008) Interplay of conjugating enzymes with OATP uptake transporters and ABCC/MRP efflux pumps in the elimination of drugs, *Expert Opin Drug Metab Toxicol* 4, 545-568.
37. Sekine, T., Miyazaki, H., and Endou, H. (2006) Molecular physiology of renal organic anion transporters, *Am J Physiol Renal Physiol* 290, F251-261.
38. Hagenbuch, B. (2009) Drug Uptake Systems in Liver and Kidney: A Historic Perspective, *Clin Pharmacol Ther* 87, 39-47.
39. Lee, W., and Kim, R. B. (2004) Transporters and renal drug elimination, *Annu Rev Pharmacol Toxicol* 44, 137-166.
40. Thiebaut, F., Tsuruo, T., Hamada, H., Gottesman, M. M., Pastan, I., and Willingham, M. C. (1987) Cellular localization of the multidrug-resistance gene product P-glycoprotein in normal human tissues, *Proceedings of the National Academy of Sciences* 84, 7735-7738.
41. Hori, R., Okamura, N., Aiba, T., and Tanigawara, Y. (1993) Role of P-glycoprotein in renal tubular secretion of digoxin in the isolated perfused rat kidney, *Journal of Pharmacology and Experimental Therapeutics* 266, 1620-1625.
42. Peng, K.-C., Cluzeaud, F., Bens, M., Duong Van Huyen, J.-P., Wioland, M. A., Lacave, R., and Vandewalle, A. (1999) Tissue and Cell Distribution of the Multidrug Resistance-Associated Protein (MRP) in Mouse Intestine and Kidney, *Journal of Histochemistry & Cytochemistry* 47, 757-767.

43. Nies, A., and Keppler, D. (2007) The apical conjugate efflux pump ABCC2 (MRP2), *Pflügers Archiv European Journal of Physiology* 453, 643-659.
44. SCHAUB, T. P., KARTENBECK, J., KÖNIG, J., SPRING, H., DÖRSAM, J., STAEHLER, G., STÖRKEL, S., THON, W. F., and KEPPLER, D. (1999) Expression of the MRP2 Gene-Encoded Conjugate Export Pump in Human Kidney Proximal Tubules and in Renal Cell Carcinoma, *Journal of the American Society of Nephrology* 10, 1159-1169.
45. Hulot, J.-S., Villard, E., Maguy, A., Morel, V., Mir, L., Tostivint, I., William-Faltaos, D., Fernandez, C., Hatem, S., Deray, G., Komajda, M., Leblond, V., and Lechat, P. (2005) A mutation in the drug transporter gene ABCC2 associated with impaired methotrexate elimination, *Pharmacogenetics and Genomics* 15, 277-285.
46. Kuroda, M., Kobayashi, Y., Tanaka, Y., Itani, T., Mifuji, R., Araki, J. U. N., Kaito, M., and Adachi, Y. (2004) Increased hepatic and renal expressions of multidrug resistance-associated protein 3 in Eisai hyperbilirubinuria rats, *Journal of Gastroenterology and Hepatology* 19, 146-153.
47. Scheffer, G. L., Kool, M., de Haas, M., de Vree, J. M. L., Pijnenborg, A. C. L. M., Bosman, D. K., Oude Elferink, R. P. J., van der Valk, P., Borst, P., and Scheper, R. J. (2002) Tissue Distribution and Induction of Human Multidrug Resistant Protein 3, *Lab Invest* 82, 193-201.
48. van Aubel, R. A. M. H., Smeets, P. H. E., Peters, J. G. P., Bindels, R. J. M., and Russel, F. G. M. (2002) The MRP4/ABCC4 Gene Encodes a Novel Apical Organic Anion Transporter in Human Kidney Proximal Tubules: Putative Efflux Pump for Urinary cAMP and cGMP, *Journal of the American Society of Nephrology* 13, 595-603.
49. Denk, G. U., Soroka, C. J., Takeyama, Y., Chen, W.-S., Schuetz, J. D., and Boyer, J. L. (2004) Multidrug resistance-associated protein 4 is up-regulated in liver but down-regulated in kidney in obstructive cholestasis in the rat, *Journal of Hepatology* 40, 585-591.
50. Russel, F. G. M., Koenderink, J. B., and Masereeuw, R. (2008) Multidrug resistance protein 4 (MRP4/ABCC4): a versatile efflux transporter for drugs and signalling molecules, *Trends in Pharmacological Sciences* 29, 200-207.
51. Kool, M., de Haas, M., Scheffer, G. L., Scheper, R. J., van Eijk, M. J. T., Juijn, J. A., Baas, F., and Borst, P. (1997) Analysis of Expression of cMOAT (MRP2),

- MRP3, MRP4, and MRP5, Homologues of the Multidrug Resistance-associated Protein Gene (MRP1), in Human Cancer Cell Lines, *Cancer Research* 57, 3537-3547.
52. Maher, J. M., Slitt, A. L., Cherrington, N. J., Cheng, X., and Klaassen, C. D. (2005) TISSUE DISTRIBUTION AND HEPATIC AND RENAL ONTOGENY OF THE MULTIDRUG RESISTANCE-ASSOCIATED PROTEIN (MRP) FAMILY IN MICE, *Drug Metabolism and Disposition* 33, 947-955.
  53. Wijnholds, J., Mol, C. A. A. M., van Deemter, L., de Haas, M., Scheffer, G. L., Baas, F., Beijnen, J. H., Scheper, R. J., Hatse, S., De Clercq, E., Balzarini, J., and Borst, P. (2000) Multidrug-resistance protein 5 is a multispecific organic anion transporter able to transport nucleotide analogs, *Proceedings of the National Academy of Sciences* 97, 7476-7481.
  54. Jedlitschky, G., Burchell, B., and Keppler, D. (2000) The Multidrug Resistance Protein 5 Functions as an ATP-dependent Export Pump for Cyclic Nucleotides, *Journal of Biological Chemistry* 275, 30069-30074.
  55. Scheffer, G. L., Hu, X., Pijnenborg, A. C. L. M., Wijnholds, J., Bergen, A. A. B., and Scheper, R. J. (2002) MRP6 (ABCC6) Detection in Normal Human Tissues and Tumors, *Lab Invest* 82, 515-518.
  56. Beck, K., Hayashi, K., Nishiguchi, B., Saux, O. L., Hayashi, M., and Boyd, C. D. (2003) The Distribution of Abcc6 in Normal Mouse Tissues Suggests Multiple Functions for this ABC Transporter, *Journal of Histochemistry & Cytochemistry* 51, 887-902.
  57. Huls, M., Brown, C. D. A., Windass, A. S., Sayer, R., van den Heuvel, J. J. M. W., Heemskerk, S., Russel, F. G. M., and Masereeuw, R. (2007) The breast cancer resistance protein transporter ABCG2 is expressed in the human kidney proximal tubule apical membrane, *Kidney Int* 73, 220-225.
  58. Jonker, J. W., Buitelaar, M., Wagenaar, E., van der Valk, M. A., Scheffer, G. L., Scheper, R. J., Plösch, T., Kuipers, F., Elferink, R. P. J. O., Rosing, H., Beijnen, J. H., and Schinkel, A. H. (2002) The breast cancer resistance protein protects against a major chlorophyll-derived dietary phototoxin and protoporphyria, *Proceedings of the National Academy of Sciences* 99, 15649-15654.
  59. Shen, H., Smith, D. E., Yang, T., Huang, Y. G., Schnermann, J. B., and Brosius, F. C. (1999) Localization of PEPT1 and PEPT2 proton-coupled oligopeptide

- transporter mRNA and protein in rat kidney, *American Journal of Physiology - Renal Physiology* 276, F658-F665.
60. Werner, A., Moore, M. L., Mantei, N., Biber, J., Semenza, G., and Murer, H. (1991) Cloning and expression of cDNA for a Na/Pi cotransport system of kidney cortex, *Proceedings of the National Academy of Sciences* 88, 9608-9612.
  61. Biber, J., Custer, M., Werner, A., Kaissling, B., and Murer, H. (1993) Localization of NaPi-1, a Na/Pi cotransporter, in rabbit kidney proximal tubules. II. Localization by immunohistochemistry, *Pflügers Arch* 424, 210-215.
  62. Uchino, H., Tamai, I., Yamashita, K., Minemoto, Y., Sai, Y., Yabuuchi, H., Miyamoto, K.-i., Takeda, E., and Tsuji, A. (2000) p-Aminohippuric Acid Transport at Renal Apical Membrane Mediated by Human Inorganic Phosphate Transporter NPT1, *Biochemical and Biophysical Research Communications* 270, 254-259.
  63. Bergwerk, A. J., Shi, X., Ford, A. C., Kanai, N., Jacquemin, E., Burk, R. D., Bai, S., Novikoff, P. M., Stieger, B., Meier, P. J., Schuster, V. L., and Wolkoff, A. W. (1996) Immunologic distribution of an organic anion transport protein in rat liver and kidney, *American Journal of Physiology - Gastrointestinal and Liver Physiology* 271, G231-G238.
  64. Yang, C.-H., Glover, K. P., and Han, X. (2009) Organic anion transporting polypeptide (Oatp) 1a1-mediated perfluorooctanoate transport and evidence for a renal reabsorption mechanism of Oatp1a1 in renal elimination of perfluorocarboxylates in rats, *Toxicology Letters* 190, 163-171.
  65. Satlin, L. M., Amin, V., and Wolkoff, A. W. (1997) Organic Anion Transporting Polypeptide Mediates Organic Anion/HCO<sub>3</sub><sup>-</sup> Exchange, *Journal of Biological Chemistry* 272, 26340-26345.
  66. Li, L., Lee, T. K., Meier, P. J., and Ballatori, N. (1998) Identification of Glutathione as a Driving Force and Leukotriene C<sub>4</sub> as a Substrate for oatp1, the Hepatic Sinusoidal Organic Solute Transporter, *Journal of Biological Chemistry* 273, 16184-16191.
  67. Lee, W., Glaeser, H., Smith, L. H., Roberts, R. L., Moeckel, G. W., Gervasini, G., Leake, B. F., and Kim, R. B. (2005) Polymorphisms in Human Organic Anion-transporting Polypeptide 1A2 (OATP1A2), *Journal of Biological Chemistry* 280, 9610-9617.
  68. Badagnani, I., Castro, R. A., Taylor, T. R., Brett, C. M., Huang, C. C., Stryke, D., Kawamoto, M., Johns, S. J., Ferrin, T. E., Carlson, E. J., Burchard, E. G., and

- Giacomini, K. M. (2006) Interaction of Methotrexate with Organic-Anion Transporting Polypeptide 1A2 and Its Genetic Variants, *Journal of Pharmacology and Experimental Therapeutics* 318, 521-529.
69. Saito, H., Masuda, S., and Inui, K.-i. (1996) Cloning and Functional Characterization of a Novel Rat Organic Anion Transporter Mediating Basolateral Uptake of Methotrexate in the Kidney, *Journal of Biological Chemistry* 271, 20719-20725.
  70. Masuda, S., Saito, H., Nonoguchi, H., Tomita, K., and Inui, K.-i. (1997) mRNA distribution and membrane localization of the OAT-K1 organic anion transporter in rat renal tubules, *FEBS Letters* 407, 127-131.
  71. Masuda, S., Ibaramoto, K., Takeuchi, A., Saito, H., Hashimoto, Y., and Inui, K.-i. (1999) Cloning and Functional Characterization of a New Multispecific Organic Anion Transporter, OAT-K2, in Rat Kidney, *Molecular Pharmacology* 55, 743-752.
  72. Takeuchi, A., Masuda, S., Saito, H., Doi, T., and Inui, K.-i. (2001) Role of kidney-specific organic anion transporters in the urinary excretion of methotrexate, *Kidney Int* 60, 1058-1068.
  73. Masuda, S. (2003) Functional Characteristics and Pharmacokinetic Significance of Kidney-specific Organic Anion Transporters, OAT-K1 and OAT-K2, in the Urinary Excretion of Anionic Drugs, *Drug Metabolism and Pharmacokinetics* 18, 91-103.
  74. Takeuchi, A., Masuda, S., Saito, H., Hashimoto, Y., and Inui, K.-i. (2000) Trans-Stimulation Effects of Folic Acid Derivatives on Methotrexate Transport by Rat Renal Organic Anion Transporter, OAT-K1, *Journal of Pharmacology and Experimental Therapeutics* 293, 1034-1039.
  75. Abe, T., Kakyo, M., Sakagami, H., Tokui, T., Nishio, T., Tanemoto, M., Nomura, H., Hebert, S. C., Matsuno, S., Kondo, H., and Yawo, H. (1998) Molecular Characterization and Tissue Distribution of a New Organic Anion Transporter Subtype (oatp3) That Transports Thyroid Hormones and Taurocholate and Comparison with oatp2, *Journal of Biological Chemistry* 273, 22395-22401.
  76. Dresser, G. K., Bailey, D. G., Leake, B. F., Schwarz, U. I., Dawson, P. A., Freeman, D. J., and Kim, R. B. (2002) Fruit juices inhibit organic anion transporting polypeptide-mediated drug uptake to decrease the oral availability of fexofenadine, *Clin Pharmacol Ther* 71, 11-20.

77. Ohtsuki, S., Takizawa, T., Takanaga, H., Terasaki, N., Kitazawa, T., Sasaki, M., Abe, T., Hosoya, K.-i., and Terasaki, T. (2003) In Vitro Study of the Functional Expression of Organic Anion Transporting Polypeptide 3 at Rat Choroid Plexus Epithelial Cells and Its Involvement in the Cerebrospinal Fluid-to-Blood Transport of Estrone-3-Sulfate, *Molecular Pharmacology* 63, 532-537.
78. Bao, Y., Pucci, M. L., Chan, B. S., Lu, R., Ito, S., and Schuster, V. L. (2002) Prostaglandin transporter PGT is expressed in cell types that synthesize and release prostanoids, *American Journal of Physiology - Renal Physiology* 282, F1103-F1110.
79. Mikkaichi, T., Suzuki, T., Onogawa, T., Tanemoto, M., Mizutamari, H., Okada, M., Chaki, T., Masuda, S., Tokui, T., Eto, N., Abe, M., Satoh, F., Unno, M., Hishinuma, T., Inui, K., Ito, S., Goto, J., and Abe, T. (2004) Isolation and characterization of a digoxin transporter and its rat homologue expressed in the kidney, *Proc Natl Acad Sci U S A* 101, 3569-3574.
80. Karbach, U., Kricke, J., Meyer-Wentrup, F., Gorboulev, V., Volk, C., Loffing-Cueni, D., Kaissling, B., Bachmann, S., and Koepsell, H. (2000) Localization of organic cation transporters OCT1 and OCT2 in rat kidney, *American Journal of Physiology - Renal Physiology* 279, F679-F687.
81. Koepsell, H., Lips, K., and Volk, C. (2007) Polyspecific Organic Cation Transporters: Structure, Function, Physiological Roles, and Biopharmaceutical Implications, *Pharmaceutical Research* 24, 1227-1251.
82. Motohashi, H., Sakurai, Y., Saito, H., Masuda, S., Urakami, Y., Goto, M., Fukatsu, A., Ogawa, O., and Inui, K.-i. (2002) Gene Expression Levels and Immunolocalization of Organic Ion Transporters in the Human Kidney, *Journal of the American Society of Nephrology* 13, 866-874.
83. Wing-Kee, L., Wolff, N. A., and Thévenod, F. (2009) Organic Cation Transporters: Physiology, Toxicology and Special Focus on Ethidium as a Novel Substrate, *Current Drug Metabolism* 10, 617-631.
84. Tamai, I., China, K., Sai, Y., Kobayashi, D., Nezu, J.-i., Kawahara, E., and Tsuji, A. (2001) Na<sup>+</sup>-coupled transport of L-carnitine via high-affinity carnitine transporter OCTN2 and its subcellular localization in kidney, *Biochimica et Biophysica Acta (BBA) - Biomembranes* 1512, 273-284.

85. Tamai, I., Nakanishi, T., Kobayashi, D., China, K., Kosugi, Y., Nezu, J.-i., Sai, Y., and Tsuji, A. (2003) Involvement of OCTN1 (SLC22A4) in pH-Dependent Transport of Organic Cations, *Molecular Pharmaceutics* 1, 57-66.
86. Yabuuchi, H., Tamai, I., Nezu, J., Sakamoto, K., Oku, A., Shimane, M., Sai, Y., and Tsuji, A. (1999) Novel membrane transporter OCTN1 mediates multispecific, bidirectional, and pH-dependent transport of organic cations, *J Pharmacol Exp Ther* 289, 768-773.
87. Tamai, I., Yabuuchi, H., Nezu, J., Sai, Y., Oku, A., Shimane, M., and Tsuji, A. (1997) Cloning and characterization of a novel human pH-dependent organic cation transporter, OCTN1, *FEBS Lett* 419, 107-111.
88. Tamai, I., Ohashi, R., Nezu, J. I., Sai, Y., Kobayashi, D., Oku, A., Shimane, M., and Tsuji, A. (2000) Molecular and functional characterization of organic cation/carnitine transporter family in mice, *J Biol Chem* 275, 40064-40072.
89. Tamai, I., Ohashi, R., Nezu, J., Yabuuchi, H., Oku, A., Shimane, M., Sai, Y., and Tsuji, A. (1998) Molecular and functional identification of sodium ion-dependent, high affinity human carnitine transporter OCTN2, *J Biol Chem* 273, 20378-20382.
90. Burckhardt, G., and Burckhardt, B. C. (2011) In Vitro and In Vivo Evidence of the Importance of Organic Anion Transporters (OATs) in Drug Therapy Drug Transporters, (Fromm, M. F., and Kim, R. B., Eds.), pp 29-104, Springer Berlin Heidelberg.
91. Kojima, R., Sekine, T., Kawachi, M., Cha, S. H., Suzuki, Y., and Endou, H. (2002) Immunolocalization of Multispecific Organic Anion Transporters, OAT1, OAT2, and OAT3, in Rat Kidney, *Journal of the American Society of Nephrology* 13, 848-857.
92. Enomoto, A., Takeda, M., Shimoda, M., Narikawa, S., Kobayashi, Y., Kobayashi, Y., Yamamoto, T., Sekine, T., Cha, S. H., Niwa, T., and Endou, H. (2002) Interaction of Human Organic Anion Transporters 2 and 4 with Organic Anion Transport Inhibitors, *Journal of Pharmacology and Experimental Therapeutics* 301, 797-802.
93. Ljubojevic, M., Balen, D., Breljak, D., Kusan, M., Anzai, N., Bahn, A., Burckhardt, G., and Sabolic, I. (2007) Renal expression of organic anion transporter OAT2 in rats and mice is regulated by sex hormones, *American Journal of Physiology - Renal Physiology* 292, F361-F372.



94. Cha, S. H., Sekine, T., Fukushima, J.-i., Kanai, Y., Kobayashi, Y., Goya, T., and Endou, H. (2001) Identification and Characterization of Human Organic Anion Transporter 3 Expressing Predominantly in the Kidney, *Molecular Pharmacology* 59, 1277-1286.
95. Masereeuw, R., and Russel, F. G. M. (2010) Therapeutic implications of renal anionic drug transporters, *Pharmacology & Therapeutics* 126, 200-216.
96. Babu, E., Takeda, M., Narikawa, S., Kobayashi, Y., Enomoto, A., Tojo, A., Cha, S. H., Sekine, T., Sakthisekaran, D., and Endou, H. (2002) Role of human organic anion transporter 4 in the transport of ochratoxin A, *Biochimica et Biophysica Acta (BBA) - Molecular Cell Research* 1590, 64-75.
97. Ekaratanawong, S., Anzai, N., Jutabha, P., Miyazaki, H., Noshiro, R., Takeda, M., Kanai, Y., Sophasan, S., and Endou, H. (2004) Human Organic Anion Transporter 4 Is a Renal Apical Organic Anion/Dicarboxylate Exchanger in the Proximal Tubules, *Journal of Pharmacological Sciences* 94, 297-304.
98. Rizwan, A., and Burckhardt, G. (2007) Organic Anion Transporters of the SLC22 Family: Biopharmaceutical, Physiological, and Pathological Roles, *Pharmaceutical Research* 24, 450-470.
99. Enomoto, A., Kimura, H., Chairoungdua, A., Shigeta, Y., Jutabha, P., Ho Cha, S., Hosoyamada, M., Takeda, M., Sekine, T., Igarashi, T., Matsuo, H., Kikuchi, Y., Oda, T., Ichida, K., Hosoya, T., Shimokata, K., Niwa, T., Kanai, Y., and Endou, H. (2002) Molecular identification of a renal urate-anion exchanger that regulates blood urate levels, *Nature* 417, 447-452.
100. Xu, G., Chen, X., Wu, D., Shi, S., Wang, J., Ding, R., Hong, Q., Feng, Z., Lin, S., and Lu, Y. (2006) Development of high-specificity antibodies against renal urate transporters using genetic immunization, *J Biochem Mol Biol* 39, 696-702.
101. Bahn, A., Hagos, Y., Reuter, S., Balen, D., Brzica, H., Krick, W., Burckhardt, B. C., Sabolić, I., and Burckhardt, G. (2008) Identification of a New Urate and High Affinity Nicotinate Transporter, hOAT10 (SLC22A13), *Journal of Biological Chemistry* 283, 16332-16341.
102. Anzai, N., Jutabha, P., Enomoto, A., Yokoyama, H., Nonoguchi, H., Hirata, T., Shiraya, K., He, X., Cha, S. H., Takeda, M., Miyazaki, H., Sakata, T., Tomita, K., Igarashi, T., Kanai, Y., and Endou, H. (2005) Functional Characterization of Rat Organic Anion Transporter 5 (Slc22a19) at the Apical Membrane of Renal

- Proximal Tubules, *Journal of Pharmacology and Experimental Therapeutics* 315, 534-544.
103. Kwak, J. O., Kim, H. W., Oh, K. J., Ko, C. B., Park, H., and Cha, S. H. (2005) Characterization of mouse organic anion transporter 5 as a renal steroid sulfate transporter, *J Steroid Biochem Mol Biol* 97, 369-375.
  104. Bleasby, K., Castle, J. C., Roberts, C. J., Cheng, C., Bailey, W. J., Sina, J. F., Kulkarni, A. V., Hafey, M. J., Evers, R., Johnson, J. M., Ulrich, R. G., and Slatter, J. G. (2006) Expression profiles of 50 xenobiotic transporter genes in humans and pre-clinical species: a resource for investigations into drug disposition, *Xenobiotica* 36, 963-988.
  105. Cheng, X., Maher, J., Chen, C., and Klaassen, C. D. (2005) TISSUE DISTRIBUTION AND ONTOGENY OF MOUSE ORGANIC ANION TRANSPORTING POLYPEPTIDES (OATPS), *Drug Metabolism and Disposition* 33, 1062-1073.
  106. Toyohara, T., Suzuki, T., Morimoto, R., Akiyama, Y., Souma, T., Shiwaku, H. O., Takeuchi, Y., Mishima, E., Abe, M., Tanemoto, M., Masuda, S., Kawano, H., Maemura, K., Nakayama, M., Sato, H., Mikkaichi, T., Yamaguchi, H., Fukui, S., Fukumoto, Y., Shimokawa, H., Inui, K.-i., Terasaki, T., Goto, J., Ito, S., Hishinuma, T., Rubera, I., Tauc, M., Fujii-Kuriyama, Y., Yabuuchi, H., Moriyama, Y., Soga, T., and Abe, T. (2009) SLCO4C1 Transporter Eliminates Uremic Toxins and Attenuates Hypertension and Renal Inflammation, *Journal of the American Society of Nephrology* 20, 2546-2555.
  107. Okabe, M., Szakács, G., Reimers, M. A., Suzuki, T., Hall, M. D., Abe, T., Weinstein, J. N., and Gottesman, M. M. (2008) Profiling SLCO and SLC22 genes in the NCI-60 cancer cell lines to identify drug uptake transporters, *Molecular Cancer Therapeutics* 7, 3081-3091.
  108. Fujii-Kuriyama, Y., and Mimura, J. (2005) Molecular mechanisms of AhR functions in the regulation of cytochrome P450 genes, *Biochemical and Biophysical Research Communications* 338, 311-317.
  109. Chu, X.-Y., Bleasby, K., Yabut, J., Cai, X., Chan, G. H., Hafey, M. J., Xu, S., Bergman, A. J., Braun, M. P., Dean, D. C., and Evers, R. (2007) Transport of the Dipeptidyl Peptidase-4 Inhibitor Sitagliptin by Human Organic Anion Transporter 3, Organic Anion Transporting Polypeptide 4C1, and Multidrug Resistance P-

- glycoprotein, *Journal of Pharmacology and Experimental Therapeutics* 321, 673-683.
110. Yamaguchi, H., Sugie, M., Okada, M., Mikkaichi, T., Toyohara, T., Abe, T., Goto, J., Hishinuma, T., Shimada, M., and Mano, N. (2010) Transport of estrone 3-sulfate mediated by organic anion transporter OATP4C1: estrone 3-sulfate binds to the different recognition site for digoxin in OATP4C1, *Drug Metab Pharmacokinet* 25, 314-317.
  111. Leuthold, S., Hagenbuch, B., Mohebbi, N., Wagner, C. A., Meier, P. J., and Stieger, B. (2009) Mechanisms of pH-gradient driven transport mediated by organic anion polypeptide transporters, *Am J Physiol Cell Physiol* 296, C570-582.
  112. Cunningham, R. E. (2010) Indirect immunofluorescent labeling of viable cells, *Methods Mol Biol* 588, 331-334.
  113. Goldinger, J. M., Khalsa, B. D., and Hong, S. K. (1984) Photoaffinity labeling of organic anion transport system in proximal tubule, *American Journal of Physiology - Cell Physiology* 247, C217-C227.
  114. Walmsley, S. J., Broeckling, C., Hess, A., Prenni, J., and Curthoys, N. P. (2010) Proteomic analysis of brush-border membrane vesicles isolated from purified proximal convoluted tubules, *American Journal of Physiology - Renal Physiology* 298, F1323-F1331.
  115. Wierdl, M., Wall, A., Morton, C. L., Sampath, J., Danks, M. K., Schuetz, J. D., and Potter, P. M. (2003) Carboxylesterase-mediated sensitization of human tumor cells to CPT-11 cannot override ABCG2-mediated drug resistance, *Mol Pharmacol* 64, 279-288.
  116. Fukada, K., Zhang, F., Vien, A., Cashman, N. R., and Zhu, H. (2004) Mitochondrial Proteomic Analysis of a Cell Line Model of Familial Amyotrophic Lateral Sclerosis, *Molecular & Cellular Proteomics* 3, 1211-1223.
  117. Zhai, J., Ström, A.-L., Kilty, R., Venkatakrishnan, P., White, J., Everson, W. V., Smart, E. J., and Zhu, H. (2009) Proteomic characterization of lipid raft proteins in amyotrophic lateral sclerosis mouse spinal cord, *FEBS Journal* 276, 3308-3323.
  118. Lai, L., and Tan, T. M. C. (2002) Role of glutathione in the multidrug resistance protein 4 (MRP4/ABCC4)-mediated efflux of cAMP and resistance to purine analogues, *Biochem. J.* 361, 497-503.

119. Hoque, M. T., Conseil, G., and Cole, S. P. C. (2009) Involvement of NHERF1 in apical membrane localization of MRP4 in polarized kidney cells, *Biochemical and Biophysical Research Communications* 379, 60-64.
120. Kidane, A., Guan, Y., Evans, P., Kaderbhai, M., and Kemp, R. (1997) Comparison of heat flux in wild-type and genetically-engineered Chinese Hamster ovary cells, *Journal of Thermal Analysis and Calorimetry* 49, 771-783.
121. Glick, B. R. (1995) Metabolic load and heterologous gene expression, *Biotechnol Adv* 13, 247-261.
122. Hirano, M., Maeda, K., Shitara, Y., and Sugiyama, Y. (2004) Contribution of OATP2 (OATP1B1) and OATP8 (OATP1B3) to the Hepatic Uptake of Pitavastatin in Humans, *Journal of Pharmacology and Experimental Therapeutics* 311, 139-146.
123. Dalmaso, G., Nguyen, H. T. T., Yan, Y., Charrier-Hisamuddin, L., Sitaraman, S. V., and Merlin, D. (2008) Butyrate Transcriptionally Enhances Peptide Transporter PepT1 Expression and Activity, *PLoS ONE* 3, e2476.
124. Laughery, M. D., Clifford, R. J., Chi, Y., and Kaplan, J. H. (2007) Selective basolateral localization of overexpressed Na-K-ATPase  $\beta$ 1- and  $\beta$ 2- subunits is disrupted by butyrate treatment of MDCK cells, *American Journal of Physiology - Renal Physiology* 292, F1718-F1725.
125. Sato, S., Ward, C. L., Krouse, M. E., Wine, J. J., and Kopito, R. R. (1996) Glycerol Reverses the Misfolding Phenotype of the Most Common Cystic Fibrosis Mutation, *Journal of Biological Chemistry* 271, 635-638.
126. Gekko, K., and Ito, H. (1990) Competing Solvent Effects of Polyols and Guanidine Hydrochloride on Protein Stability, *Journal of Biochemistry* 107, 572-577.
127. Piepenhagen, P. A., Peters, L. L., Lux, S. E., and Nelson, W. J. (1995) Differential expression of Na(+)-K(+)-ATPase, ankyrin, fodrin, and E-cadherin along the kidney nephron, *American Journal of Physiology - Cell Physiology* 269, C1417-C1432.
128. Truesdell, P. F., Zirngibl, R. A., Francis, S., Sangrar, W., and Greer, P. A. (2009) fps/fes knockout mice display a lactation defect and the fps/fes tyrosine kinase is a component of E-cadherin-based adherens junctions in breast epithelial cells during lactation, *Experimental Cell Research* 315, 2929-2940.

129. Old, W. M., Meyer-Arendt, K., Aveline-Wolf, L., Pierce, K. G., Mendoza, A., Sevinsky, J. R., Resing, K. A., and Ahn, N. G. (2005) Comparison of Label-free Methods for Quantifying Human Proteins by Shotgun Proteomics, *Molecular & Cellular Proteomics* 4, 1487-1502.
130. Liu, H., Sadygov, R. G., and Yates, J. R. (2004) A Model for Random Sampling and Estimation of Relative Protein Abundance in Shotgun Proteomics, *Analytical Chemistry* 76, 4193-4201.
131. Sabolic, I., Valenti, G., Verbavatz, J. M., Van Hoek, A. N., Verkman, A. S., Ausiello, D. A., and Brown, D. (1992) Localization of the CHIP28 water channel in rat kidney, *American Journal of Physiology - Cell Physiology* 263, C1225-C1233.
132. Bindels, R. J., Hartog, A., Timmermans, J. A., and van Os, C. H. (1991) Immunocytochemical localization of calbindin-D28k, calbindin-D9k and parvalbumin in rat kidney, *Contrib Nephrol* 91, 7-13.
133. Leggas, M., Adachi, M., Scheffer, G. L., Sun, D., Wielinga, P., Du, G., Mercer, K. E., Zhuang, Y., Panetta, J. C., Johnston, B., Scheper, R. J., Stewart, C. F., and Schuetz, J. D. (2004) Mrp4 confers resistance to topotecan and protects the brain from chemotherapy, *Mol Cell Biol* 24, 7612-7621.
134. Matter, K., and Mellman, I. (1994) Mechanisms of cell polarity: sorting and transport in epithelial cells, *Current Opinion in Cell Biology* 6, 545-554.
135. Cao, X., Surma, M. A., and Simons, K. (2012) Polarized sorting and trafficking in epithelial cells, *Cell Res*.
136. Fölsch, H., Ohno, H., Bonifacino, J. S., and Mellman, I. (1999) A Novel Clathrin Adaptor Complex Mediates Basolateral Targeting in Polarized Epithelial Cells, *Cell* 99, 189-198.
137. Kruh, J. (1982) Effects of sodium butyrate, a new pharmacological agent, on cells in culture, *Mol Cell Biochem* 42, 65-82.
138. Gry, M., Rimini, R., Stromberg, S., Asplund, A., Ponten, F., Uhlen, M., and Nilsson, P. (2009) Correlations between RNA and protein expression profiles in 23 human cell lines, *BMC Genomics* 10, 365.
139. Shankavaram, U. T., Reinhold, W. C., Nishizuka, S., Major, S., Morita, D., Chary, K. K., Reimers, M. A., Scherf, U., Kahn, A., Dolginow, D., Cossman, J., Kaldjian, E. P., Scudiero, D. A., Petricoin, E., Liotta, L., Lee, J. K., and Weinstein, J. N.

- (2007) Transcript and protein expression profiles of the NCI-60 cancer cell panel: an integrative microarray study, *Molecular Cancer Therapeutics* 6, 820-832.
140. Yokomizo, A., Shiota, M., Kashiwagi, E., Kuroiwa, K., Tatsugami, K., Inokuchi, J., Takeuchi, A., and Naito, S. (2011) Statins reduce the androgen sensitivity and cell proliferation by decreasing the androgen receptor protein in prostate cancer cells, *The Prostate* 71, 298-304.
  141. Brown, C. R., Hong-Brown, L. Q., Biwersi, J., Verkman, A. S., and Welch, W. J. (1996) Chemical chaperones correct the mutant phenotype of the delta F508 cystic fibrosis transmembrane conductance regulator protein, *Cell Stress Chaperones* 1, 117-125.
  142. Wakabayashi, K., Nakagawa, H., Tamura, A., Koshiba, S., Hoshijima, K., Komada, M., and Ishikawa, T. (2007) Intramolecular Disulfide Bond Is a Critical Check Point Determining Degradative Fates of ATP-binding Cassette (ABC) Transporter ABCG2 Protein, *Journal of Biological Chemistry* 282, 27841-27846.
  143. Maliepaard, M., Scheffer, G. L., Faneyte, I. F., van Gastelen, M. A., Pijnenborg, A. C. L. M., Schinkel, A. H., van de Vijver, M. J., Scheper, R. J., and Schellens, J. H. M. (2001) Subcellular Localization and Distribution of the Breast Cancer Resistance Protein Transporter in Normal Human Tissues, *Cancer Research* 61, 3458-3464.
  144. Liu, B., Sun, D., Xia, W., Hung, M. C., and Yu, D. (1997) Cross-reactivity of C219 anti-p170(mdr-1) antibody with p185(c-erbB2) in breast cancer cells: cautions on evaluating p170(mdr-1), *J Natl Cancer Inst* 89, 1524-1529.
  145. Murer, H., and Gmaj, P. (1986) Transport studies in plasma membrane vesicles isolated from renal cortex, *Kidney Int* 30, 171-186.
  146. Yoshioka, S., Suzuki, T., and Kawakita, M. (1997) Analysis of the Distribution of Na<sup>+</sup>/H<sup>+</sup> Exchanger Isoforms among the Plasma Membrane Subfractions of Bovine Kidney Cortex: Reevaluation of Methods for Fractionating the Brush-Border and the Basolateral Membranes, *Journal of Biochemistry* 122, 641-646.
  147. Yusufi, A. N. K., Murayama, N., Gapstur, S. M., Szczepanska-Konkel, M., and Dousa, T. P. (1994) Differential properties of brush-border membrane vesicles from early and late proximal tubules of rat kidney, *Biochimica et Biophysica Acta (BBA) - Biomembranes* 1191, 117-132.

148. Kaufmann, M., Muff, R., Stieger, B., Biber, J., Murer, H., and Fischer, J. A. (1994) Apical and basolateral parathyroid hormone receptors in rat renal cortical membranes, *Endocrinology* 134, 1173-1178.
149. Scalera, V., Huang, Y. K., Hildmann, B., and Murer, H. (1981) A simple isolation method for basal-lateral plasma membranes from rat kidney cortex, *Membr Biochem* 4, 49-61.
150. Inui, K., Okano, T., Takano, M., Kitazawa, S., and Hori, R. (1981) A simple method for the isolation of basolateral plasma membrane vesicles from rat kidney cortex. Enzyme activities and some properties of glucose transport, *Biochim Biophys Acta* 647, 150-154.
151. Wright, K., Collins, D. C., Musey, P. I., and Preedy, J. R. (1978) A specific radioimmunoassay for estrone sulfate in plasma and urine without hydrolysis, *J Clin Endocrinol Metab* 47, 1092-1098.
152. Breithaupt, H., and Kuenzlen, E. (1982) Pharmacokinetics of methotrexate and 7-hydroxymethotrexate following infusions of high-dose methotrexate, *Cancer treatment reports* 66, 1733-1741.
153. Deguchi, T., Kusuhara, H., Takadate, A., Endou, H., Otagiri, M., and Sugiyama, Y. (2004) Characterization of uremic toxin transport by organic anion transporters in the kidney, *Kidney Int* 65, 162-174.
154. Deguchi, T., Takemoto, M., Uehara, N., Lindup, W. E., Suenaga, A., and Otagiri, M. (2005) Renal Clearance of Endogenous Hippurate Correlates with Expression Levels of Renal Organic Anion Transporters in Uremic Rats, *Journal of Pharmacology and Experimental Therapeutics* 314, 932-938.
155. Mutsaers, H. A., van den Heuvel, L. P., Ringens, L. H., Dankers, A. C., Russel, F. G., Wetzels, J. F., Hoenderop, J. G., and Masereeuw, R. (2011) Uremic toxins inhibit transport by breast cancer resistance protein and multidrug resistance protein 4 at clinically relevant concentrations, *PLoS One* 6, e18438.
156. Li, L., Sham, Y. Y., Bikadi, Z., and Elmquist, W. F. (2011) pH-Dependent Transport of Pemetrexed by Breast Cancer Resistance Protein, *Drug Metabolism and Disposition* 39, 1478-1485.
157. Breedveld, P., Pluim, D., Cipriani, G., Dahlhaus, F., van Eijndhoven, M. A. J., de Wolf, C. J. F., Kuil, A., Beijnen, J. H., Scheffer, G. L., Jansen, G., Borst, P., and Schellens, J. H. M. (2007) The Effect of Low pH on Breast Cancer Resistance Protein (ABCG2)-Mediated Transport of Methotrexate, 7-Hydroxymethotrexate,

- Methotrexate Diglutamate, Folic Acid, Mitoxantrone, Topotecan, and Resveratrol in In Vitro Drug Transport Models, *Molecular Pharmacology* 71, 240-249.
158. Satlin, L. M., Amin, V., and Wolkoff, A. W. (1997) Organic Anion Transporting Polypeptide Mediates Organic Anion/HCO<sub>3</sub><sup>-</sup> Exchange, *Journal of Biological Chemistry* 272, 26340-26345.
  159. Meier-Abt, F., Faulstich, H., and Hagenbuch, B. (2004) Identification of phalloidin uptake systems of rat and human liver, *Biochimica et Biophysica Acta (BBA) - Biomembranes* 1664, 64-69.
  160. Kobayashi, D., Nozawa, T., Imai, K., Nezu, J.-i., Tsuji, A., and Tamai, I. (2003) Involvement of Human Organic Anion Transporting Polypeptide OATP-B (SLC21A9) in pH-Dependent Transport across Intestinal Apical Membrane, *Journal of Pharmacology and Experimental Therapeutics* 306, 703-708.
  161. Buerkert, J., Martin, D., and Trigg, D. (1983) Segmental analysis of the renal tubule in buffer production and net acid formation, *American Journal of Physiology - Renal Physiology* 244, F442-F454.
  162. DuBose, T. D., Pucacco, L. R., Lucci, M. S., and Carter, N. W. (1979) Micropuncture determination of pH, PCO<sub>2</sub>, and total CO<sub>2</sub> concentration in accessible structures of the rat renal cortex, *The Journal of Clinical Investigation* 64, 476-482.
  163. Malnic, G., De Mello Aires, M., and Giebisch, G. (1972) Micropuncture study of renal tubular hydrogen ion transport in the rat, *American Journal of Physiology -- Legacy Content* 222, 147-158.
  164. Vieira, F., and Malnic, G. (1968) Hydrogen ion secretion by rat renal cortical tubules as studied by an antimony microelectrode, *American Journal of Physiology -- Legacy Content* 214, 710-718.
  165. Goh, L.-B., Spears, K. J., Yao, D., Ayrton, A., Morgan, P., Roland Wolf, C., and Friedberg, T. (2002) Endogenous drug transporters in in vitro and in vivo models for the prediction of drug disposition in man, *Biochemical Pharmacology* 64, 1569-1578.
  166. Hyafil, F., Vergely, C., Du Vignaud, P., and Grand-Perret, T. (1993) In vitro and in vivo reversal of multidrug resistance by GF120918, an acridonecarboxamide derivative, *Cancer Res* 53, 4595-4602.



167. Wallstab, A., Koester, M., Bohme, M., and Keppler, D. (1999) Selective inhibition of MDR1 P-glycoprotein-mediated transport by the acridone carboxamide derivative GG918, *Br J Cancer* 79, 1053-1060.
168. Qian, Y.-M., Song, W.-C., Cui, H., Cole, S. P. C., and Deeley, R. G. (2001) Glutathione Stimulates Sulfated Estrogen Transport by Multidrug Resistance Protein 1, *Journal of Biological Chemistry* 276, 6404-6411.
169. Williams, G. C., Liu, A., Knipp, G., and Sinko, P. J. (2002) Direct evidence that saquinavir is transported by multidrug resistance-associated protein (MRP1) and canalicular multispecific organic anion transporter (MRP2), *Antimicrob Agents Chemother* 46, 3456-3462.
170. Vellonen, K.-S., Honkakoski, P., and Urtti, A. (2004) Substrates and inhibitors of efflux proteins interfere with the MTT assay in cells and may lead to underestimation of drug toxicity, *European Journal of Pharmaceutical Sciences* 23, 181-188.
171. Pedersen, J. M., Matsson, P., Bergström, C. A. S., Norinder, U., Hoogstraate, J., and Artursson, P. (2008) Prediction and Identification of Drug Interactions with the Human ATP-Binding Cassette Transporter Multidrug-Resistance Associated Protein 2 (MRP2; ABCC2), *Journal of Medicinal Chemistry* 51, 3275-3287.
172. Özvegy, C., Litman, T., Szakács, G., Nagy, Z., Bates, S., Váradi, A., and Sarkadi, B. (2001) Functional Characterization of the Human Multidrug Transporter, ABCG2, Expressed in Insect Cells, *Biochemical and Biophysical Research Communications* 285, 111-117.
173. Glavinas, H., Méhn, D., Jani, M., Oosterhuis, B., Herédi-Szabó, K., and Krajcsi, P. (2008) Utilization of membrane vesicle preparations to study drug-ABC transporter interactions, *Expert Opinion on Drug Metabolism & Toxicology* 4, 721-732.
174. Chen, L., and Tai, P. C. (1986) Effects of nucleotides on ATP-dependent protein translocation into Escherichia coli membrane vesicles, *Journal of Bacteriology* 168, 828-832.
175. Komatsu, M., Sato, Y., Yamada, S., Yamauchi, K., Hashizume, K., and Aizawa, T. (2002) Triggering of insulin release by a combination of cAMP signal and nutrients: an ATP-sensitive K<sup>+</sup> channel-independent phenomenon, *Diabetes* 51 Suppl 1, S29-32.

176. Masuda, N., Ohnishi, T., Kawamoto, S., Monden, M., and Okubo, K. (1999) Analysis of chemical modification of RNA from formalin-fixed samples and optimization of molecular biology applications for such samples, *Nucleic Acids Research* 27, 4436-4443.
177. Cronin, M., Pho, M., Dutta, D., Stephans, J. C., Shak, S., Kiefer, M. C., Esteban, J. M., and Baker, J. B. (2004) Measurement of Gene Expression in Archival Paraffin-Embedded Tissues: Development and Performance of a 92-Gene Reverse Transcriptase-Polymerase Chain Reaction Assay, *The American Journal of Pathology* 164, 35-42.
178. Godfrey, T. E., Kim, S. H., Chavira, M., Ruff, D. W., Warren, R. S., Gray, J. W., and Jensen, R. H. (2000) Quantitative mRNA expression analysis from formalin-fixed, paraffin-embedded tissues using 5' nuclease quantitative reverse transcription-polymerase chain reaction, *J Mol Diagn* 2, 84-91.
179. Imai, Y., Asada, S., Tsukahara, S., Ishikawa, E., Tsuruo, T., and Sugimoto, Y. (2003) Breast Cancer Resistance Protein Exports Sulfated Estrogens but Not Free Estrogens, *Molecular Pharmacology* 64, 610-618.
180. Scharenberg, C. W., Harkey, M. A., and Torok-Storb, B. (2002) The ABCG2 transporter is an efficient Hoechst 33342 efflux pump and is preferentially expressed by immature human hematopoietic progenitors, *Blood* 99, 507-512.
181. Özvegy-Laczka, C., Köblös, G., Sarkadi, B., and Váradi, A. (2005) Single amino acid (482) variants of the ABCG2 multidrug transporter: major differences in transport capacity and substrate recognition, *Biochimica et Biophysica Acta (BBA) - Biomembranes* 1668, 53-63.
182. de Bruin, M., Miyake, K., Litman, T., Robey, R., and Bates, S. E. (1999) Reversal of resistance by GF120918 in cell lines expressing the ABC half-transporter, MXR, *Cancer Letters* 146, 117-126.
183. Tanigawara, Y., Okamura, N., Hirai, M., Yasuhara, M., Ueda, K., Kioka, N., Komano, T., and Hori, R. (1992) Transport of digoxin by human P-glycoprotein expressed in a porcine kidney epithelial cell line (LLC-PK1), *Journal of Pharmacology and Experimental Therapeutics* 263, 840-845.

## VITA

### Kuei-Ling Kuo

**Date and place of birth:** September 7, 1981; Taipei, Taiwan

### Education:

2000-2004 B.S.(Pharmacy) Taipei Medical University, Taipei, Taiwan

2004-2006 M.S.(Pharmaceutical Sciences) National Taiwan University, Taipei, Taiwan

2006-present Ph.D. candidate (Pharmaceutical Sciences) University of Kentucky, Lexington, Kentucky, USA

### Professional Experiences:

2004-2006 Graduate Assistant, Department of Pharmaceutical Sciences, National Taiwan University, Taipei, Taiwan

2006-2008 Teaching Assistant, Department of Pharmaceutical Sciences, University of Kentucky, Lexington, Kentucky

2008-present Research Assistant, Department of Pharmaceutical Sciences, University of Kentucky, Lexington, Kentucky

### Publications:

Kuo KL, Zhu H, McNamara PJ, Leggas M. Localization and functional characterization of the rat Oatp4c1 transporter in an *in vitro* cell system and rat tissues. (accepted, PLOS One)

Tsakalozou E, Adane ED, Kuo KL, Daily A, Moscow JA, Leggas M. The effect of BCRP and OATP1B3 on the antitumor efficacy of the lipophilic camptothecin AR-67 *in vitro* (in preparation)

Leggas M, Kuo KL, Robert F, Cloud G, deShazo M, Zhang R, Li M, Wang H, Davidson S, Rinehart J. Intensive anti-inflammatory therapy with dexamethasone in patients with non-small cell lung cancer: effect on chemotherapy toxicity and efficacy. Cancer Chemother Pharmacol. 2009; 63(4):731-43.

Lee PH, Kuo KL, Chu PY, Liu EM, Lin JH. SLITHER: a web server for generating contiguous conformations of substrate molecules entering into deep active sites of proteins or migrating through channels in membrane transporters. Nucleic Acids Res. 2009; 37(Web Server issue):W559-64